Direct Surface Sampling of Dried Blood Spots Coupled with Mass Spectrometry for Haemoglobin Analysis

by

REBECCA LOUISE EDWARDS

A thesis submitted to the University of Birmingham for the degree of DOCTOR OF PHILOSOPHY

School of Biosciences

University of Birmingham

October 2013

Abstract

Haemoglobinopathies are inherited disorders, typically detected during neonatal healthcare screening programmes. Haemoglobinopathies are characterised by either a reduction in the synthesis of the globin chains or by point mutations in the globin gene often leading to a single amino acid substitution in the globin chain. Current screening techniques analyse samples from resolubilised dried blood spots (DBS) by HPLC and/or isoelectric focusing. These methods are characterised by lengthy sample preparation and/or ambiguous variant determination. Further analysis is required for unequivocal diagnosis. The work presented here describes a method for the unambiguous diagnosis of haemoglobin variants in neonatal DBS samples using a surface sampling technique called liquid extraction surface analysis (LESA) coupled with high resolution top-down mass spectrometry. LESA allows DBS samples to be sampled directly and the material recovered to be directly electrosprayed into a mass spectrometer. Both the sampling and MS/MS (CID/ETD) parameters were optimised to yield maximum globin chain sequence coverage (up to 81 %) allowing for the unambiguous diagnosis of common Hb variants such as HbS and so-called unknown variants (variants unable to be diagnosed during the standard screening protocol). The LESA sampling technique has also successfully been applied to study Hb non-covalent interactions.

Acknowledgements

Firstly I would like to thank my supervisor Dr Helen J. Cooper for her guidance and support thorough the entirety of my PhD studies, as well as Dr Andrew J. Creese and Dr Cleidiane Zampronio for their much appreciated practical help, assistance and advice.

I wish to thank Paul Griffiths at Birmingham Children's Hospital for supplying the DBS samples and Advion for their technical assistance. I would also like to thank the rest of the Cooper research group and all the members of the 5th floor for their kindness and support.

Finally, I would like to gratefully acknowledge the EPSRC for funding.

Table of Contents

List of Figures

Abbreviations:

AGC, automatic gain control

ce, cation exchange

CID, collision induced dissociation

DBS, dried blood spots

DNA, deoxyribonucleic acid

ETD, electron transfer dissociation

Hb, haemoglobin

HbA, adult haemoglobin

HbF, foetal haemoglobin

HPLC**,** high pressure liquid chromatography

IEF, isoelectric focusing

LESA, liquid extraction surface analysis

LMJ, liquid microjunction

MS/MS, tandem mass spectrometry

NHS, National Health Service (UK)

SCD, sickle cell disease

SIM, selected ion monitoring

Chapter 1: Introduction

Overview

Abnormalities of haemoglobin, haemoglobinopathies, are the most common type of inherited disorder. Haemoglobinopathies including HbS which is responsible for sickle cell disease are typically detected during population wide neonatal healthcare screening programmes. Current screening techniques analyse samples from resolubilised dried blood spots (DBS) by HPLC and/or isoelectric focusing. These methods are characterised by lengthy sample preparation and/or ambiguous variant determination. Further analysis by either DNA sequencing or mass spectrometry (MS) analysis is required for a definitive diagnosis.

Tandem mass spectrometry (MS/MS) is the standard technique used in newborn screening for inherited metabolic disorders such as phenylketonuria. For convenience, it would be advantageous to use the same technique to screen Hb variants as well. Mass spectrometry accurately determines the *m/z* of globin chains, pinpoint the precise location of a variant without the need to perform any further confirmatory analysis. For this reason MS has been studied has an alternative to the current screening method. However, mass spectrometery-based screening techniquuies have been typically categorised by lengthy sample preparation (including resolubilisation of the dried blood spot (DBS), tryptic digests, removal of salts from the sample and HPLC-MS coupled runs) and often the inability to diagnose Hb variants with very small mass shift.

The aim of the work presented in this thesis is to assess the viability of liquid extraction surface analysis (LESA) of DBS coupled with top-down mass spectrometry for the diagnosis of a variety of Hb variants in neonatal samples.

1.1 Mass Spectrometry

The origin of mass spectrometry (MS) as an analytical technique occurred over a century ago when J.J. Thomson built an apparatus that could measure *e/m* (charge to mass ratio) of an electron. Two years later, he developed an instrument that could simultaneously measure *e/m* and *e* from which the mass of an electron could be determined and for this discovery he was awarded the Nobel Prize in Physics in 1906 [1]. In 1912 Thomson along with F.W. Aston introduced what is widely acknowledged as the first mass spectrometer and which could measure the mass of charged molecules [2]. Since then biological mass spectrometry has undergone a revolution, principally due to the development of the soft ionisation techniques electrospray ionisation (ESI) [3] and matrix-assisted laser desorption ionisation (MALDI) [4]. These developments removed the restrictions to the molecular weight and type of samples that could be analysed, making MS the technique of choice across a variety of disciplines.

Mass spectrometers consist of three fundamental components: an ion source, a mass analyser and a detector. Ions are separated according to their mass to charge ratio (*m/z*) by measuring the response of an ion's trajectory to electric and/or magnetic fields under vacuum [5].

1.2 Ionisation

In electron impact/electron ionisation (EI), a beam of electrons are formed from a heated metallic filament, accelerated by an electric field and collided with a vaporised sample causing electron expulsion from the analytes and the subsequent formation of positively charged radical cations $M^{+\cdot}$ [6]. EI is an energetic process responsible for extensive and reproducible in-source fragmentation. This is advantageous in structural elucidation and compound identification studies where comparisons are made with reference spectra, however, due to the excessive fragmentation the molecular ion is often absent rendering the technique unsuitable for molecular weight determination [7]. Chemical ionisation is an alternative ionisation technique in which ions are produced through the collision of the analyte molecules (added at low pressure) with reaction gas molecules [8]. Fast atom bombardment (FAB) is a technique that was developed in 1981 [9] with the aim of overcoming some of the problems associated with the ionisation of biological samples, namely their non- volatility and large molecular weights. The process involves the interaction of the sample dissolved in a non- volatile liquid matrix such as glycerol with a high intensity molecular beam of a neutral gas (argon). Energetic particles hit the sample solution producing a spluttering effect (momentum transfer from Ar ions to the target sample) which ejects positively and negatively charged ions from the solution [10]. The technique allows for the analysis of thermally labile biological molecules up to about 25, 000 Da producing mainly singly charged ions which places limitation on the mass analyser that can be used [11].

Matrix- assisted laser desorption ionisation (MALDI) was established in the late 1980s by Karas and Hillenkamp [4] and Tanaka [12]. For the first time, it allowed for the

measurement of intact proteins larger than 25,000 Da [13]. It is also a soft ionisation technique meaning the process itself results in little or no fragmentation. The key feature in the MALDI ion generation process is the presence of an organic matrix which is present in excess with comparison to the sample. The sample is dissolved in the matrix solvent. The mixture is dried and the matrix which strongly absorbs (N_2) laser wavelengths, is co-crystallised with the sample. The analyte molecules are completely separated from one another by the matrix molecules. Under vacuum, irradiation of the crystalline sample causes the crystals to heat up rapidly due to the excitation of the matrix molecules which causes an accumulation of energy. This heating causes sublimation of the crystal surface and expands the matrix into gas phase along with the analyte into the expanding matrix plume.

1.2.1 Electrospray ionisation

Electrospray ionisation (ESI) was originally proposed in the 1960s by Malcolm Dole [14] and was developed further by John Fenn [15] for which he was awarded a Noble prize in 2002. An ESI source creates ions through the nebulization of a solution phase sample into electrically charged droplets from which ions are released. A typical ESI solution suitable for protein/peptide analysis consists of water with the addition of an organic solvent which aids the ESI process (increases ionisation efficiency) as it decreases the surface tension. In positive mode formic acid is also added for protonation [16].

The process begins by the mechanical injection of a solution through a stainless steel needle or capillary under atmosphere pressure at a flow rate of between 1 and 20 μl/min. In positive mode electrospray a high voltage of 3-6 kV is applied. The resulting electric field leads to positive charge accumulation at the tip. The repulsion between the positive ions

accumulated at the tip overcomes surface tension causing an expansion of the emerging liquid [17, 18] forming a Taylor cone [19]. In the presence of a suitably high electric field a fine jet arises from the cone which then breaks into small charged droplets [20]. See **Figure 1.1.**

At ambient temperature the charged droplet travels towards the counter electrode during which the droplet decreases in size due to solvent evaporation. The charge density of each droplet increases until the Rayleigh limit is reached. Coulomb repulsion between charges overcomes surface tension breaking the droplet apart (Coulomb fission) producing smaller daughter droplets. This sequence of events continues to repeat itself causing fission of the daughter droplets formed [21], producing very small, highly charged droplets.

Two mechanisms have been proposed to describe how gas-phase ions are formed from these small highly charged droplets. The first mechanism, termed charged residue model (CRM), was suggested by Dole [14]. It states that the gas phase ions of globular proteins are produced from very small droplets that only contain one macromolecule, so called ultimate droplets.

As the ultimate droplet completely evaporates the small ions on the surface of the droplet transfer to the macromolecule, providing the macromolecule with a charge [22]. The second mechanism is termed ion evaporation model (IEM) and was proposed by Iribarne and Thomson [23] whose studies were conducted on small analytes. The IEM proposes that direct ion emission occurs when an electric field at the surface of the droplet with a radius of 10 nM or less has become suitably high. Ion evaporation in these droplets is faster than Coulombic fission. An assumption is made that the evaporating ion is a charge located at the surface of the droplet. The emitted ion is repelled by the remaining charges on the droplet pushing the ion into the ambient gas forming a gas-phase ion [20, 24].

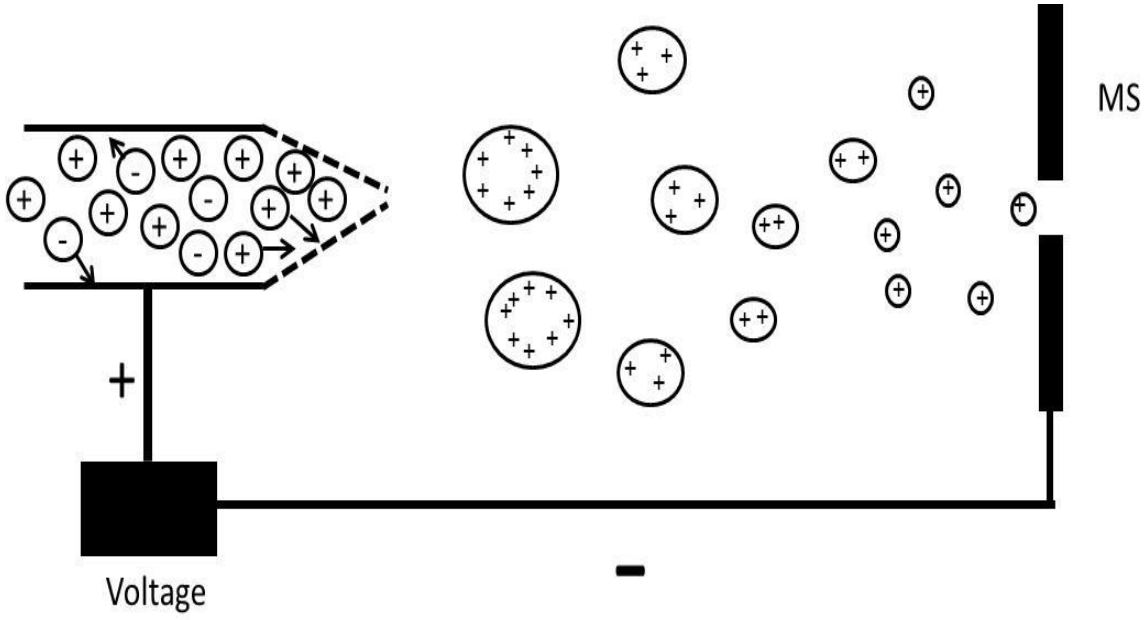

Figure 1.1. The electrospray ionisation process showing the formation of small highly charged droplets.

ESI is an effective so-called soft ionisation technique because the transfer of analyte ions from the solution to the gas phase is a non-energetic process therefore the structure of analyte ions remains intact (no fragmentation). ESI can produce multiply charged ions of biomolecules with large molecular masses due to the increased amount of proton accepting (or realising) sites. This is advantageous as it means mass analyzers with a relatively small *m/z* range (up to *m/z* 3000) are capable of accurately determining the mass of large intact proteins [16]. Reduction in the efficiency of the ESI process is caused by high sample concentration (above 10^{-5} M) [25] and ion suppression (which is produced by the presence of salts/drugs or molecules with larger masses in the ESI solution that produce a greater signal than the analyte of interest which is less readily ionised) [26]. The development of nanoelectrospray helped alleviate some of these issues, subsequently making the technique even more widely used.

1.2.2 Nanoelectrospray

Nanoelectrospray (nano-ESI) uses a smaller capillary (often made of fused silica) with an inner diameter of approximately 1 μm resulting in the formation of smaller droplets. The smaller droplet size is responsible for the reduction in contaminants such as salt observed during nano-ESI. The initial droplets are often 1000 times smaller than the initial droplets formed by standard ESI reducing the number of solvent evaporation (which would increase the concentration of the salt/analyte) and Coulombic fission steps required for the generation of the ions, consequently reducing the concentration of the contaminants and increasing the sensitivity of the analytes [27]. In ESI analyte sample flow rate through a capillary is typically a few μl/min. The application of nano-ESI, with flow rates of nl/min,

reduces sample consumption meaning very low sample volumes are sufficient for analysis [28]. Henion *et al.* [29, 30] have developed an automated nano-ESI system for sample infusion. It allows for automated high throughput sample analysis with increased spray stability. A robotic probe (Triversa NanoMate) controlled by ChipSoft (Advion) software picks up a disposable pipette tip to collect the sample from a well of a standard 96-well plate and then positions the pipette tip containing the sample flush with the inlet of ESI chip (which is composed of 400 silica based nozzles/capillaries). A spray voltage (kV) and nitrogen gas pressure (psi) is applied to the sample in the tip which initiates the nano-ESI process. Once sample infusion and analysis is complete the tip is automatically discarded. The next sample to be analysed uses a fresh tip and nozzle. The system of one tip and one nozzle per sample eliminates sample carry over.

1.2.3 Desorption electrospray ionisation

In 2004 Cooks *et al.* introduced an alternative ambient ionisation technique desorption electrospray ionisation (DESI) [31]. Ionized solvent droplets created by the electrospray ionization (ESI) source are directed at a sample surface of interest. The charged solvent ion droplets from ESI source impact with the sample surface. The ions bounce off the surface and are transported to the mass spectrometer via the inlet capillary of an atmosphere pressure ion transfer line. The precise mechanism is not fully known but is believed to occur because the initial droplets that have been electrosprayed onto the sample pre-wet the surface, causing surface analytes to dissolve in a localised solvent layer. Subsequent droplets impact with and disturb this solvent layer emitting secondary droplets which contain dissolved analytes from the sample surface. Therefore analyte desorption occurs due to the momentum transfer from charged droplets that are the ionised by ESI [32].

DESI produces similar mass spectra to those of ESI. This technique has been used in a number of applications such as: *in vivo* sampling of living tissue surfaces, imaging to determine the spatial distribution of compounds across a sample surface, such as a fingerprint [33]. The development of this technique has triggered interest into a range of techniques know as ambient surface sample techniques (ionization occurs at atmosphere pressure) and their associated ionization techniques [34].

1.2.4 Liquid extraction surface analysis

The development of liquid microjunction-surface sampling probe (LMJ-SSP) latterly termed liquid extraction surface analysis (LESA) (Advion Biosciences) is a technique that has reported applications on a wide variety of samples including drugs captured in solid phase extraction cards and compounds such as metabolites from thin tissue sections [35]. It is performed using a combined surface sampling probe and an electrospray emitter, such as the Advion Triversa Nanomate [29]. A key feature of liquid extraction surface sampling is the formation of the probe-to-surface liquid microjunction. A robotic probe (solvent flow channel) is positioned an appropriate distance from the sample surface, the ESI solvent is dispensed on the sample surface and a wall-less liquid microjunction is formed by dispensing the liquid (electrospray solvent) from the sample extraction/dispensing end of the probe and onto the sample surface. There is often a small delay time of a few seconds where the LMJ is maintained allowing for species on the surface dissolved by the electrospray solvent are drawn back into the probe. The surface analytes are then electrosprayed into a mass spectrometer. The technique can theoretically be performed with any probe capable of both dispensing and recovering solution from the sample surface. LESA has been investigated has a tool in large scale proteomic studies in recent

work by Quanico *et al.* [36]. It describes a protocol consisting of a direct on tissue digest, followed by LESA and instead of direct sampling into a mass spectrometer; the extracted sample is collected and then subjected nanoLC-MS/MS. This allowed for the identification of 1500 proteins.

1.3 Mass analysers

There are five major types of mass analyser: quadrupole, time-of-flight (TOF), ion trap (IT), Fourier transform ion cyclotron resonance (FT-ICR) and orbitrap analysers. Each of the analysers has different characteristics regarding mass accuracy, *m/z* range, sensitivity and scanning speed. To take advantage of their differing characteristics often multiple analysers are coupled together to create hybrid instruments such as a quadrupole-TOF or ion trap-FT-ICR [37]. The mass analysers used in this work are presented below.

1.3.1 Ion traps

An ion trap uses an oscillating electric field to store ions and a radio frequency (RF) quadrupolar field to trap ions in either two dimensions (linear ion trap) or three dimensions (quadrupole ion trap). Quadrupole ion traps (QIT), known as Paul traps, consist of a central ring electrode positioned between two ellipsoid end cap electrodes. The upper cap electrode has an inlet to allow ions to enter the trap from the source and the lower cap electrode has an inlet to allow ions to exit trap and reach the detector, **figure 1.2**. Inside the trap, ion repulsion results in an expansion of its trajectory. Helium gas (10^{-3} Torr) present in the trap eliminates the ions' excess kinetic energy preventing ion escape through trajectory expansion directing the ions towards the centre of the trap, trapping the ions in the presence of RF potential [38, 39]. Ions are ejected sequentially from the QIT by the

linearly ramping the amplitude of the RF potential that is applied to an electrode. Ions of the same species are ejected from the trap at specific RF amplitude, the m/z ratio for the ion species is determined from initial amplitude and ramping rate [40].

In contrast a linear ion trap (LIT) on is made up of four parallel electrode rods with opposite electrodes possessing the same polarity. A quadrupolar field (RF) is used to trap ions radially and an electric field applied to the tip of the rods to trap ions axially. Ions are trapped along the *z* axis through the centre of rods when a balanced dipolar RF potential is applied to opposing rod pairs. Simultaneous ion oscillation in the *xy* plane occurs is due to the application of a RF voltage. Inside the LIT the ions collide with inert buffer gas with the purpose of reducing the ions' kinetic energy and the DC voltage applied to the tip of the rods contribute to containing the ions inside the trap [41, 42]. Ions are either ejected axially following the presence of a so-called fringe field produced by applying an AC voltage between the rods and an exit lens [43] or by radial (perpendicular) ejection through application of an AC current to opposing rods with slots cut into them. The advantages of a LIT over a QIT include a greater ion trapping capacity and ejection efficiency [39].

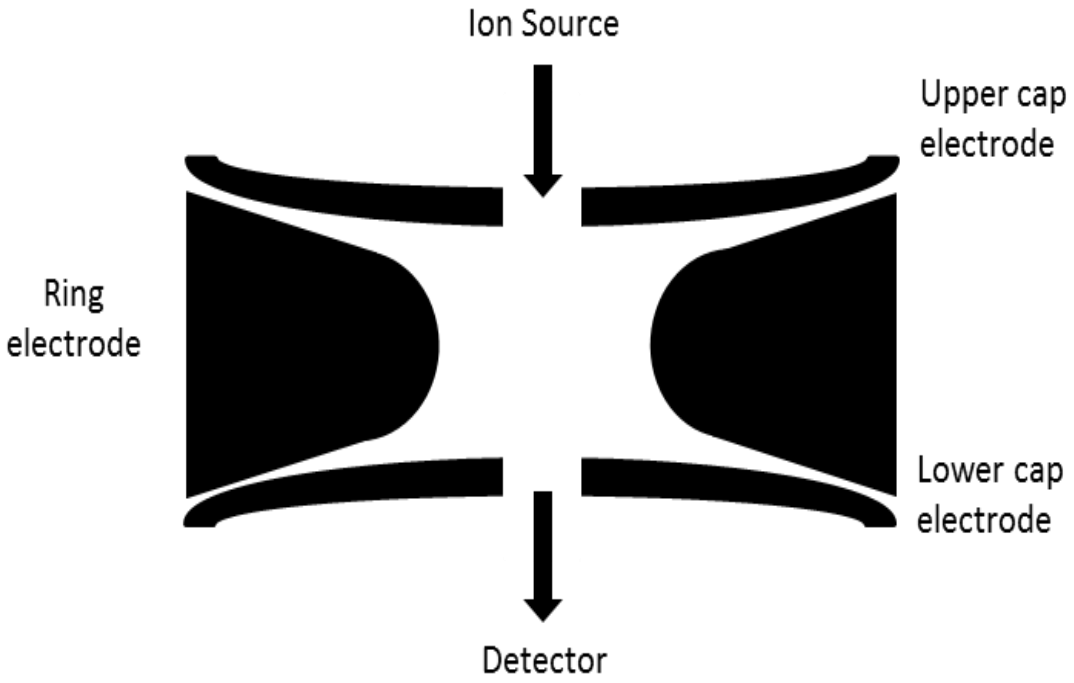

Figure 1.2 Schematic of a 3D ion trap.

1.3.2 The orbitrap

The recently developed orbitrap mass analyser is an electrostatic ion trap that utilizes an electrostatic field for ion trapping. It does not require RF or magnetic fields and uses Fourier transform to obtain mass spectra. It was originally proposed by Makarov in 1996 [44]. The orbitrap, **figure 1.3** consists of a thin-wire central electrode and an electrically isolated barrel- like outer cylindrical electrode. Ions are injected tangentially into the orbitrap after the voltage on the central electrode has been switched on but before the electrode has reached its target voltage. As a consequence the ions undergo what is known as electrodynamic squeezing because of the increase in electric field strength. Ions are squeezed towards the central electrode, responding with a reduction in the rotational radius which prevents unwanted collisions with the outer electrode. This initiates the ion packet's oscillation along the *z* axis without the need for any additional excitation. Once the voltage incline ceases ion packet trajectories become a stable spiral. The ions all have the same amplitude but ions of different m/z ratios will oscillate along the z axis at a specific frequency [45, 46].

The direct current (DC) voltage is applied between the two axially symmetric inner and outer electrodes which creates an electrostatic potential. See equation 1.

$$U(r,z) = \frac{k}{2}\left(z^2 - \frac{r^2}{2}\right) + \frac{k}{2}\,(R_m)^2 \ln\left(\frac{r}{R_m}\right) + C$$

Equation 1

In the equation *r* and *z* are cylindrical coordinates z = 0 is the axis of symmetry of the field, *k* is the field curvature, C is a constant and R_m is the characteristic radius [45].

The voltage gradient *z* (in the horizontal direction through the orbitrap) is defined in equation 2.

$$\frac{\partial U(r,z)}{\partial z} = kz$$

Equation 2

An ion with a mass *m* and overall charge *q*=*ze* accelerates along the *z* axis as a consequence of the force induced by the electric field. This electric force *–qkz* is equal to mass times acceleration i.e $m(d^2_Z/d_t^2)$.

$$\frac{d^2 z}{dt^2} = -\frac{q}{m}\, kz$$

Equation 3

Ion motion along the z axis is described as a harmonic oscillation, see equation 4, independent of both r and φ (φ is the angular coordinate). E_z is the energy characteristic in the *z* direction.

$$qE_Z = \left(\frac{m}{2}\right)\left(\frac{dz_0}{dt}\right)^2$$

Equation 4

The solution to equation 3 is

$$z(t) = z_0 \cos \omega t + \sqrt{2E/K} \sin \omega t$$

Equation 5

Whereby

$$\omega = \sqrt{\left(\frac{q}{m}\right)k}$$

Equation 6

The information shown in equation 6 shows frequency of axial oscillations is proportional to the *m*/*q* ratio independent of the kinetic energy of the injected ions. Detection of the ions requires a signal voltage that is induced by the oscillations of the ions. The signal (the image current) is detected by the Orbitrap analyser's outer electrodes. The ions are observed for a time period, often several seconds. This time domain signal (transient) is composed of sinusoids of the frequencies of the measured ions at intensities corresponding to the amount of the molecular species in the sample [39, 47]. The acquired image signal/transient is converted from the time domain into a frequency spectrum by applying a fast Fourier transform algorithm [48]. The frequency components are then calibrated andsubsequently converted into a mass spectrum [49, 50].

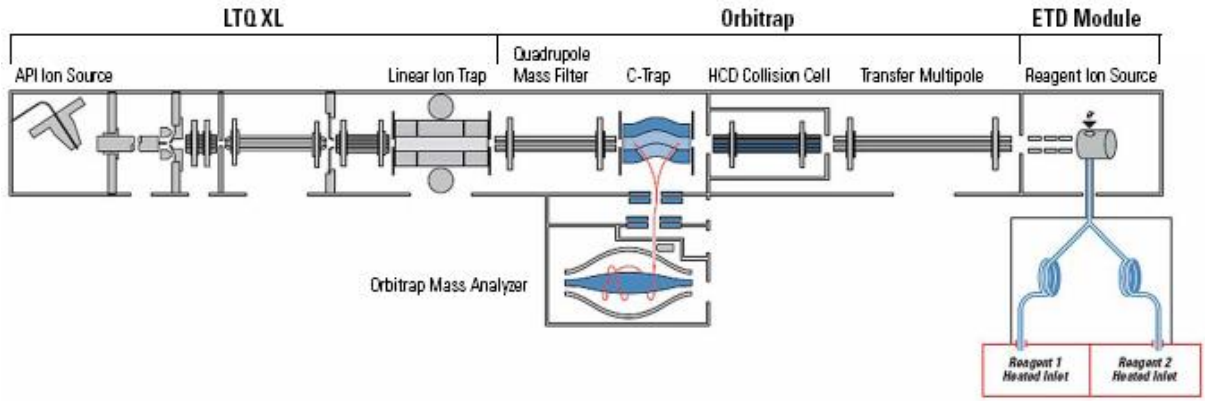

Figure 1.3 A schematic of an Orbitrap Velos mass spectrometer used in this work. (Thermo Scientfic).

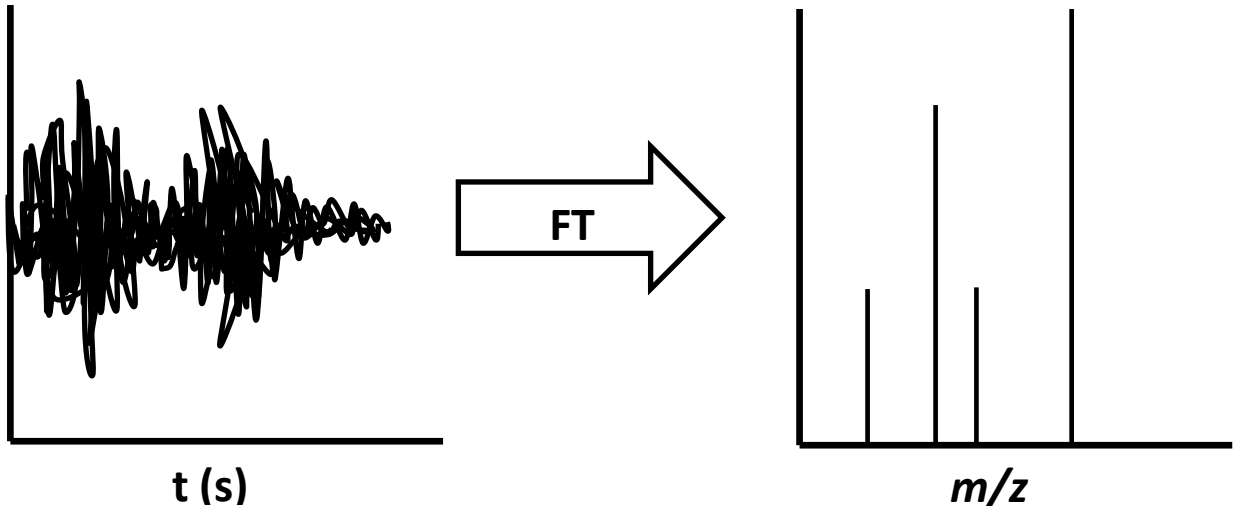

Figure 1.4. (Left) A schematic of a time domain frequency transient and (right) a mass spectrum.

1.4 Tandem Mass Spectrometry

Tandem mass spectrometry (MS/MS) is the process in which an ion is characterised according to its fragments. Following generation in an ion source (e.g. by ESI) an ion is selected in MS^1 then fragmented, then product ions are analysed in MS^2 [51]. The fragmented ions are displayed as a mass spectrum [52].

1.4.1 Collision induced dissociation

Collision induced dissociation (CID) also known as collisional activated dissociation (CAD) was first described by McLafferty [53] and Jennings [54]. CID involves the collision of the ion with non-reactive gas molecules such as helium or nitrogen [55]. Upon collision, a portion of the ion's kinetic energy is converted into internal vibrational energy. This is termed the activation/ excitation stage. The resultant bond breakage is known as the dissociation stage. CID is a slow activation method where the activation stage is longer than the dissociation stage. The slow activation stage involves multiple discrete reactions that give time for other processes to occur, including deactivation events. Competition between activation and de-activation events results in distribution of internal energy throughout the ion causing cleavage of the most labile bonds. In peptides, this tends to be the amide N–CO bond [56, 57] resulting in a series of N-terminal b and C-terminal y fragment ions [58], see **figure 1.5**. During CID the most labile bond is preferentially cleaved [59].

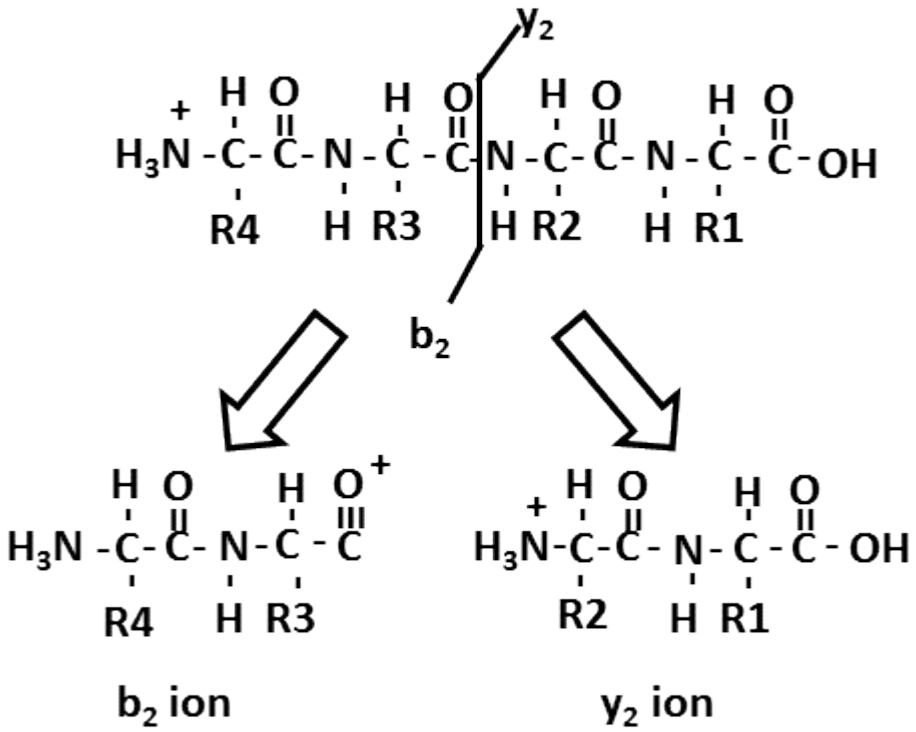

Figure 1.5. Schematic of the b and y fragment ions formed by collision induced dissociation.

1.4.2 Electron capture dissociation

Electron capture dissociation (ECD) was developed by Zubarev *et al.* in 1998 [60]. Multiply charged peptide ions are irradiated with a beam of low energy electrons (< 0.2 eV) dispensed by a cathode. The result is electron capture (e^-) by the multiply charged ion producing a radical charge-reduced species which then dissociates [39]. Peptide fragmentation occurs along the backbone N-Cα bond producing a series of informative N-terminal c and C-terminal z fragment ions. During the fragmentation process transfer of a hydrogen atom often occurs leading to the formation of additional fragments $c^{\bullet}$ and z fragment ions (**figure 1.5**) [57, 61]. In contrast to CID the most labile bond is not the favoured site of fragmentation. One advantage of this behaviour is that it results in the retention of post-translational modifications and therefore the ability to determine the site of modification [62].

The precise mechanism of the production of fragment ions by ECD is subject to much debate. Two proposed mechanisms, the Cornell mechanism [60] and the Utah-Washington mechanism [63, 64] are considered the most likely candidates. The Cornell mechanism states that following electron capture to high-*n* Rydberg state, the electron is localized to protonation site forming a hypervalent radical. Transfer of a hydrogen atom from a $–NH_3^+$ group to an amide oxygen results in the cleavage of the nearby N-Cα bond [65]. The Utah-Washington mechanism proposes that following its capture an electron is localised to the amide π* orbital increasing the amide bond's basicity. This results in proton abstraction from a proximal amino acid side site resulting in the formation of an aminoketyl radical

that undergoes dissociation by cleavage of the [64, 66]. The beam of low energy electrons used in ECD require a high vacuum therefore standard ion trap vacuum is insufficient limiting ECD to mainly FT-ICR mass analysers [16].

1.4.3 Electron transfer dissociation

Electron transfer dissociation (ETD), first described in 2004 by Syka *et al.* [67], is an ECD- like dissociation technique suitable for use in instruments with reduced vacuum specifications, such as an ion trap [68]. In this work ETD has been performed on a Thermo Scientific LTQ Orbitrap Velos. The multiply charged analyte ions are injected into the linear trap for precursor cation isolation [69]. The ETD reagent radical anions (e.g anthracene) are generated in the CI source and are transferred into the linear trap via RF-only ion guides (transfer multipoles), the gas-filled HCD collision cell, and the C-Trap. The reagent ions pass a quadrupole mass filter between C-Trap and linear trap. Like ECD the initial capture of an electron by a multiply charged ion occurs at an amide carbonyl group that is hydrogen bonded to a protonated basic amino acid side chain. The radical anion then abstracts a proton and generates an amino-ketal radical site which triggers dissociation into a series of ECD analogous c and z type fragment ions. The resulting product ions are analyzed in either the linear ion trap or when an increase in mass resolution and accuracy is required, in the orbitrap [70].

1.5 Mass spectrometry-based proteomics

In the post-genomic era DNA sequence information has been collected for entire genomes, including the human genome [71, 72]. However defining the function of each protein

encoded by the genes is more challenging. The human proteome is diverse and complex. The same protein may have several different functions, alter in disease state and undergo dynamic post-translation modifications. A conservative estimate put the total number of proteins between 60,000 and 70,000 but including post-translational modifications the number could reach 700,000 [16]. Changes in the composition of proteins may yield disease pathology information and biomarker discovery. Proteomics is the global analysis of all the proteins in a cell, tissue or organism. The analysis of complex protein-laden samples by mass spectrometry has become the method of choice [37]. The vast majority of proteomic experiments are completed using a bottom-up proteomic work flow.

1.5.1 Bottom-up proteomics

Bottom-up proteomics is the established high-throughput method used in protein identification. In a gel based approach, proteins in complex biological samples are often separated by sodium dodecyl sulphate polyacrylamide gel electrophoresis (SDS-PAGE) or 2-dimensional gel electrophoresis (2D-GE). The gel is stained with either coomassie brilliant blue [73] or silver staining [74] to locate the proteins. Bands are cut out, the gel digested with an enzyme (e.g. trypsin), producing numerous short peptides. The short peptides are separated by online reverse phased high-pressure liquid chromatography (HPLC) MS and MS/MS (CID) analysis. Removal of containments such as detergents, staining and salts by dialysis an important step in the preparation of complex biological samples such as plasma or urine for MS analysis [75]. Very complex samples such as whole cell lysates often require an extra separation step (2D LCMS/MS), strong cation exchange (SCX) chromatography, prior to online HPLC [76]. The obtained CID spectra are searched against protein databases such as MASCOT [77] and SEQUEST [78] which

contains lists of peptides generated by *in-silico* digestion of known proteins. A probability score, based on sequence coverage obtained and mass accuracy is given for each peptide/protein identified to assess the likelihood of its presence in the sample. An alternative non-gel based approach involves the digestion of a mixture of proteins in a solution. This is often coupled with peptide labelling techniques such as isotope-coded affinity tag (ICAT) [79] or stable isotope labelling by amino acids in cell culture (SILAC) [80] to study protein expression [81].

1.5.2 Top-down proteomics

Top-down proteomics is the measurement of the molecular weight of intact protein ions and direct fragmentation of gas-phase protein ions [82]. Top-down proteomics is often performed with ESI which produces intact multiply charged gas-phase ions coupled with high-resolution mass spectrometers. The high mass accuracy is vital for the accurate assignment of large multiply charged intact protein ions [46]. Top-down proteomics usually involves the isolation of a single protein or small number of proteins from a protein rich complex sample. The protein sample is then either further separated by online reverse phase HPLC or directly infused into the mass spectrometer [83]. Top-down methodology [84, 85] removes the need for lengthy proteolysis and addresses the problems of 'information loss' inherent in bottom-up approaches [86]. There is no loss of regions of the protein due to poor ionisation or confusion due to the presence of isomeric peptides.

The potential of top-down proteomics was first demonstrated by Loo *et al.* [87] in 1990 where intact multiply charged bovine ribonuclease A (14 kDa) was fragmented by CID resulting in a series of sequence specific product ions. The same group demonstrated top-down MS with a significantly larger intact protein serum albumin (66 kDa) from a variety

of species including bovine and human. However, sequence assignment is restricted to the first 30 amino acid residues of the N-terminus and first 10 of the C-terminus due to the limited *m/z* range and sensitivity of the mass analyser used [88]. Top-down proteomics results in the generation of complex spectra that requires lengthy manual interpretation.

Extensive work led by Kelleher *et al.* since 1996 [89] focuses on the development of a suitable database capable of identifying intact proteins by matching MS/MS against sequence databases to aid with spectra interpretation. MS/MS spectra of intact bovine ubiquitin (8.6 kDa), human muscle creatine kinase (43 kDa), bovine carbonic anhydrase B (29 kDa) and chicken cyctochrome C (12 kDa) where trialled in the study. Results showed identification of proteins from intact MS/MS data was possible. It also showed the importance of high resolution (high mass accuracy) Fourier transform mass spectrometry (FTMS) data for such identifications. The study demonstrated the effectiveness of the web-based ProSight PTM software for the automatic identification of single proteins and protein mixtures including those with post translational modifications [90, 91] from top-down MS and MS/MS spectra. Currently ProSight PTM is viewed as the most effective software available for the analysis of top-down data [92].

1.6 Haemoglobin and its variants

Adult haemoglobin (HbA) exists as a tetramer of non-covalently bound globin chains, consisting of two α- and two β- subunits each containing a single oxygen binding heme B complex with an iron atom at its core **(Figure 1.6)**. HbA has a total molecular weight of 68 000 Da. Foetal haemoglobin (HbF), with its increased oxygen affinity, is composed of two α and two γ subunits (α2γ2). The gamma subunits are homologous to the β chain, differing by 39 amino acids. Foetal haemoglobin is usually present in the blood until six months

after birth. The γ subunits comprise of one $^{A}\gamma$ and one $^{G}\gamma$ which corresponds to the amino acid at position 136 in the globin chains ($^{A}\gamma$ an alanine and $^{G}\gamma$ a glycine) [93].

Abnormalities of haemoglobin, haemoglobinopathies, are the most common single gene recessive disorder with approximately 269 million carriers worldwide [94]. Haemoglobinoapthies are classified into two major types; Thalassemias which are characterised by a reduction in the synthesis of the globin chains and structural haemoglobin variants which are caused by point mutations in the globin gene typically leading to a single amino acid substitution in the globin chain. There are over 1000 Hb variants [95] classified and in the majority of cases occur on the β chain are clinically silent. The most well-known structural Hb variant is the sickle variant, HbS [96].

In the 1950s Ingram was the first to demonstrate that HbA differed from HbS by just a single amino acid substitution, a glutamic acid for a valine [97] (Δm -29.9745 Da) which is a consequence of a single substitution (GTG for GAG) on the sixth codon of the β globin chain. The heterozygous inheritance of the sickle variant (HbAS), sickle trait/ carrier results in mild complications. The phenotypic consequences of inheriting HbS variant in homozygous form is sickle cell disease (SCD) with all the serious clinical complications associated with the disease [98]. Sickle cell disease affects the oxygen-carrying capacity of red blood cells. Patients with sickle cell disease experience reduced life spans [99] and 15% of young children with sickle cell disease die due to acute infections and other sickle-related complications. The rapid detection of sickle cell disease dramatically reduces mortality rates [100]. Clinical complications include vaso-occlusion, caused by the characteristic sickle-shaped red blood cells obstructing blood vessels leading to ischemic damage. An increase in the risk of infections especially in infants is caused by infarction of the spleen and the subsequent decrease in splenic function, is also observed [101]. There is

no cure for SCD. Some studies suggest that penicillin prophylaxis reduces the rate of infections and mortality rate in infants from infection related complications [102, 103].

Another sickling disorder, sickle cell haemoglobin C (HbSC) disease is caused by the inheritance of HbS from one parent and HbC (substitution of a glutamic acid to lysine, also at position 6 on the β chain Δm = -0.9476 Da) from another. The phenotype for the HbSC variant is variable, it is generally expressed as a milder form of sickle cell anaemia requiring medical intervention and careful monitoring although in some cases it can be equally/more severe than HbSS [104-106]. Patients with SCD experience reduced life-spans, typically mid 40s [107]. Rapid diagnosis during newborn blood screening programmes which allow for the implementation of a suitable healthcare strategy has been credited with the ability to reduce childhood mortality in SCD and SCD-related disorders [108, 109]. Haemoglobin C disorder requires both abnormal genes, HbCC (homozygote), whereas trait, HbAC (heterozygote), is asymptomatic. Symptoms of the disease state include mild/ moderate anaemia and haemolysis [110].

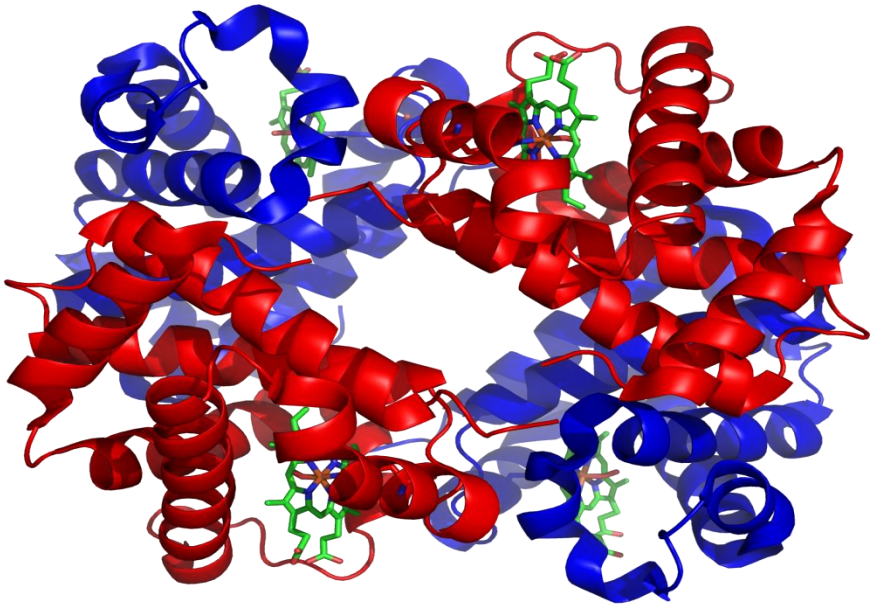

Figure 1.6. The structure of haemoglobin. The red ribbons represent the α- globin chains, blue ribbons represent β- globin chains and the green represent the heme groups. Image courtesy of PDB and PDB ENZYME.

The haemoglobin D variant is a caused by a mutation on the β chain at position 121 (glutamic acid for a glutamine), also resulting in a mass shift of less than -1Da (Δm = 0.9840 Da). Haemoglobin D (HbAD) trait (heterozygote) again causes no clinical manifestations but if co-inherited with sickle (HbSD) causes considerable sickle-like health problems. In its homozygous state HbD causes haemoglobin D disease which manifests as mild to moderate anaemia [111, 112].

HbE is another common variant occurring on the β chain position 26, a glutamic acid substituted for a lysine, resulting in a mass shift of Δm 0. 9476 Da. HbE inherited in homozygous or heterozygous form is asymptomatic, however inherited in combination with β thalassemia (HbE/β thalassemia) can result in severe anaemia [113]. Hb variants with significant clinical outcomes, such as homozygous sickle cell disease, have a prevalence rate of 1 in 2000 births [114]'[115]. Over a two year screening period 17,000 carriers (heterozygous for Hb variants) were identified from almost 1.2 million infants [115].

1.7 Newborn screening

Annually the UK newborn screening programme screens ~700 000 neonates for five genetic disorders; PKU, congenital hypothyroidism (CHT), cystic fibrosis (CF), medium chain acyl-CoA dehydrogenase deficiency (MCADD) and sickle cell disease (SCD)[116]. SCD has the highest prevalence of all the disorders screened for by the NHS in England with a rate of 1 in 2000 [117]. The term SCD refers to a set of disorders characterized by the inheritance of the structural variant haemoglobin S (HbS). SCD also includes

compound heterozygotes disorders whereby one HbS variant has been co-inherited with another haemoglobinopathy for example HbC, HbE or HbD Punjab/ Los Angeles [118]. Clinical significance of these compound heterozygote variants differ. For example HbSE syndrome is uncommon and the vast majority of patients experience no sickle-like symptoms. Rarely symptoms may develop requiring medical assistance [119]. The compound heterozygotes HbSD- Punjab/ Los Angeles and the rare HbSO-Arab (β121 Glu→Lys Δm -0.9476 Da) phenotypes are severe with a similar pathology to HbSS [120]. Neonatal screening for the sickle variant allows for early detection, appropriate genetic counselling and treatment to reduce deaths from sickle related complications [121, 122]. As well as screening for the sickle variant the NHS newborn screening programme requires that methods used in the screening process must be able to reliably detect the following clinically significant structural haemoglobin variants: HbC, HbD Punjab/ Los Angeles, HbE and HbO-Arab [123]. Inheritance of these variants (without HbS) in either heterozygous or homozygous state is usually clinically benign.

The current screening protocol for haemoglobinopathies uses blood samples collected by midwives via heel prick onto standard NHS Guthrie (dried blood spot) cards from neonates between 5-8 days old. The initial labour intensive stage in the screening process involves manually punching out small discs (approx. 3 mm in diameter) from the dried blood card and eluting the sample for around 30 mins [124]. The samples are usually analysed by cation exchange high-performance liquid chromatography (ceHPLC) and/or isoelectric focusing (IEF) [125]. IEF results are interpreted by comparison with known standards. Samples that merge or are insufficiently focused require repeating [126] and IEF is unable to separate some Hb variants [127]. ceHPLC detects Hb variants by comparing the characteristic retention time of HbA to any deviations from the retention time,

problematically some variants co-elute [128]. Separation of Hb variants has also recently been reported using a technique called capillary electrophoresis (CEP) [129, 130]. These methods involve lengthy sample preparation and identification of an Hb variant these methods are presumptive. Conclusive diagnosis of an Hb variant can only be determined by second line testing with DNA analysis (sequencing) or amino acid analysis (mass spectrometry) [131].

1.8 Mass spectrometry and haemoglobin variant analysis

Tandem mass spectrometry (MS/MS) is now the standard method for PKU and MCADD screening in the newborn dried blood spot screening programmes [132]. Logically also using this technique as first line test to screen for haemoglobinopathies without the need to perform any further confirmatory analysis would reduce work flow in newborn screening laboratories. MS/MS is able to diagnose Hb structural variants accurately measuring the monoistopic mass of intact globin, digested or fragmented peptide chains

Analysis of Hb and variant globin chains by mass spectrometry was first described in 1981 by Wada *et al*. [133] using field desorption ionisation. Whole blood samples were purified by chromatography and the heme groups removed by addition of acetone. The globin chains were separated by further chromatography and a trypsin digest was performed to yield a series of sequence informative shorter peptide chains. Detection of Hb variants with large mass shifts on both the α-globin (Hb Boston α58 His→Tyr, Δm + 26.0044 Da) and the β-globin (HbS and Hb Genova (β28 Leu → Pro, Δm -16.1066 Da) was demostrated.

In the early 1990s, Witkowska and co-workers [134, 135] applied a combination of electrospray ionisation (ESI), liquid secondary ion mass spectrometry (LSIMS) [136] ionisation and tandem mass spectrometry (MS/MS) to the analysis of haemoglobin variants in whole blood samples. Sample preparation was a lengthy process, it involved the lysis of red blood cells combined with two separate chromatography steps and aminoethylation of cysteine residues and an overnight trypsin digestion. ESI of the intact globin chains enabled preliminary detection of the Hb variants. Data were collected by use of a low resolution quadrupole mass spectrometer. The results suggested that variants separated by greater than 14 Da could be diagnosed from examination of the intact globin molecule. For mass shifts < 14 Da, and to determine the site of the substitution, HPLC fractionation followed by LSIMS analysis of the tryptic peptides by CID was performed [53, 54].

Wild et al. [137] described a two-stage protocol for identifying Hb variants using electrospray ionization mass spectrometry. The procedure used a 1 in 50 fold dilution of whole blood which was then de-salted. In the first step, the intact globin chains are analysed and the variant containing globin chain was identified by a difference in the expected molecular weight. These researchers suggested that the minimum variant mass shift that could be observed in this step was ~6 Da. In the second step, the diluted whole blood sample was subjected to a 12-15 hr tryptic digestion. The resulting peptides were analysed by ESI-MS to identify the variant-containing peptide, which was subsequently analysed by MS/MS to identify the precise location of amino acid substitution.

In 2001, Rai et al. applied a similar approach [138]. Seventy blood samples from patients exhibiting unexplained erythrocytosis, but which had behaved normally in IEF and HPLC analyses, were analysed using mass spectrometry of the intact globins, followed by

MS/MS of the tryptic peptides where indicated. Three samples were diagnosed as Hb variants. In two cases, Hb Olympia (β20 Val→Met, Δm +31.9721 Da) was identified. The third variant was identified as Hb Coimbra/Ingelheim (β99 Asp→Glu, Δm +14.0157 Da). The study was successful in demonstrating the advantages of mass spectrometry over the standard screening methods, HPLC and IEF. In 2003, Rai et al. showed that provided the variant was present in abundance >10%, variants of mass shifts between 1 and 4 Da could be detected by use of quadrupole instrumentation [139].

The approaches described above, however, are not suitable for large-scale population screening. In 2005, Daniel *et al.* [140] proposed a high-throughput MS/MS approach based on multiple reaction monitoring (MRM) and pseudo-MRM. In screening programmes, it is not necessary to identify all haemoglobin variants but simply those which are clinically significant. Those defined variants display characteristic tryptic peptides: For example, to confirm the HbS variant, it is sufficient to identify and sequence by MS/MS the [1-8] tryptic peptide which contains the Glu→Val substitution at position 6. The nature of the variant (homozygous or heterozygous) can be determined by concomitant analysis of the wild-type tryptic peptide. Daniel and co-workers [140] analysed 200 whole blood samples on a triple quadrupole mass spectrometer. The peptides of interest were sequentially isolated in the first quadrupole (MS1), subjected to collision induced dissociation (CID) MS/MS in the second quadrupole and the fragment ions detected in the third quadrupole (MS2). A series of pre-determined product and parent ion scans ((pseudo)MRM transitions) allow for the rapid identification of abnormal haemoglobins. Sample preparation time was ~30 mins but the total mass spectrometry acquisition time was 60 s.

Boemer *et al.* [141] applied the MRM approach to the detection of HbS, HbC, HbE and β-thalassemia in dried blood spot eluates and compared the results with those obtained from

isoelectric focusing. No discrepancies between the two techniques were observed in over 2000 samples thus demonstrating the reliability of the mass spectrometry-based approach. The approach was subsequently adopted by the neonatal screening programme of the French Community of Belgium [142]. Scherl and co-workers [143] have recently developed an MRM-based approach for the analysis of intact globin chains from HbS and HbC variants. The method utilises electron transfer dissociation (ETD) [67] for fragment ion generation. The advantage of this approach is that it negates the requirement for trypsin digestion of the sample.

Therefore an ideal technique for accurate identification of Hb variants would comprise of high resolution data with minimal sample preparation. The work presented here fulfils both these criteria coupling high resolution top-down mass spectrometry with liquid extraction surface analysis (LESA) of DBS to eliminate the need for any sample preparation.

1.9 Aims and objectives

Then initial aim of this work was to determine if direct surface sampling (LESA) of dried blood spots (DBS) coupled with high resolution mass spectrometry could be used and subsequently optimised for the extraction/analysis of normal adult haemoglobin (see chapter 3). The technique's suitability would then be investigated as an alternative to the current Hb variant screening protocol (ce-HPLC and/or IEF) for diagnosis of common structural Hb variants including HbS and HbD using clinical neonatal DBS samples (see chapter 4).

After establishing that the direct surface sampling technique was suitable for the diagnosis of common Hb variants in neonates the robustness of the techniques was probed by attempting to diagnose six unknown Hb variants. The current Hb screening protocol

employed in a clinincal laboratory showed the presence of a variant was suspected in the six samples but a diagnosis could not be made (see chapter 5). A subsequent aim of the project was to investigate an appropriate method for the analysis of the complex MS/MS spectra generated from top-down analysis of the globin chains. Manual analysis of mass spectra was compared with analysis completed with the freely available ProSight PTM data analysis software (see chapter 5).

Chapter 6 aims to investigate the suitability of LESA of dried blood as a technique to probe Hb non-covalent interactions.

Chapter 2: Materials and Methods

2.1 Materials

2.1.1 General Reagents

HPLC grade water (J. T. Baker, Deventer, The Netherlands)

Methanol (J. T. Baker, Deventer, The Netherlands)

Formic acid (Sigma-Aldrich Company Ltd., Dorset, UK)

Ammonium acetate (Fisher Scientific, Loughborough, UK.)

Drabkin's reagent (Sigma-Aldrich Company Ltd., Dorset, UK)

Haemoglobin standard (200 g/L) for spectrophotometry based quantitative assay (Stanbio Laboratory, Boerne, Texas, USA)

30 % (w/v) Brij 35 Solution (Sigma-Aldrich Company Ltd., Dorset, UK)

Human haemoglobin lyophilized powder (Sigma-Aldrich Company Ltd., Dorset, UK)

m-nitrobenzyl alcohol (received from Dr Malgorzata Kaczorowska)

2.1.2 Adult dried blood spots

Blood samples were taken from volunteers by either finger prick or by venipuncture carried out by a trained phlebotomist using syringes or BD vacutainer system® (BD, Oxford, UK) without the presence of an anticoagulant. The blood was either directly dispensed from finger prick or 20 µl of blood pipetted (Gilson Scientific Ltd, Bedfordshire,

UK) from the sample collected by venepuncture onto the standard NHS blood spot (Guthrie) cards, Ahlstrom grade 226 filter paper (ID Biological Systems, Greenville, South Carolina, USA).

2.1.3 Neonatal dried blood spots

Blood was collected by midwives from neonates 5-8 days after birth via heel prick onto standard NHS blood spot cards (ID Biological Systems). Anonoymized dried blood spots (DBS) were supplied by Birmingham Children's Hospital in accordance with the Code of Practice for the Retention and Storage of Residual spots [144] All samples have previously undergone analysis by the standard NHS screening protocols using cation exchange liquid chromatography and isoelectric focusing. The dried blood spots were stored at -20 ºC with 1 g desiccant packets (Whatman International Ltd, Kent, UK).

2.2 Methods

2.2.1 Surface Sampling

Dried blood spots were placed onto the Advion LESA (Liquid Extraction Surface Analysis) universal plate adapter (Advion, Ithaca, NY, USA) and an image of the DBS was acquired using an Epson Perfection V300 photo scanner. Using the LESA Points software (Advion), the precise location of the DBS to be samples was selected using the scanned image. The universal plate adapter was placed into the Triversa Nanomate chip-based electrospray device (Advion) shown in **figure 2.1a**.

Sample analysis was performed using the LESA feature of the Triversa Nanomate ChipSoft Manager software. This platform was used to set the parameters for the surface

sampling routine based on robotic arm movements (X,Y,Z) of the nanomate probe. The method described here was optimised in chapter 3. The routine begins with the Nanomate probe collecting a conductive tip, which is used for sample recovery and delivery, from the tip rack. The tip then moved to a solvent well containing the electrospray/extraction solution and collects 7 µl of the solution (**figure 2.1b**). The robotic arm relocates to a predetermined position above the surface of the DBS and the tip is lowered towards the surface of the DBS leaving a gap between the sample surface and the tip. Six µl of the electrospray solution is dispensed onto the DBS forming the sample surface to tip liquid microjuction (LMJ) (**figure 2.2a**). The LMJ is maintained for 5 seconds and then 5 µl is reaspirated (**figure 2.2b**) and introduced via nanoelectrospray into the mass spectrometer.

The advance user interface (AUI) of the ChipSoft software (Advion) was used instead of LESA for the direct surface sampling in some cases, for example when following surface sampling the sample was collected instead of immediately electrosprayed into the mass spectrometer. The sampling parameters remain the same but the DBS was mounted onto a 96 well microtiter plate (Thermo Scientific, Leicestershire, UK) instead of the universal plate adapter and the ESI solvent is picked up from a well on the microtiter plate opposed to the separate solvent well. Also sampling location could not be determined using a combination of the LESA points software and a scanner, so sampling location was determined by a more rudimentary method of employing a 'dry' test run where a location co-ordinate (estimated by eye) would be inputted into the AUI and the surface sampling routine would be executed (without any solvent or picking up the sample) to ensure an accurate location co-ordinate had been established before sampling could occur.

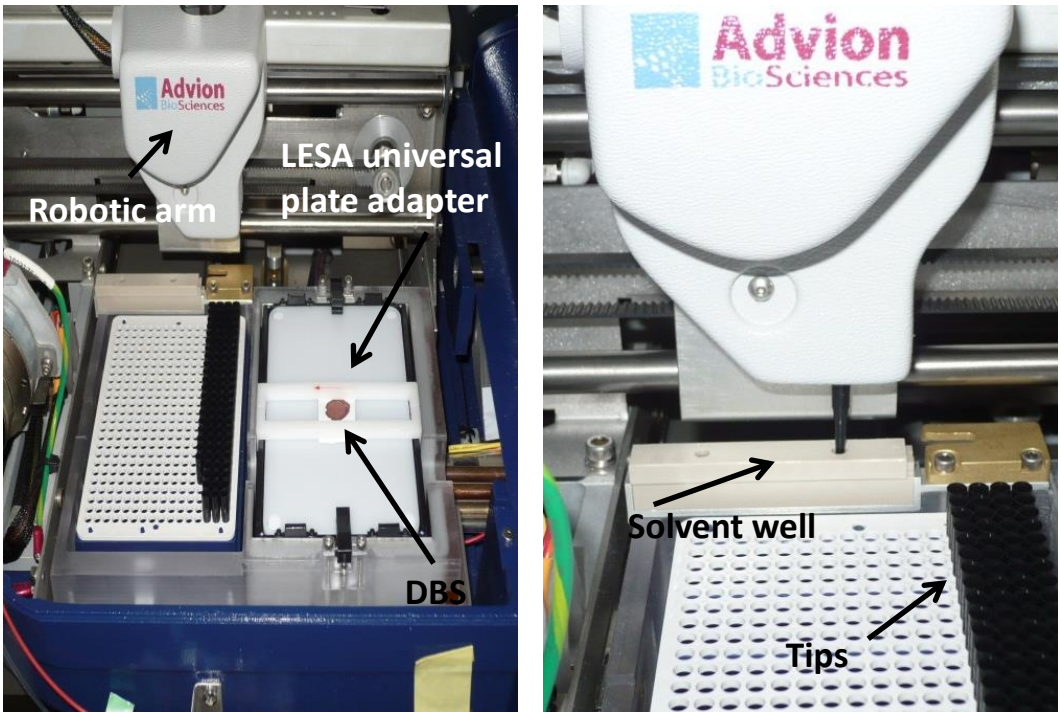

Figure 2.1. (Left) LESA apparatus and (right) aspiration of ESI solvent from the solvent well.

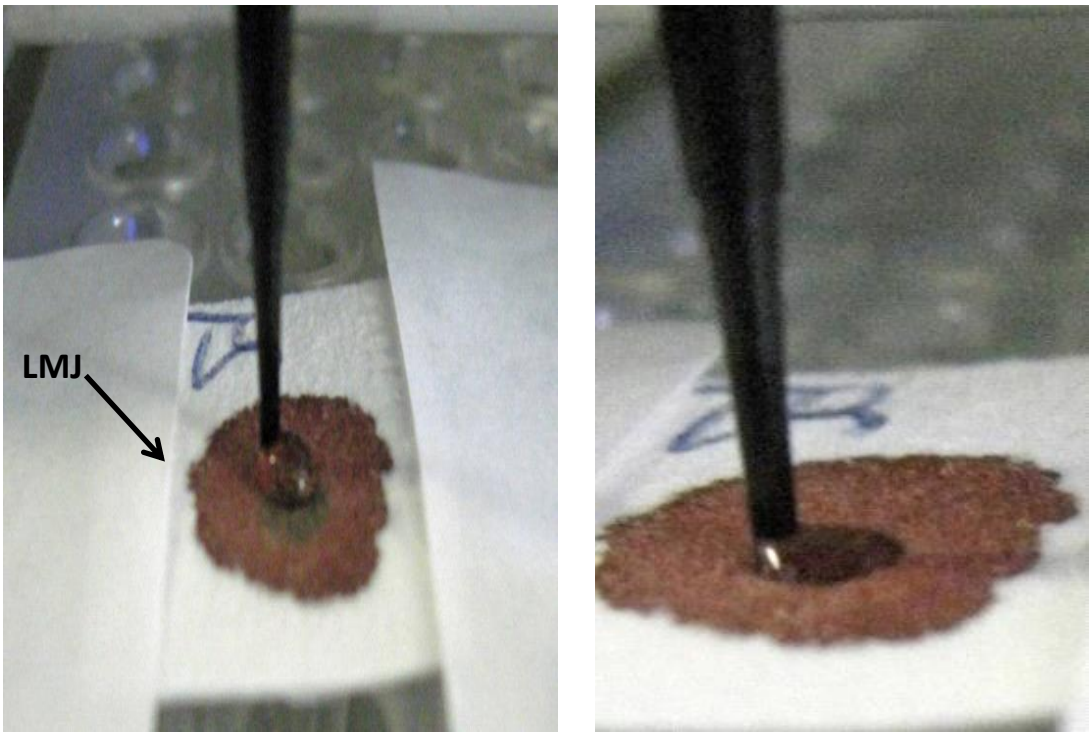

Figure 2.2 (Left) The formation of a liquid microjuction and (right) the reaspiration of the solvent.

2.2.2 Mass Spectrometry

All samples were analysed using the ThermoFisher Scientific Orbitrap Velos ETD (ThermoFisher Scientific, Bremen, Germany). Samples were introduced at a flow rate of ~ 80 nl/min with as gas pressure of 0.5 psi, a tip voltage of 1.75 kV and a capillary temperature of 250 ºC. MS data collected in full MS mode (*m/z* 600-2000) and in selected ion monitoring (SIM) mode *(m/z* 1055-1090) at a resolution of 100,000 at *m/z* 400. Each scan comprises 30 co-added microscans. Automatic gain control (AGC) target was 1×10^6 with a maximum fill time of 2 seconds. Collision induced dissociation (CID) was performed in the ion trap and the fragment ions detected in the orbitrap with a resolution of 100,000 at *m/z* 400. The isolation window was 8-10 Th and the AGC target for CID was 1×10^6 with a maximum fill time of 2 seconds. CID experiments were performed with helium gas at a normalized collision energy of 30 %. Each CID scan comprises 30 co-added microscans. Electron transfer dissociation (ETD) was performed in the ion trap and the fragments detected in the orbitrap with a resolution of 100,000 at *m/z* 400. The isolation width was 10 Th. The AGC target for ETD was 1×10^6 with a maximum fill time of 2 seconds. The reagent ion (fluroranthene ion) AGC target was 1×10^5 with a maximum fill time of 1 second. ETD activation time was 20 ms. Each ETD scan comprises 30 co-added microscans.

2.3 Data Analysis

2.3.1 Mass spectral analysis

The acquired spectra were analysed using Xcalibur 2.10 software (ThermoFisher Scientific). For the SIM mode mass spectra the Xtract program (44 % fit factor, 25 %

reminder, signal/noise threshold 2:1) was used to calculate the singly charge deconvoluted monoisotopic masses and their relative intensities (Arbitray units, AU). The program calculates the monoisotopic masses as the sum of all charge weighted isotope pattern contributions. See equation 7 below.

$$\text{IntNorm } A_n = \sum \text{Int } A_n^{m+} / m$$

Equation 7

Where An are the isotopes A0 (monoisotopic), A1, A2….An, m is the charge of the ion IntNorm is the normalized intensity, and n is the ion (A0 = M, A1 = M+1, An = M+n).

The deconvoluted singly charged monoisotopic masses are calculated as the sum of all contributing isotope intensities see equation 8.

$$\text{IntNorm}_{\text{monoiso}} = \sum \text{IntNorm } A_n$$

Equation 8

2.3.2 Manual MS/MS Fragment Assignment

For manually assigned MS/MS spectra experimentally measured singly and multiply charged CID or ETD m/z values were compared with the theoretical m/z values (fragment tolerance Δ 10 ppm) that were calculated in Protein Prospector (http://prospector.uscf.edu/prospector/mshome.htm). Fragment ion maps were then generated manually, displaying globin chain sequence coverage.

2.3.3 Automated MS/MS Fragment Assignment

For automated analysis the MS/MS spectra were first deconvoluted using the Xtract program as described in section 2.3.1. The generated list of singly charged CID/ETD fragment ions was then copied and pasted into an excel spreadsheet. Using the web based program ProsightPTM [145] in single protein mode the fragment ion list was the pasted into ProsightPTM from excel. The amino acid sequence of the globin chains and the intact mass of the globin chain (determined from Xtracted SIM spectrum) was also inputted into the program. A list of observed fragment ions (fragment tolerance Δ 10 ppm) along with an fragment ion map are automatically generated.

2.4. Quantitative analysis of whole blood

2.4.1 Preparation of reagents

In order to determine the concentration of Hb in whole blood samples, internationally recommended cyanmethemoglobin technique was used [146]. The method employs the use of Drabkin's reagent [147] (Sigma-Aldrich Company Ltd) which contains sodium bicarbonate, potassium ferricyanide and potassium cyanide. A single vial of the dry Drabkin's reagent is reconstituted with 1 L of water with the addition of 0.5 ml of the surfactant 30 % Brij 35 Solution **(**Polyoxyethylene (23) lauryl ether) (Sigma-Aldrich Company Ltd) which reduces any turbidity caused by the addition of erythrocytes. The reconstituted Drabkin's reagent is stable at room temperature for approximately six months

when stored in an amber glass bottle and sheltered from light. Drabkin's reagent oxidizes all forms of haemoglobin excluding sulfhemoglobin to methemoglobin in the presence of alkaline potassium cyanide. The methemoglobin reacts with the potassium cyanide to form cyanmethemoglobin which has peak absorption at 540 nm. The absorption intensity measured is proportional to the total haemoglobin concentration.

2.4.2 Calibration Curve

The cyanmethemoglobin standard haemoglobin solution 200 g/L (Stanbio Laboratory) was subsequently diluted with reconstituted Drabkin's reagent to create a series of five working standards with Hb concentrations of 0, 5, 100, 150 and 200 g/L. Each of these solutions (n=3) were pipetted into plastic semi-micro cuvettes (10 x 4 x 45 mm) (Sarstedt AG & Co., Numbrecht, Germany) with an optical path of 10 mm. Using a Camspec M501 single beam scanning UV/visible spectrometer (Spectronic Camspec Ltd, Leeds, UK) the absorbance (ABS) of solutions were measured at wavelength 540 nm with the spectrophotometer blanked against cuvette containing Drabkin's reagent between each absorbance reading. Results were plotted on a graph in excel where the linear relationship between Hb concentration and absorbance, the coefficient of determination (R^2) is calculated. The equation for the plotted line was determined.

The relationship between absorbance and the concentration of a solution can be described in the Beer-Lambert law see equation 9.

$$A = \varepsilon bc$$

Equation 9

(Where absorbance = ABS, molar absorptivity (coefficient) = ε , path length in cm (b) and molar concentration = c)

2.4.3 Determination of whole blood Hb concentration

Adult whole blood samples from a number of healthy donors taken by venipuncture carried out by a trained phlebotomist using syringes or BD vacutainer system® (BD, Oxford, UK) in the presence of the anticoagulants EDTA or lithium heparin. A 1 in 251 fold dilution of the whole blood sample with Drabkin's reagent was prepared (5 µl of whole blood per 1250 of Drabkin's reagent) and left to stand for 10 mins to ensure conversion of haemoglobin to cyanmethemoglobin. The solutions were transferred into semi-micro cuvettes (Sarstedt AG & Co) and absorbance at 540 nM were recorded. The equation of the line on the standard curve was used to calculate the whole blood haemoglobin concentration. Normal adult whole blood haemoglobin concentration ranges from 135-175 g/L for males and 115 – 155 g/L for females [148].

2.4.4 Determination of Hb contraction following LESA of DBS

Adult DBS underwent direct surface sampling in accordance with the sampling routine described in section 2.2.1.The AUI was used to sample the DBS instead of the LESA settings. The 5 µl of extracted material sampled from the DBS was not directly infused into the mass spectrometer but was deposited into an empty well of the microtiter plate then transferred into a eppendorf to prevent sample evaporation. Each DBS spot was sampled three times at discrete locations and pooled to give a total extraction volume of 15 µl. This solution was then added to 1250 µl of Drabkin's reagent, left to react for 10 mins

and absorbance at 540 nm was recorded. The Hb concentration of the sample was determined as section 2.4.3.

Chapter 3: Development of a Method for the Direct Surface Sampling of Dried Blood Spots Couple with Mass Spectrometry for the Analysis of Haemoglobin

3.1 Overview

The aim of the work presented in this chapter was optimisation of direct surface sampling using liquid extraction surface analysis (LESA) of adult dried blood spots (DBS) for haemoglobin (Hb) analysis. The principal aim of the method optimisation was to maximise the abundance of the β globin chain in the resultant mass spectra. Abnormalities of the β globin chain are more prevalent and are highly clinically significant. They are responsible for sickle cell disease (SCD) as well as other important Hb disorders. This becomes challenging when analysing neonatal dried blood spots due to the presence of foetal haemoglobin (HbF) in the samples resulting in the reduction of HbA (normal adult Hb, i.e, two α- and two β globin chains) in the sample to about 25 %. Optimisation of surface sampling was completed by investigating the following parameters; electrospray solvent composition, sampling time delay, sample dispense tip height and sampling reproducibility of the DBS cards.

The next stage of method development focused on the optimisation of the tandem mass spectrometry (MS/MS) experimental parameters. The aim was to maximise sequence coverage to aid in the identification of common Hb variants and diagnosis of unknown Hb variants from DBS samples. The parameters investigated were as follows; precursor ion charge state, collision induced dissociation (CID) energy and electron transfer dissociation (ETD) activation time.

3.2 Surface sampling optimisation

3.2.1 Formic acid concentration of the electrospray solvent

Four electrospray/ extraction solutions were prepared with equal parts methanol and water and varying formic acid composition *(v/v)* as follows: 49.5:49.5 methanol: water, with 1 % formic acid, 49:49 methanol: water with 2 % formic acid, 48.5:48.5 methanol: water with 3 % formic acid and 47.5:47.5 methanol: water with 5 % formic acid. For each of the four ESI solutions, three DBS (containing 20 µL of whole blood) were each sampled at three discrete locations (n=9). The (deconvoluted) β-chain abundance was calculated for each spectrum using the Xtract program as described in section 2.3.1. The overall average β intensity across all the technical replicates for the same donor one calculated for each of the ESI solutions is shown in **figure 3.1.** The data suggest that changing the overall formic acid composition of the ESI solution from 1 to 3 % has little to no effect on extracted β chain intensities observed. An ESI solution of 5 % appears to improve the observed extracted intensities, however spray stability was reduced. A one-way ANOVA statistical test was performed using the Microsoft office excel program. The null hypothesis is that there is no difference in average observed β- globin chain intensity with the differing % formic acid used in the ESI solution (the alpha value, for rejection of null hypothesis was set at 0.05). Following one-way ANOVA (table shown in **Appendix 1**) no significant difference [$F(3,32) = 1.46$, $p = 0.24$] in observed β- globin chain intensity when % formic acid in ESI solution increases. Empirical observations on neonatal samples, where β chain abundance is lower revealed that 3 % formic acid was optimum and this was used throughout the work published in this thesis.

3.2.2 methanol composition of electrospray solution

Five ESI solutions were prepared with the following solvent compositions, each with 3 % formic acid (v/v); 10:87 methanol: water, 30:67 methanol: water, 48.5:48.5 methanol: water, 70: 27 methanol: water and 90: 7 methanol: water. The overall average β chain intensity across all the technical replicates from a single donor was calculated for each of the ESI solvents with increasing % of methanol compositions ranging from 10 to 70 %. 90 % methanol solution was also trailed but LMJ repeatedly failed to form. **Figure 3.2** shows the average β chain abundance for each of the solvent compositions. The data show an ESI solution with a methanol content ranging between 10 and 50 % results in similar β-chain abundances. There is a reduction in the average β chain abundance with a solution comprised of 70 % methanol. A one-way ANOVA statistical test was performed using the Microsoft office excel program. The null hypothesis is that there is no difference in average observed β- globin chain intensity with the differing % methanol used in the ESI solution (the alpha value, for rejection of null hypothesis was set at 0.05). The results one-way ANOVA (results shown in **Appendix 2**) [$F(3,32) = 1.14$, $p = 0.35$] no significant difference in observed β- globin chain intensity when % methanol in ESI solution increases. The high methanol content of the solution caused the LMJ to collapse. This finding rules out the use of a solution of 90 % methanol for direct surface sampling of DBS using LESA. Based on the data shown in **figure 3.2** the ESI solution used in all subsequent experiments is 48.5:48.5 methanol: water with 3% formic acid. A full scan mode mass spectrum of an adult DBS with these solvent conditions is shown in **figure 3.3**.

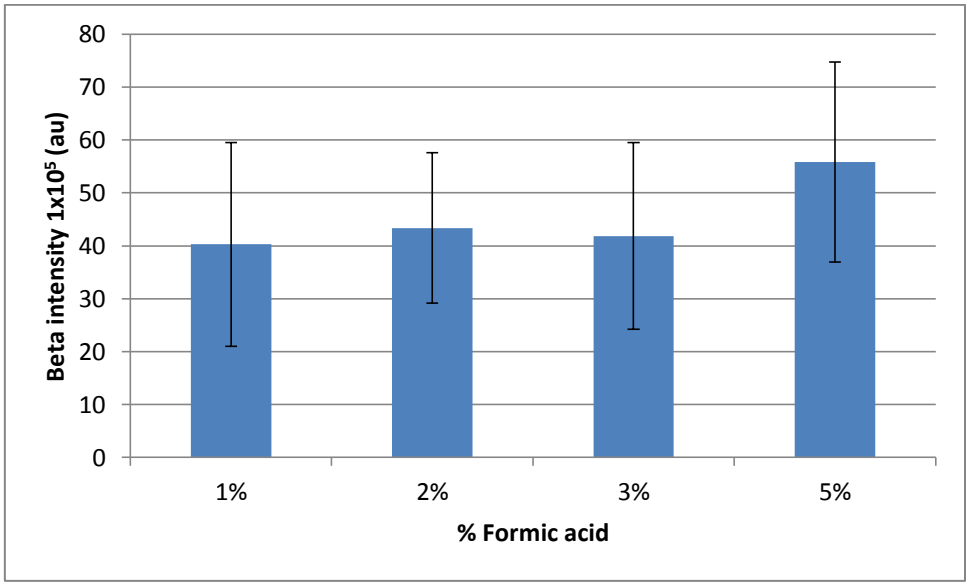

Figure 3.1 The average deconvoluted β- globin chain intensity (n=9) with ESI solution containing varying (1-5 %) formic acid composition. The error bars represent the standard deviation of the data set.

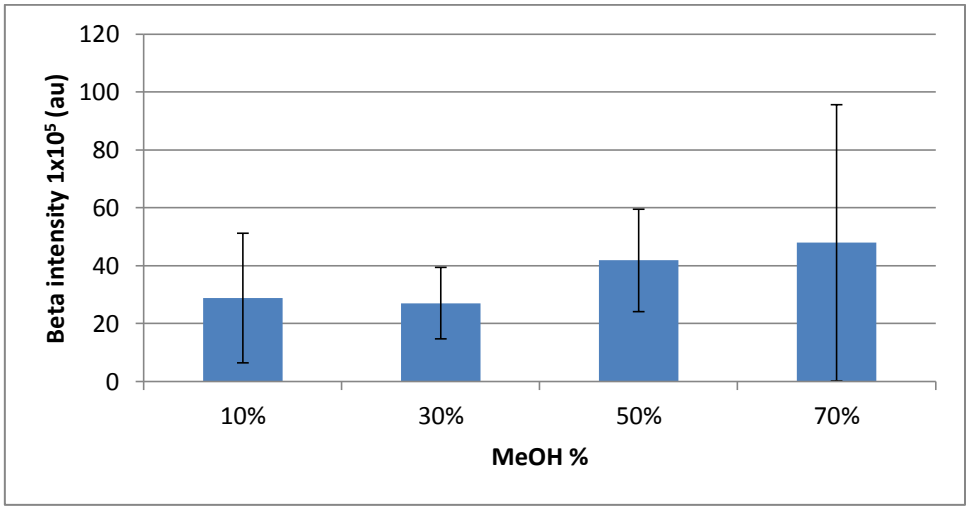

Figure 3.2 The average deconvoluted β chain intensity with ESI solution containing varying (10-70 %) methanol composition (n=9). The error bars represent the standard deviation of the data set.

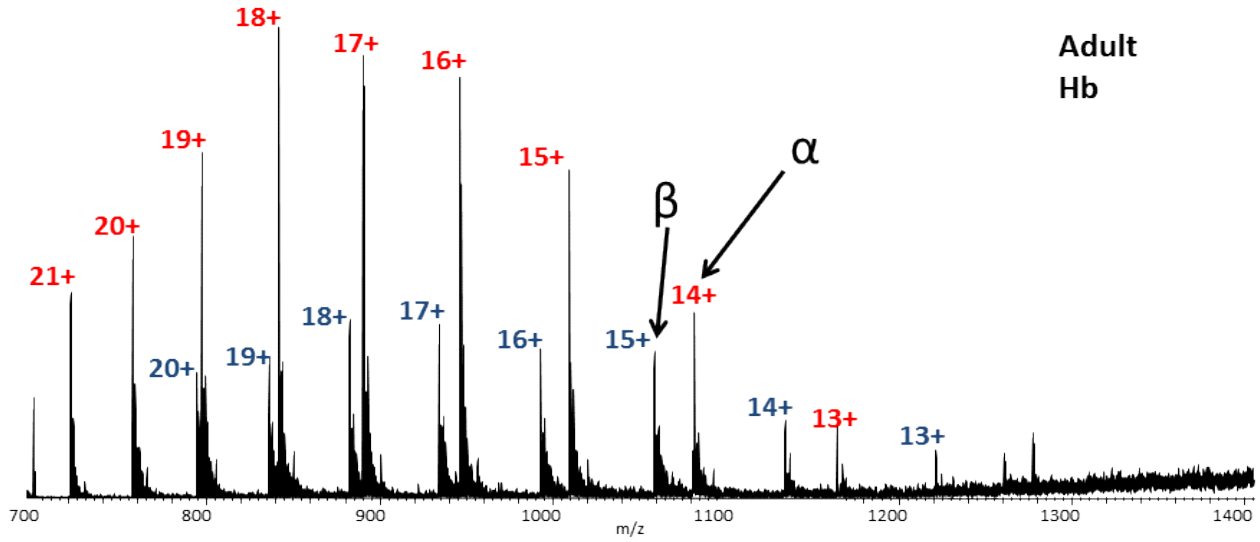

Figure 3.3 Full scan mass spectrum obtained following direct surface sampling of a normal adult DBS using an extraction/ ESI solution made up of 48.5:48.5 methanol: water with 3% formic acid. Peaks corresponding to Hb (α = red, β= blue) are observed.

3.2.2 Sampling time delay

One of the variable parameters in the liquid extraction surface analysis sampling method is termed 'post dispense time delay'. It is the time between the ESI/ extraction solvent being dispensed and re-aspirated. Essentially, it is the amount of time the liquid microjunction remains intact between sample surface and tip. The purpose of a delay is to allow for the analyte of interest to mix with the ESI-extraction solvent prior to mass spectrometry analysis. Delay times measured in this investigation were 0, 2.5, 5, 7.5 and 10 seconds respectively. MS parameters are the same as described previously with each spectrum comprising of 30 co-added microscans. Data shown comprise five scans. Dispense height (the distance between the sample surface and the tip) remained at 1.6 mm across all experiments. The data shown in **figure 3.4** suggest that a time delay of zero seconds is insufficient for appropriate sampling mixing to occur due to the relatively low amount β globin chain observed in the spectra. A one-way ANOVA statistical test was performed using the Microsoft office excel program. The null hypothesis in this case being that there is no difference in average observed β- globin chain intensity with relation to the sampling time delay (the amount of time the LMJ is maintained for) (the alpha value, for rejection of null hypothesis was set at 0.05). The results one-way ANOVA (results shown in **Appendix 3**) [$F(4,40) = 53.03$, $p = 1.82 \times 10^{-15}$] means the null hypothesis is rejected. The data is shown to be statistically significant difference, the amount of time the ESI/sampling solution is able to mix with the DBS sample effects the average β- globin chain intensity observed. A post hoc analysis was perfomed using the Tukey HSD (Honestly Significant Difference) test to determine which specific time delay period/s was responsible for producing a significant difference in obserbed β- globin chain intensity. Results of the Tukey test revealed that mean score for the 0 sec [$M = 2.07 \times 10^5$, SD =

1.86] and for the 2.5 sec [M = 18.61 x10^5, SD = 9.5] results is significantly different to all the other time delay intervels (5, 7.5, 10 sec) including each other. The mean score for time dealy of 5, 7.5 and 10 sec are not significantly from each other. The conclusion drawn from experiment is that a delay of 5 seconds is optimum. This delay has a small standard deviation [SD = 3.6] and yields high extracted β- globin chain intensity with minimum time delay as lengthing the amount of time the LMJ is maintiend to 7.5 and 10 does not significantly improve the intensity of the obserbed β- globin chain ions.

3.2.3 Dispense tip height

The height at which the ESI/ extraction solvent is dispensed onto the surface of the DBS card, which equates to the distance between the sample surface and the tip in which the liquid microjunction is formed, was also studied with regards to its effect on β globin chain intensity/ mass spectrometer response. For each of the tip height intervals chosen, three DBS (containing 20 µL of whole blood) from a single donors were each sampled . The surface sampling parameters (5 second LMJ delay, ESI solvent dispense volume of 6 µl and a reaspiration volume of 5µl) remained the same throughout and the tip height was varied between 1 mm, 1.2 mm, 1.6 mm, 2 mm, 2.4 mm, 2.8 mm and 3 mm respectively. The MS parameters are the same as described above. **Figure 3.5** shows the average β - globin chain intensity across the multiple technical replicates varying tip height. A one-way ANOVA statistical test was performed using the Microsoft office excel program. The null hypothesis in this case being that there is no difference in average observed β- globin chain intensity with relation to tip height (the amount of time the LMJ is maintained for) (the alpha value, for rejection of null hypothesis was set at 0.05). The results one-way ANOVA (results shown in **Appendix 4**) [F(5,12) = 1.16, p = 0.38] shows there is

statistically no significant difference, between tip height and the average β- globin chain intensity observed. Overall there is no significant difference in β- globin chain intensity by varying the tip height between 1 mm to 2.8 mm however a tip height of 3 mm (**figure 3.6**) for the surface of the DBS appeared to be too large and the liquid microjuction's collapsed. A tip height of 1.6 mm (**figure 3.6**) was chosen and used through all LESA experiments.

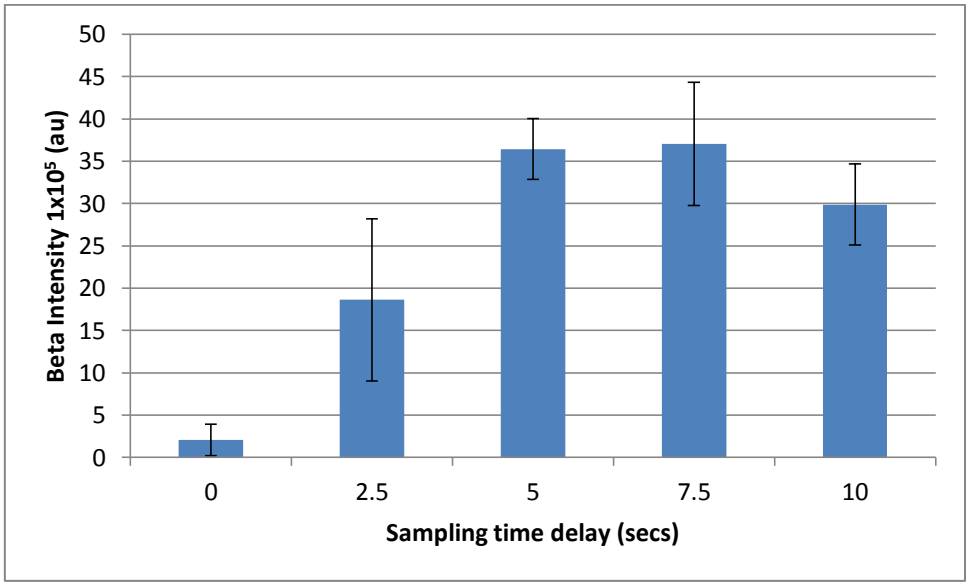

Figure 3.4 The average β chain intensity with various LMJ time delays (0-10 secs). The error bars represent the standard deviation of the data set.

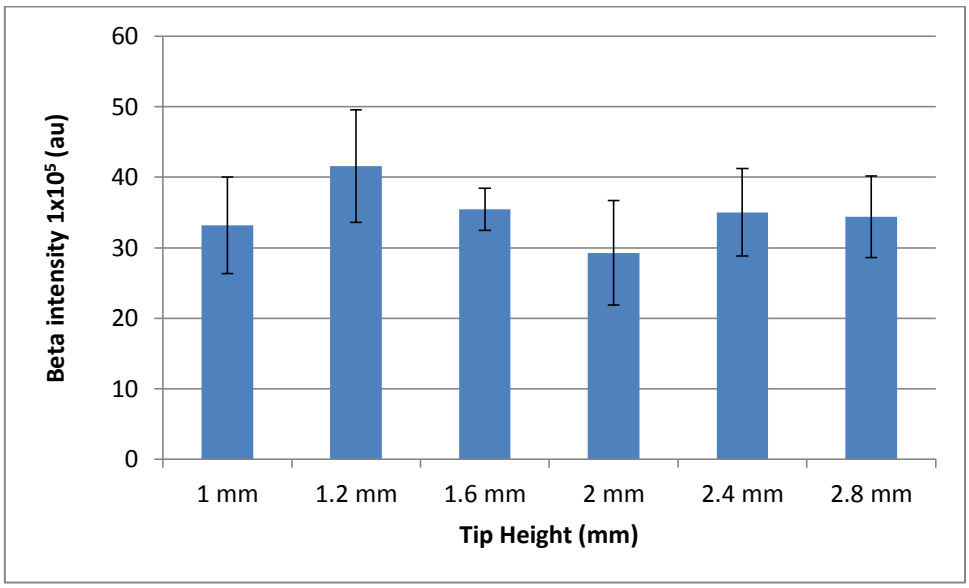

Figure 3.5 The average β chain intensity in response to varying tip height (1- 2.8 mm) (n=9). The error bars represent the standard deviation of the data set.

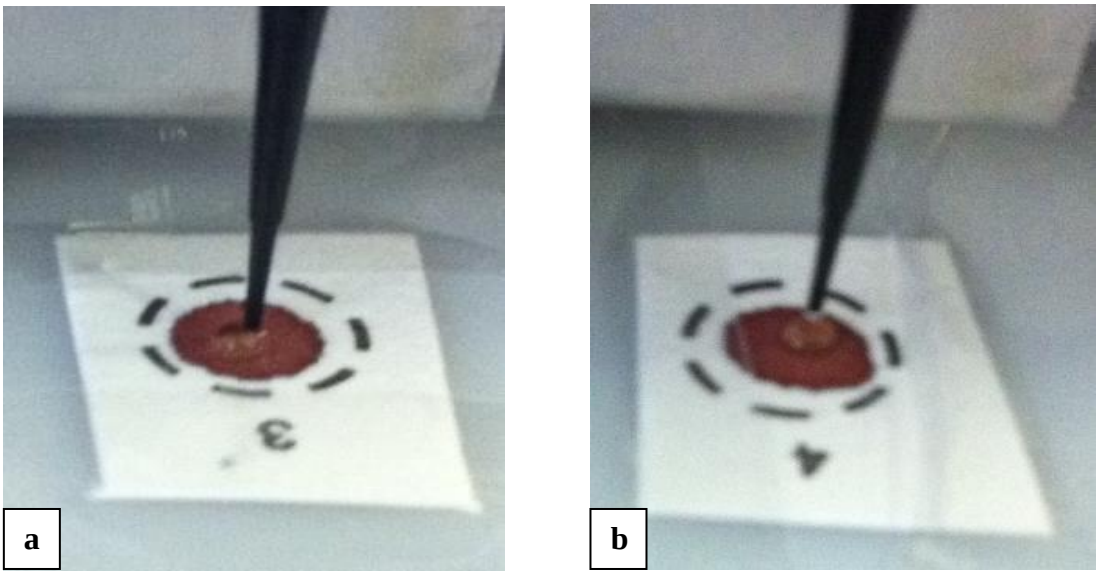

Figure 3.6. LMJ formation 1.6 mm (a) vs 3 mm (b)

3.3 Sampling Reproducibility

The reproducibility of the surface sampling process was investigated using 20 µl of whole blood (collected in the absence of an anticoagulant) from three separate adult donors. The whole blood was spotted onto dried blood spot cards multiple times (producing nine technical replicates for each donor) and left to dry for 24hrs. Whole blood from the same three donors (taken at the same time) was also collected in the presence of an anticoagulant (lithium heparin or EDTA). The whole blood samples collected in the presence of an anticoagulant were used to determine donor total whole blood Hb concentration by diluting the whole blood with Drabkin's reagent (Sigma) and measuring the absorbance at 540 nm of the solution by use of a Campspec M501 spectrophotometer.

The whole blood Hb concentration for each of the three donors was determined by spectrophotometry as described in section 2.4.3. A standard curve was created using a set of standards with known Hb concentrations of 0, 50, 100, 150 and 200 g/l (Stanbio). A plot of absorbance at 540 nm against Hb concentration (g/l) is shown in **figure 3.7** (R^2 = 0.99948). Using the equation determined in excel (y = 0.00275 + 0.00460), donor whole blood Hb concentration could be calculated: The whole blood samples were diluted by 251 using Drabkin's reagent (four replicates for each donor) and the absorbance at 540 nM was measured. The whole blood Hb concentration was calculated using the average absorbance value for each donor and was determined to be 155, 137 and 165 g/L (all within expected Hb concentration range for a normal adult) for donors one, two, and three respectively. See Table 3.1. Figure 3.8, 3.9 and 3.10 show example full mass spectra from donors 1,2 and 3 respectively.

In order to investigate the reproducibility of the surface sampling method whole blood collected without anticoagulant was taken from the same three separate donors. For each donor 3x 20 µl of the whole blood was pipetted onto a DBS card (yielding 3 separate spots for each donor). Each of these spots was sampled at three discrete locations. 5 µl of sampled material was electrosprayed in to the mass spectrometer. The deconvoluted globin chain mass spectral intensity was recorded and an average intensity for each of the three spots (nine separate measurements) was calculated. **Figure 3.11** shows the average α-globin intensity and **figure 3.12** shows the average β- globin chain intensity for each donor. This tentatively fits the pattern seen in the data shown in table 3.1 whereby donor three has the highest average intensity and donor two the lowest. The investigations described above show that sampling reproducibility is poor, demonstrated by the error bars representing standard deviation on figures 3.11 and 3.12.

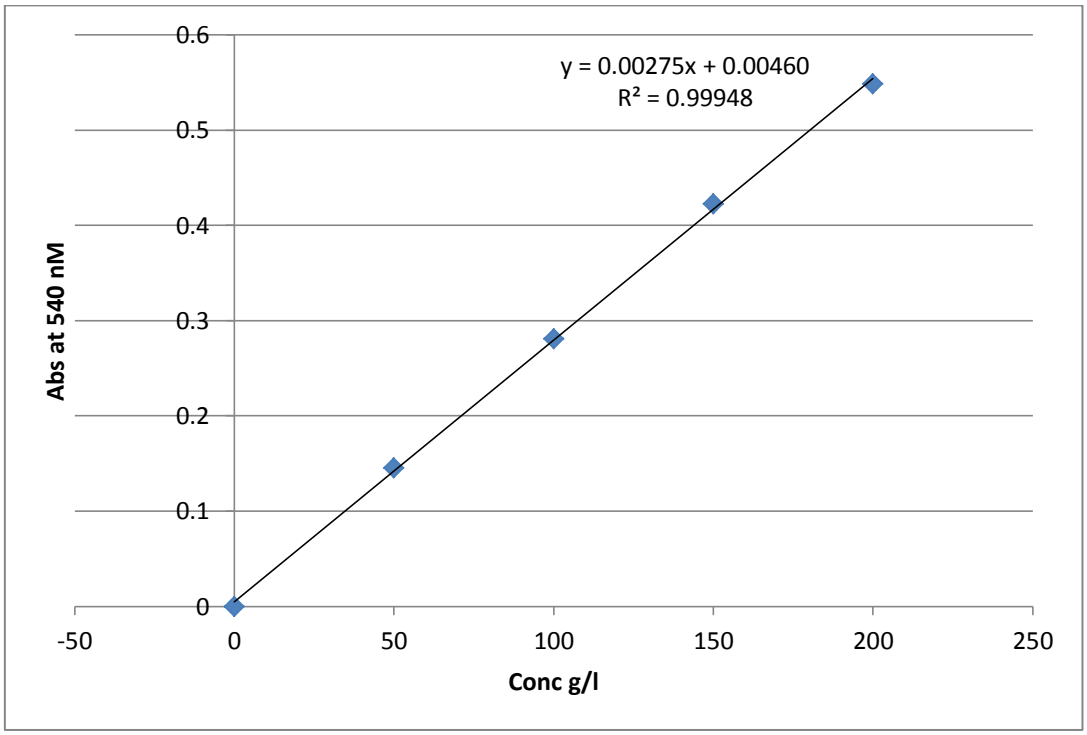

Figure 3.7. Standard curve: Absorbance at 540 nM versus Hb concentration (0-200g/L).

	Abs at 540 nM				Ave	Calc Conc g/l
	Abs 1	Abs 2	Abs 3	Abs 4		
Donor 1	0.423	0.422	0.423	0.422	0.4225	155.31
Donor 2	0.371	0.371	0.373	0.371	0.3715	136.78
Donor 3	0.449	0.449	0.449	0.449	0.449	164.96

Table 3.1 Absorbance at 540 nm of Hb solutions derived from whole blood samples.

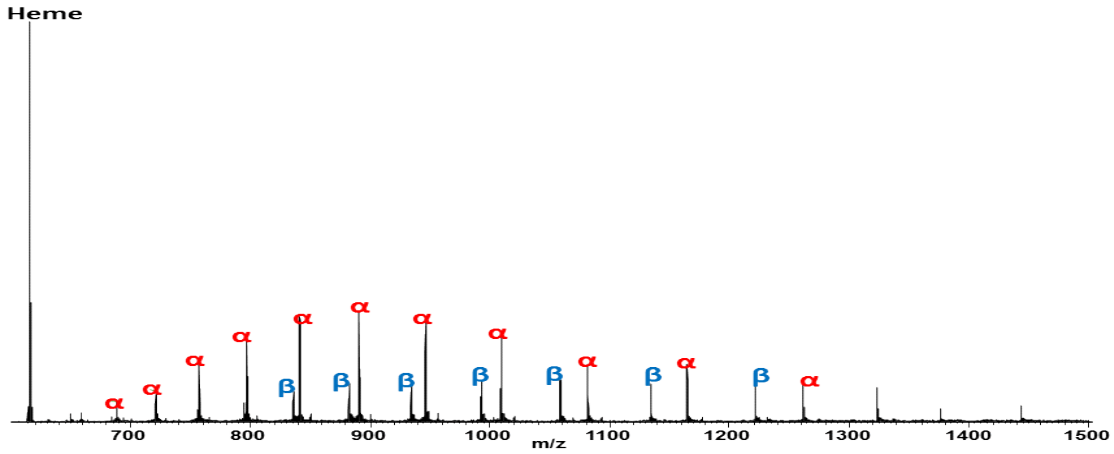

Figure 3.8. Donor 1 full mass spectrum.

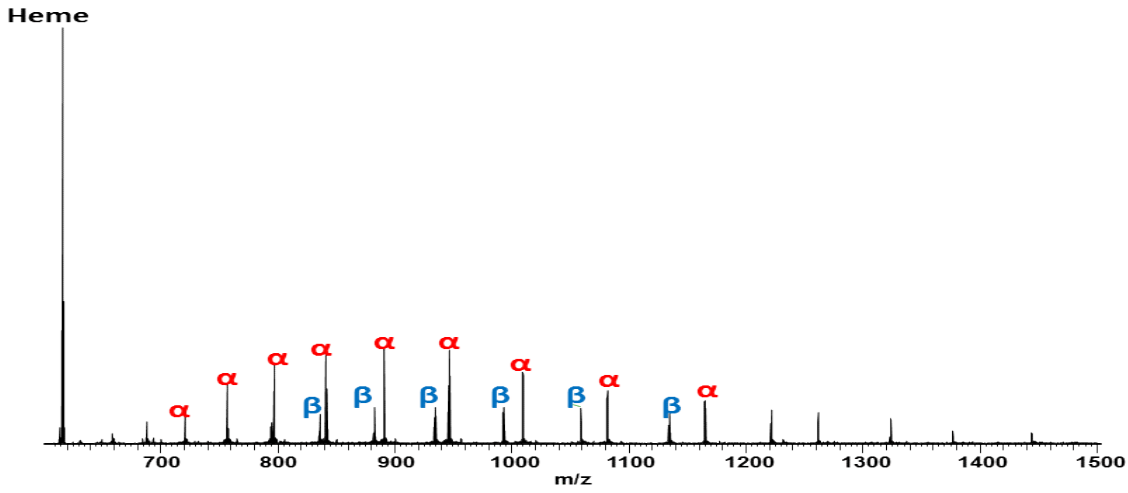

Figure 3.9. Donor 2 full mass spectrum

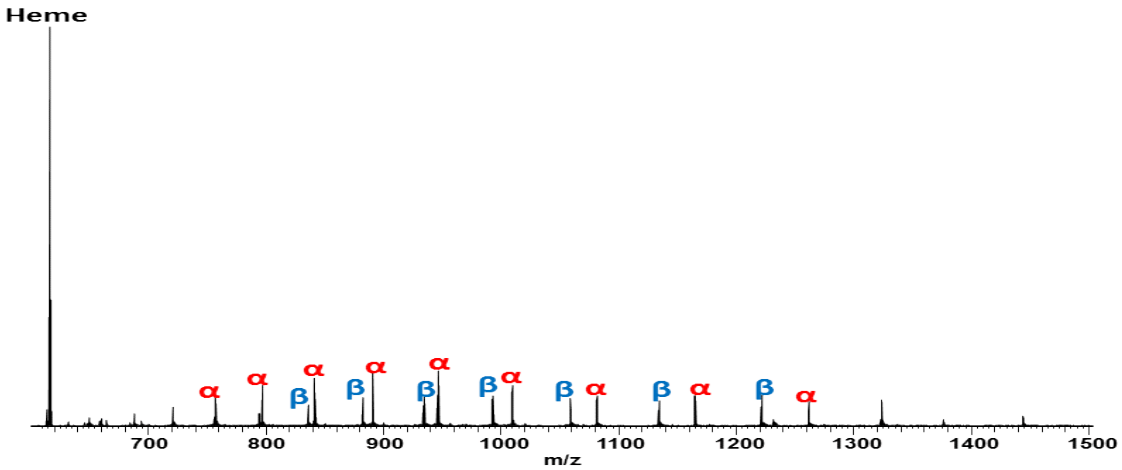

Figure 3.10. Donor 3 full mass spectrum

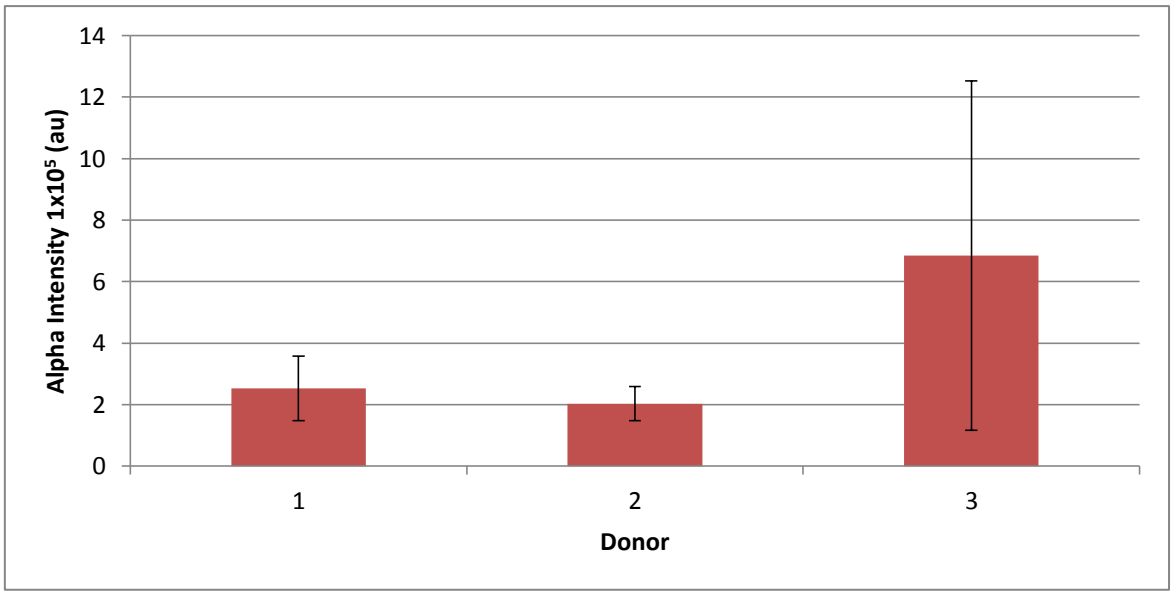

Figure 3.11. Average alpha globin chain intensity across multiple technical replicates for donors 1 to 3. Error bars show the standard deviation calculated in excel where n=9.

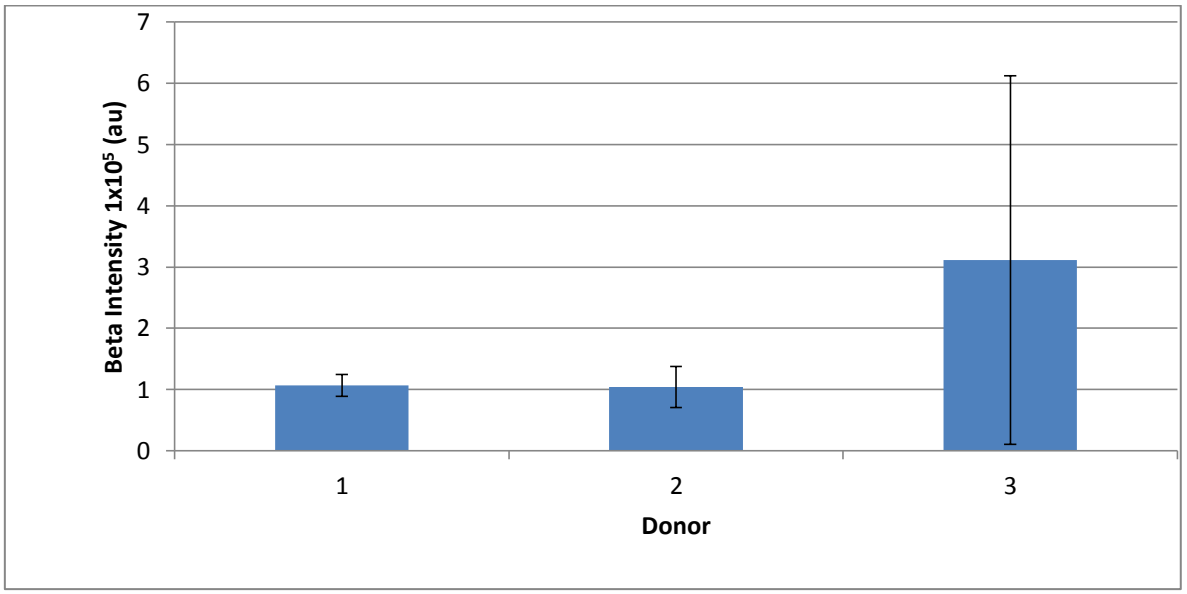

Figure 3.12. Average beta globin chain intensity across multiple technical replicates for donors 1 to 3. Error bars show the standard deviation calculated using excel where n=9.

The relationship between whole blood Hb concentration and the Hb concentration following LESA extraction of the DBS was investigated. For each donor, 20 µl (anticoagulant free) whole blood was pipetted onto DBS cards to give a total of three DBS per donor. Each spot was sampled in three discrete locations. The sampled solution (5 µl) was collected into eppendorf tubes for spectrophotometry analysis rather than being electrosprayed into the mass spectrometer. The sampled solutions were diluted with Drabkin's reagent (251x) and the absorbance at 540 nm was measured. Data are shown in Table 3.2. Note the very low absorbance measurements, with some even not registering a response, suggesting that the Hb concentration is low and on the edge of the limits of detection of the spectroscopy technique, and questioning the reliability of the data collected. Nevertheless, the Hb concentration was calculated using the standard curve shown in figure 3.7. The concentration of Hb in LESA samples (and hence typically electrosprayed into the mass spectrometer) was determined to be between 1.7 to 2.6 g/L. The sample recovery rate was also calculated, see Table 3.1. Sample recovery rate was determined as the percentage of LESA sampled Hb concentration to the Hb concentration in whole blood for each donor. The average sample recovery rate across all donors and spots was 1.31 %. Despite the low sample recovery rate, high quality mass spectra data of Hb are able to be obtained. This is because the 1.7 to 2.6 g/L that is electrosprayed into the mass spectrometer equates to an Hb concentration of 26 µM to 40 µM, when only 1 µM - 2µM is required for good quality spectra. In order to overcome the detection limit issue, LESA samples were combined/ pooled. Three repeats (5 µl each) from each DBS were pooled (forming a 15 µl sample volume for each DBS), diluted by 84x in Drabkin's reagent and the absorbance at 540 nm measured, see Table 3.3. The Hb concentration in the pooled sample was calculated by use of the standard curve. Using this approach, the

concentration of LESA sampled was determined to be between 1.6 and 2.8 g/L, 25 μM to 43 μM Hb concentration which is very similar to the results obtained without sample pooling. The average sample recovery rate across all donors and spots was 2.24 %. The conclusion drawn from this work is that sampling reproducibility appears non-consistent and there is little relationship between mass spectral response and Hb concentration suggesting direct quantitation in this manner is not possible.

		ABS Repeats				Hb Conc	
Donor	**DBS**	**a**	**b**	**c**	**Average**	**g/L**	**%Recovery**
1	1	0.002	0	0.002	0.001	2.2	1.39
	2	0	0.001	0.001	0.001	1.9	1.22
	3	0	0.002	0	0.001	1.9	1.22
2	1	0	0	0	0.000	1.7	1.24
	2	0	0	0.001	0.000	1.8	1.32
	3	0	0	0	0.000	1.7	1.24
3	1	0.002	0.002	0.002	0.002	2.4	1.45
	2	0.004	0.002	0.002	0.003	2.6	1.58
	3	0.001	0	0.001	0.001	1.9	1.15

Table 3.2 Absorbance at 540 nm of Hb solutions collected by direct surface sampling.

Donor	DBS Pooled 3x	Abs	g/L	%Recovery
1	1	0.002	2.4	1.55
	2	0.003	2.8	1.80
	3	0.006	3.9	2.51
2	1	0.003	2.8	2.05
	2	0.003	2.8	2.05
	3	0.003	2.8	2.05
3	1	0.007	4.2	2.55
	2	0.008	4.6	2.79
	3	0.008	4.6	2.79

Table 3.3 shows the absorbance at 540 nm of Hb solutions collected by direct surface sampling that have been pooled together.

3.4 Tandem mass spectrometry

3.4.1 Collision induced dissociation

The unambiguous diagnosis of Hb variants is dependent on a high % sequence coverage of the globin chains. In order to maximise the sequence coverage obtained from collision induced dissociation (CID) of the intact β globin chain, the $[M + 15H]^{15+}$ ions were isolated with a width of 10 Th and subjected to collision with helium gas at a normalised collision energy between 20 and 40 % at intervals of 5 %. See section 2.2.2. MS parameters are the same as described previously with spectra comprising of 30 co-added microscans. Each spectrum was acquired for 5 scans. Assignment of the product ions was performed manually. The experimentally measured fragment m/z values were compared with theoretical *m/z* values calculated using Protein Prospector (http://prospector.ucsf.edu/prospector/mshome.htm). The experiment was repeated three times for each energy interval with the average sequence coverage shown in **figure 3.13.** The data appear to be highly reproducible with small standard deviations represented by the error bars. A normalized CID energy of 30 % resulted in the the highest sequence coverage of 68 % and this was used throughout unless otherwise stated. An example of the sequence coverage from an individual experiment for each of the CID energies in shown in **figure 3.14.**

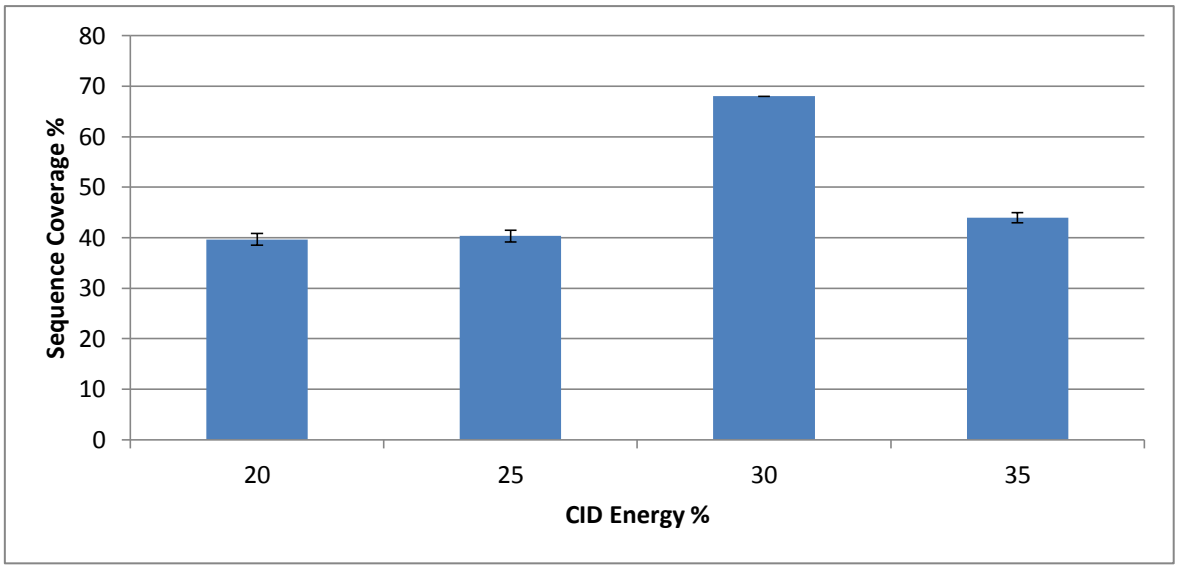

Figure 3.13 Average β -globin chain sequence coverage of the $[M + 15H]^{15+}$ ions obtained by varying CID normalised collision energy. Error bars represent the standard deviation.

Figure 3.14 Fragment ion maps showing the sequence coverage obtained using a CID collision energy of (a) 20 %, (b) 25 % , (c) 30 % and (d) 35 % .

3.4.2 Charge state optimisation

The work of Bakhtiar *et al*. [149] describes differences in fragment ions produced and sequence coverage when different charge states of α globin are isolated and fragmented. The effect the charge state of the precursor ions would have on the β globin chain sequence coverage obtained following CID was investigated. Isolation width of all the precursor ions was 10 Th. Fragmentation spectra from each charge state were acquired in triplicate. Charge states $[M+14H]^{14}$ to $[M+19H]^{19}$ were investigated. Fragment ion assignment was performed manually. **Figure 3.15** shows the average sequence coverage obtained with different precursor ion charge states at a normalised collision energy of 30 % and **figure 3.16** shows representative fragment ion maps of each charge state showing the sequence coverage. The results show that a precursor ion charge state of $[M+15H]^{15}$ yields greatest sequence coverage and is used throughout this work.

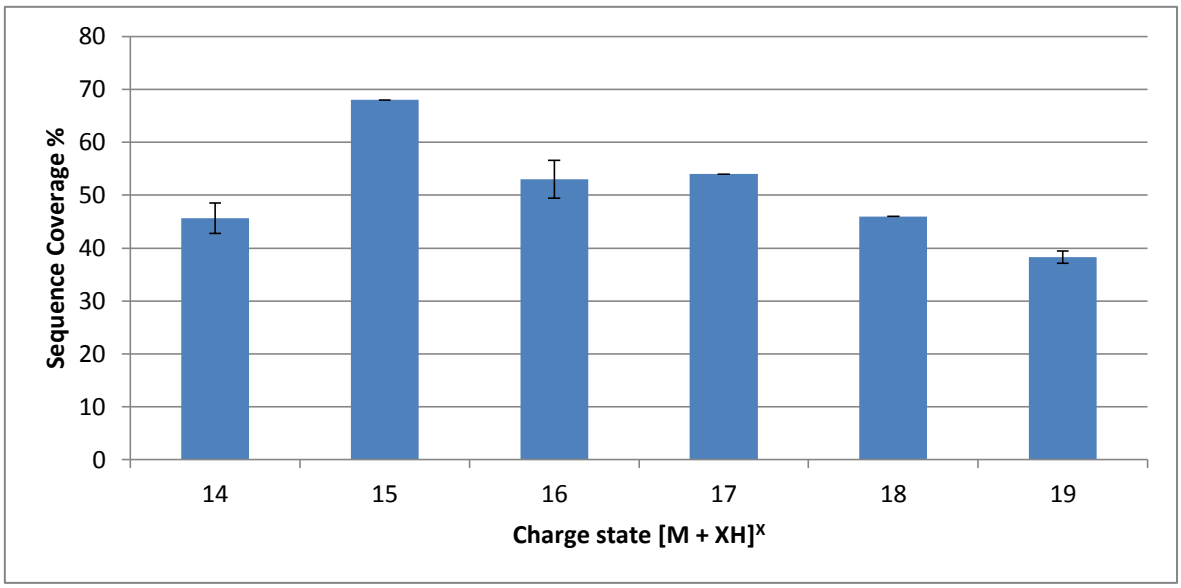

Figure 3.15. Average β globin chain sequence coverage for charge states $[M + 14H]^{14+}$ to $[M + 19H]^{19+}$.

a

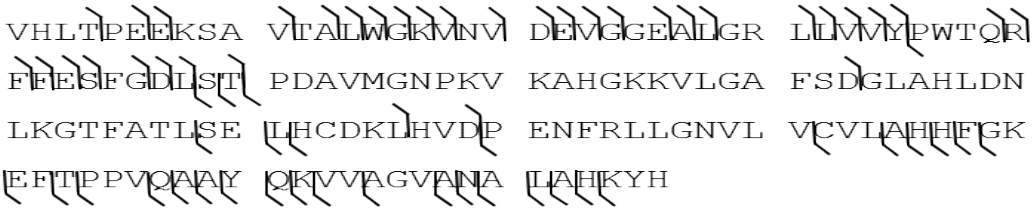

b

c

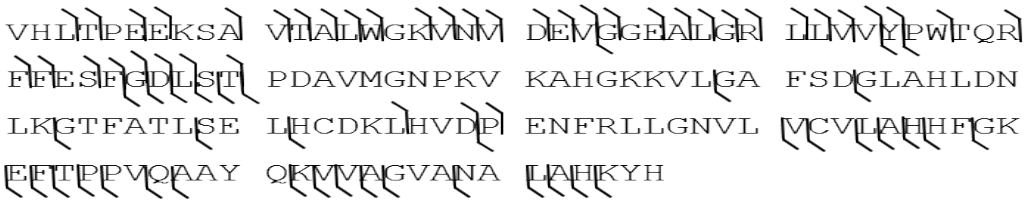

d

e

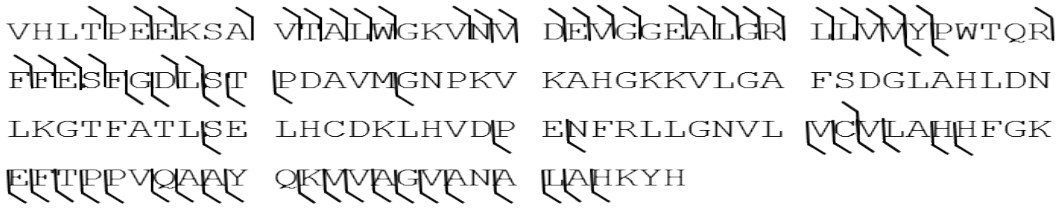

f

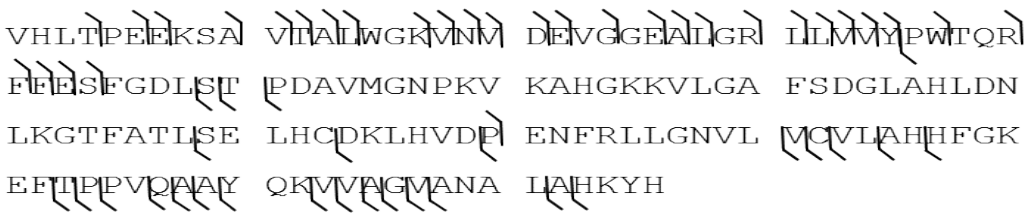

Figure 3.16. Example of sequence coverage achieved from charge state (a) $[M + 14H]^{14+}$, (b) $[M + 15H]^{15+}$, (c) $[M + 16H]^{16+}$, (d) $[M + 17H]^{17+}$, (e) $[M + 18H]^{18+}$ and (f) $[M + 19H]^{19+}$.

3.4.2 Electron transfer dissociation

With the aim of improving overall sequence coverage, electron transfer dissociation (ETD without supplemental activation was optimised for use as a complementary fragmentation technique. Firstly sequence coverage was optimised by fragmenting the $[M + 15H]^{15+}$, β globin chain ions with different ETD activation times from 15 to 25 ms. Results are shown in **figure 3.17**. These reveal that an activation time of 20 ms is optimal in order to maximise sequence coverage. The sequence coverage (43 %) is displayed in figure **3.18.** When combining the sequence coverage obtained at a CID normalised collision energy of 30 % (see figure 3.11) with the sequence coverage generated from ETD with an activation time of 20 ms, the overall sequence coverage achieved (CID + ETD) was 81 %.

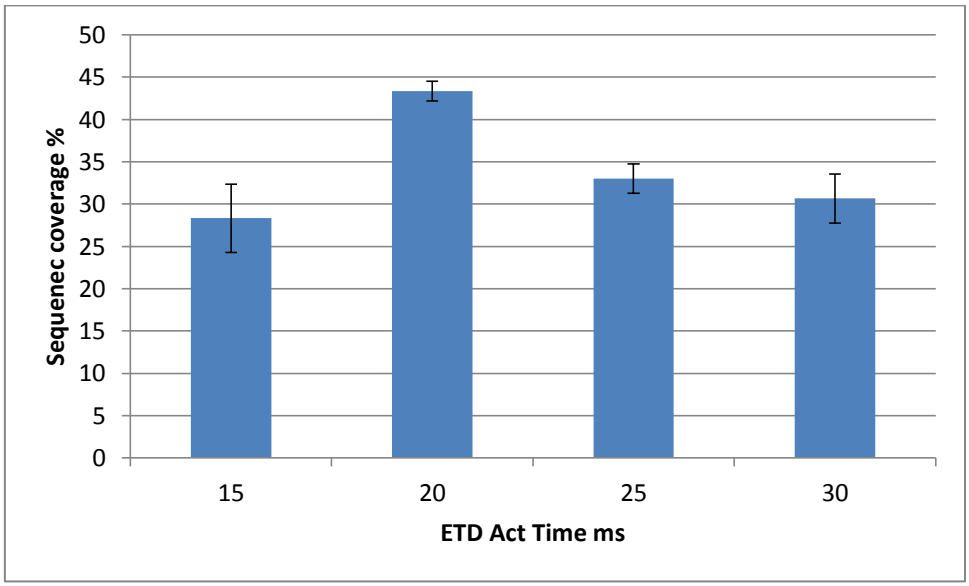

Figure 3.17 β globin chain sequence coverage obtained using different ETD activation times.

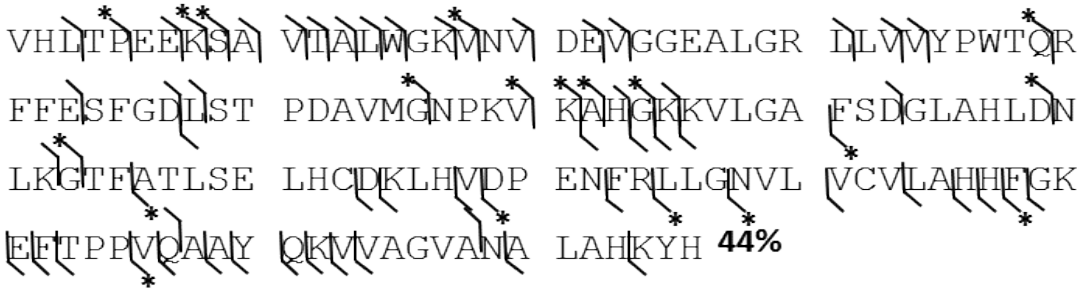

Figure 3.18 β -globin chain sequence coverage obtained using ETD activation times of 20 ms * = fragments unique to ETD fragmentation when combine with fragments produced by CID at a normalised collision energy of 30 % total sequence coverage = 81 %.

3.4 Conclusion

The data described in this chapter suggest that the optimum parameters for the LESA of DBS for identification of known and unknown Hb variants include an ESI/ extraction solvent of 48.5:48.5 (v/v) methanol: water with 3 % (v/v) formic acid, a sampling time delay of 5 seconds and a tip height at 1.6 mm. Investigation into the potential of directly quantifying Hb concentration with mass spectrometer response suggest quantitation is not possible due to the non- reproducible sampling process and poor sample recovery. For MS/MS experiments, a CID normalised collision energy of 30 % and an ETD activation energy of 20 ms yield highest β globin chain coverage. Results from the two fragmentation techniques can be combined to further increase the sequence coverage. These parameters were used to obtain data in the following chapters unless otherwise stated.

Having optimised the parameters for Hb analysis by direct surface sampling mass spectrometry of adult DBS, the approach was applied to neonatal DBS to investigate the suitability of the method for newborn screening.

Chapter 4: Direct Surface Sampling of Dried Blood Spots Coupled with Mass Spectrometry Analysis of Common Haemoglobin Variants in Neonates

4.1 Overview

This chapter describes the application of liquid extraction surface analysis (LESA) of neonatal dried blood spots coupled to a high-resolution orbitrap mass spectrometer for the analysis of common Hb variants routinely screened for in newborn screening programmes. Neonatal samples afford more of challenge than normal adult DBS for the diagnosis of Hb variants, particularly β- globin variants due to the presence of foetal haemoglobin in the samples and the subsequent reduction in the amount of β-globin present. In a practical sense the collection of neonatal blood samples is more difficult than adult samples as only a small amount of blood can be taken, hence the preference of using DBS opposed to whole blood. A successful Hb variant diagnosis method must use a minimal amount of blood. The common variants presented in this chapter are HbS, HbC, HbD and HbE. Using an orbitrap mass spectrometer it was possible, in selected ion monitoring (SIM) mode, to identify both homozygous (HbSS) and heterozygous (HbAS) sickle cell disease (Δm - 29.9745 Da). The variants HbC (both homo- and heterozygous), HbD (heterozygous), HbE (heterozygous) ($\Delta m < 1$ Da) and the compound heterozygotes disorders HbSC and HbSD were unambiguously identified and distinguished from HbAS using collision-induced dissociation tandem mass spectrometry (CID MS/MS). That is significant because whereas FAS is generally benign, the clinical severity of FSC is similar to that of homozygous sickle. The suitability of this method to diagnose thaslassemic disorders was also investigated using five neonatal DBS β thalassemia samples. The results shown that

Data shown in this chapter was published in Edwards RL, Creese AJ, Baumert M, Griffiths P, Bunch J, Cooper HJ: Hemoglobin Variant Analysis via Direct Surface Sampling of Dried Blood Spots Coupled with High-Resolution Mass Spectrometry. *Analytical Chemistry* 83(6), 2265-2270 (2011).

LESA offers a fast, direct, and unambiguous determination of Hb variants with no sample preparation. It allows for repeated analysis of the dried blood spots.

This thesis resulted in a publication in which I am first author, and which included work carried out by other collaborators and which was written in collaboration with other authors and with my supervisor

4.2 Results

4.2.1 Normal adult haemoglobin

As shown in **figure 4.1** in the spectrum for normal adult haemoglobin the β globin chains are less intense than the α globin chain. The β chain contains fewer basic amino acid residues than the α -globin chain and consequently ionizes less readily. Selected ion monitoring mode is used to increase the S/N of the β- globin peaks (especially important in neonatal samples) and there is no need see all of the charge states (as in full MS) for screening. Figure 4.1b shows a mass spectrum acquired in SIM mode over the m/z range 1056-1084. Peaks corresponding to the 14+ charge state of α globin chain (MW_{meas} 15 117.8883, MW_{calc} 15 117.8924, Δ -0.27 ppm) and the 15+ charge state of the β chain (MW_{meas} 15 858.2835, MW_{calc} 15 858.2570, Δ 1.67 ppm) are observed. The $[M + 14H]^{14+}$ of the α chain and $[M + 15H]^{15+}$ of the β chain were isolated (separately) with a width of 10 Th and subjected to a collision with helium gas at a normalised collision energy of 35 %, producing fragment (product ion) laden MS/MS spectra f**igure 4.2**. The spectra were analysed manually to determine sequence coverage for both globin chains. The percentage coverage for the α chain and β chain was 67 % and 68 % respectively, **figure 4.3**. All the assigned fragments for the α and β chain are shown in appendices 5 and 6.

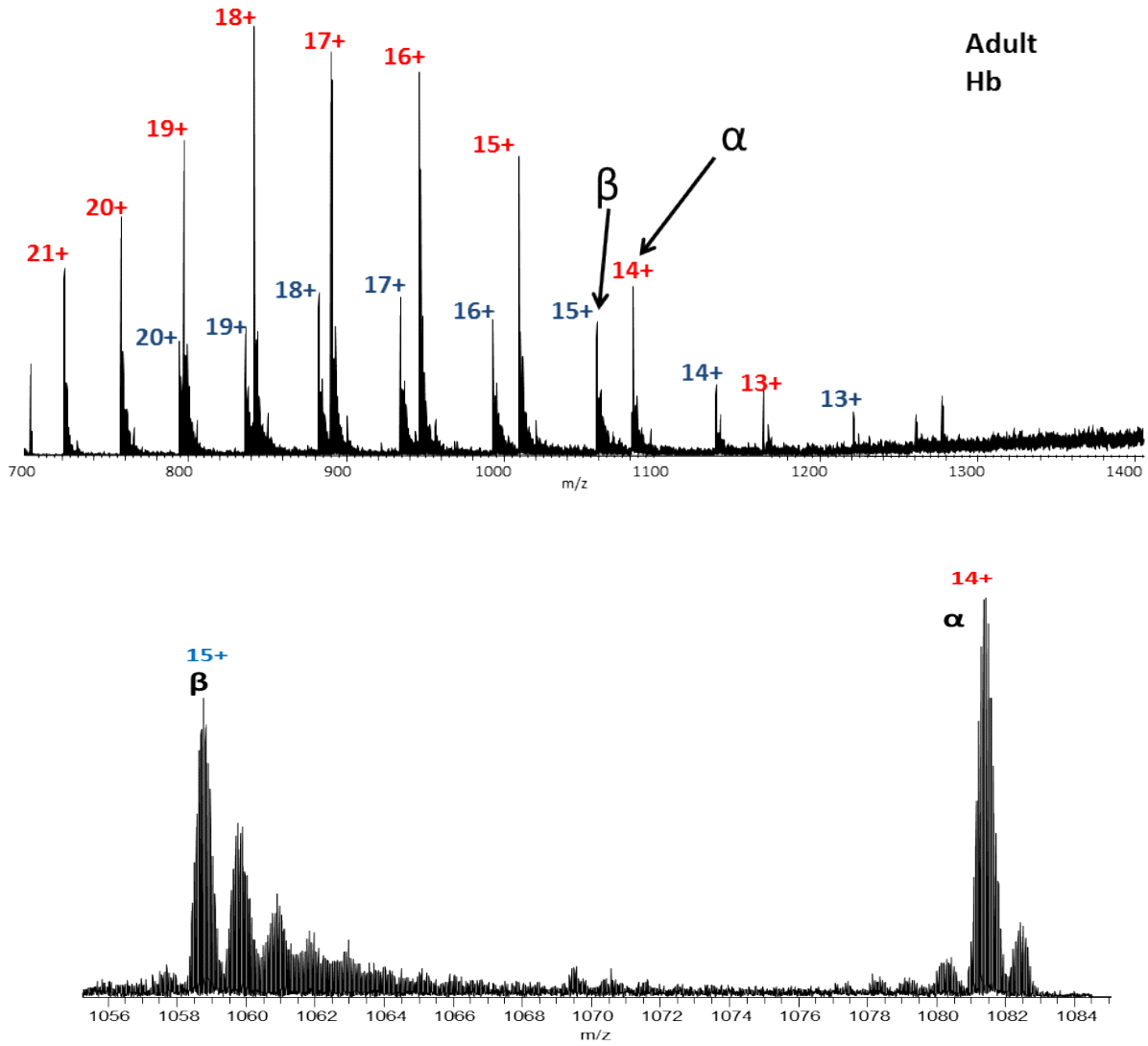

Figure 4.1 (a) Full scan and (b) selected ion monitoring (SIM) mode mass spectra of adult hemoglobin HbA. Peaks labelled in red correspond to the α chains and blue to the β chain

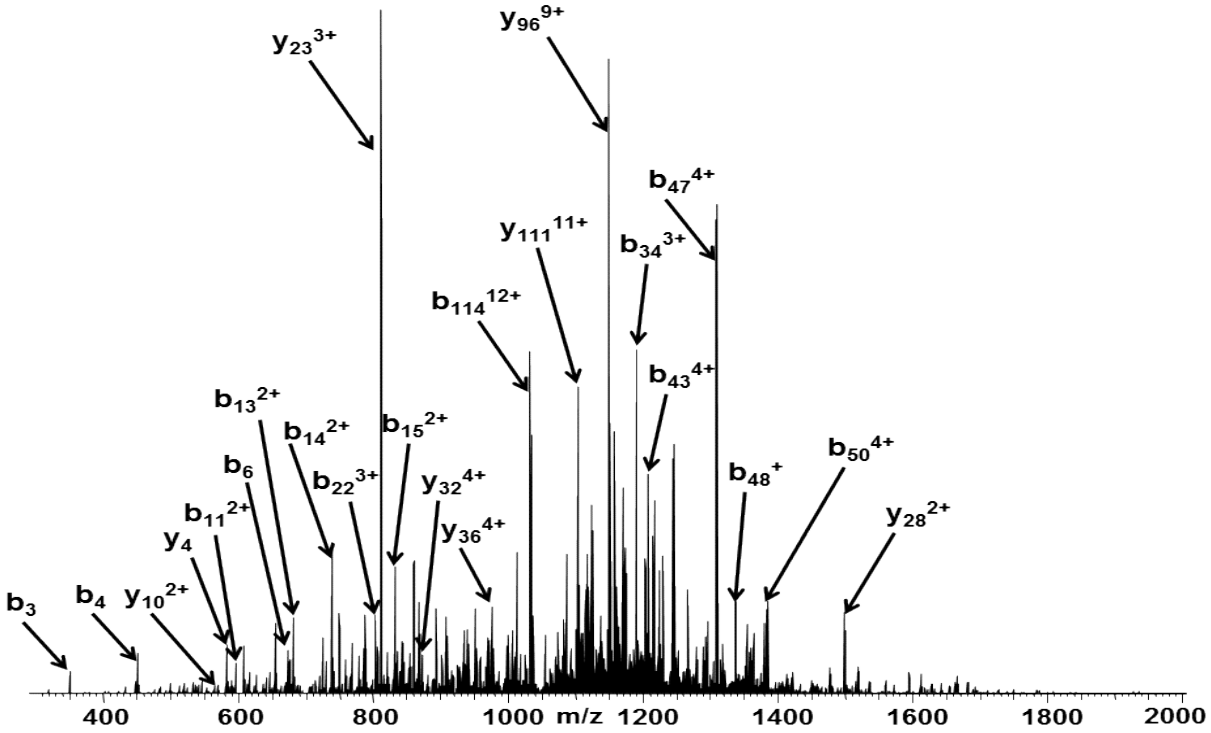

Figure 4.2 Top down CID spectrum of adult $[M + 15H]^{15}$ β chain ions.

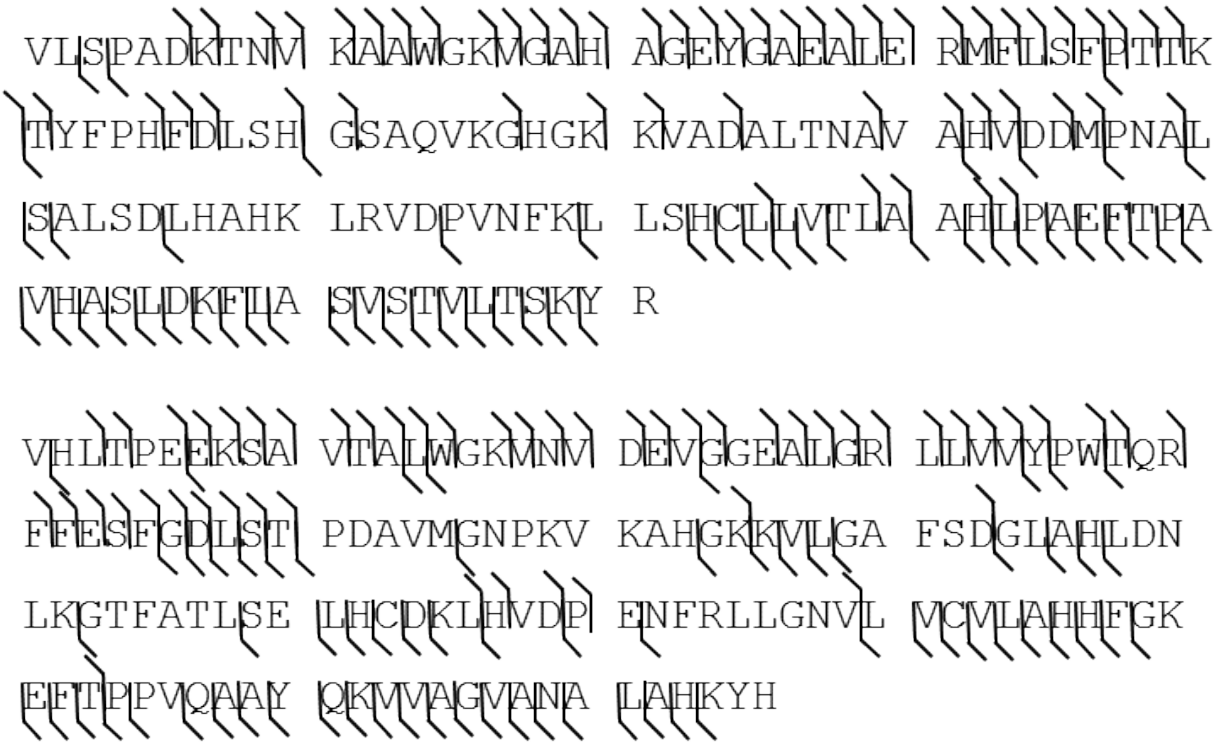

Figure 4.3. The CID sequence coverage of adult α chain (top) (67 %) and the β chain (bottom) (68 %).

4.2.1 Normal foetal haemoglobin

Peaks corresponding to ions of three major species are observed in the full scan mass spectrum obtained following LESA of a dried blood spot from a normal neonate: α chain, fetal γ chain, and very low abundance β chain (**Figure 4.4a**). Given that the most severe Hb variants occur in the β chain, the low abundance of these ions could be a problem. However, with acquisition of data in the SIM mode, the signal-to-noise is improved significantly, see **Figure 4.4b**. The measured masses of the globin chains were as follows; α MW_{meas} 15 117.8842 Da, β MW_{meas} 15 858.2687 Da γ_G MW_{meas} 15 986.2683 Da (MW_{calc} 15 986.2626 Da Δ 0.36 ppm) and γ_A MW_{meas} 16 000. 2592 Da (MW_{calc} 16 000.2782 Da, Δ -1.19 ppm). These chains were isolated and fragmented by CID the sequence coverage for each of the α (64 %), β (64 %), γ_G (43 %) and γ_A (32 %) globin chains is shown in **figure 4.5**. For the respective fragment ion lists see appendices 7-10.

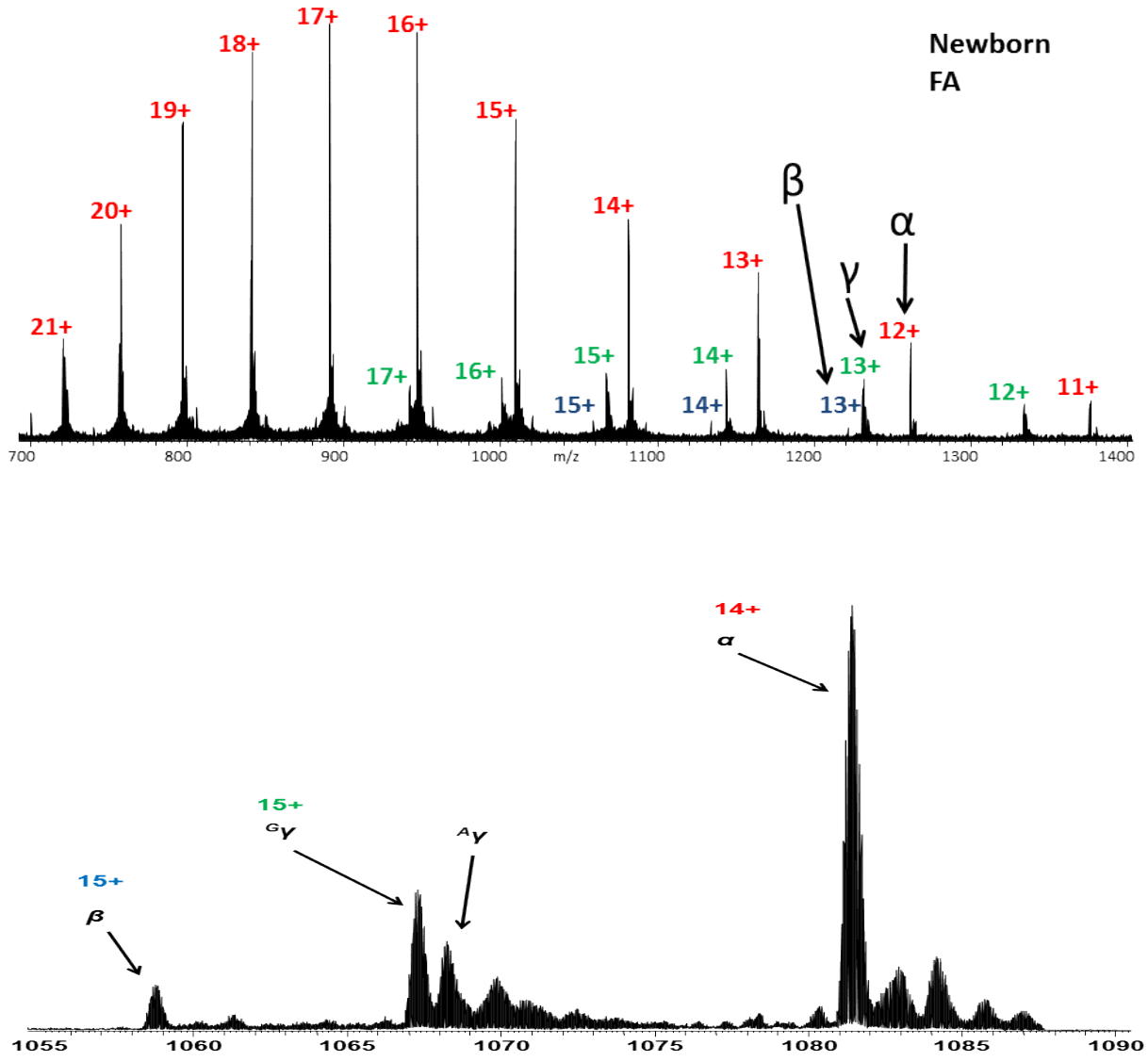

Figure 4.4 (a) Full scan and (b) selected ion monitoring (SIM) mode mass spectra of neonatal hemoglobin HbA. Peaks labeled in red correspond to the α chains, blue to the β chains and green to the γ chains. Peaks labeled Gγ and Aγ denote γ chains containing glycine or alanine at position 136, respectively.

Figure 4.5 The CID sequence coverage of neonatal (a) α chain and (b) the β chain (c) Gγ chain and (d) Aγ chain.

4.2.2. HbS Variant

With confirmation that the method was suitable for the analysis of neonatal samples, it was applied to samples homozygous and heterozygous for HbS. It was not possible to determine the presence of HbS from the full scan mass spectra; however, with the data acquired in SIM mode, the variant could be identified unambiguously (MW_{meas} 15 828.2408 Da; MW_{calc} 15 828.2828 Da, Δ 2.7 ppm) **Figure 4.6**. The sickle trait sample (heterozygous) can clearly be identified as such by the presence of both the β-chain and the sickle chain, whereas the SIM mode mass spectrum of homozygous sample shows no peak corresponding to the β-chain. The $[M + 15H]^{15+}$ ions of the β and sickle chains from the heterozygous (FAS) sample were each selected for CID and the fragments detected in the orbitrap. Seven heterozygous and five homozygous sickle samples were analysed. Results presented are representative examples. For the sickle chain ions, sequence coverage was 32% in the heterozygous sample shown in **Figure 4.7a** and sequence coverage in the homozygous sickle sample was 45 %, **Figure 4.7b,** fragment ion list appendix 11. The sickle variant is the result of the HbS variant substitution at position 6 on the β chain, Glu→ Val (+ 29.9745). Following CID of the β chain ions, the singly charged b_6 fragment was observed at m/z meas 677.3628 (m/z_{calc} 677.3617) **Figure 4.8**. No peak was observed at that *m/z* following CID of the sickle ions; however, a peak was observed at 647.3854, corresponding to a mass shift of -29.9745 Da (m/z_{calc} 647.3875). Expanded *m/z* regions showing representative fragments b_{22}^{3+} and b_{47}^{4+} are shown in **Figure 4.9**.

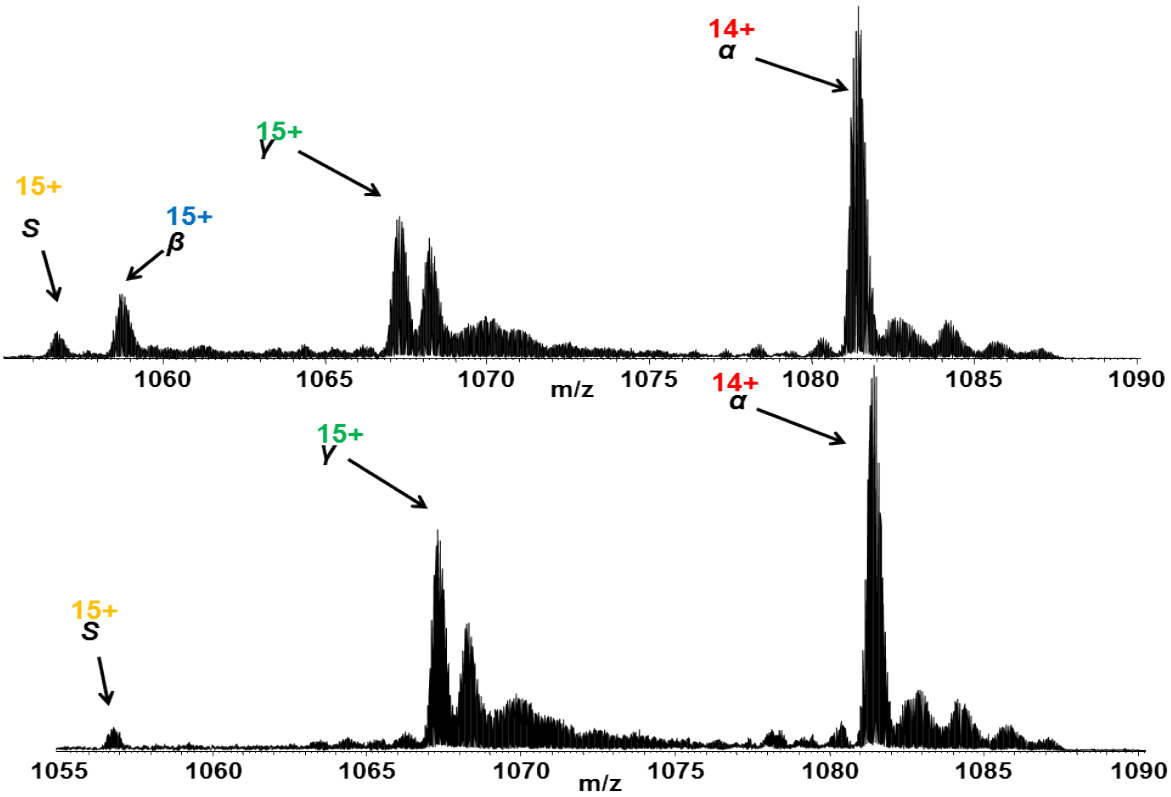

Figure 4.6 Selected ion monitoring (SIM) mode mass spectra of neonatal (a) heterozygous sickle FAS and (b) homozygous sickle hemoglobin FS. Red = α- globin chain, green = γ-globin chains, blue = β- globin chain and yellow = sickle chain.

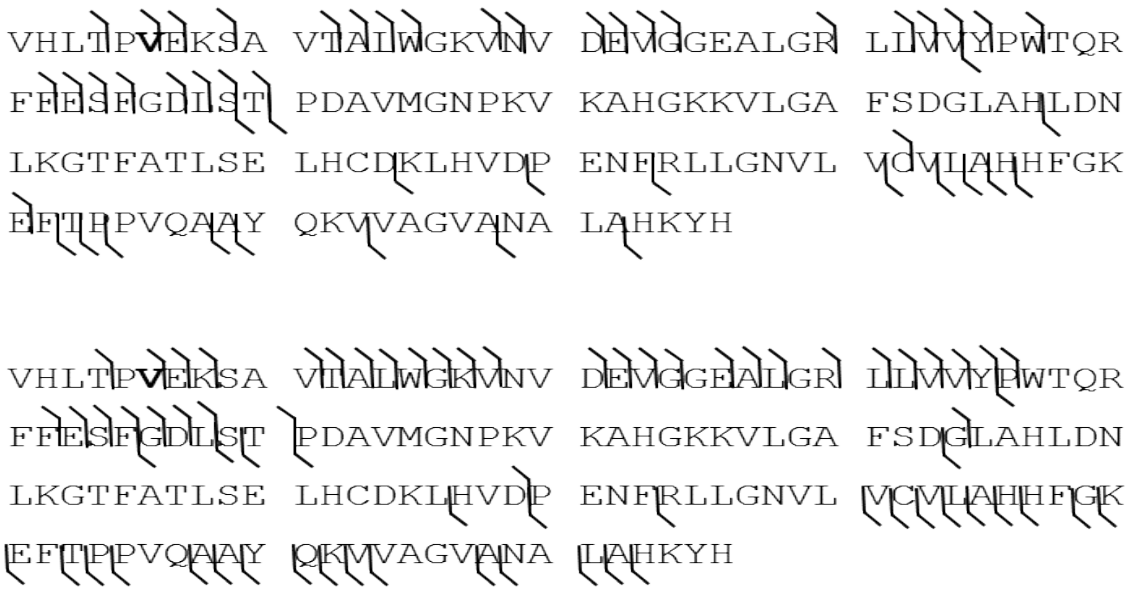

Figure 4.7 The CID sequence coverage of (a) heterozygous FAS and (b) homozygous sickle FS chains.

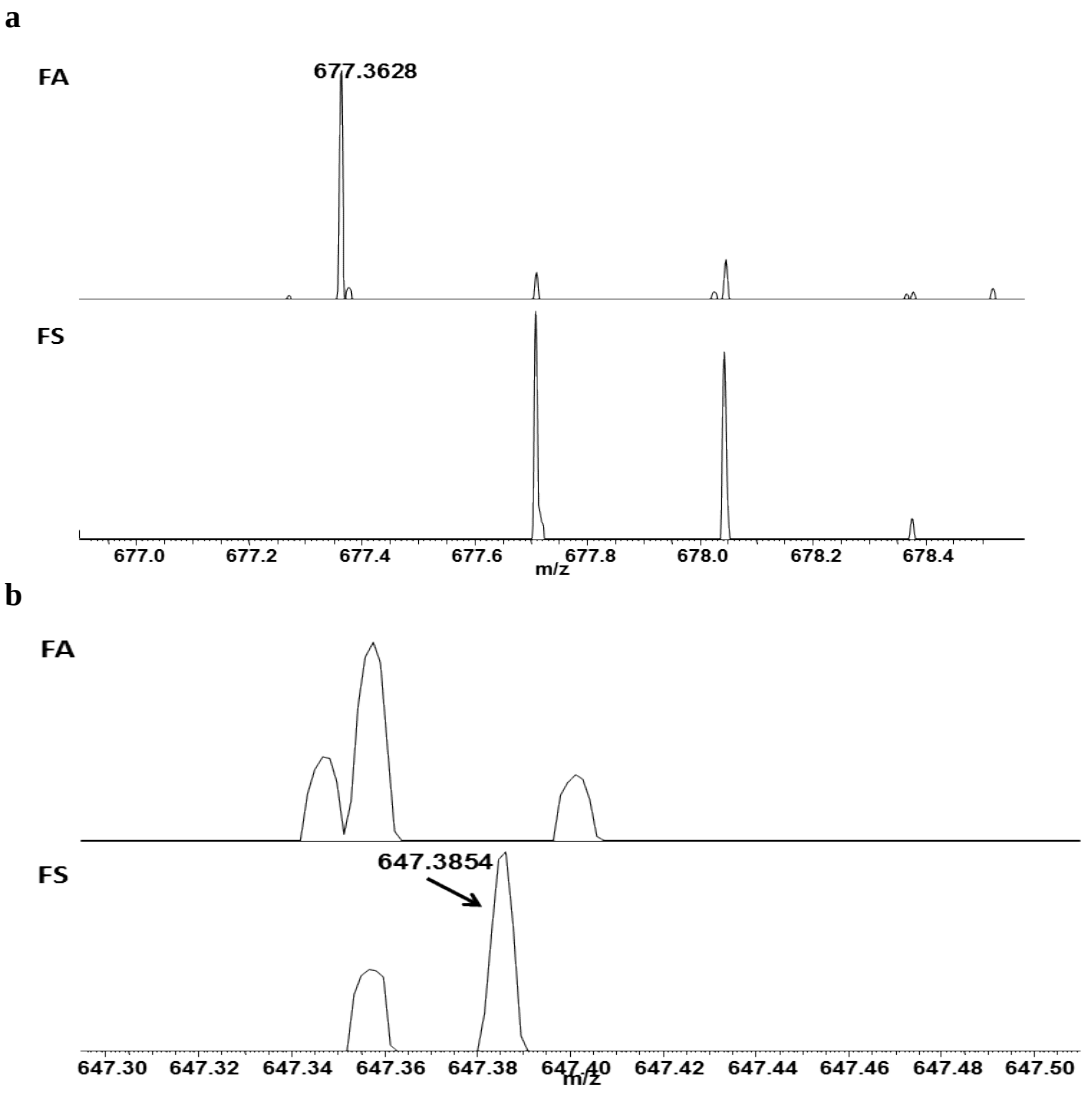

Figure 4.8 Expanded m/z regions showing the b_6 fragments observed following CID of the β chain ions (top) and HbS variant ions.

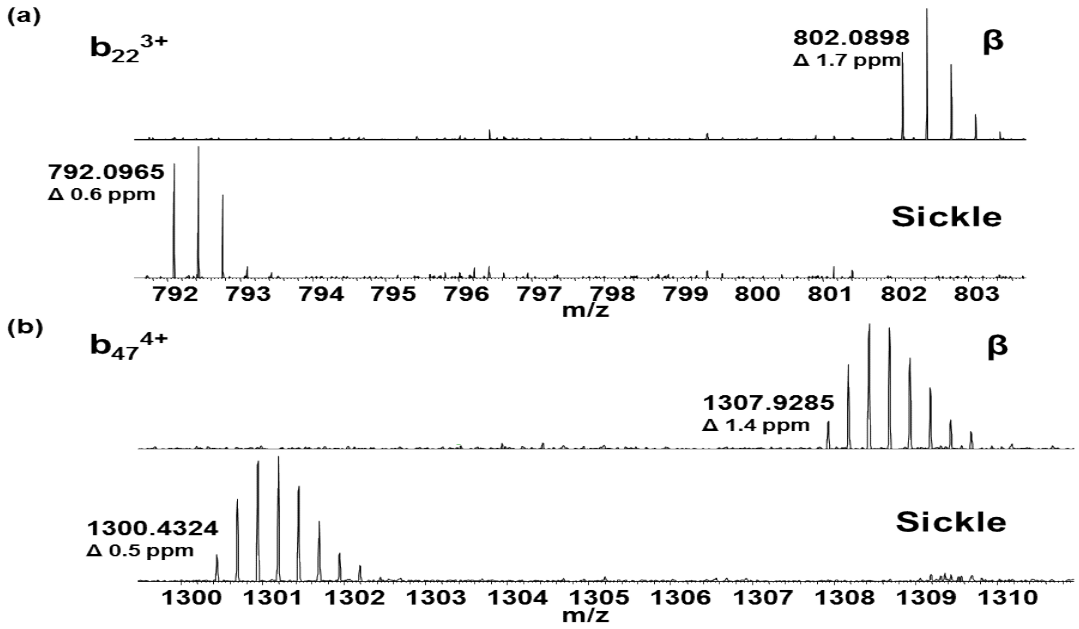

Figure 4.9 Expanded regions of CID MS/MS spectra showing peaks corresponding to (a) b_{22}^{3+} fragment ions and (b) b_{47}^{4+} fragment ions of the β chain and sickle variant. Measured monoisotopic m/z values are given.

4.2.3 HbC Variant

The HbC variant is the result of a Glu (129.0426 Da) → Lys (128.0950 Da) substitution at position 6 on the β chain with an associated mass shift of 0.9476 Da. **Figure 4.10** shows the mass spectra obtained in SIM mode from normal, heterozygous HbC and homozygous HbC samples. Comparison of these SIM mode spectra does not reveal the presence of the HbC variant in either the heterozygous or homozygous form (Figure 4.10). Five heterozygous HbC variant samples were analysed and two homozygous HbC variant samples were analysed and the results presented here are representive examples. The spectra were deconvoluted by use of the Xtract software (Thermo Fisher Scientific) to determine the monoisotopic masses of the ions. The measured MW of the β chain from the normal neonate sample was 15 858.2680 Da. For the homozygous variant C sample, the measured MW was 15 857.4033 Da (MW_{calc} 15 857.3094, Δ 5.9 ppm), suggesting the presence of a variant with a mass shift of -1 Da. However, the molecular weight obtained following deconvolution of the heterozygous sample was 15857.2442 Da suggesting the presence of the variant but failing to reveal the presence of the β chain. To confirm the presence or otherwise of the HbC variant, in each sample the ions centered at m/z 1058 were selected and subjected to CID. Assigned fragment ions are shown in appendix 8. **Figure 4.11** shows an expanded m/z region containing the b_{22}^{3+} fragment ion of the β chain (monoisotopic m/z_{meas} 802.0898, m/z_{calc} 802.0884). That fragment was also observed for the heterozygous sample (Figure 4.11 (middle)) and is accompanied by the b_{22}^{3+} fragment of the HbC variant (monoisotopic m/z_{meas} 801.7727, m/z_{calc} 801.7725). In the MS/MS spectrum obtained from the homozygous sample (Figure 4.11 (bottom)), only the b_{22}^{3+} fragment of the HbC variant is observed. Another example, b_{14}^{2+} is given in **Figure 4.12**.

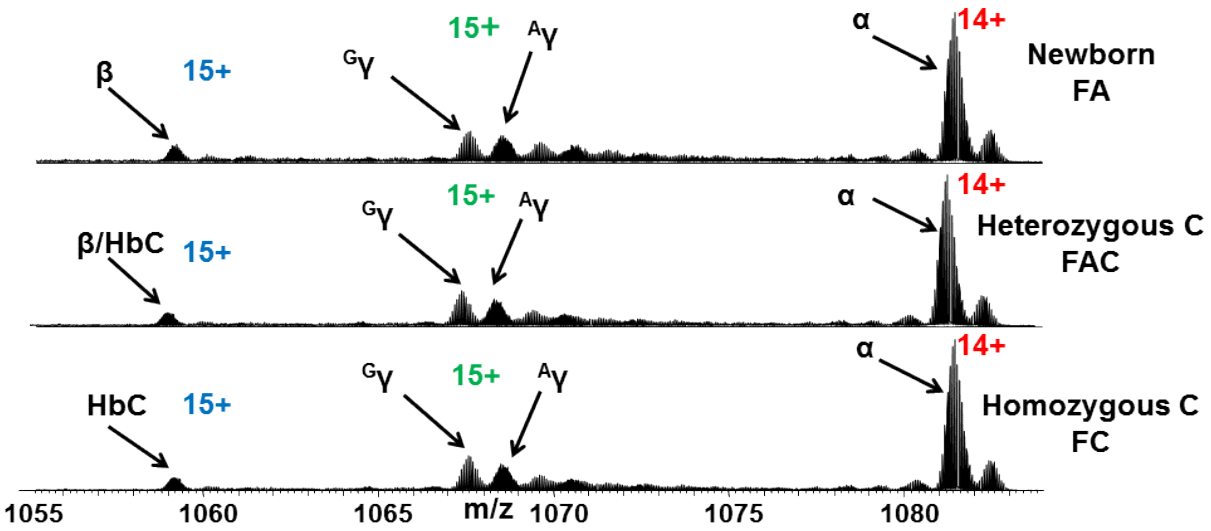

Figure 4.10 SIM mode mass spectra from normal FA (top), heterozygous HbC (middle), and homozygous HbC (bottom). Red = α- globin chain, green = γ- globin chains and blue = β- globin chain.

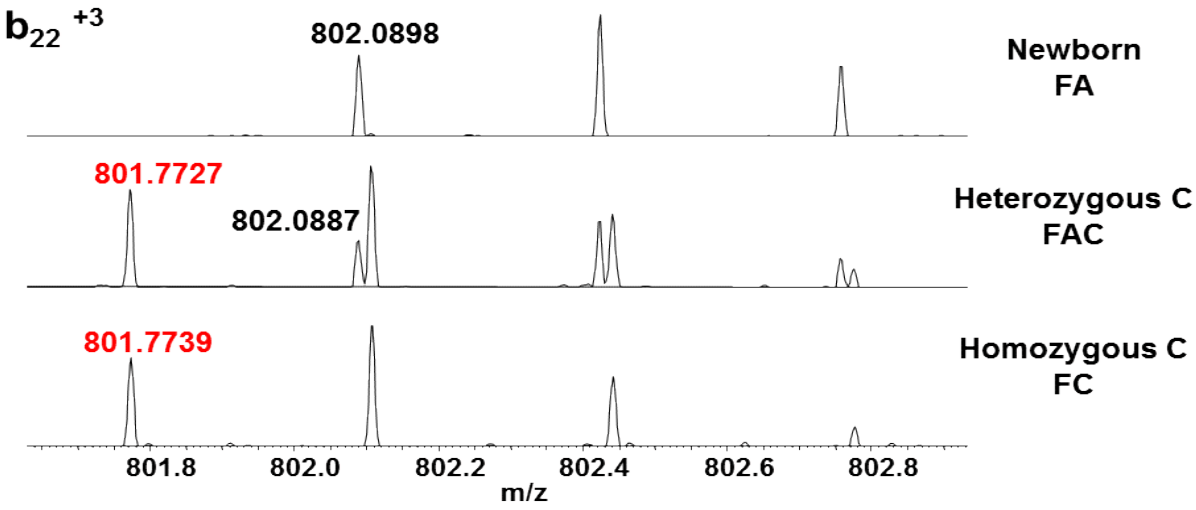

Figure 4.11. Expanded m/z regions showing the b_{22}^{3+} fragments observed following CID of the β chain ions (m/z_{calc} 802.0884) (black) and HbC variant ions (m/z_{calc} 801.7725) (red).

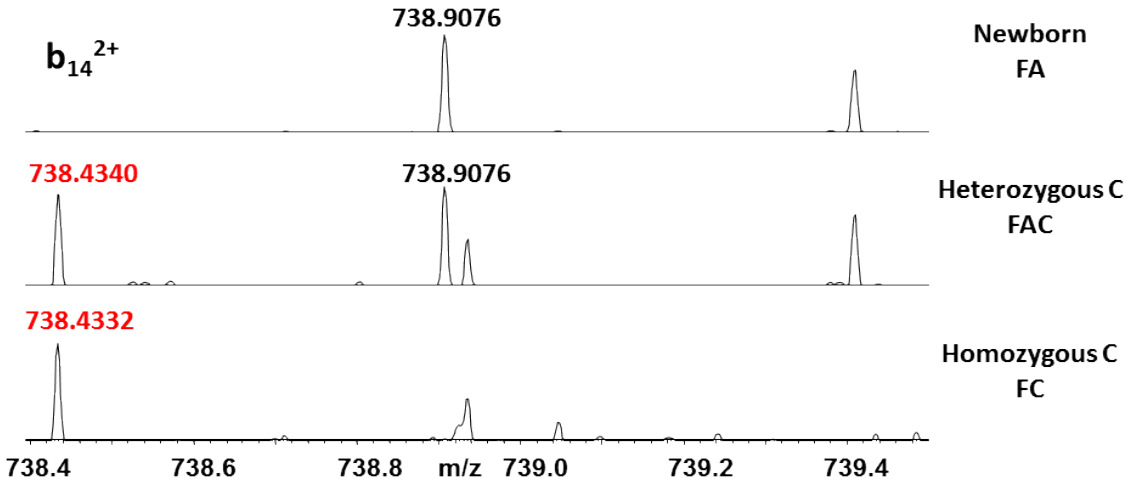

Figure 4.12. Expanded m/z regions showing the b_{14}^{2+} fragments observed following CID of the β chain ions (m/z_{calc} 738.9065) (black) and HbC variant ions (m/z_{calc} 738.4327) (red).

4.2.4 HbD Variant

The HbD (Punjab/Los Angeles) variant is the result of a Glu (129.0426 Da) → Gln (128.0586 Da) substitution at position 121 of the β chain resulting in a mass shift of-0.9840 Da. Although the mass shift is greater than for HbC, the HbD variant is more challenging to identify because of the problem of overlapping isotope peaks. The difference in mass between the 13C isotope of HbD and the 12C isotope of the β chain is 0.0194 Da. Four heterozygous HbD samples were analysed. **Figure 4.13** shows the SIM mode mass spectra obtained from normal and heterozygous HbD. As for HbC, we are unable to confirm the presence of the variant directly from the SIM spectrum. The $[M+15H]^{15+}$ ions of HbD/β were isolated and subjected to CID. The resulting mass spectrum was compared with that obtained following CID of $[M+15H]^{15+}$ ions of the β chain. Expanded m/z regions showing the y_{32}^{4+} fragments are shown in **Figure 4.14**. Note that for the peaks at m/z 872.7 and m/z 872.95 in the lower spectrum (heterozygous D), the peak shapes suggest the presence of the two species. A further example y_{47}^{5+} is shown in **Figure 4.15**. The HbD variant ion sequence coverage of the heterozygous HbD sample is 50 % for the variant D ions only (fragments corresponding to the normal β –globin chain were excluded), as shown in **Figure 4.16**. Appendix 13 shows the assigned variant HbD ions only.

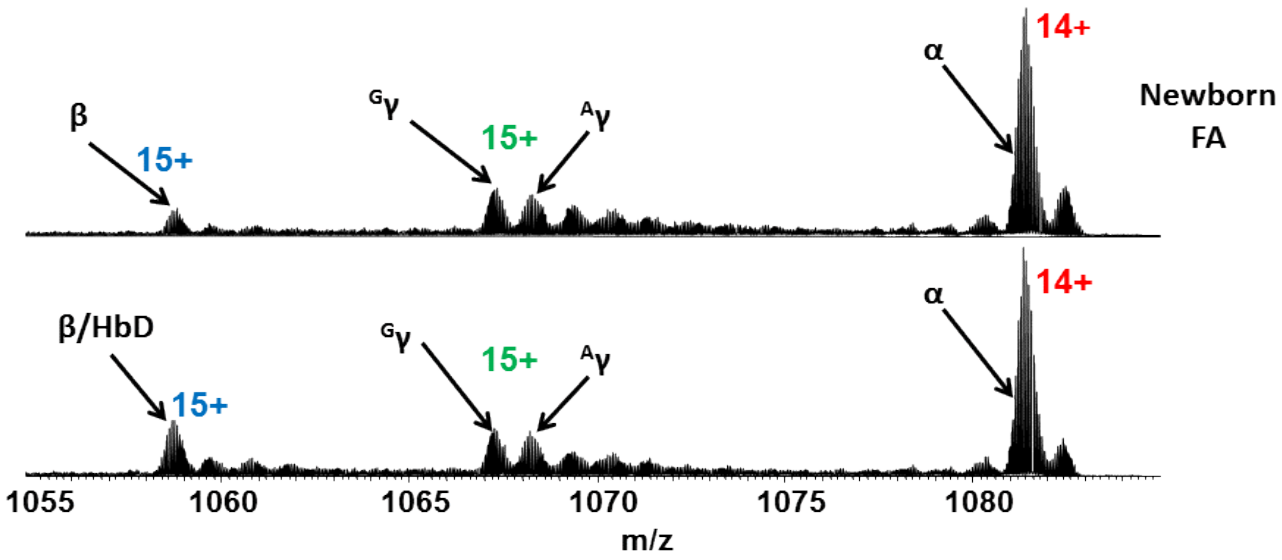

Figure 4.13 SIM mode mass spectra from normal FA (top) and heterozygous HbD (bottom). Red = α- globin chain, green = γ- globin chains and blue = β/D- globin chain.

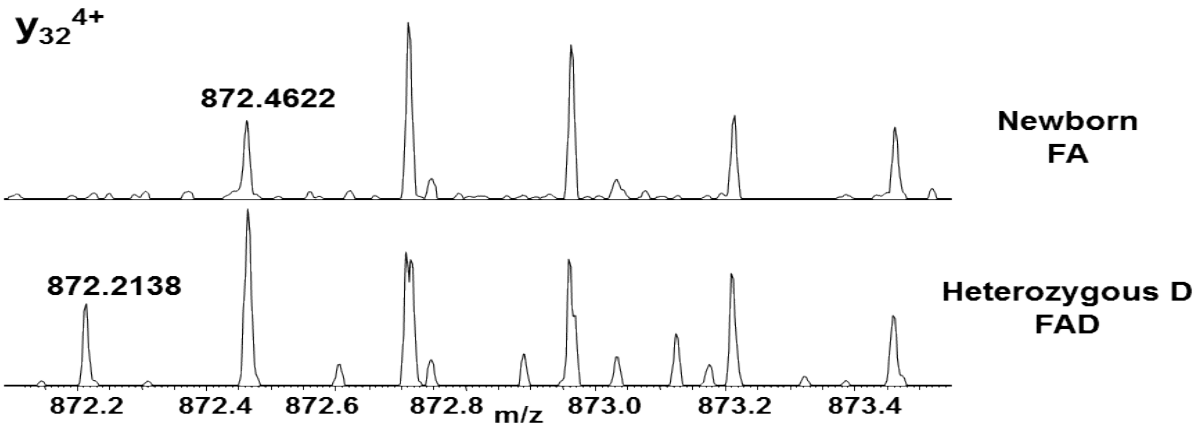

Figure 4.14 Expanded m/z region showing peaks corresponding to y_{32}^{4+} fragments observed following CID of β chain ions (m/z_{meas} 872.4622, m/z_{calc} 872.4600), and variant HbD (m/z_{meas} 872.2138, m/z_{calc} 872.2140).

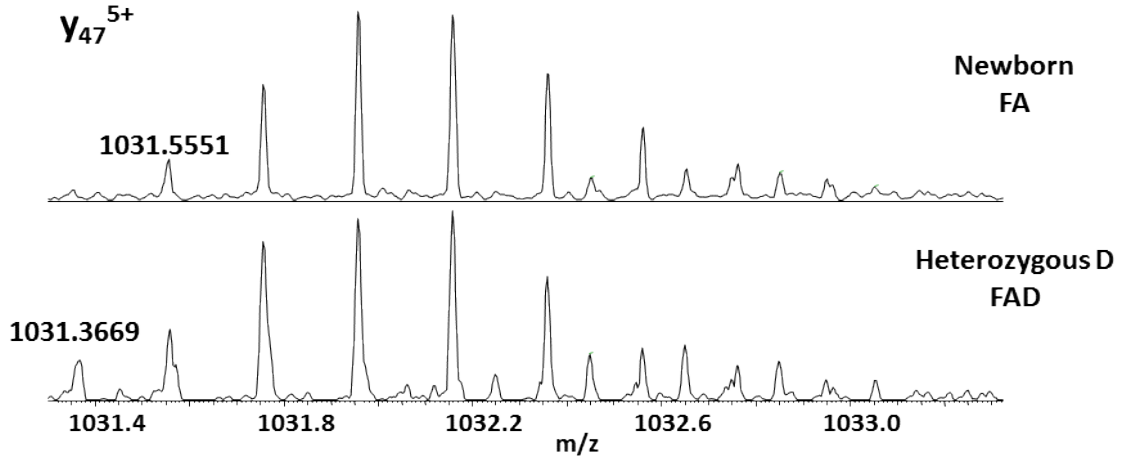

Figure 4.15 Expanded m/z region showing peaks corresponding to y_{47}^{5+} fragments observed following CID of β chain ions and variant HbD.

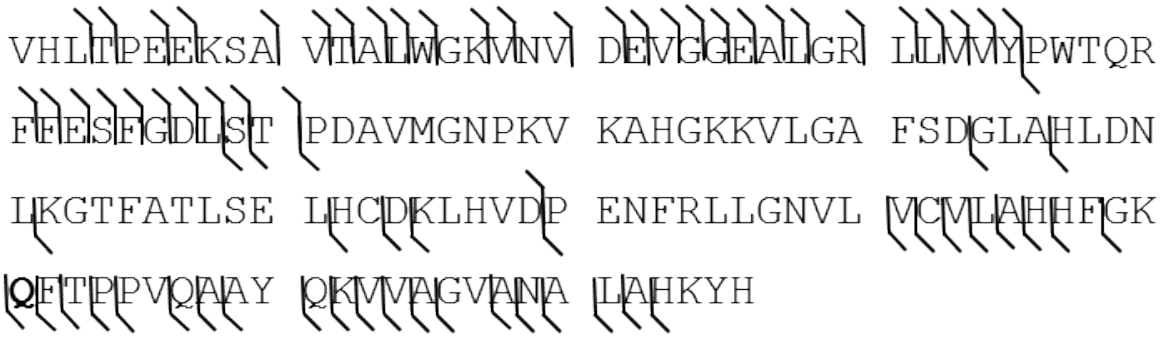

Figure 4.16 The CID sequence coverage of heterozygous FAD.

4.2.5 HbE Variant

The HbE variant occurs at position 26 on the β- globin chain where a glutamic acid is substituted for a lysine, resulting in a mass shift of Δm 0. 9476 Da [113]. **Figure 4.17** shows a comparison of SIM-mode mass spectra from a normal (FA) and FAE neonatal sample. In total, six heterozygous HbE samples were analysed. The spectra shows peaks corresponding to $[M + 14H]^{14+}$ ions of the α- chain (MW_{calc} 15117.8924), $[M + 15H]^{15+}$ ions of the β- chain (MW_{calc} 15117.8924) and $[M + 15H]^{15+}$ ions of the γ- chains (γ_A MW_{calc} 15986.2626 and γ_G MW_{calc} 16000.2782). It is not possible to unambiguously determine the presence of the HbE variant because the small shift (Δm -0.9476 Da) of the variant means that peaks from the intact globin overlap with those from the β-globin. Precursor ions corresponding to both the β-globin and the HbE variant were isolated and subjected to CID. The resulting fragmentation allowed unambiguous diagnosis of the phenotype can be made. CID resulted in a sequence coverage of 43% (**Figure 4.18)**. The assigned fragment ion list is shown in appendix 14. The variant is located at position 26 on the globin chain, no fragments were observed at this position. The normal b_{24}^{3+} fragment ion was observed (*m/z* 852.1195) verifying that the Hb variant is not present before position 25 on the globin chain. A peak at *m/z* 842.9724 corresponds to the b_{32}^{4+} with a mass shift of -0.9476 Da shown in **Figure 4.19**. A mass shift of -0.9476 is the result of a substitution of a glutamic acid for a lysine. The only glutamic acid between position 24 and 32 on the β -globin chain is located at position 26 therefore the amino acid substitution must have occurred there, diagnosing the neonate with an HbE variant. The CID fragmentation results are also able to determine if the variant is present in the carrier or

homozygous state. This is shown in **Figure 4.20**. The spectrum shows the b_{35}^{4+} fragment ion is present in both variant (MW_{meas} 933.2719) and normal (MW_{meas} 933.5097) form. The neonate is a carrier of HbE. In England, FAE carrier rate has been reported as 1 in 639 neonates [150].

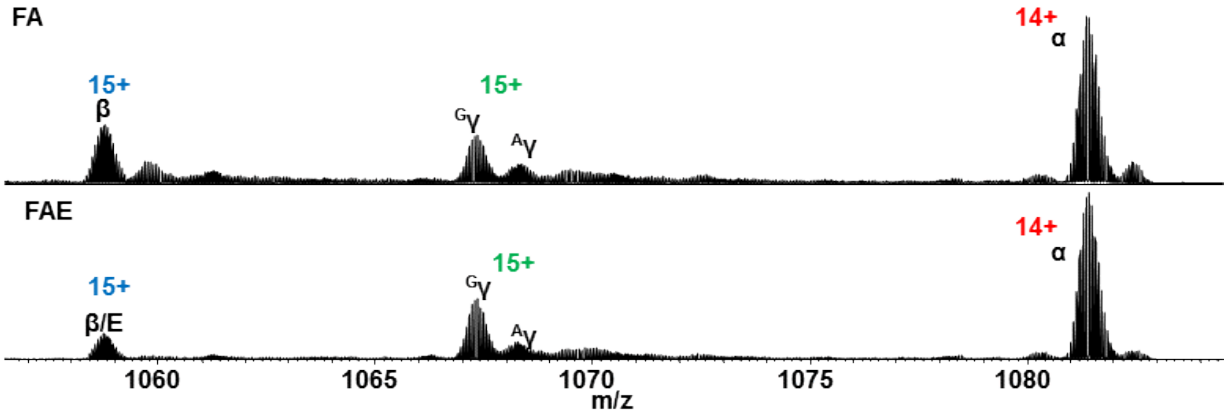

Figure 4.17 SIM mode mass spectra from normal FA (top) and heterozygous HbE (bottom). Red = α- globin chain, green = γ- globin chains and blue = β/E- globin chain.

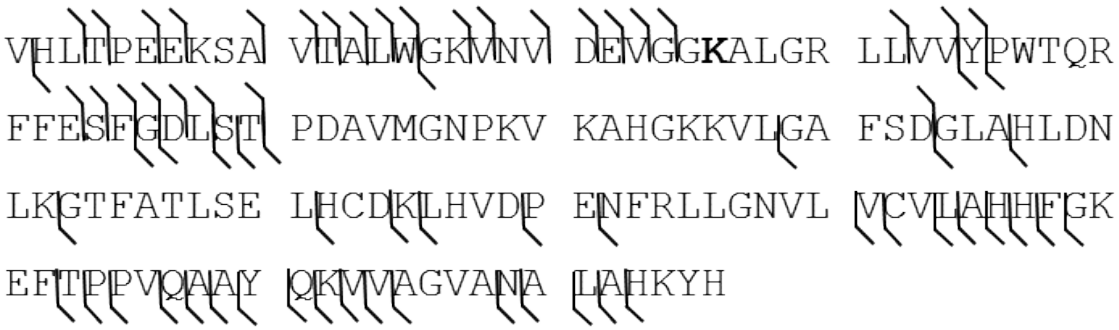

Figure 4.18 The CID sequence coverage of heterozygous FAE.

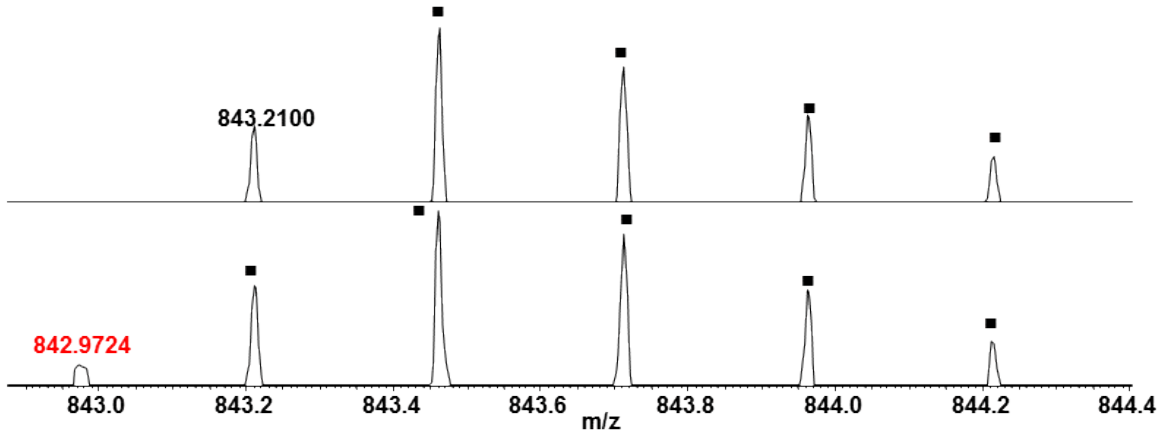

Figure 4.19 Expanded *m/z* region showing peaks corresponding to the isotopic distributions of b_{32}^{4+} fragments observed following CID of β chain ions (m/z_{calc} 843.2096) and (red) variant HbE (m/z_{calc} 842.9727).

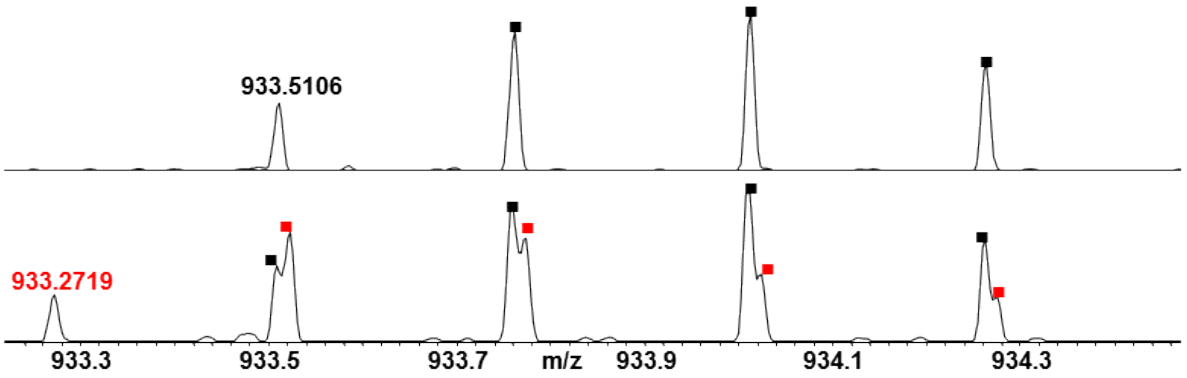

Figure 4.20 Expanded *m/z* region showing peaks corresponding to the isotopic distributions of b_{35}^{4+} fragments following CID of β chain ions(m/z_{calc} 933.5096) and HbE variant ions (m/z_{calc} 933.2727).

4.2.6 Hb SC

Figure 4.21 shows SIM mode mass spectra of heterozygous sickle (FAS) and compound heterozygous FSC samples. HbSC is a compound heterozygote composed of two normal α chains and two variant β chains. One abnormal chain is caused by a substitution of a Glu→ Lys at position 6 (HbC) on the β chain resulting in a mass shift of -0.9476 Da and the other abnormal chain is caused by the HbS variant, a substitution also at position 6 on the β chain, Glu→ Val (- 29.9745 Da). As described above it is possible to determine the presence of the sickle variant and its nature (homo- or heterozygous) in this mode. Nevertheless, there exists the possibility of misdiagnosis of compound heterozygotes- the mass spectra in figure 4.21 top (FAS) and bottom (FSC) appear identical. FSC has a prevalence rate of 1 in 7174 in England [150]. Two FSC samples were analysed in this study and the data presented are representative of both samples. For both the FAS and FSC sample, ions centred at *m/z* 1056 were isolated and subjected to CID. The protein sequence coverage observed for the Hb C variant ions was 26% (**Figure 4.22**). The fragment ion list is shown in appendix 15. **Figure 4.23** shows the expanded *m/z* region containing the b_{47}^{4+} fragments of the FAS and FSC variants. The peaks at m/z 1300.4444 and 1307.6914 in figure 4.23, bottom, confirm the presence of both HbS and HbC, i.e., that the sample is a compound heterozygote FSC. **Figure 4.24** is another example that confirms that the HbC variant is present.

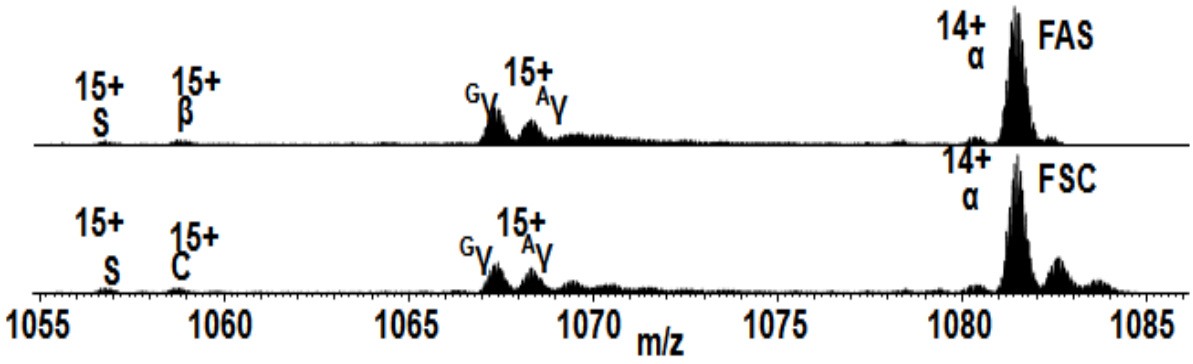

Figure 4.21 Selected ion monitoring mass spectra of normal neonate haemoglobin heterozygous and homozygous FAS (top) and FSC (bottom).

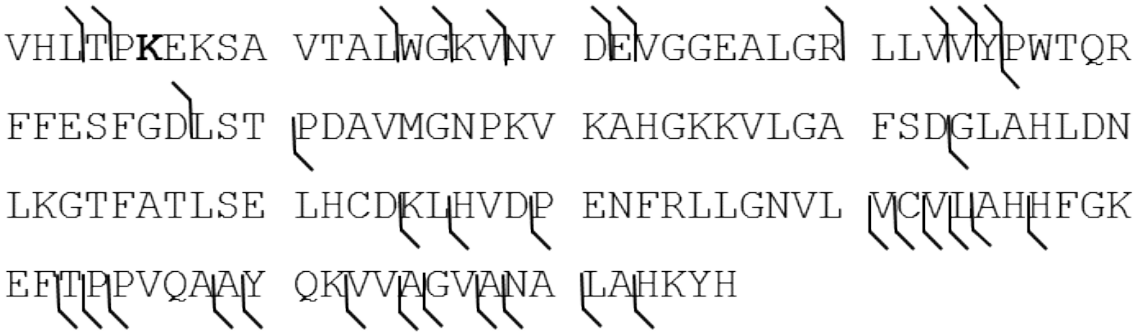

Figure 4.22 The CID sequence coverage (26 %) of the variant HbC ions in a heterozygous FSC sample.

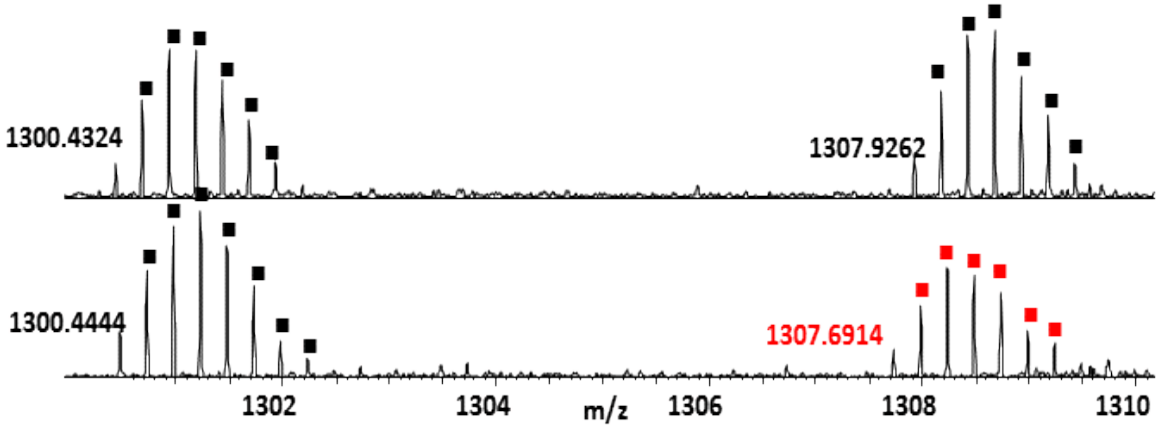

Figure 4.23 Expanded *m/z* region showing the b_{47}^{4+} fragments observed following CID of the sickle ions (m/z_{calc} 1300.4330), β chain ions (m/z_{calc} 1307.9266) and HbC variant ions (m/z_{calc} 1307.6897) (red).

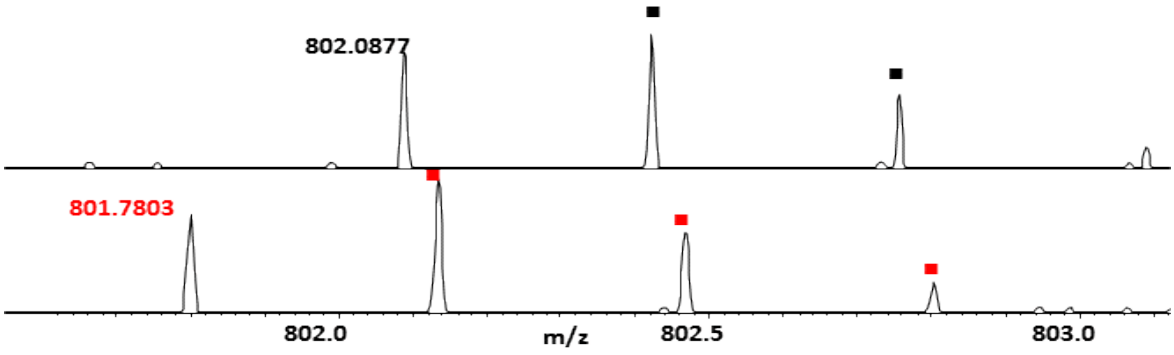

Figure 4.24 Expanded m/z region showing b_{22}^{3+} fragments for the β chain ions (m/z_{calc} 802.0884) and HbC variant ions (m/z_{calc} 801.7726) (red).

4.2.7 Hb SD

HbSD is another compound heterozygote where two variant chains are inherited instead of normal β chains: one HbS chain (substitution also position 6 on the β chain, Glu→ Val (+ 29.974)) and one HbD chain (Glu→Gln substitution at position 121 of the β chain, Δ -0.9840 Da). Only one Hb SD sample was available for analysis. The SIM-mode mass spectra of FAS and FSD samples shown in **figure 4.25** look identical. This is because the normal β globin chain differs in mass from the variant D Punjab/ Los Angeles chain by only 0.9840 Da. The presence of the sickle variant in both samples is clear in SIM mode. CID fragmentation is required to differentiate between clinically benign FAS and the severe medical disorder FSD. **Figure 4.26** shows the HbD variant ions assigned yielding protein sequence coverage of 14 %, appendix 16. Despite the low sequence coverage FSD is diagnosed. The y_{23}^{4+} (m/z_{meas} 608.8415) is obserbed at the expected m/z for normal β-globin chain the next fragment observed y_{32}^{4+} is present at m/z_{meas} 872.4143 corresponding to a variant with a mass shift of -0.9840 Da Glu→Gln (**Figure 4.27**). The only glutamic acid in the region between y_{23} and y_{32} is at position 121 diagnosing HbD Punjab/ Los Angeles (β121 Glu→Gln Δm -0.9840 Da).

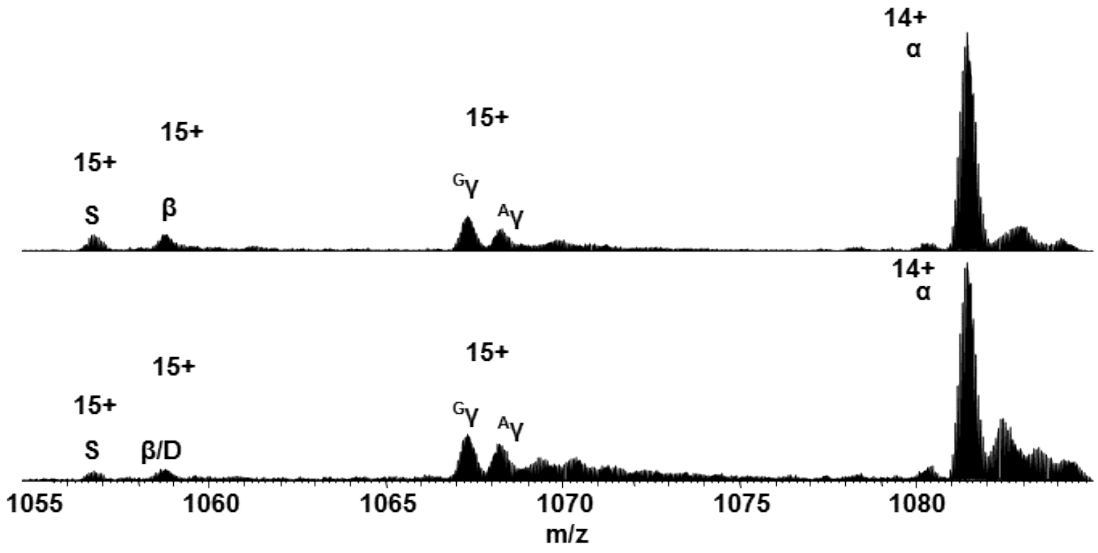

Figure 4.25 Selected ion monitoring mass spectra of normal neonate haemoglobin heterozygous and homozygous FAS (top) and FSD (bottom).

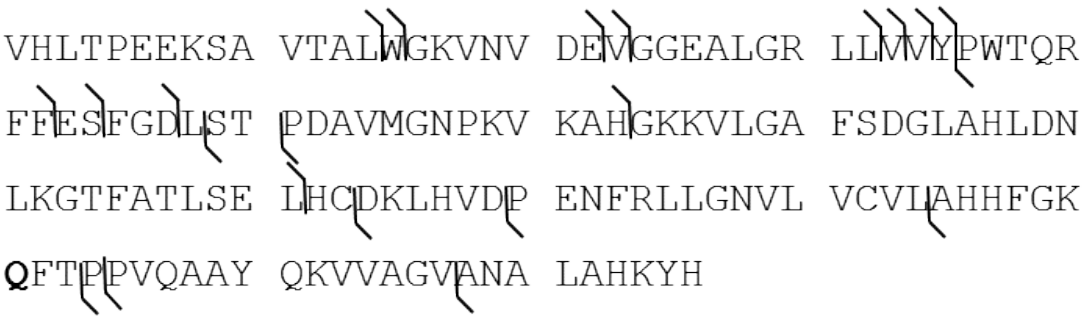

Figure 4.26 The CID sequence coverage of heterozygous FSD, variant HbD ions only.

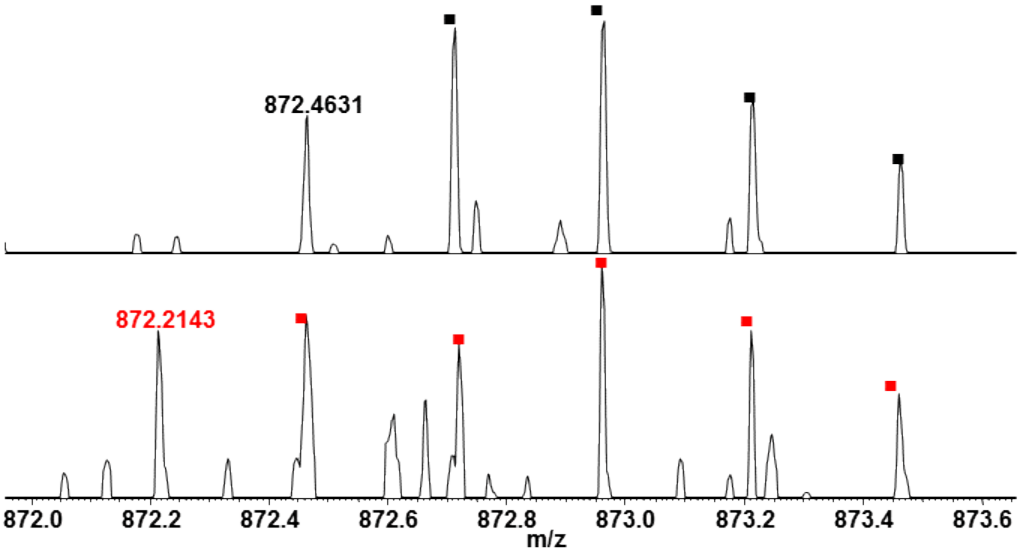

Figure 4.27 Expanded *m/z* region showing the y_{32}^{4+} fragments observed following CID of the β chain ions (m/z_{calc} 1307.9266) in the FAS sample and HbD variant ions (m/z_{calc} 872.2140) (red) in the FSD sample.

4.2.8 Beta thalassemia

The diagnosis of thalassemic variants poses a different challenge than the diagnosis the structural variants described above. Thalassemic variants result in the reduction in the synthesis of the globin chain and are not caused by amino acid substitutions that result in measureable mass shifts. Five different β thalassemia DBS samples were investigated in this study. The variant DBS underwent standard hospital screening (ceHPLC) and the samples were diagnosed as being β thalassemic. All the samples were then analysed by use of the LESA protocol. In full MS mode no peaks corresponding to β -globin chains were observed in any of the five β thalassemia samples. **Figure 4.28** shows a full MS spectrum for a β thalassemia variant. The spectrum was deconvoluted by use of the Xtract software to determine the monoisotopic masses of the measured ions. The measured MW of the α chain from the spectrum shown in figure 4.28 was 15 117.8346 Da (Δ -3.8 ppm), γ_G chain 15 986.1963 Da (Δ -4.2 ppm) and for the γ_A is 16 000.2017 (Δ -4.8 ppm). The β- globin chain was absent. The SIM mode mass spectrum (m/z range 1055-1090) also shows the absence of any peaks corresponding to the β- globin chain, **Figure 4.29**. All samples were analysed from full term neonates so the absence of β -globin cannot be explained by neonatal prematurity (production of β chain not yet switched on). The absence of the β chain in the samples must therefore be explained by the presence of the β thalassemia variant. The method offers the potential for diagnosis of β thalassemia.

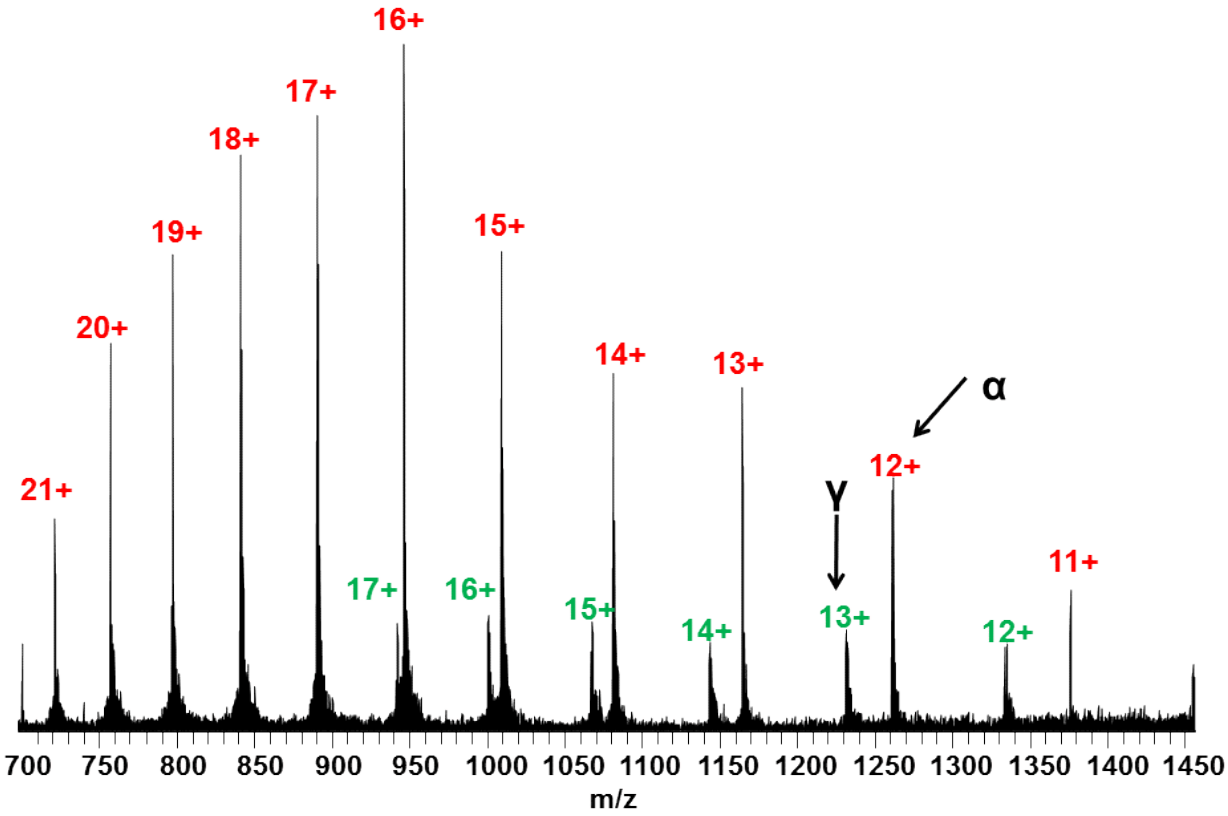

Figure 4.28. Full MS spectra of β thalassamina sample.

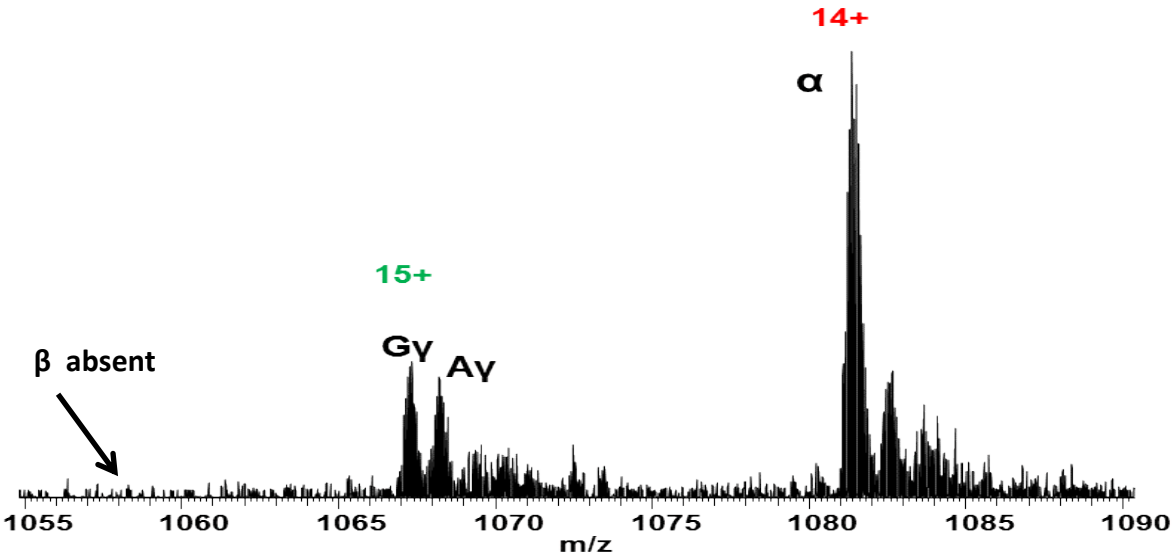

Figure 4.29 SIM mode mass spectrum of β thalassemia sample

4.3 Conclusion

The results presented in this chapter show that LESA method used in this investigation is able to diagnose clinically significant structural variants including HbS as well as variants with mass shifts of less than 1 Da (HbC, HbE etc) from neonatal DBS without the need for any sample digestion or preparation. The diagnosis of four (HbS, HbC, HbD and HbE) out of the five structural variants that must be detected during neonatal screening is presented above. The HbO-Arab variant is rare [120], no samples were available for analysis during this study. The O-Arab variant occurs at position 121 on the β -globin chain like the HbD variant and caused by a substitution of a glutamic acid for a lysine causing a mass shift of -0.9476 Da the same as variants HbC and HbE variants. As all these variants have been diagnosed using this direct surface sampling MS/MS diagnosis of HbO-Arab should also be possible.

The method also allowed for the successful diagnosis of the compound heterozygotes samples FSC and FSD. Further sickle compound heterozygote variant samples were not available to sample during this study due to their rarity. Variants FSE, FSO-Arab and other sickle compound heterozygotes including FSD have a combined prevalence of rate of 1 in 24, 871 [150]. The ability to determine other common structural variants suggests the diagnosis other sickle compound heterozygotes would be possible.

The method also has potential to be used in the diagnosis of β thalassimic disorders however further investigation (larger sample number, adult samples) is required.

Chapter 5: The Diagnosis of Unknown Variants in Neonatal Samples

5.1 Overview

The previous chapter revealed liquid extraction surface analysis (LESA) of newborn dried blood spots (DBS) coupled with high resolution mass spectrometry for the screening of common Hb variants [151]. The work presented in this chapter aims to demonstrate the robustness and versatility of the surface sampling method by applying the technique for the diagnosis of unknown variants. The method was applied to six unknown neonate samples (FAV1-6). The samples had been identified as variants using ceHPLC and IEF by the Birmingham Children's Hospital haemoglobinopathy department; however, the nature of the variant had not been diagnosed. In this analysis five of the six were diagnosed unambiguously. The sixth was either mis-assigned as a variant by the standard screening methods, or was an isomeric substitution (Ile→Leu or vice versa). All data were analyzed manually, with the attendant time costs, constituting a bottle-neck in the workflow and highlighting the need for data analysis software specifically for the diagnosis of Hb variants from top-down MS/MS data. Therefore, the freely available web based top-down protein characterization software Prosight PTM [91] (described in section 2.3.3) was investigated as an alternative to manual data analysis.

5.2. Results

5.2.1 FAV 1

Figure 5.1 shows the SIM-mode mass spectrum obtained from sample FAV1. Initially the mass spectrum appears identical to that expected for a normal neonatal sample[151]. Peaks corresponding to $[M + 14H]^{14+}$ ions of the α-chain and $[M + 15H]^{15+}$ ions of the γ-chains

Data shown in this chapter was published in Edwards RL, Griffiths P, Bunch J, Cooper HJ: Top-Down Proteomics and Direct Surface Sampling of Neonatal Dried Blood Spots: Diagnosis of Unknown Hemoglobin Variants. *Journal of The American Society for Mass Spectrometry* 23(11), 1921-1930 (2012).

(γA and γG) are present. However, the peak at m/z 1058 corresponds to a measured mass MWmeas 15856.3072 Da, suggesting the presence of a variant with a -1 Da mass shift. (The calculated mass of the β-chain is 15857.2497 Da). The ions centred at m/z 1058 were selected and subjected to CID. The resulting fragments were compared with those observed for CID of $[M + 15H]^{15+}$ ions of the β-chain. The fragment peaks observed in the CID mass spectrum of FAV1 and their assignments are shown in Appendix 17. The sample was identified as heterozygous Hb D-Iran. Hb D-Iran is caused by an amino acid substitution at position 22 on the β chain, glutamic acid to glutamine, causing a mass shift Δm 0.9840Da [152]. **Figure 5.2** shows an expanded m/z region containing the b_{21}^{3+} fragment ions of the β-chain (monoisotopic m/z_{calc} 759.0742) (top) and the equivalent region for the variant (bottom). **Figure 5.3** shows the expanded m/z region containing the b_{22}^{3+} fragment ions of the β-chain (monoisotopic m/z_{calc} 802.0884) (top) and the equivalent region for the variant (bottom). Whereas the regions containing the b_{21} fragments are identical, the regions containing the b_{22} fragments are not. Two sets of peaks are observed for the variant sample: One set corresponds to the isotope distribution of the b_{22}^{3+} fragment of the β-chain (monoisotopic m/z_{meas} 802.0865), confirming the heterozygous nature of the variant. The second set corresponds to the b_{22}^{3+} fragment of Hb D-Iran (m/z_{meas} 801.7623, m/z_{calc} 801.7604, Δ 2.4 ppm). Similar observations are made for the b_{23}^{3+} fragment ions shown in **Figure 5.4.** The protein sequence coverage obtained was 54 %, see **Figure 5.5.** It should be noted, however, that as this sample is heterozygous and the mass shift is <1 Da, both the normal β-chain and the variant ions were selected for CID. This is an unavoidable consequence of instrumental resolution limitations and overlapping isotopic distributions. Fifteen of the observed fragments were unique to Hb D-Iran, whereas the remaining 62 are common to both.

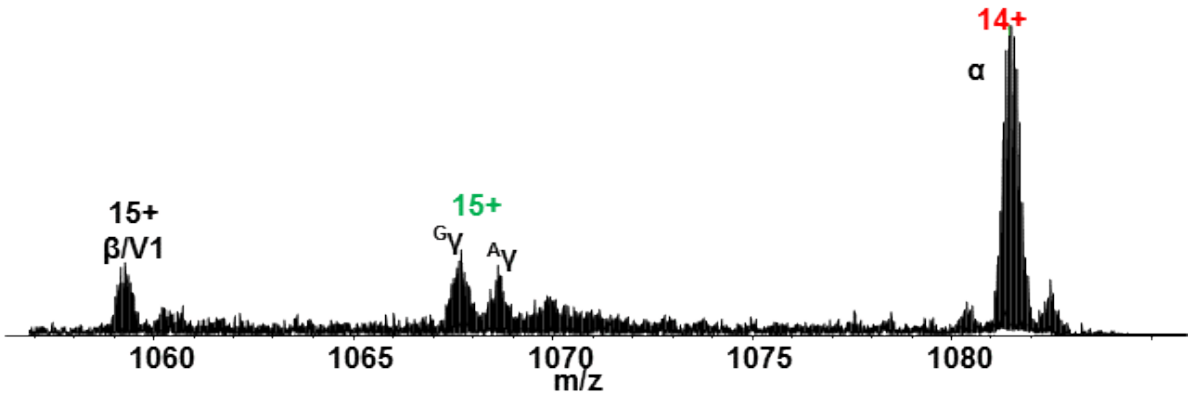

Figure 5.1. Selected ion monitoring mode mass spectrum of unknown variant FAV1. Red = α- globin chain, green = γ- globin chains and black = β/ variant chain.

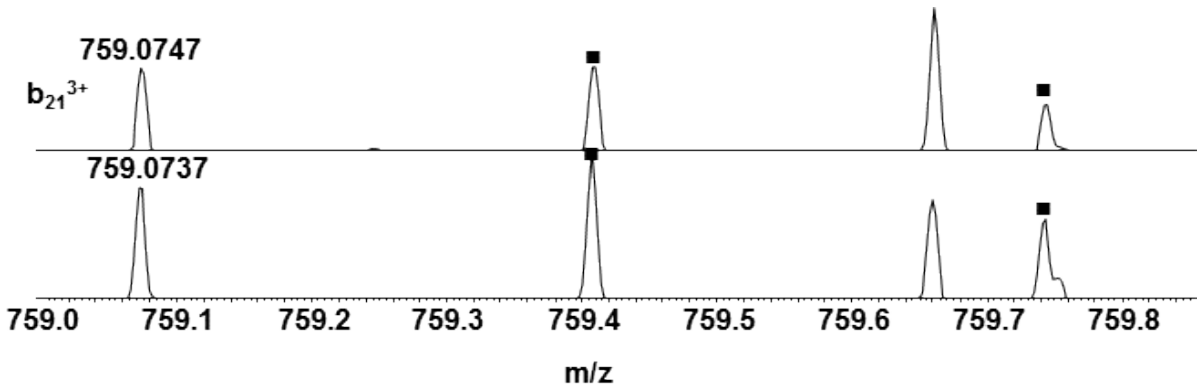

Figure 5.2 Expanded m/z region showing peaks corresponding to the isotopic distributions of (b) b_{21}^{3+} fragments (m/z calc 759.0742) observed following CID of $[M + 15H]^{15+}$ ions of β- chain (top) and variant Hb D-Iran (bottom).

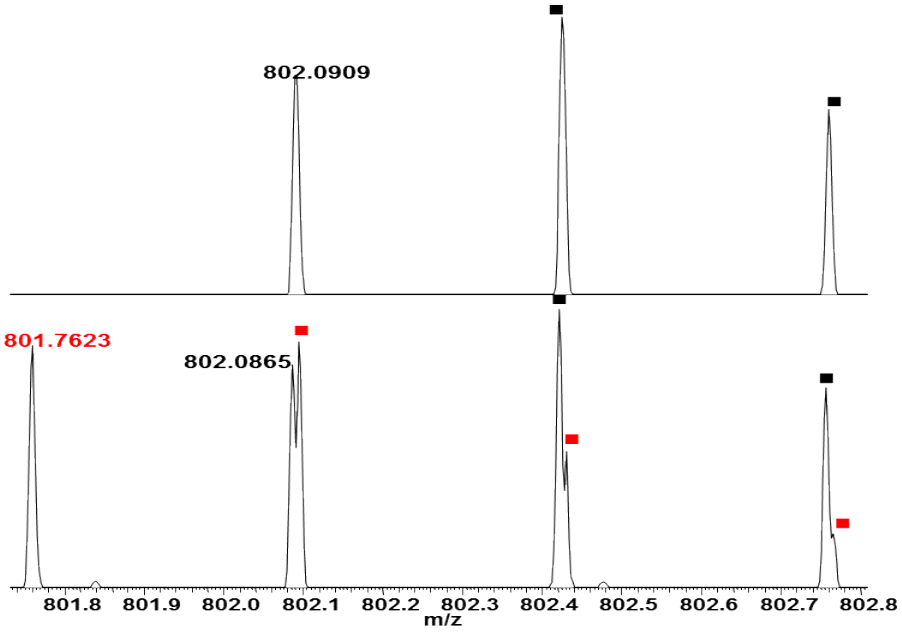

Figure 5.3 Expanded m/z region showing peaks corresponding to the isotopic distributions of b_{22}^{3+} fragments observed following CID of $[M + 15H]^{15+}$ ions of β chain (m/z_{calc} 802.0884) (top) (black) and variant Hb D-Iran (m/z_{calc} 801.7604) (bottom) (red).

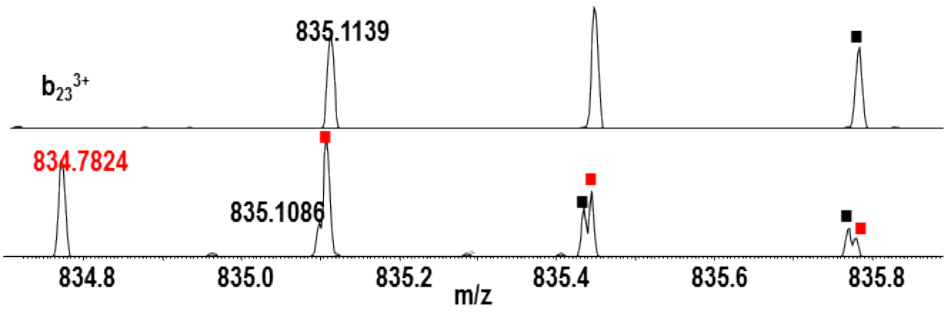

Figure 5.4 Expanded m/z region showing peaks corresponding to the isotopic distributions of b_{23}^{3+} fragments following CID of $[M + 15H]^{15+}$ ions β chain ions (m/z_{calc} 835.1112) (top) (black) and Hb D-Iran variant ions (m/z_{calc} 834.7832) (bottom) (red).

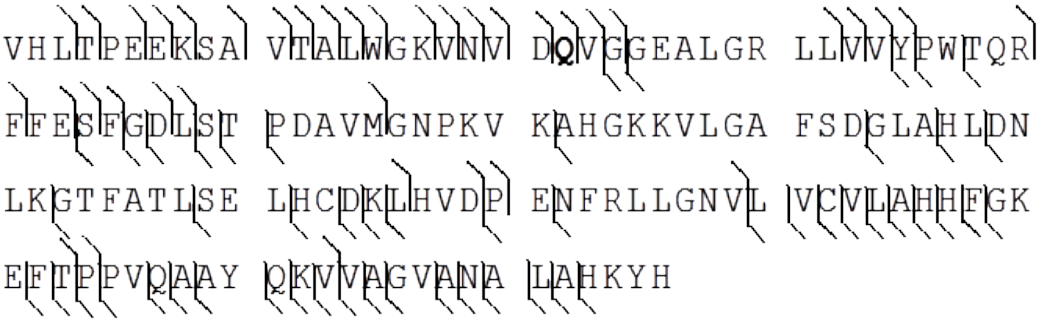

Figure 5.5 Manually assigned protein sequence coverage obtained following CID of the Hb D-Iran variant (54 %).

Figure 5.6 Data-base assigned protein sequence coverage obtained following CID of the Hb D-Iran variant (43 %). Fragment ion map generated by ProSight PTM.

Clearly, manual analysis of top-down mass spectrometry data for the diagnosis of hemoglobin variants is time consuming and is a potential barrier to adoption in the clinical laboratory. Ideally, data collection would be followed by automated searching against a hemoglobin variant database. To test that approach, CID MS/MS data for FAV1 was searched against the Hb D-Iran sequence using ProSightPTM 1.0 (the data-base analysis is described in detail in section 2.33). The aim was to mimic a search against a dedicated Hb variant database. The protein sequence coverage for the Hb D-Iran variant chain generated using ProSightPTM was 43 % (see **Figure 5.6**). The source of the discrepancy in sequence coverage was investigated further. For example, fragment ions b_{32}^{4+} and b_{33}^{4+} were assigned manually but were not identified by ProSightPTM (see **Figure 5.7 and 5.8**). For these fragments, the Xtract program had failed to distinguish the presence of two overlapping isotope distributions, one from the β-chain and one from the Hb D-Iran variant. Despite the difference in sequence coverage, the site of the substitution was identified and the variant could be unequivocally diagnosed.

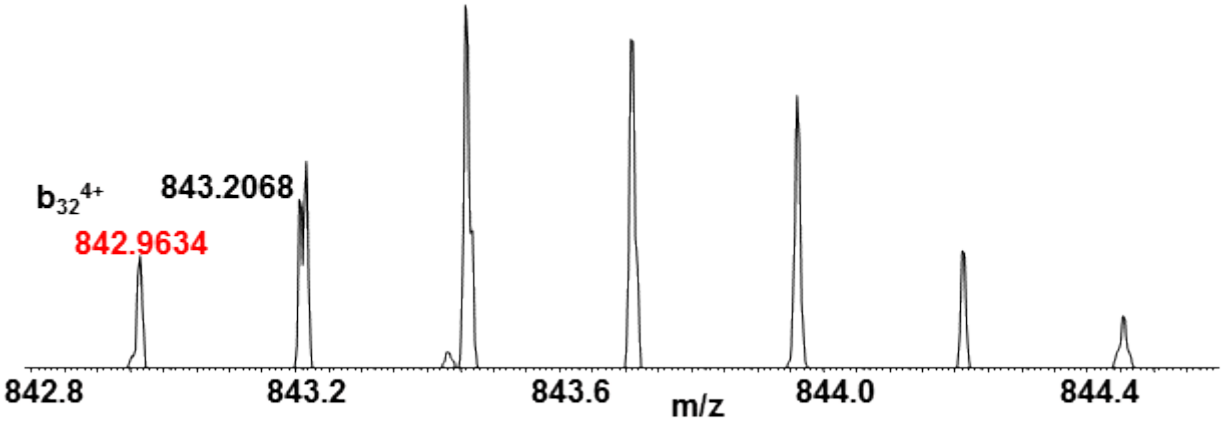

Figure 5.7 Expanded m/z region showing peaks corresponding to the isotopic distributions of b_{32}^{4+} fragments following CID of $[M + 15H]^{15+}$ ions β chain ions (m/z_{calc} 843.2096) (black) and Hb D-Iran variant ions (m/z_{calc} 842.9636) (red) .

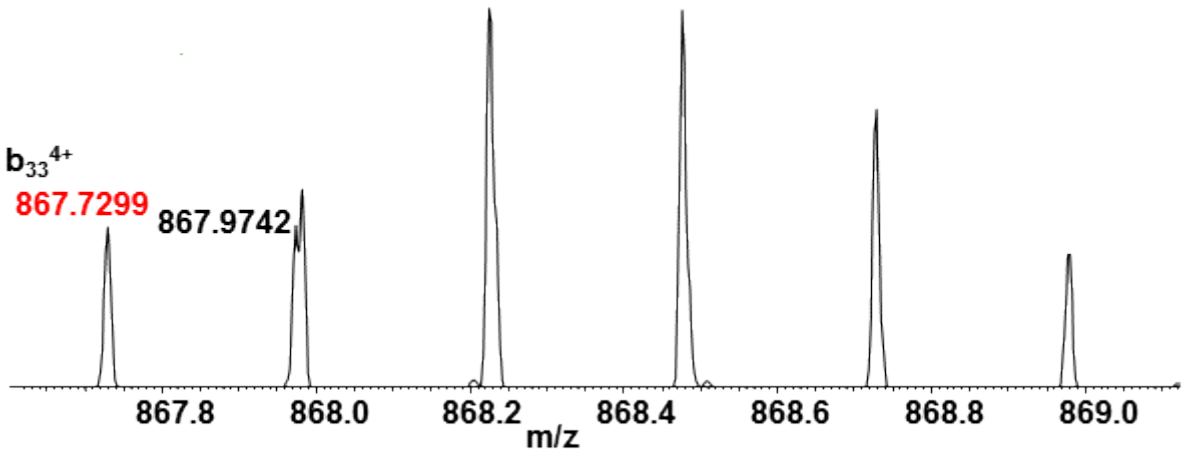

Figure 5.8 Expanded m/z region showing peaks corresponding to the isotopic distributions of b_{33}^{4+} fragments following CID of $[M + 15H]^{15+}$ ions β chain ions (m/z_{calc} 867.9767) (black) and Hb D-Iran variant ions (m/z_{calc} 867.7307) (red).

5.2.2. FAV2

A second unknown variant, FAV2, was also identified as heterozygous Hb D-Iran. Again, because of the small mass difference, both the variant and the β-chain were selected for CID. The fragment peaks observed in the CID mass spectrum of FAV2 and their assignments are shown in Appendix 18. **Figure 5.9** shows two sets of peaks are observed for the variant sample: One set corresponds to the isotope distribution of the b_{22}^{3+} fragment of the β-chain (monoisotopic m/z_{meas} 802.0884), confirming the heterozygous nature of the variant. The second set corresponds to the b_{22}^{3+} fragment of Hb D-Iran (m/z_{meas} 801.7624, m/z_{calc} 801.7604, Δ 2.5 ppm). As a further example, the $b23^{3+}$ fragment ions are shown in **Figure 5.10.** The protein sequence coverage obtained manually was 57 % (**Figure 5.11**). Again, the data were searched against the Hb D-Iran sequence using ProSightPTM and gave a coverage of 56 % **(Figure 5.12)**, and unequivocal diagnosis. A study reviewing screening results over a 10 year period in the North Thames health region showed that Hb D variants are the third most common variants with a carrier incidence rate of 1 in 631. Hb D-Iran is the second most prevalent of the Hb D variants after Hb D Punjab (Los Angeles) [12]. Heterozygous Hb D-Iran is clinically benign.

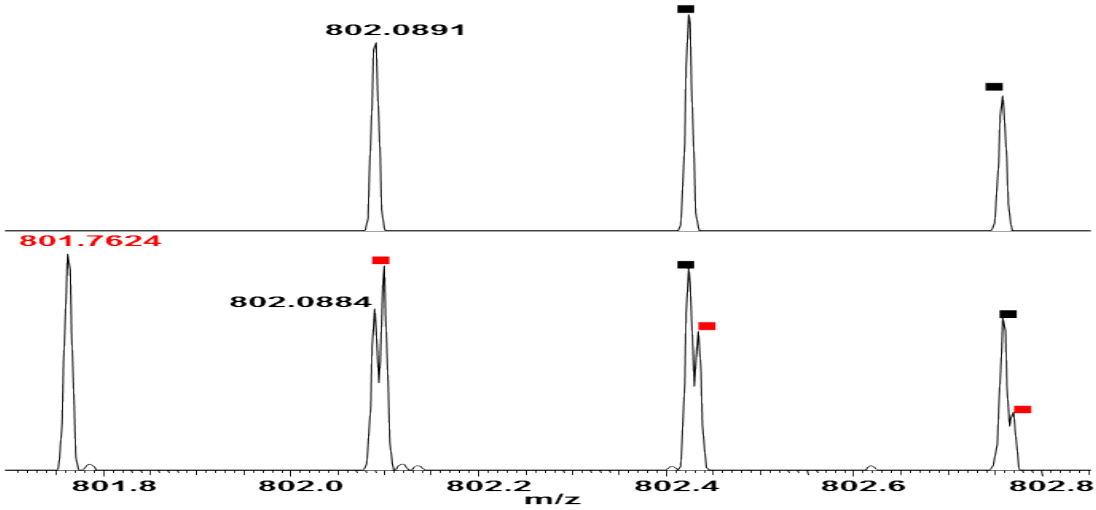

Figure 5.9 Expanded m/z region showing peaks corresponding to the isotopic distributions of b_{22}^{3+} fragments observed following CID of 15+ ions of FAV2 β chain (m/z_{calc} 802.0884) (top) (black) and variant Hb D-Iran (m/z_{calc} 801.7604) (bottom) (red).

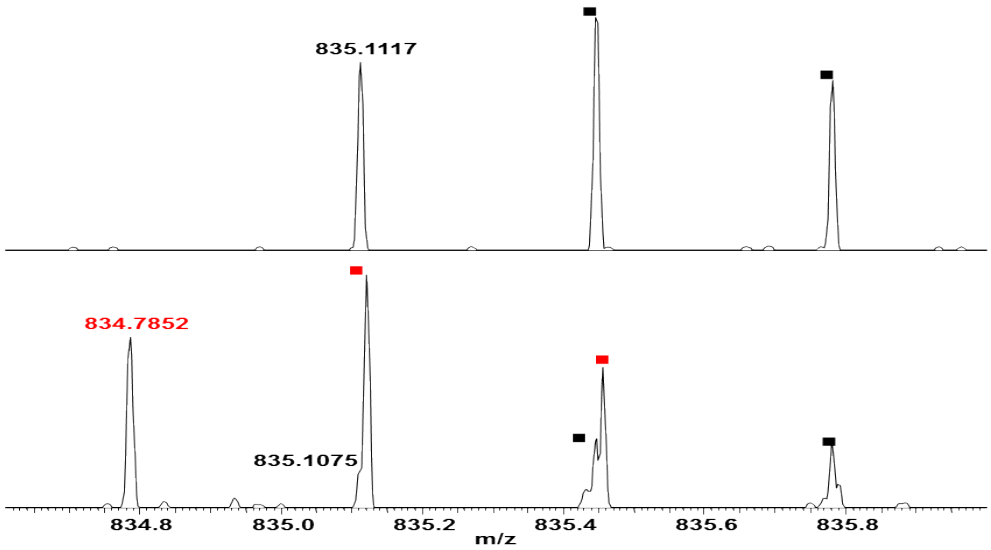

Figure 5.10 Expanded m/z region showing peaks corresponding to the isotopic distributions of b_{23}^{3+} fragments following CID of FAV2 15+ ions β chain ions (m/z_{calc} 835.1112) (top) (black) and Hb D-Iran variant ions (m/z_{calc} 834.7832) (bottom) (red).

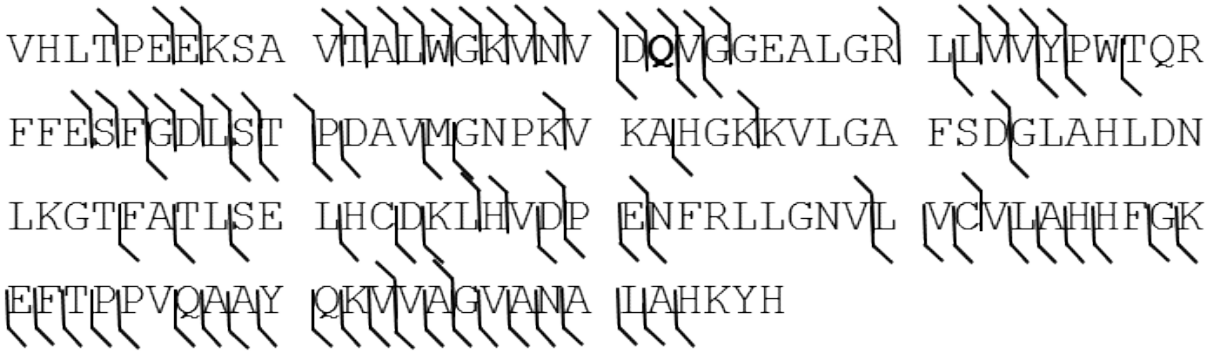

Figure 5.11 Manually assigned protein sequence coverage obtained following CID of the Hb D-Iran variant (57 %).

Figure 5.12 Data-base assigned protein sequence coverage obtained following CID of the Hb D-Iran variant (56 %).

5.2.3 FAV3

Figure 5.13 shows the SIM-mode mass spectrum obtained for variant FAV3. In addition to the peaks corresponding to the α, β, and γ chains, a peak is observed at m/z 1063 (MW*meas* 15926.24 Da) which corresponds to a β-chain mass shift Δm + 69.06 Da (i.e., substitution of a serine for an arginine residue). The presence of both the β-chain and the variant confirm the sample as heterozygous. The variant ions were isolated and fragmented by CID and ETD. The fragment peaks observed in the CID mass spectrum and their assignments are shown in Appendix 15. The β-chain contains five serine residues: Ser9, Ser44, Ser49, Ser72, Ser89. Two Ser→Arg variants are known: Hb Headington (Ser72→Arg) and Hb Vanderbilt (Ser89→Arg). The protein sequence coverage observed following CID was 46 % and is summarised in **Figure 5.14**. (Note, unlike Hb D Iran, there is no interference from β-chain fragments as the larger mass shift makes it possible to fully isolate the variant precursor ions). Potential substitution of Ser9, Ser44 and Ser49 are ruled out by the presence of the b_{11} through b_{49} fragments at the expected masses. The nature of the variant (Hb Vanderbilt or Hb Headington) could not be confirmed by the CID data due to the lack of fragments in the central region of the protein. The protein sequence coverage observed following ETD was 34 %, see **Figure 5.15**. The assigned fragment ions are shown in Appendix 20. Hb Vanderbilt is ruled out by the presence of fragments z_{61-63}, z_{67-70} and z_{74} at the expected masses. The variant is confirmed as Hb Headington [153] by the presence of the c + H_{72}^{6+} fragment (m/z_{meas} 1309.0297, m/z_{calc} 1309.0339, Δ 3.2 ppm) and the $z77^{7+}$ fragment (m/z_{meas} 1208.7861, m/z_{calc} 1208.7754, Δ 8.9 ppm), see **Figure 5.16** and **5.17**. The combined protein sequence coverage (CID + ETD) was 63 %. The diagnostically informative ETD spectrum was searched against the Hb Headington sequence using ProSightPTM, which returned a coverage of 20 % (**Figure 5.18**). The

variant was assigned on the basis of the c_{77}^{6+} fragment ion. That fragment was not assigned in the manual analysis due to the very low signal-to-noise of the monoisotopic peak.

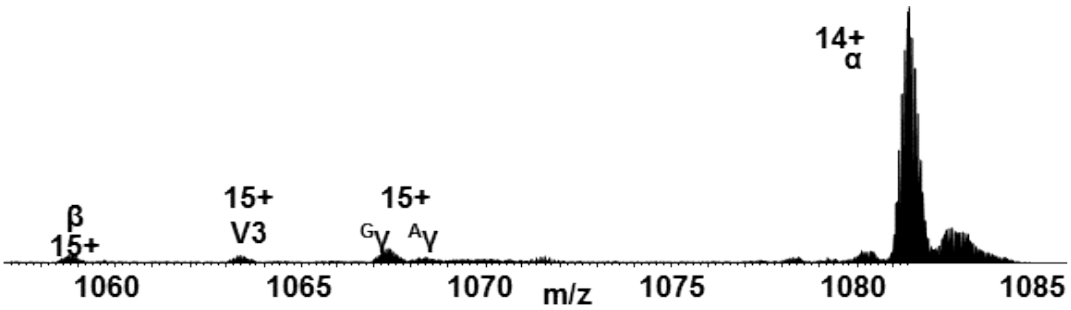

Figure 5.13 Selected ion monitoring mode mass spectrum of an unknown variant FAV3.

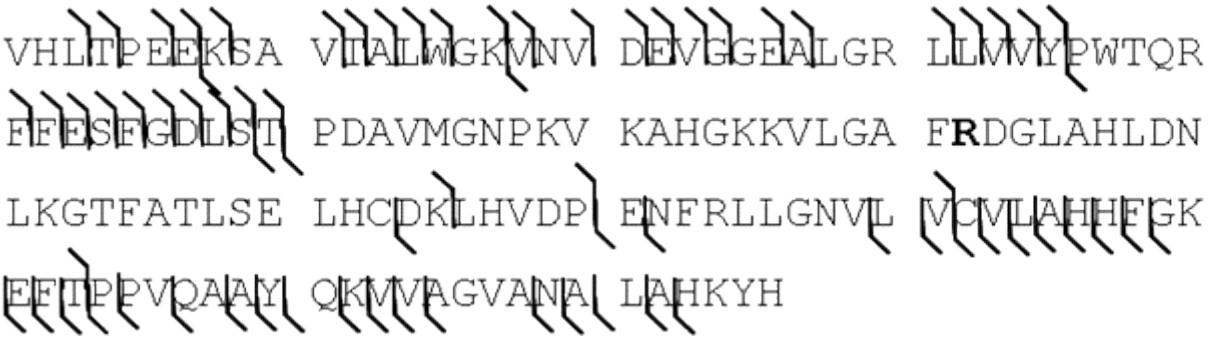

Figure 5.14 Protein sequence coverage observed following CID (46 %) of V3.

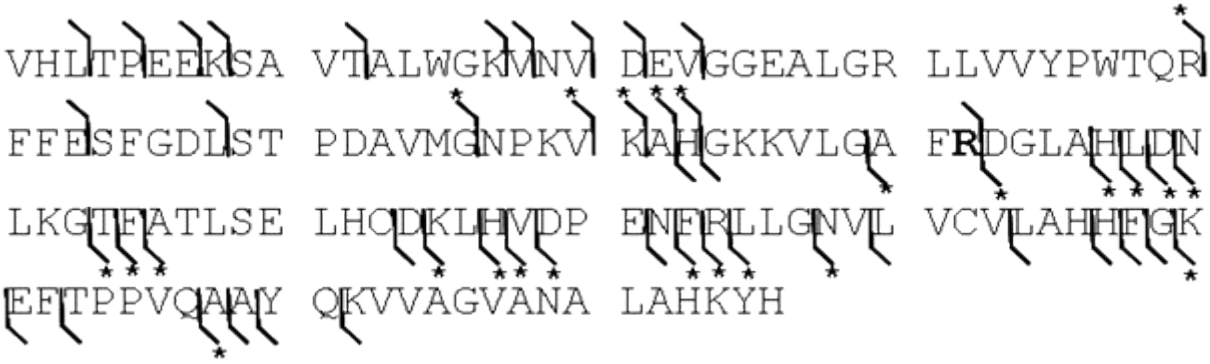

Figure 5.15 Protein sequence coverage observed following ETD (34 %) of V3. Site of substitution (Ser72→Arg) is shown in both but can only be confirmed by ETD. * Indicates fragments unique to ETD.

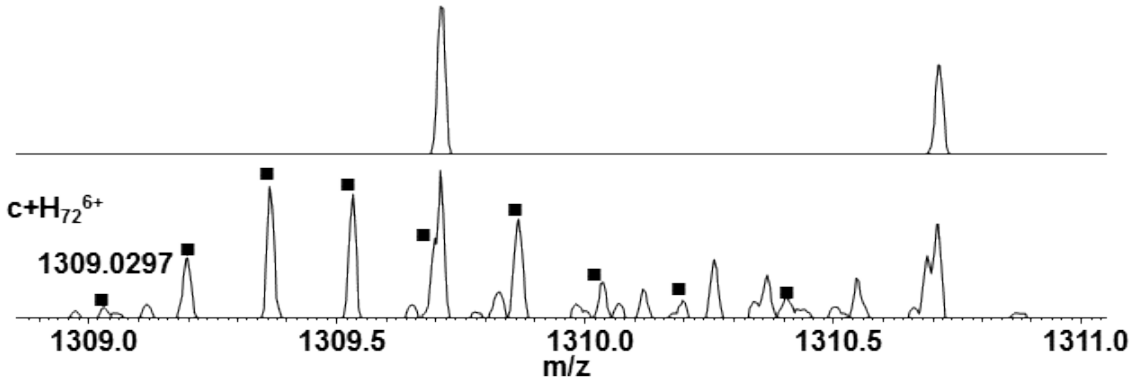

Figure 5.17 Expanded m/z region showing peaks corresponding to c + H_{72}^{6+} (m/z_{calc}1309.0339) fragment ions following ETD of 15+ ions of V3 (bottom) and the equivalent regions (above) from the ETD of 15+ ions of β chain.

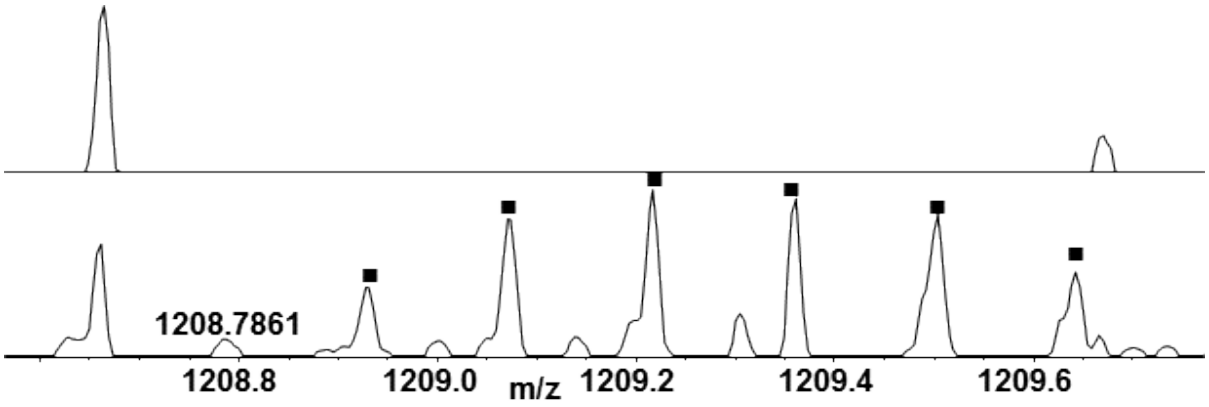

Figure 5.18 Expanded m/z region showing peaks corresponding to z_{77}^{7+} (m/z_{calc} 1208.7754) fragment ions following ETD of 15+ ions of V3 (bottom) and the equivalent regions (above) from the ETD of 15+ ions of β chain.

Figure 5.19 Data-base assigned protein sequence coverage obtained following ETD of the Hb Headington (20 %).

5.2.4 FAV4

Figure 5.20 shows the SIM-mode mass spectrum obtained for unknown variant FAV4. An additional peak is observed at m/z 1062, corresponding to a β-chain variant with mass shift Δm +58.01 Da (MW_{meas} 15915.27). A mass shift of +58.01 Da could either result from a Gly→Asp substitution or an Ala→Glu substitution. The β-chain contains thirteen glycine residues and fifteen alanine residues, offering numerous possibilities for variation. The ions at m/z 1062 were isolated and subjected to CID. The fragment peaks observed in the CID mass spectrum and their assignments are shown in Appendix 21. The protein sequence coverage, see **Figure 5.21** was 28 %, the lowest of all the variants studied. Nevertheless, the fragmentation observed narrows down the region of substitution to between Gly16 and Glu22: The b_{15}^{2+} fragment is observed at the expected mass m/z_{meas} 831.9470 (m/z_{calc} 831.9461, Δ 1.1 ppm) while the b_{22}^{3+} fragment is observed with the +58.01 mass shift, m/z_{meas} 821.4248 (m/zcalc 821.4236 Δ –1.7 ppm), see **Figure 5.22** and **5.23**. The only glycine or alanine residue in this region is Gly16. Thus the variant corresponds to a Gly16→Asp substitution (i.e., Hb J-Baltimore) [154]. The ProsightPTM search of the data against the Hb J-Baltimore sequence gave a sequence coverage of 19 % (**Figure 5.24**). Again the reduced coverage appears to be the result of incomplete deconvolution by the Xtract program. Nevertheless, the variant could be diagnosed unambiguously.

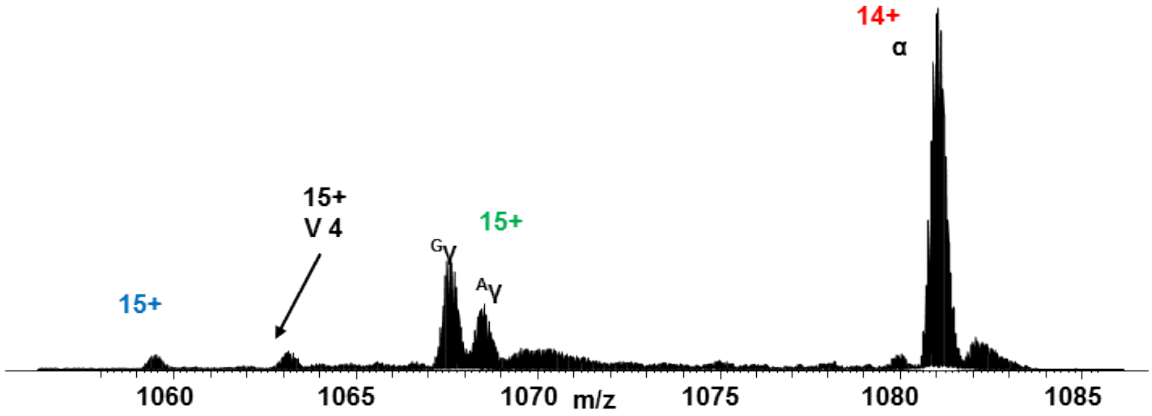

Figure 5.20 Selected ion monitoring mode mass spectra spectrum of an unknown variant FAV4. Red = α- globin chain, green = γ- globin chains and blue = β- globin chain.

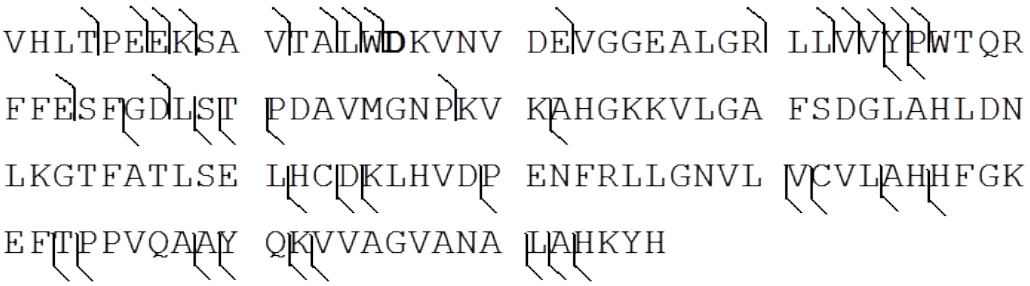

Figure 5.21. Manually assigned protein sequence coverage observed following CID of V4 (Hb J-Baltimore), 28 %.

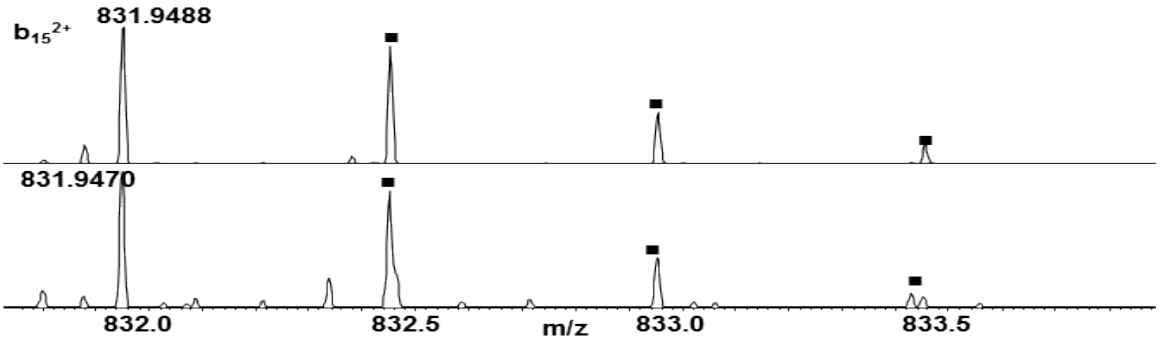

Figure 5.22 Expanded m/z region showing peaks corresponding to isotopic distributions of the b_{15}^{4+} fragments (m/zcalc 831.9461) observed following CID of 15+ ions of β-chain (top) and variant Hb J Baltimore (bottom).

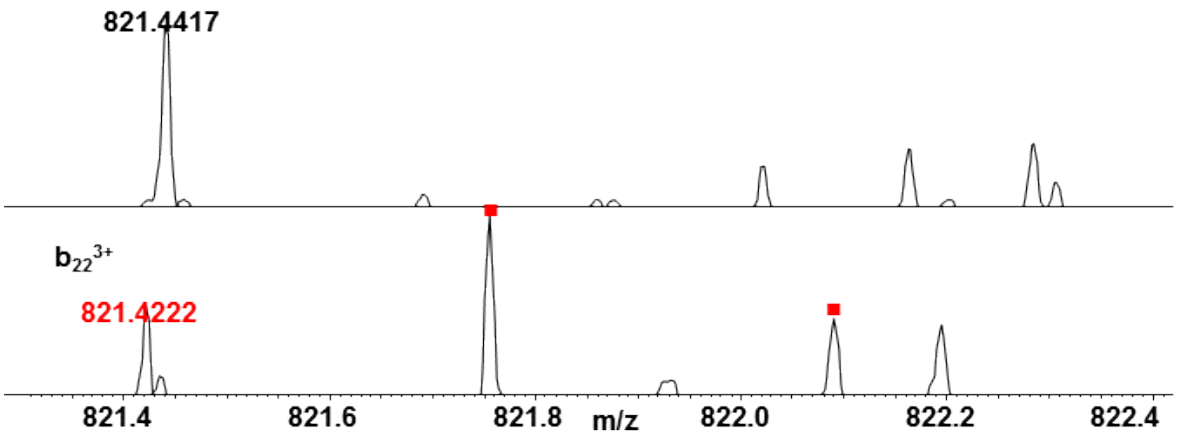

Figure 5.23 Expanded m/z region showing peaks corresponding to isotopic distributions of b_{22}^{3+} fragments following CID of $[M + 15H]^{15+}$ ions of variant Hb J-Baltimore (m/z_{calc} 821.4248), (bottom) and the equivalent m/z region from the CID mass spectrum of $[M + 15H]^{15+}$ ions of β-chain (top).

Figure 5.24 Data-base assigned protein sequence coverage obtained following CID of the Hb J-Baltimore (19 %)

5.2.5 FAV5

The SIM-mode mass spectrum obtained for the variant FAV5 is shown in **Figure 5.25**. Peaks corresponding to 15+ ions of β and γ chains and 14+ ions of α-chains are observed, confirming the variant is heterozygous. In addition, a peak corresponding to 14+ ions was observed at m/z 1090 suggesting the presence of an α-chain variant. β variants are more common than α variants: ~60 % are β variants [155]. In addition, β variants are more abundant because only two β globin chains are inherited (one per chromosome) by an individual compared with four α globin chains, therefore inheritance of an β variant makes up 50 % of the Hb content whereas an α variant would be 25 % [156]. The measured mass of the α-chain was MW_{meas} 15116.95 Da (MW_{calc} 15116.89 Da) and the measured mass of the variant was 15229.88 Da, a mass shift Δm of +113 Da. That mass shift does not correspond to any possible amino acid substitution, however it does correspond to insertion of an isoleucine or leucine residue within the sequence. The α-chain and the variant were each selected for CID. The fragments observed for the α-chain are shown in Appendix 18. The α-chain sequence coverage was 54 %. The CID fragments observed for the variant are shown Appendix 23. The variant was identified as Hb Phnom Penh which arises through insertion of an isoleucine between position 117 and 118 on the α-chain coded by the α -1 gene [157]. The protein sequence coverage was 46 % and is summarised in **Figure 5.26**. Fragments y_3 through y_{24} were observed at the expected masses. **Figure 5.27** shows an expanded m/z region containing the y_{25}^{3+} of the Hb Phnom Penh variant (m/z_{meas} 902.1746, m/z_{calc} 902.1726 Δ 2.2 ppm) (i.e., the fragment adjacent to the insertion, and the corresponding region from the CID of the α- chain). Another example, the y_{48}^{4+} fragment (m/z_{meas} 1305.4803, m/z_{calc} 1305.4768 Δ 2.7 ppm), is shown in **Figure 5.28**. The

ProsightPTM search of the data against the Hb Phnom Penh sequence gave a sequence coverage of 44 % (**Figure 5.29**) and unequivocal diagnosis.

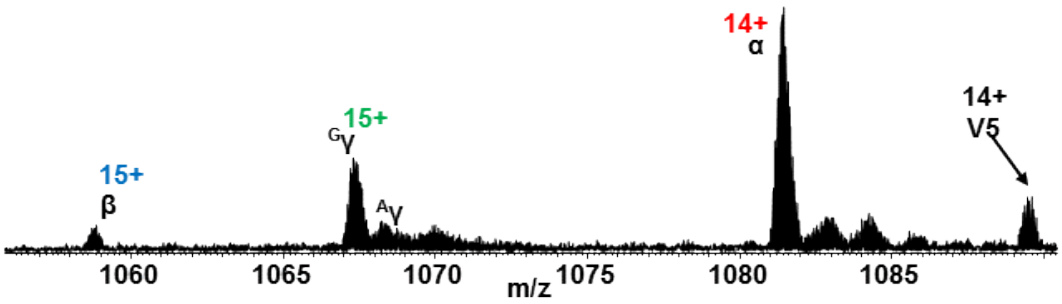

Figure 5.25 Selected ion monitoring mode mass spectrum of an unknown variant FAV5.

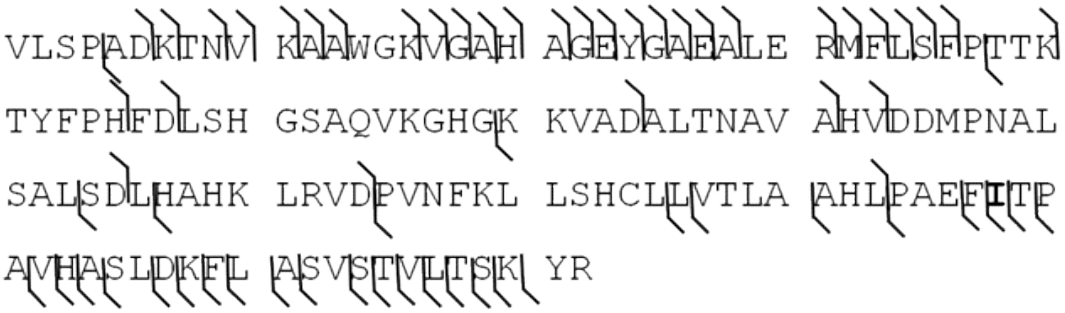

Figure 5.26 Manually assigned protein sequence coverage observed following CID of V5 (Hb Phnom Penh), 46%.

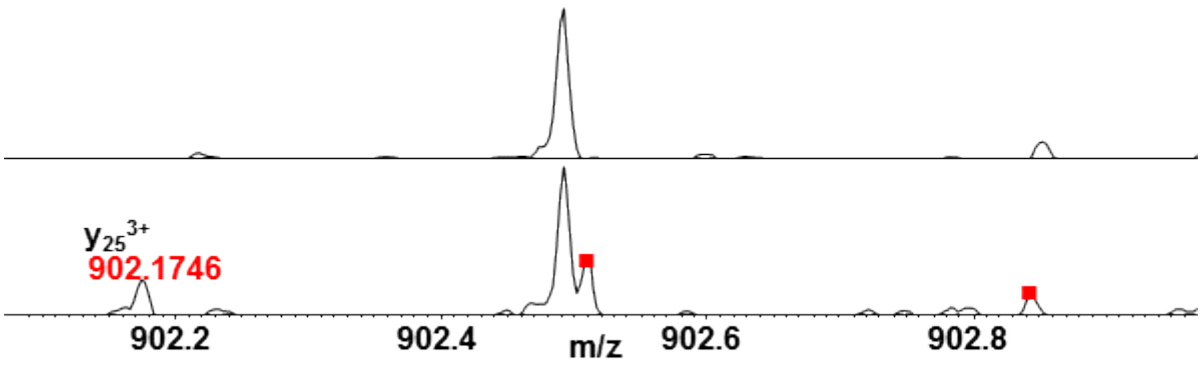

Figure 5.27 Expanded m/z regions showing peaks corresponding to isotopic distributions of (c) y_{25}^{3+} fragments (m/z_{calc} 902.1726) observed following CID of 14+ ions of variant V5 (Hb Phnom Penh) (bottom) and the equivalent m/z regions from the CID mass spectrum of 14+ ions of α-chain (top)

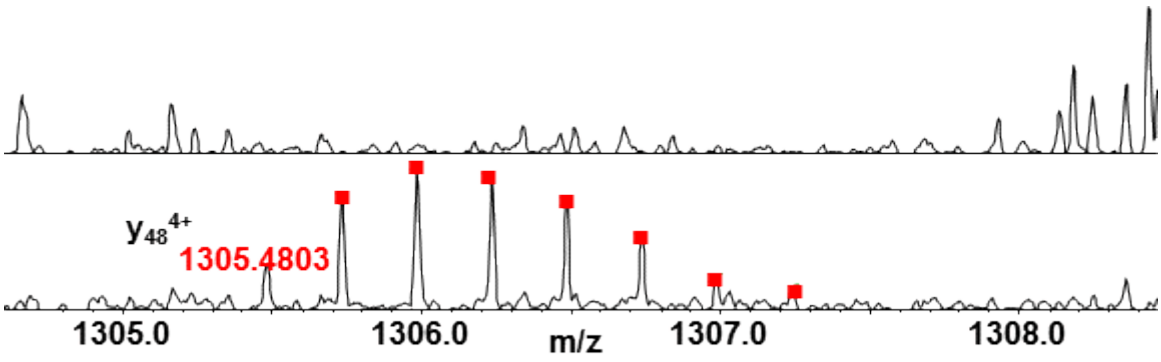

Figure 5.28 Expanded m/z regions showing peaks corresponding to isotopic distributions of y_{48}^{4+} fragments (m/z_{calc} 1305.4768) observed following CID of $[M + 14H]^{14+}$ ions of variant V5 (Hb Phnom Penh) (bottom) and the equivalent m/z regions from the CID mass spectrum of $[M + 14H]^{14+}$ ions of α-chain (top).

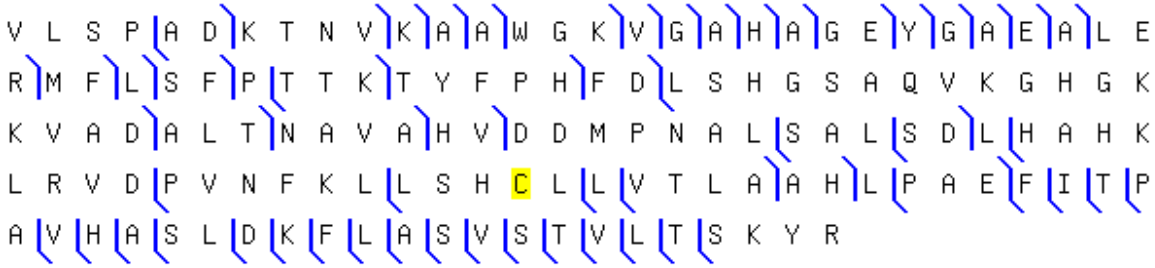

Figure 5.29 Data-base assigned protein sequence coverage obtained following CID of the Hb Phnom Penh (44%).

5.2.6 FAV6

The SIM-mode mass spectrum for the final unknown variant FAV6 is shown in **Figure 5.30**. The mass spectrum does not reveal the presence of any additional peaks. The measured masses of the α, β, Gγ and Aγ chains were MW_{meas} 15117.8211 (MW_{calc} 15117.8924 Δ -4.7 ppm), MW_{meas} 15858.3217 (MW_{calc} 15858.2570 Δ 4.1 ppm), MW_{meas} 15986.3329 (MW_{calc} 15986.2626 Δ 4.4 ppm), MW_{meas} 16000.2849 (MW_{calc} 16000.2782 Δ 0.4 ppm), respectively. Therefore CID of the peaks centered at m/z 1059 (β-chains), m/z 1068 (γ-chains) and m/z 1081 (α- chains). The CID protein sequence coverages were 46 % (β- chain), 45 % (α-chain), 43 % (Gγ-chain) and 32 % (Aγ-chain). The ETD protein sequence coverages were 17 % (β-chain), 44 % (α-chain), 28 % (Gγ-chain) and 15 % (Aγ-chain). The CID and ETD fragments observed are detailed in Appendix 24-30. No erroneous fragment peaks were observed for any of the globin chains suggesting that either the sample had been incorrectly identified as a variant in the screening process or contains an isomeric substitution (i.e., Leu→Ile or vice versa). (It is worth noting that no such substitution is currently described in the HbVar database [3].) It was not possible to reconfirm the screening results because the sample was anonymized prior to mass spectrometry analysis. The estimated false positive rate in screening is ~1 % [158] and documented sources of error include administration errors or unfocused/merged bands in IEF [159].

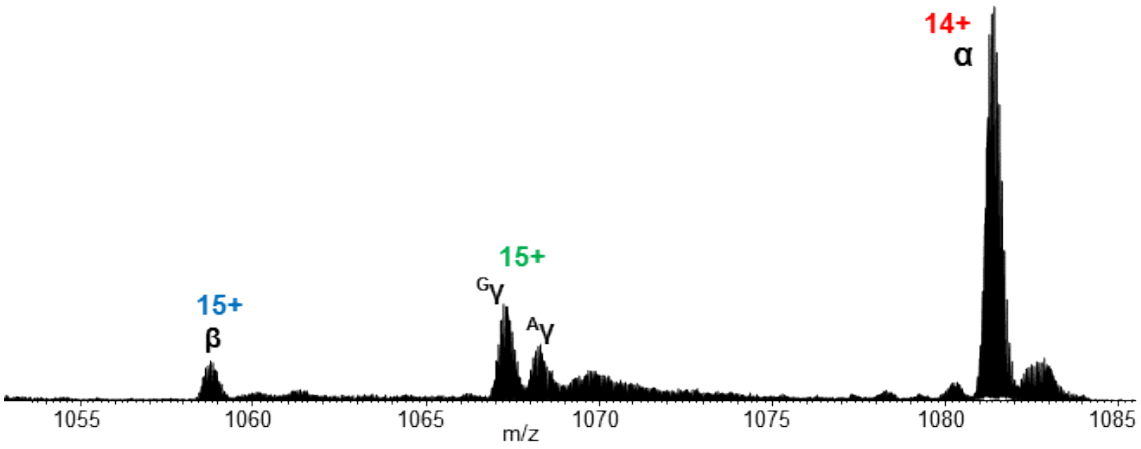

Figure 5.30 Selected ion monitoring mode mass spectrum of an unknown variant FAV6.

Red = α- globin chain, green = γ- globin chains and blue = β- globin.

5.3. Conclusion

The results presented in this chapter demonstrate the robustness of the direct surface sampling top-down proteomics approach and confirm that the approach is applicable both for screening and diagnosis. Results show direct surface sampling of newborn dried blood spots coupled with top down mass spectrometry may be used for the diagnosis of unknown haemoglobin variants. Six samples which had been identified as variants by ceHPLC and IEF, but which could not be diagnosed by those methods, were analyzed. Two of the samples were determined to be heterozygous Hb D-Iran following CID of the overlapping β-chain and variant peaks. Mass analysis of the third sample revealed the presence of a Ser→Arg β-chain variant. CID of the variant narrowed the possibilities to Hb Headington or Hb Vanderbilt. ETD confirmed the variant as Hb Headington. Mass analysis of the fourth variant suggested either a Gly→Asp or Ala→Gln β-chain substitution. CID confirmed the variant as Hb J Baltimore. The fifth sample was confirmed as a rare α-variant with a mass shift of +113 Da. CID revealed it to be the insertion variant Hb Phnom Penh. The mass analysis, CID and ETD of the sixth sample do not indicate the presence of a variant. Either the sample had been incorrectly identified as a variant by the ceHPLC and IEF (the false positive rate in screening is estimated as ~1 % [158]) or contained an isomeric substitution (Ile→Leu or vice versa).

Chapter 6: Native Mass Spectrometry of Haemoglobin

6.1 Overview

The previous two chapters have demonstrated the effectiveness of direct surface sampling of DBS coupled with electrospray ionisation mass spectrometry of intact (heme free) apo - α and apo-β -globin chains [151, 160]. Several studies have demonstrated the potential of ESI mass spectrometry as a tool for the analysis of intact Hb non-covalent protein-protein and protein-ligand complexes [161, 162], often termed native mass spectrometry [163], in purified Hb aqueous solution phase samples. Native mass spectrometry allows for the study of structural aspects of proteins and protein complexes [164] by combining soft ionisation techniques with volatile buffers (ammonium acetate based). These volatile buffers allow for the preservation of non- covalent interactions, whereas traditional ESI solutions containing an acidified organic solvent (e.g. methanol) serve to denature quaternary and tertiary protein structure [165].

The work presented in this chapter investigates the viability of LESA coupled with native MS for the study of Hb non-covalent interactions. The rationale for the study was to assess the potential application of the technique for the study of thalassemic variants. Thalassemia is responsible for the formation of abnormal Hb tetramers. For example β-thalassemia is caused by a reduction in the synthesis of β- globin chains resulting in a surplus of α- globin chains which can lead to the formation of all α – chain tetramers, Hb Barts [166]. Preserving the quaternary structure of Hb by native MS could allow for observation of these abnormal tetramers, and therefore the identification of thalassemic disorders.

6.2. Results

6.2.1 Direct infusion of haemoglobin solution

Figure 6.1 shows a full mass spectrum (*m/z* range 600- 4000) obtained following direct infusion ESI of a 10 μM solution of Hb. The ESI solution consisted of water/methanol/formic acid (48.5:48.5:3,*v/v*). The capillary temperature was 250 ºC. The free heme (m/z_{meas} 616.1765, m/z_{calc} 616.1773, Δ -1.30 ppm) is the dominant species in the mass spectrum. The mass spectrum also contains multiply-charged peaks corresponding to apo-α (MW 15117.8924) and apo-β chains (MW 15858.2570). No multiply-charged species are observed above *m/z* ~1800.

Figure 6.2 shows a full 'native' mass spectrum obtained following direct infusion ESI of a 10 μM solution of Hb in 10 mM ammonium acetate at a reduced capillary temperature of 200 ºC. The high *m/z* range of 600-4000 was chosen to maximise the chance of observing tetramer ions and because no peaks corresponding to Hb were observed below m/z 600 in any data presented here. The sheath gas pressure was 0.7 psi and a voltage of 0.75 kV was applied to the analyte containing tip. The change in ESI solution dramatically affects the species observed in the spectrum. The free heme is no longer the dominant species. Multiply charged (heme attached) holo α- and holo β- chain ions are now observed. The non-covalent interactions between the heme group and the globin chains has been maintained. Two types of dimers are also observed:α- plus β- globin with either one or two heme groups attached. Species can be confidently assigned up to *m/z* ~3000. There is a low abundance multiply charged peak at m/z 3800. It was not possible to deconvolute the suspected tetramer using the Xcalibur xtract programme so its presence could not be

confirmed. This proved the case for all suspected tetramers in data obtained throughout this chapter. A major problem encountered when using ammonium acetate as the electrospray solution was poor spray stability. To overcome this, small amounts of methanol were added to the electrospray solution with the aim of improving electrospray stability while maintaining Hb non-covalent interactions. An electrospray solution of 10 mM ammonium acetate with 5 % methanol (containing 10 μM Hb) proved optimal in maximising spray stability and yielding reproducible results without denaturing non-covalent interactions, **Figure 6.3**. The mass spectra obtained both with and without the addition of methanol appear identical. **Figure 6.4** shows a mass spectrum obtained when ammonium acetate concentration was increased from 10 mM to 100 mM in the ESI solution. The resultant mass spectrum shows an increase in the relative abundance of the $\alpha^{h}\beta^{h12+}$ and $\alpha^{h}\beta^{h11+}$ dimers and an increase in relative abundance of the suspected tetramer peaks. Nevertheless, it was still not possible to confirm these species as tetramers, probably due to their low abundance. Charge states observed in this spectrum range from $[M + 20H]^{20+}$ to $[M + 7H]^{7+}$.

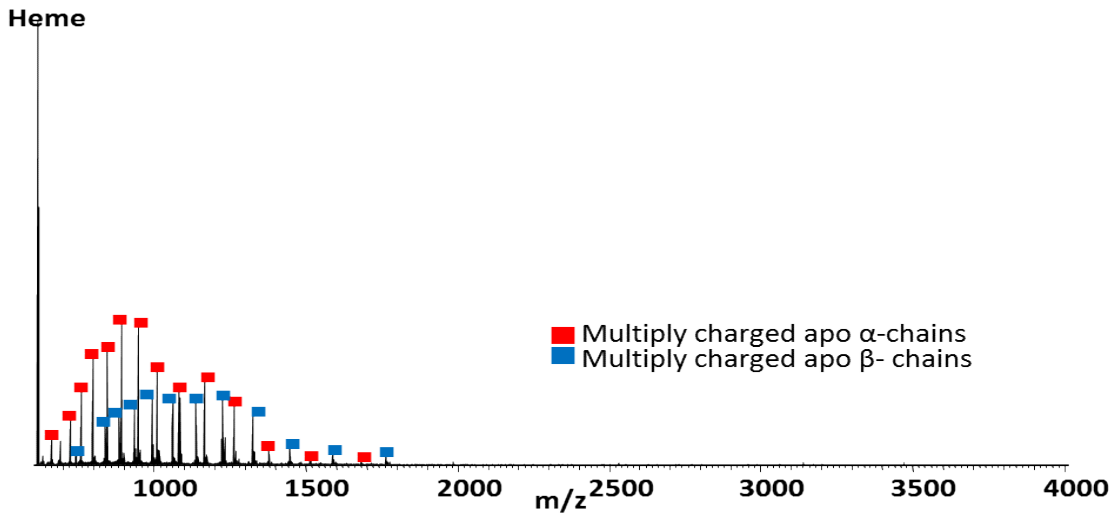

Figure 6.1 Full MS spectrum obtained following direct infusion electrospray of 10 µM Hb. ESI solution consisted of water/methanol/formic acid (48.5:48.5:3,*v/v*).

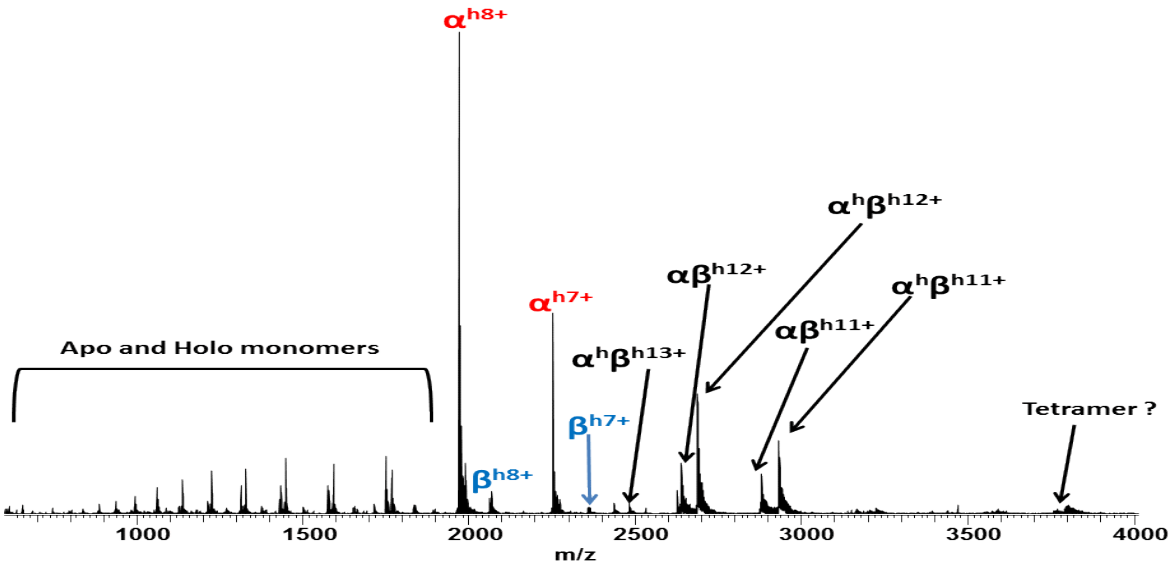

Figure 6.2 Full MS spectrum obtained following direct infusion electrospray of 10 µM Hb. ESI solution consisting of 10 mM ammonium acetate, h = heme attached.

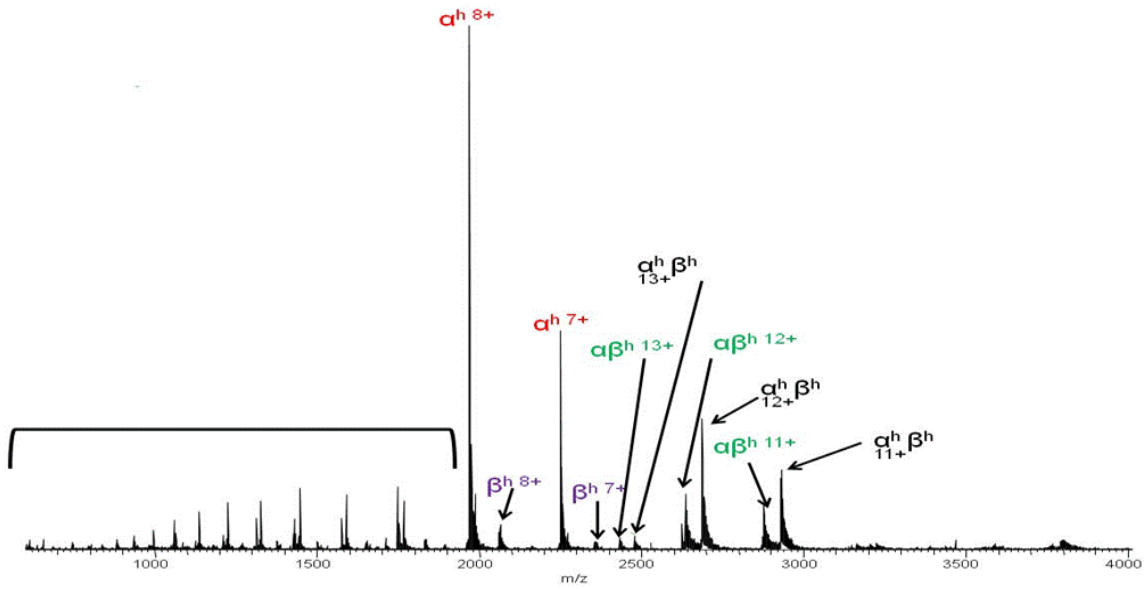

Figure 6.3 Full MS spectrum obtained following direct infusion electrospray of 10 μM Hb. ESI solution consisting of 10 mM ammonium acetate in 5% methanol, h = heme attached.

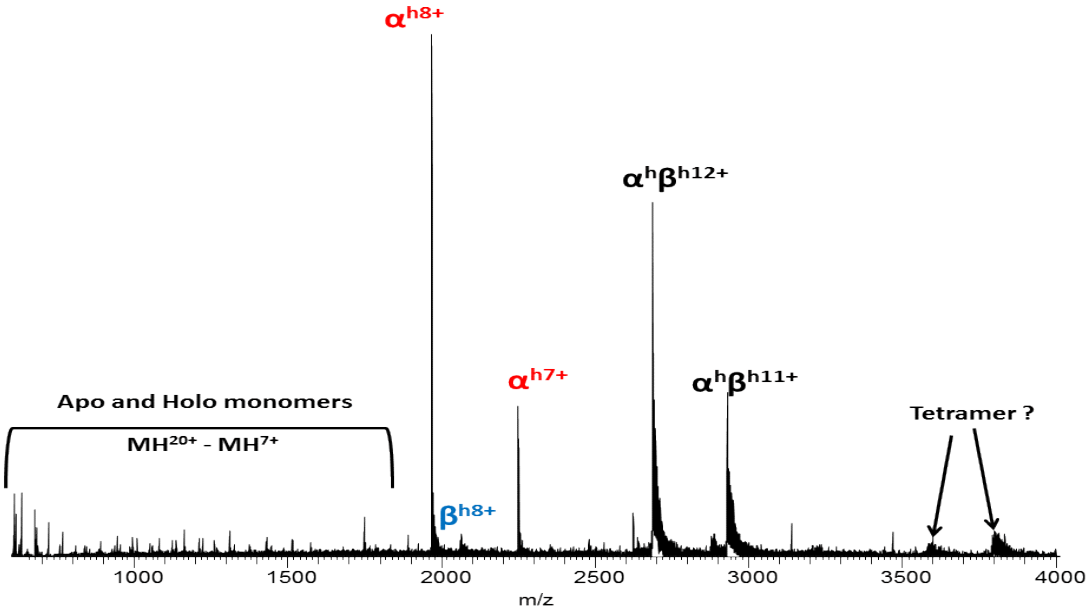

Figure 6.4 Full MS spectrum obtained following direct infusion electrospray of 10 μM Hb. ESI solution consisting of 100 mM ammonium acetate in 5% methanol, h = heme attached.

The super charging agent m-nitrobenzyl alcohol (0.5 % m-NBA) [167, 168] was added to the ESI solution comprising of 10 Mm ammonium acetate in 5 % methanol, with aim of increasing the number of charged species visible in the spectrum, **figure 6.5**. The aim was to supercharge the tetramer to provide confident identification of the presence of the non-covalently bond tetramer molecule in sample. It did increase the charge states of the apo- and holo- globin chains from $[M + 20H]^{20+}$ to $[M + 22H]^{22+}$ however the addition of 0.5 % m-NBA and 0.75 % m-NBA (**figure 6.6**) served to denature the protein complex. Hb tetramers and globin chain dimers were no longer observed in the spectra. This observation can be explained by work presented by Sterling and Williams [169] which concludes that supercharging of a protein upon the addition of m-NBA is due to increased ESI droplet heating caused by m-NBA's increased boiling point leading to the dissociation of non-covalent complexes.

The above results show that use of an ESI solution comprising ammonium acetate with a 5% methanol is able to preserve (to some degree) Hb non- covalent interactions, figure 6.4. The same conditions were subsequently employed to investigate Hb non-covalent interactions following LESA of DBS.

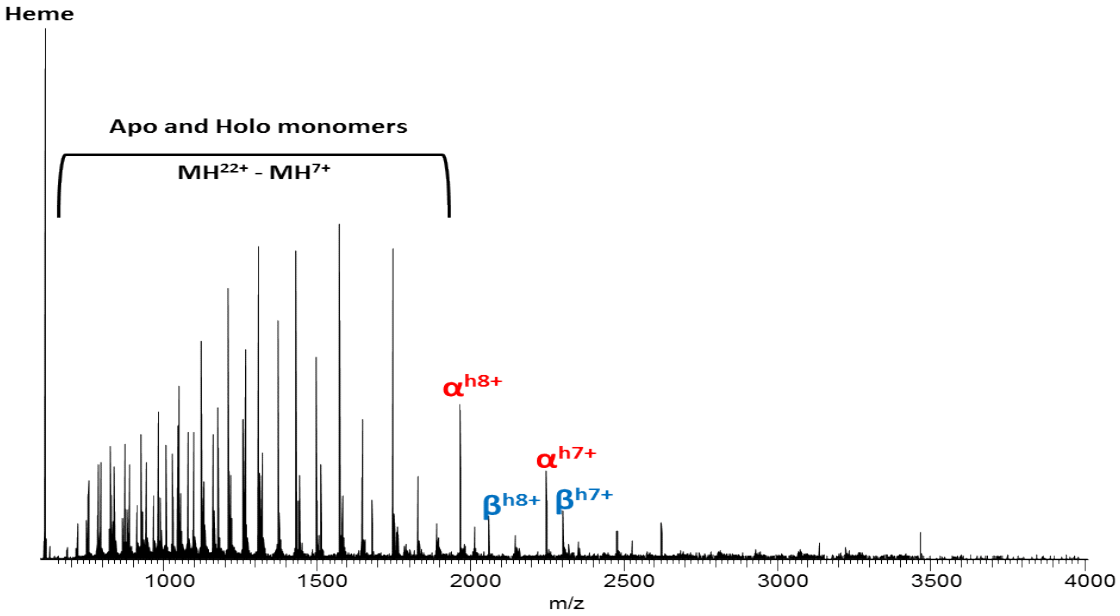

Figure 6.5 Full MS spectrum obtained following direct infusion electrospray of 10 µM Hb. ESI solution consisting of 100 mM ammonium acetate in 5% methanol, with 0.5 % m-NBA, h = heme attached.

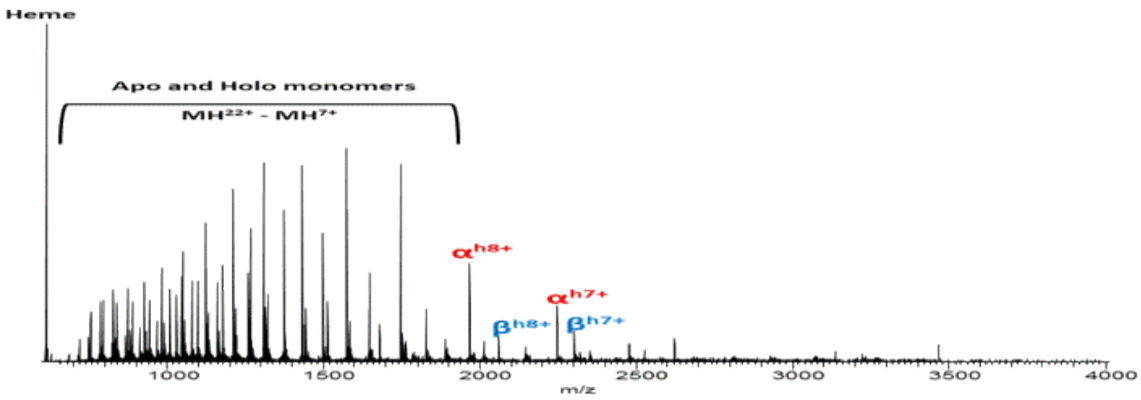

Figure 6.6 Full MS spectrum obtained following direct infusion electrospray of 10 µM Hb. ESI solution consisting of 100 mM ammonium acetate in 5% methanol, with 0.75 % m-NBA, h = heme attached.

6.2.2. Adult DBS

Figure 6.7 shows a full 'native' mass spectrum following liquid extraction surface analysis (LESA) of a normal adult DBS using an extraction/ESI solution of 100 mM ammonium acetate in 5% methanol and capillary temperature of 200 ºC (*m/z* range 600-4000). The surface sampling routine is identical to the method described in the previous section. The only difference is the extraction/ESI solution used. It appears Hb was not extracted from the DBS under these conditions. The concentration of ammonium acetate in the ESI solution was reduced to 50 mM, but again Hb was not extracted as shown in **figure 6.8**. It was possible, by use of an ESI solution comprising 10 mM ammonium acetate with 5 % methanol, to extract Hb from the DBS by LESA as shown in **figure 6.9**. The mass spectrum produced is similar to the spectrum obtained when 10 μM Hb (in the same ESI solution) was directly infused into the mass spectrometer, figure 6.3. In figure 6.9 the presence of multiply charged holo α- and holo β- chains as well as multiple dimers is also observed. This shows that 'native' Hb MS spectra can be produced directly from DBS without the need for any sample preparation.

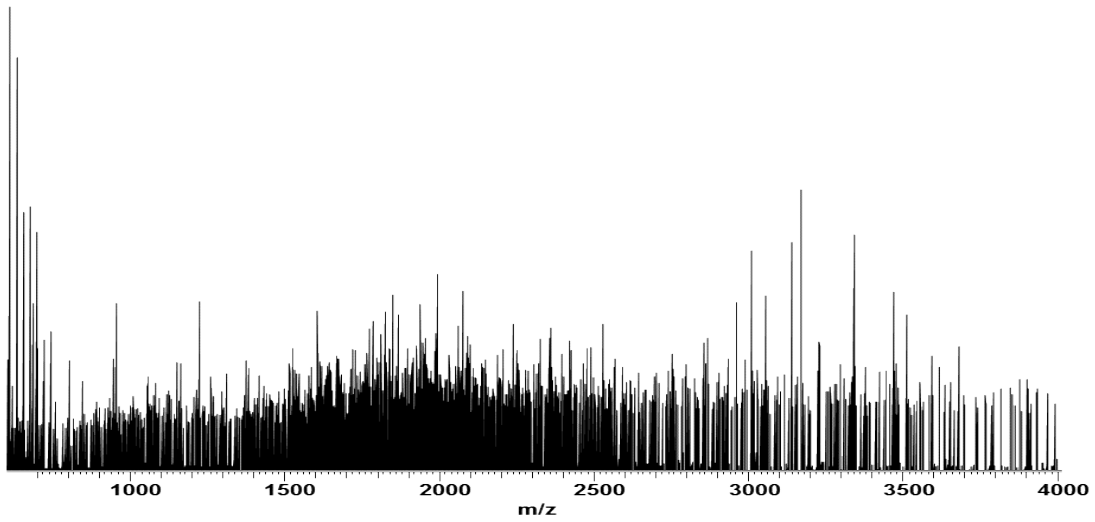

Figure 6.7 Full MS spectrum obtained following LESA of an adult DBS. ESI solution consisting of 100 mM ammonium acetate in 5% methanol.

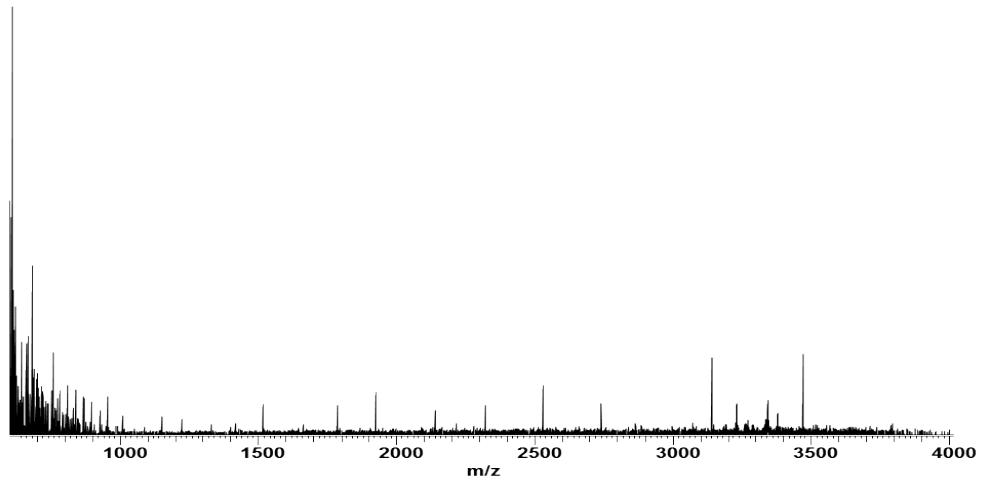

Figure 6.8 Full MS spectrum obtained following LESA of an adult DBS with an ESI solution consisting of 50 mM ammonium acetate in 5% methano

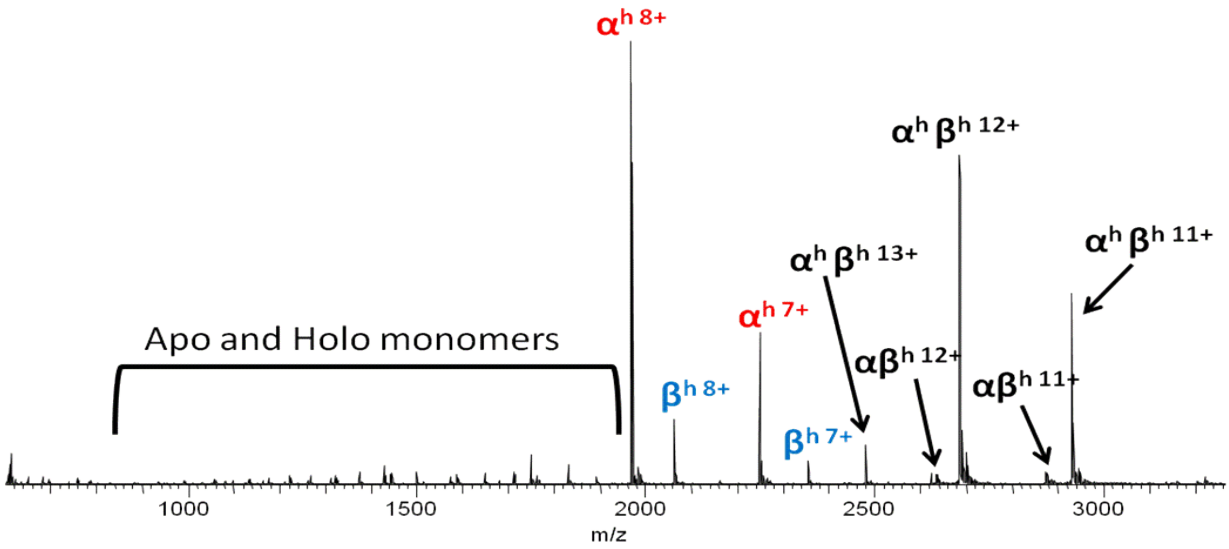

Figure 6.9 Full MS spectrum obtained following LESA of a DBS. ESI solution consisting of 10 mM ammonium acetate in 5% methanol, h = heme attached.

6.2.3 Neonatal DBS

The ESI solution consisting of 10 mM ammonium acetate in 5% methanol was used and applied to neonatal DBS. The resultant mass spectrum is shown in **figure 6.10**. Numerous (> 20) neonatal DBS were sampled, however no informative mass spectra were obtained. The only two peaks able to be successfully assigned were holo α- globin chains, that is α-globin+heme. This result demonstrates that although mass spectra were poor quality; some non- covalent interactions were preserved. One possible reason for the difference in spectra quality obtained between adult and neonatal samples could be sample age. Spectra acquired from adult DBS in this chapter were all obtained within a few days of the sample being initially taken (1-7 days) whereas neonatal samples were several months old. This may have an effect on the efficiency of Hb extraction process and the increased age of the newborn DBS may have allowed for increased haemoglobin denaturation, breaking some of the non-covalent interactions. This is backed up by observations reported by others the ability to distinguish between haemoglobin disorders by electrophoresis decreases the older the sample is before analysis [170].

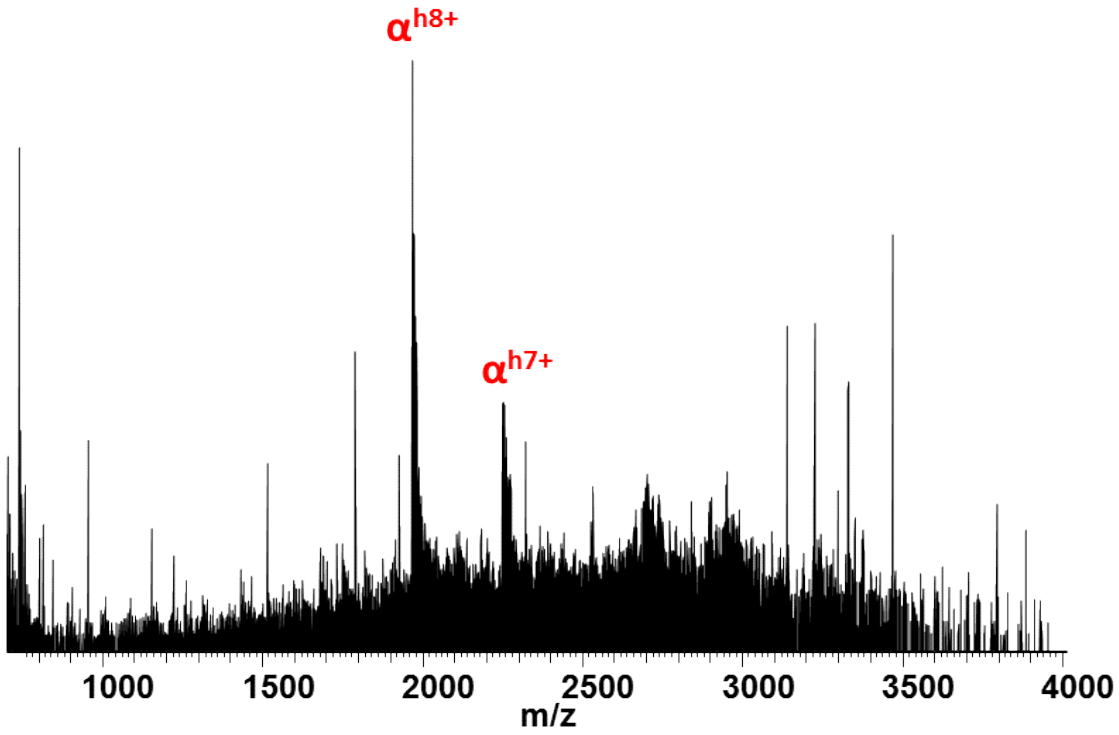

Figure 6.10 Full MS spectrum of LESA of a neonatal DBS using an ESI solution composed of of 10 mM ammonium acetate in 5% methanol.

6.3 Conclusion

When whole blood is dried onto blood spot cards the red blood cells lyse. The cells contents are then released into solution upon resolubilisation of the DBS [171]. LESA resolubilises the dried blood spot during the liquid microjunction formation in the sampling process. Results obtained from native MS of liquid extraction surface analysis of adult DBS look promising: Hb non-covalent interactions were able to be maintained during the ionisation and analysis process in the presence of an ammonium acetate buffer. Non-covalent interactions between the heme group and the globin chains (holo α- and holo β- globin) as well as dimers of the globin chains were observed. No unexpected non-covalent interactions such as two alpha globin chains or one globin chain plus two heme groups were observed. These interactions do usually not occur naturally. This suggests that native non-covalent interactions are preserved from sampling rather than formed during the ESI process. The presence of tetramers could not be confirmed in any of the spectra obtained during this investigation. This could be due to a combination of poor molecule charging and the need for a higher mass-to-charge range (greater than m/z 4000). An Hb tetramer has a large mass ~ 65 kDa, and for it to be observed within the mass range of the instrument, it would need to be highly multiply charged. An alternative instrument with a higher mass range may offer the opportunity to observe these species.

Neonatal DBS were sampled in an identical fashion to adult DBS, however only poor quality spectra were obtained. Nevertheless, some non-covalent interactions were maintained.

Results obtained from this work show that native mass spectrometry can be coupled to LESA to study a proteins non-covalent interactions from a complex sample without any

sample preparation. However the initial aim of being able to screen for abnormal Hb tetramers or dimers with the aim of detecting thalassimc disorders in newborn samples was not able to be completed in this study due to the difficultly of applying the native MS method to the neonatal samples.

Chapter 7: Discussion and future work

The work presented in this thesis demonstrates the effectiveness of liquid extraction surface analysis (LESA) as a direct surface sampling technique to probe haemoglobin and haemoglobin variants in dried blood spot (DBS) samples by mass spectrometry. It offers a rapid, sample preparation free alternative screening technique to current protocols without the need for further confirmatory analysis. This would reduce the work flow Hb variant analysis in the clinical setting.

7.1 Development of a method for the direct surface sampling of dried blood spots coupled with mass spectrometry for the analysis of haemoglobin

Following investigations presented in chapter three, an optimal surface sampling method was determined to allow for the sampling of DBS for the extraction, detection and MS/MS of haemoglobin. Optimal surface sampling conditions to assure liquid microjunction formation and Hb extraction from the surface of a DBS and the detection of Hb by mass spectrometry were as follows; an ESI/ extraction solvent of 48.5:48.5 (v/v) methanol: water with 3 % (v/v) formic acid, a sampling time delay of 5 seconds and a tip height at 1.6 mm from surface of the DBS. Further work to optimise the surface sampling routine to improve the detection of Hb by mass spectrometry could include investigating the use of other solvents such as acetonitrile and investigating the role the age of the DBS sample may play in spectra quality.

Data presented in chapter three reveals that between 12 and 40 μM of Hb is electrosprayed into the mass spectrometer following LESA. Results also show that a directly quantitative

technique to diagnose quantitative globin chain variants showed that surface sampling technique is not reproducible under the conditions described in the chapter. An alternative approach for the diagnosis of quantitative Hb variants such as β thalassemia would need to be investigated.

The optimisation of CID (normalised collision energy of 30 %) and ETD (activation energy of 20) fragmentation parameters to yield maximum sequence coverage (of up to 81 %) increases the chance of Hb variant diagnosis while the semi- automated (and potentially automated) nature of the sampling technique allows for the sequential analysis of multiple samples. Future work to improve the % sequence coverage would be to investigate alternative fragmentation techniques such as higher energy collision induced dissociation (HCD) [172]. An alternative approach could be to combine the top-down approach described in this thesis with a bottom-up approach by performing automated [173] or on-spot tryptic digests to ensure maximum sequence coverage of Hb variants.

7.2 Diagnosis of common haemoglobin variants in neonatal samples

Liquid extraction surface analysis (LESA) was employed for the diagnosis of structural variants including HbS (which can be identified in SIM mode and confirmed by top-down CID analysis). The technique also diagnosed common Hb variants with mass shifts of less than 1 Da (HbC, HbD, and HbE). The technique can also successfully diagnose the clinically significant compound heterozygotes FSC and FSD. The ability to diagnose common structural variants without any sample preparation and minimal sampling handling offers considerable advantages in the clinical setting. However, high resolution mass spectrometers such as the Orbitrap are not routinely used in clinical laboratories. Quadrupoles are often used in clinical based screening programmes such as for the

diagnosis of phenylketonuria (PKU) [174], further work to assess the application of the direct surface sampling method to diagnose Hb variants using other mass spectrometers, particularly those instruments commonly used in a clinical setting would be useful. Other interesting further experiments would be to investigate what other proteins and small molecules can be extracted from DBS and observed by mass spectrometry using this surface sampling technique.

Investigation of this technique to diagnosis of β thalassemia disorders revealed that in all samples analysed β- globin chains were not detected. This result indicates the potential of the technique to diagnose quantitative Hb variants. However, the failure to obserb β-globin chain cannot be used to definitively conclude the absence of β- globin in the sample. The absence of β- globin chain in the mass spectra could be due to ion suppression, particularly due to presence of foetal Hb in relatively large quantities in neonatal samples. A comparison of data obtained when sampling DBS of adult β thalassemia patients to see if only α- globin chains where observed would be worthwhile. If reliable diagnosis of β thalassemia proved possible using this technique could be considered a viable alternative to the current screening methods employed.

7.3 Diagnosis of unknown haemoglobin variants in neonatal samples

The robustness of the technique is demonstrated by the ability to use LESA of DBS coupled with top-down proteomics to diagnose unknown variants. Six samples which had been identified as variants by ceHPLC and IEF, but from which the nature of the variant was not determined, were analysed. Two of the samples were determined to be heterozygous Hb D-Iran following CID of the overlapping β-chain and variant peaks. ETD

confirmed a third variant as Hb Headington. Mass analysis of the fourth variant suggested either a Gly→Asp or Ala→Gln β-chain substitution. CID confirmed the variant as Hb J Baltimore. The fifth sample was confirmed as a rare α- variant with a mass shift of +113 Da. CID revealed it to be the insertion variant Hb Phnom Penh. The mass analysis, CID and ETD of the sixth sample did not indicate the presence of a variant. This sample was likely to have been mis-diagnosed as a variant during ceHPLC and IEF analysis.

A comparison of manual and automated data analysis of the same resultant unknown Hb variants studied. Following spectrum deconvolution, the ProSightPTM software was used to search against (the manually assigned) Hb variant sequences to illustrate such an approach. In all cases, the automated search identified unique fragment ions, allowing variant diagnosis, albeit with reduced overall protein sequence coverage. Efficient application of automated data analysis would require improvements to Xtract programme and the use or/development of software capable of searching top-down MS/MS data (CID, ETD) against a dedicated haemoglobin variant database. These results demonstrates the both the potential of using top-down proteomics (with is associated complex data analysis) in clinical diagnostics with automated data analysis procedure.

7.4 Analysis of haemoglobins non-covalent reactions by mass spectrometry

Data presented in chapter six show that Hb non-covalent interactions can be probed by liquid extraction surface analysis of DBS. Hb non-covalent interactions were able to be maintained during the ionisation and analysis process in the presence of an ammonium acetate buffer. Non-covalent interactions between the heme group and the globin chains (holo α- and holo β- globin) as well as interactions between the globin chains (dimers)

were observed however, spectra obtained under these conditions were often not reproducible due to problems with spray stability.

Sampling of neonatal DBS with an ammonium acetate buffer containing 5 % methanol produced poor quality mass spectra. Results obtained from this work show that native mass spectrometry can be coupled to LESA to yield some structural information from a complex sample without any sample preparation. However the initial aim of being able to screen for abnormal Hb tetramers or dimers with the aim of detecting thalassemias was not able to be met due to the difficultly of applying the native MS method to the neonatal samples. Further interesting work to study Hb covalent and non-covalent structure could include coupling the surface sampling with ion mobility mass spectrometry. Ion mobility mass spectrometry could also be used to separate Hb variants where changes to the molecules' structure has occurred (i.e. it could potentially be used to separate HbA from HbS).

References

1. Griffiths, J., *A Brief History of Mass Spectrometry.* Analytical Chemistry, 2008. **80**(15): p. 5678-5683.
2. Budzikiewicz, H. and R.D. Grigsby, *Mass spectrometry and isotopes: A century of research and discussion.* Mass Spectrometry Reviews, 2006. **25**(1): p. 146-157.
3. Fenn, J., et al., *Electrospray ionization for mass spectrometry of large biomolecules.* Science, 1989. **246**(4926): p. 64-71.
4. Karas, M., et al., *Matrix-assisted ultraviolet laser desorption of non-volatile compounds.* International Journal of Mass Spectrometry and Ion Processes, 1987. **78**(0): p. 53-68.
5. Washburn, H., H. Wiley, and S. Rock, *Mass Spectrometer as Analytical Tool.* Industrial & Engineering Chemistry Analytical Edition, 1943. **15**(9): p. 541-547.
6. Crandall, D.H., *Electron impact ionization of multicharged ions.* Physica Scripta, 2007. **23**(2): p. 153.
7. Cappiello, A., G. Famiglini, and P. Palma, *Peer Reviewed: Electron Ionization for LC/MS.* Analytical Chemistry, 2003. **75**(23): p. 496 A-503 A.
8. Munson, M.S.B. and F.H. Field, *Chemical Ionization Mass Spectrometry. I. General Introduction.* Journal of the American Chemical Society, 1966. **88**(12): p. 2621-2630.
9. Barber, M., et al., *Fast atom bombardment of solids (F.A.B.): a new ion source for mass spectrometry.* Journal of the Chemical Society, Chemical Communications, 1981(7): p. 325-327.
10. Barber, M., et al., *Fast Atom Bombardment Mass Spectrometry.* Analytical Chemistry, 1982. **54**(4): p. 645A-657A.
11. Banerjee, S. and S. Mazumdar, *Electrospray Ionization Mass Spectrometry: A Technique to Access the Information beyond the Molecular Weight of the Analyte.* International Journal of Analytical Chemistry, 2012. **2012**.
12. Tanaka, K., et al., *Protein and polymer analyses up to m/z 100 000 by laser ionization time? of? flight mass spectrometry.* Rapid Communications in Mass Spectrometry, 1988. **2**(8): p. 151-153.
13. Karas, M. and F. Hillenkamp, *Laser desorption ionization of proteins with molecular masses exceeding 10,000 daltons.* Analytical Chemistry, 1988. **60**(20): p. 2299-2301.
14. Dole, M., et al., *Molecular beams of macroions.* The Journal of Chemical Physics, 1968. **49**: p. 2240.
15. Yamashita, M. and J.B. Fenn, *Electrospray ion source. Another variation on the free-jet theme.* The Journal of Physical Chemistry, 1984. **88**(20): p. 4451-4459.
16. Kraj, A. and J. Silberring, *Introduction to Proteomics*2008: Wiley.
17. Cech, N.B. and C.G. Enke, *Practical implications of some recent studies in electrospray ionization fundamentals.* Mass Spectrometry Reviews, 2002. **20**(6): p. 362-387.
18. Bruins, A.P., *Mechanistic aspects of electrospray ionization.* Journal of Chromatography A, 1998. **794**(1): p. 345-357.
19. Taylor, G., *Disintegration of Water Drops in an Electric Field.* Proceedings of the Royal Society of London. Series A. Mathematical and Physical Sciences, 1964. **280**(1382): p. 383-397.
20. Kebarle, P. and M. Peschke, *On the mechanisms by which the charged droplets produced by electrospray lead to gas phase ions.* Analytica Chimica Acta, 2000. **406**(1): p. 11-35.

21. Kebarle, P., *A brief overview of the present status of the mechanisms involved in electrospray mass spectrometry.* Journal of Mass Spectrometry, 2000. **35**(7): p. 804-817.
22. Peschke, M., U.H. Verkerk, and P. Kebarle, *Features of the ESI mechanism that affect the observation of multiply charged noncovalent protein complexes and the determination of the association constant by the titration method.* Journal of the American Society for Mass Spectrometry, 2004. **15**(10): p. 1424-1434.
23. Iribarne, J. and B. Thomson, *On the evaporation of small ions from charged droplets.* The Journal of Chemical Physics, 1976. **64**: p. 2287.
24. Nguyen, S. and J.B. Fenn, *Gas-phase ions of solute species from charged droplets of solutions.* Proceedings of the National Academy of Sciences, 2007. **104**(4): p. 1111-1117.
25. Sterner, J.L., et al., *Signal suppression in electrospray ionization Fourier transform mass spectrometry of multi-component samples.* Journal of Mass Spectrometry, 2000. **35**(3): p. 385-391.
26. Annesley, T.M., *Ion suppression in mass spectrometry.* Clinical chemistry, 2003. **49**(7): p. 1041-1044.
27. Karas, M., U. Bahr, and T. Dülcks, *Nano-electrospray ionization mass spectrometry: addressing analytical problems beyond routine.* Fresenius' journal of analytical chemistry, 2000. **366**(6): p. 669-676.
28. Wilm, M. and M. Mann, *Analytical Properties of the Nanoelectrospray Ion Source.* Analytical Chemistry, 1996. **68**(1): p. 1-8.
29. Zhang, S., C.K. Van Pelt, and J.D. Henion, *Automated chip-based nanoelectrospray-mass spectrometry for rapid identification of proteins separated by two-dimensional gel electrophoresis.* ELECTROPHORESIS, 2003. **24**(21): p. 3620-3632.
30. Van Pelt, C., S. Zhang, and J. Henion, *Characterization of a fully automated nanoelectrospray system with mass spectrometric detection for proteomic analyses.* Journal of biomolecular techniques: JBT, 2002. **13**(2): p. 72.
31. Takats, Z., et al., *Mass spectrometry sampling under ambient conditions with desorption electrospray ionization.* Science, 2004. **306**(5695): p. 471-473.
32. Venter, A., M. Nefliu, and R. Graham Cooks, *Ambient desorption ionization mass spectrometry.* TrAC Trends in Analytical Chemistry, 2008. **27**(4): p. 284-290.
33. Ifa, D.R., et al., *Latent fingerprint chemical imaging by mass spectrometry.* Science, 2008. **321**(5890): p. 805-805.
34. Van Berkel, G.J., S.P. Pasilis, and O. Ovchinnikova, *Established and emerging atmospheric pressure surface sampling/ionization techniques for mass spectrometry.* Journal of Mass Spectrometry, 2008. **43**(9): p. 1161-1180.
35. Van Berkel, G.J., et al., *Liquid microjunction surface sampling probe electrospray mass spectrometry for detection of drugs and metabolites in thin tissue sections.* Journal of Mass Spectrometry, 2007. **43**(4): p. 500-508.
36. Quanico, J., et al., *Development of liquid microjunction extraction strategy for improving protein identification from tissue sections.* Journal of Proteomics, 2013. **79**(0): p. 200-218.
37. Aebersold, R. and M. Mann, *Mass spectrometry-based proteomics.* Nature, 2003. **422**(6928): p. 198-207.
38. March, R.E., *Ion trap mass spectrometry.* International Journal of Mass Spectrometry and Ion Processes, 1992. **118**: p. 71-135.
39. de Hoffmann, E. and V. Stroobant, *Mass Spectrometry: Principles and Applications*2007: John Wiley & Sons.
40. March, R.E., *An introduction to quadrupole ion trap mass spectrometry.* Journal of Mass Spectrometry, 1997. **32**(4): p. 351-369.
41. Douglas, D.J., A.J. Frank, and D. Mao, *Linear ion traps in mass spectrometry.* Mass Spectrometry Reviews, 2005. **24**(1): p. 1-29.

42. Xu, W., et al., *Ion Trap Mass Analysis at High Pressure: A Theoretical View.* Journal of the American Society for Mass Spectrometry, 2009. **20**(11): p. 2144-2153.
43. Hager, J.W., *A new linear ion trap mass spectrometer.* Rapid Communications in Mass Spectrometry, 2002. **16**(6): p. 512-526.
44. Makarov, A.A., *Resonance ejection from the Paul trap: A theoretical treatment incorporating a weak octapole field.* Analytical Chemistry, 1996. **68**(23): p. 4257-4263.
45. Hu, Q., et al., *The Orbitrap: a new mass spectrometer.* Journal of Mass Spectrometry, 2005. **40**(4): p. 430-443.
46. Mann, M. and N.L. Kelleher, *Precision proteomics: The case for high resolution and high mass accuracy.* Proceedings of the National Academy of Sciences, 2008. **105**(47): p. 18132-18138.
47. Makarov, A., *Electrostatic axially harmonic orbital trapping: a high-performance technique of mass analysis.* Analytical Chemistry, 2000. **72**(6): p. 1156-1162.
48. Cooley, J.W. and J.W. Tukey, *An algorithm for the machine calculation of complex Fourier series.* Mathematics of computation, 1965. **19**(90): p. 297-301.
49. Amster, I.J., *Fourier transform mass spectrometry.* Journal of Mass Spectrometry, 1996. **31**(12): p. 1325-1337.
50. Mathur, R. and P.B. O'Connor, *Artifacts in Fourier transform mass spectrometry.* Rapid Communications in Mass Spectrometry, 2009. **23**(4): p. 523-529.
51. Glish, G.L. and D.J. Burinsky, *Hybrid mass spectrometers for tandem mass spectrometry.* Journal of the American Society for Mass Spectrometry, 2008. **19**(2): p. 161-172.
52. de Hoffmann, E., *Tandem mass spectrometry: A primer.* Journal of Mass Spectrometry, 1996. **31**(2): p. 129-137.
53. McLafferty, F. and T. Bryce, *Metastable-ion characteristics: characterization of isomeric molecules.* Chemical Communications (London), 1967(23): p. 1215-1217.
54. Jennings, K.R., *Collision-induced decompositions of aromatic molecular ions.* International Journal of Mass Spectrometry and Ion Physics, 1968. **1**(3): p. 227-235.
55. Paizs, B. and S. Suhai, *Fragmentation pathways of protonated peptides.* Mass Spectrometry Reviews, 2004. **24**(4): p. 508-548.
56. McLuckey, S.A. and D.E. Goeringer, *SPECIAL FEATURE:TUTORIAL Slow Heating Methods in Tandem Mass Spectrometry.* Journal of Mass Spectrometry, 1997. **32**(5): p. 461-474.
57. Jones, A.W. and H.J. Cooper, *Dissociation techniques in mass spectrometry-based proteomics.* Analyst, 2011. **136**(17): p. 3419-3429.
58. Roepstorff, P., *J.(1984), Proposal for a common nomenclature for sequence ions in mass spectra of peptides.* Biomed Mass Spectrom. **11**(11): p. 601.
59. Seo, J. and K.J. Lee, *Post-translational modifications and their biological functions: proteomic analysis and systematic approaches.* Journal of biochemistry and molecular biology, 2004. **37**(1): p. 35-44.
60. Zubarev, R.A., N.L. Kelleher, and F.W. McLafferty, *Electron capture dissociation of multiply charged protein cations. A nonergodic process.* Journal of the American Chemical Society, 1998. **120**(13): p. 3265-3266.
61. Zubarev, R.A., *Electron-capture dissociation tandem mass spectrometry.* Current Opinion in Biotechnology, 2004. **15**(1): p. 12-16.
62. Cooper, H.J., K. Håkansson, and A.G. Marshall, *The role of electron capture dissociation in biomolecular analysis.* Mass Spectrometry Reviews, 2005. **24**(2): p. 201-222.
63. Sobczyk, M., et al., *Coulomb-Assisted Dissociative Electron Attachment: Application to a Model Peptide.* The Journal of Physical Chemistry A, 2004. **109**(1): p. 250-258.
64. Syrstad, E.A. and F. Tureček, *Toward a general mechanism of electron capture dissociation.* Journal of the American Society for Mass Spectrometry, 2005. **16**(2): p. 208-224.

65. Jones, A.W., et al., *Electron Capture Dissociation Mass Spectrometry of Tyrosine Nitrated Peptides.* Journal of the American Society for Mass Spectrometry, 2010. **21**(2): p. 268-277.
66. Neff, D., S. Smuczynska, and J. Simons, *Electron shuttling in electron transfer dissociation.* International Journal of Mass Spectrometry, 2009. **283**(1–3): p. 122-134.
67. Syka, J.E.P., et al., *Peptide and protein sequence analysis by electron transfer dissociation mass spectrometry.* Proceedings of the National Academy of Sciences of the United States of America, 2004. **101**(26): p. 9528-9533.
68. Coon, J.J., et al., *Anion dependence in the partitioning between proton and electron transfer in ion/ion reactions.* International Journal of Mass Spectrometry, 2004. **236**(1): p. 33-42.
69. Chi, A., et al., *Analysis of phosphorylation sites on proteins from Saccharomyces cerevisiae by electron transfer dissociation (ETD) mass spectrometry.* Proceedings of the National Academy of Sciences, 2007. **104**(7): p. 2193-2198.
70. Wiesner, J., T. Premsler, and A. Sickmann, *Application of electron transfer dissociation (ETD) for the analysis of posttranslational modifications.* PROTEOMICS, 2008. **8**(21): p. 4466-4483.
71. Lander, E.S., et al., *Initial sequencing and analysis of the human genome.* Nature, 2001. **409**(6822): p. 860-921.
72. Venter, J.C., et al., *The sequence of the human genome.* Science Signalling, 2001. **291**(5507): p. 1304.
73. Meyer, T.S. and B.L. Lamberts, *Use of coomassie brilliant blue R250 for the electrophoresis of microgram quantities of parotid saliva proteins on acrylamide-gel strips.* Biochimica et Biophysica Acta (BBA) - General Subjects, 1965. **107**(1): p. 144-145.
74. Switzer Iii, R.C., C.R. Merril, and S. Shifrin, *A highly sensitive silver stain for detecting proteins and peptides in polyacrylamide gels.* Analytical Biochemistry, 1979. **98**(1): p. 231-237.
75. Bodzon-Kulakowska, A., et al., *Methods for samples preparation in proteomic research.* Journal of Chromatography B, 2007. **849**(1): p. 1-31.
76. Gygi, S.P. and R. Aebersold, *Mass spectrometry and proteomics.* Current Opinion in Chemical Biology, 2000. **4**(5): p. 489-494.
77. Cottrell, J.S. and U. London, *Probability-based protein identification by searching sequence databases using mass spectrometry data.* ELECTROPHORESIS, 1999. **20**(18): p. 3551-3567.
78. Eng, J.K., A.L. McCormack, and J.R. Yates, *An approach to correlate tandem mass spectral data of peptides with amino acid sequences in a protein database.* Journal of the American Society for Mass Spectrometry, 1994. **5**(11): p. 976-989.
79. Gygi, S.P., et al., *Quantitative analysis of complex protein mixtures using isotope-coded affinity tags.* Nature biotechnology, 1999. **17**(10): p. 994-999.
80. Ong, S.-E., et al., *Stable isotope labeling by amino acids in cell culture, SILAC, as a simple and accurate approach to expression proteomics.* Molecular & cellular proteomics, 2002. **1**(5): p. 376-386.
81. Monteoliva, L. and J.P. Albar, *Differential proteomics: an overview of gel and non-gel based approaches.* Briefings in functional genomics & proteomics, 2004. **3**(3): p. 220-239.
82. Kelleher, N.L., *Peer Reviewed: Top-Down Proteomics.* Analytical Chemistry, 2004. **76**(11): p. 196 A-203 A.
83. Garcia, B.A., *What Does the Future Hold for Top Down Mass Spectrometry?* Journal of the American Society for Mass Spectrometry, 2010. **21**(2): p. 193-202.
84. Kelleher, N.L., et al., *Top down versus bottom up protein characterization by tandem high-resolution mass spectrometry.* J. Am. Chem. Soc., 1999. **121**: p. 806-812.

85. Reid, G.E. and S.A. McLuckey, *'Top down' protein characterization via tandem mass spectrometry.* Journal of Mass Spectrometry, 2002. **37**(7): p. 663-675.
86. Cui, W., H.W. Rohrs, and M.L. Gross, *Top-down mass spectrometry: Recent developments, applications and perspectives.* Analyst, 2011. **136**: p. 3854-3864.
87. Loo, J., C. Edmonds, and R. Smith, *Primary sequence information from intact proteins by electrospray ionization tandem mass spectrometry.* Science, 1990. **248**(4952): p. 201-204.
88. Loo, J.A., C.G. Edmonds, and R.D. Smith, *Tandem mass spectrometry of very large molecules: serum albumin sequence information from multiply charged ions formed by electrospray ionization.* Analytical Chemistry, 1991. **63**(21): p. 2488-2499.
89. Mørtz, E., et al., *Sequence tag identification of intact proteins by matching tanden mass spectral data against sequence data bases.* Proceedings of the National Academy of Sciences, 1996. **93**(16): p. 8264-8267.
90. Taylor, G.K., et al., *Web and Database Software for Identification of Intact Proteins Using "Top Down" Mass Spectrometry.* Analytical Chemistry, 2003. **75**(16): p. 4081-4086.
91. LeDuc, R.D., et al., *ProSight PTM: an integrated environment for protein identification and characterization by top-down mass spectrometry.* Nucleic acids research, 2004. **32**(suppl 2): p. W340-W345.
92. Cui, W., H.W. Rohrs, and M.L. Gross, *Top-down mass spectrometry: Recent developments, applications and perspectives.* Analyst, 2011. **136**(19): p. 3854-3864.
93. Edoh, D., C. Antwi-Bosaiko, and D. Amuzu, *Fetal hemoglobin during infancy and in sickle cell adults.* Afr Health Sci, 2006. **6**(1): p. 51-4.
94. Trent, R.J.A., *Diagnosis of the Haemoglobinopathies.* Clin Biochem Rev, 2006. **27**: p. 27-38.
95. Giardine B, v.B.S., Kaimakis P, Riemer C, Miller W, Samara M, Kollia P, Anagnou N P, Chui D H K, Wajcman H, Hardison R C, Patrinos G P., *HbVar Database of Human Hemoglobin Variants and Thalassemia Mutations: 2007 Update.* Hum Mutat, 2007. **28**: p. 1-10.
96. Hardison, R.C., et al., *HbVar. A relational database of human hemoglobin variants and thalassemia mutations at the globin gene server.* Human Mutation, 2002. **19**(3): p. 225-233.
97. Ingram, V.M., *Abnormal human haemoglobins. III the chemical difference between normal and sickle haemoglobins.* Biochim Biophys Acta, 1959. **36**: p. 402-411.
98. Embury, S.H., *The Clinical Pathophysiology of Sickle Cell Disease.* Ann Rev Med, 1986. **37**: p. 361-76.
99. Platt, O.S., et al., *Mortality in sickle-cell disease - life expectancy and risk-factors for early death.* New England Journal of Medicine, 1994. **330**(23): p. 1639-1644.
100. Vichinsky, E., et al., *Newborn screening for sickle-cell disease-effect on mortality.* Pediatrics, 1988. **81**(6): p. 749-755.
101. Fixler J, S.L., *Sickle cell disease.* Pediatr Clin N Am 2002. **49**: p. 1193-1210.
102. Gaston M H, V.J.I., Woods G, Peglow C, Kelleher J, Presbury G, Zarkowsky H, Vichinsky E, Iyer R, Lobel J S, Diamond S, Holbrook T, Gill F M, Ricthey K, Falletta J M. , *Prophylaxis with Oral Penicillin in Children with Sickle Cell Anemia.* N Engl J Med, 1986. **314**: p. 1593-99.
103. Cummins D, H.R., Davies S C, *Penicillin prophylaxis in children with sickle disease in Brent.* BMJ, 1991. **302**: p. 989-990.
104. Nagel, R.L., M.E. Fabry, and M.H. Steinberg, *The paradox of hemoglobin SC disease.* Blood Reviews, 2003. **17**(3): p. 167-178.
105. A J Black, P.I.C., B M Gompels, R L Green, R G Huntsman, G C Jenkins, *Sickle-cell haemoglobin C disease in London.* J Clin Path, 1972. **25**: p. 49-55.
106. River G L, R.A.B., Schwartz S O, *S-C Hemoglobin: A Clinical Study.* Blood, 1961. **18**: p. 385-416.
107. Scott R B, *Health Care Priority and Sickle Cell Anemia.* JAMA, 1970. **214**: p. 731-734.

108. Davis H, S.K.C., Gergen P J, Moore R M. , *National Trends in the Mortality of Children with Sickle Cell Disease, 1968 throught 1992.* Am J Public Health, 1997. **87**: p. 1317-1322.
109. Telfer, P., et al., *Clinical outcomes in children with sickle cell disease living in England: a neonatal cohort in East London.* Haematologica, 2007. **92**(7): p. 905-912.
110. Charache, S., Lockard Conley, C., Waugh, D. F., Ugoretz, R. J., Spurrell, J. R., *Pathogenesis of Hemolytic Anemia in Homozygous Hemoglobin C Disease.* J. Clin Invest, 1967. **46**: p. 1795-1811.
111. Vella, F. and H. Lehmann, *Hemoglobin-D Punjab (D Los-Angeles).* Journal of Medical Genetics, 1974. **11**(4): p. 341-348.
112. Mukherjee, M.S., Gangakedkar, R.R., Mohanty, R.R., Colah, R.B, *Hemoglobin sickle D Punjab-a case report.* Indian. J. Hum. Genet, 2005. **11**: p. 154-155.
113. Rees, D., et al., *The hemoglobin E syndromes.* Annals of the New York Academy of Sciences, 1998. **850**(1): p. 334-343.
114. Streetly, A.C., M. Downing, M. Farrar, L. Foo, Y. Hall, K. Kemp, H. Newbold, J. Walsh, P. Yates, P. Henthorn, J, *Implementation of the newborn screening programme for sickle cell disease in England: results for 2003-2005.* J. Med. Screen, 2008. **15**: p. 9-13.
115. Streetly, A., et al., *Implementation of universal newborn bloodspot screening for sickle cell disease and other clinically significant haemoglobinopathies in England: screening results for 2005-7.* Journal of Clinical Pathology, 2009. **62**(1): p. 26-30.
116. Pollitt, R., *Introducing new screens: Why are we all doing different things?* Journal of Inherited Metabolic Disease, 2007. **30**(4): p. 423-429.
117. Streetly, A., R. Latinovic, and J. Henthorn, *Positive screening and carrier results for the England-wide universal newborn sickle cell screening programme by ethnicity and area for 2005–07.* Journal of Clinical Pathology, 2010. **63**(7): p. 626-629.
118. Ashley-Koch, A., Q. Yang, and R.S. Olney, *Sickle Hemoglobin (Hb S) Allele and Sickle Cell Disease: A HuGE Review.* American Journal of Epidemiology, 2000. **151**(9): p. 839-845.
119. Knox-Macaulay, H.H.M., et al., *Sickle cell–haemoglobin E (HbSE) compound heterozygosity: a clinical and haematological study.* International Journal of Laboratory Hematology, 2007. **29**(4): p. 292-301.
120. Rees, D.C., T.N. Williams, and M.T. Gladwin, *Sickle-cell disease.* The Lancet, 2010. **376**(9757): p. 2018-2031.
121. Lee, A., et al., *Improved survival in homozygous sickle cell disease: lessons from a cohort study.* BMJ, 1995. **311**(7020): p. 1600-1602.
122. Quinn, C.T., Z.R. Rogers, and G.R. Buchanan, *Survival of children with sickle cell disease.* Blood, 2004. **103**(11): p. 4023-4027.
123. *NHS Sickle Cell and Thalassaemina Screening Programme, Sickle Cell and Thalassaemia Handbook For Laboratories* 2009.
124. Almeida, A.M., J.S. Henthorn, and S.C. Davies, *Neonatal screening for haemoglobinopathies: the results of a 10-year programme in an English Health Region.* British Journal of Haematology, 2001. **112**(1): p. 32-35.
125. Ryan, K., et al., *Significant haemoglobinopathies: guidelines for screening and diagnosis.* British Journal of Haematology, 2010. **149**(1): p. 35-49.
126. Campbell, M., J.S. Henthorn, and S.C. Davies, *Evaluation of Cation-Exchange HPLC Compared with Isoelectric Focusing for Neonatal Hemoglobinopathy Screening.* Clin Chem, 1999. **45**(7): p. 969-975.
127. Ou, C. and C. Rognerud, *Rapid analysis of hemoglobin variants by cation-exchange HPLC.* Clin Chem, 1993. **39**(5): p. 820-824.
128. Joutovsky, A., J. Hadzi-Nesic, and M.A. Nardi, *HPLC Retention Time as a Diagnostic Tool for Hemoglobin Variants and Hemoglobinopathies: A Study of 60000 Samples in a Clinical Diagnostic Laboratory.* Clin Chem, 2004. **50**(10): p. 1736-1747.

129. Borbely, N., et al., *Capillary zone electrophoresis for haemoglobinopathy diagnosis.* Journal of clinical pathology, 2013. **66**(1): p. 29-39.
130. Alauddin, H., et al., *HbA2 levels in normal,-thalassaemia and haemoglobin E carriers by capillary electrophoresis.*
131. Old, J.M., *Screening and genetic diagnosis of haemoglobin disorders.* Blood Reviews, 2003. **17**(1): p. 43-53.
132. Naylor, E.W. and D.H. Chace, *Automated Tandem Mass Spectrometry for Mass Newborn Screening for Disorders in Fatty Acid, Organic Acid, and Amino Acid Metabolism.* Journal of Child Neurology, 1999. **14**(1 suppl): p. S4-S8.
133. Wada, Y., et al., *Structural analysis of human hemoglobin variants with field desorption mass spectrometry.* Biochimica et Biophysica Acta (BBA) - Protein Structure, 1981. **667**(2): p. 233-241.
134. Shackleton, C., et al., *Electrospray mass spectrometry in the clinical diagnosis of variant hemoglobins.* Journal of Chromatography B: Biomedical Sciences and Applications, 1991. **562**(1): p. 175-190.
135. Falick, A.M., et al., *Tandem mass spectrometry in the clinical analysis of variant hemoglobins.* Rapid communications in mass spectrometry : RCM, 1990. **4**(10): p. 396-400.
136. Aberth, W., K.M. Straub, and A. Burlingame, *Secondary ion mass spectrometry with cesium ion primary beam and liquid target matrix for analysis of bioorganic compounds.* Analytical Chemistry, 1982. **54**(12): p. 2029-2034.
137. Wild, B.J., et al., *Rapid Identification of Hemoglobin Variants by Electrospray Ionization Mass Spectrometry.* Blood Cells, Molecules, and Diseases, 2001. **27**(3): p. 691-704.
138. Rai, D.K., et al., *Electrospray Mass Spectrometry: An Efficient Method to Detect Silent Hemoglobin Variants Causing Erythrocytosis.* Clinical chemistry, 2001. **47**(7): p. 1308-1311.
139. Rai, D.K., et al., *Accurate Mass Measurement by Electrospray Ionization Quadrupole Mass Spectrometry: Detection of Variants Differing by <6 Da from Normal in Human Hemoglobin Heterozygotes.* Analytical Chemistry, 2003. **75**(9): p. 1978-1982.
140. Daniel, Y.A., et al., *Rapid and specific detection of clinically significant haemoglobinopathies using electrospray mass spectrometry–mass spectrometry.* British Journal of Haematology, 2005. **130**(4): p. 635-643.
141. Boemer, F., et al., *Newborn screening for sickle disease using tandem mass spectrometry.* Clinical Chemistry, 2008. **54**(12): p. 2036-2041.
142. Boemer, F., et al., *3-years experience review of neonatal screening for hemoglobin disorders using tandem mass spectrometry.* Clin. Chim. Acta, 2011. **412**: p. 1476-1479.
143. Graca, D.C., et al., *Electron transfer dissociation mass spectrometry of hemoglobin on clinical samples.* J. Am. Soc. Mass Spectrom., 2012. **23**: p. 1750-1756.
144. *Newborn Blood Spot Screening in the UK- Polices and Standards* 2005.
145. Zamdborg, L., et al., *ProSight PTM 2.0: improved protein identification and characterization for top down mass spectrometry.* Nucleic Acids Research, 2007. **35**: p. W701-W706.
146. Eilers, R., *Notification of final adoption of an international method and standard solution for hemoglobinometry specifications for preparation of standard solution.* American journal of clinical pathology, 1967. **47**(2): p. 212.
147. Drabkin, D.L. and J.H. Austin, *SPECTROPHOTOMETRIC STUDIES: II. PREPARATIONS FROM WASHED BLOOD CELLS; NITRIC OXIDE HEMOGLOBIN AND SULFHEMOGLOBIN.* Journal of Biological Chemistry, 1935. **112**(1): p. 51-65.
148. Hoffbrand, V. and P. Moss, *Essential haematology*2011: Wiley-Blackwell.

149. Bakhtiar, R., et al., *Charge state specific facile gas-phase cleavage of Asp 75–met 76 peptide bond in the α-chain of human apohemoglobin probed by electrospray ionization mass spectrometry.* Biological mass spectrometry, 2005. **23**(11): p. 707-710.
150. Streetly, A., et al., *Implementation of universal newborn bloodspot screening for sickle cell disease and other clinically significant haemoglobinopathies in England: screening results for 2005–7.* Journal of Clinical Pathology, 2009. **62**(1): p. 26-30.
151. Edwards, R.L., et al., *Hemoglobin Variant Analysis via Direct Surface Sampling of Dried Blood Spots Coupled with High-Resolution Mass Spectrometry.* Analytical Chemistry, 2011. **83**(6): p. 2265-2270.
152. Rahbar, S., *Haemoglobin D Iran: β222 Glutamic Acid→ Glutamine (B4).* British Journal of Haematology, 1973. **24**(1): p. 31-35.
153. Rochette, J., et al., *Association of a novel high oxygen affinity haemoglobin variant with δβ thalassaemia.* British Journal of Haematology, 1994. **86**(1): p. 118-124.
154. Vandenesch, F., et al., *Hemoglobin J-Baltimore (β16 (A13) Gly→ Asp): Interference with the assay of HbA< sub> 1c</sub>.* Clinica chimica acta, 1987. **168**(2): p. 121-128.
155. Giardine, B., et al., *HbVar database of human hemoglobin variants and thalassemia mutations: 2007 update.* Human Mutation, 2007. **28**(2): p. 206-206.
156. Fucharoen, S. and P. Winichagoon, *Thalassemia and abnormal hemoglobin.* International journal of hematology, 2002. **76**: p. 83-89.
157. Wajcman, H., et al., *Hemoglobin Phnom Penh [α117Phe (H1)-Ile-α118Thr (H2)]; evidence for a hotspot for insertion of residues in the third exon of the α1-globin gene.* Human Mutation, 1998. **11**(S1): p. S20-S22.
158. Programme, N.S.C.a.T.S., *Data Report: 2008/09. Informing policy and improving quality.*, 2008-9.
159. Papadea, C., et al., *Comparison of liquid and dried blood for neonatal hemoglobinopathy screening: Laboratory and programmatic issues.* Pediatrics, 1994. **93**(3): p. 427-432.
160. Edwards, R., et al., *Top-Down Proteomics and Direct Surface Sampling of Neonatal Dried Blood Spots: Diagnosis of Unknown Hemoglobin Variants.* Journal of The American Society for Mass Spectrometry, 2012. **23**(11): p. 1921-1930.
161. Simmons, D.A., et al., *Subunit disassembly and unfolding kinetics of hemoglobin studied by time-resolved electrospray mass spectrometry.* Biochemistry, 2004. **43**(46): p. 14792-14801.
162. Griffith, W.P. and I.A. Kaltashov, *Highly Asymmetric Interactions between Globin Chains during Hemoglobin Assembly Revealed by Electrospray Ionization Mass Spectrometry†.* Biochemistry, 2003. **42**(33): p. 10024-10033.
163. Heuvel, R.H.H.v.d. and A.J.R. Heck, *Native protein mass spectrometry: from intact oligomers to functional machineries.* Current Opinion in Chemical Biology, 2004. **8**(5): p. 519-526.
164. van Duijn, E., *Current Limitations in Native Mass Spectrometry Based Structural Biology.* Journal of the American Society for Mass Spectrometry, 2010. **21**(6): p. 971-978.
165. Heck, A.J., *Native mass spectrometry: a bridge between interactomics and structural biology.* Nature methods, 2008. **5**(11): p. 927-933.
166. Cao, A. and R. Galanello, *Beta-thalassemia.* Genet Med, 2010. **12**(2): p. 61-76.
167. Iavarone, A.T. and E.R. Williams, *Mechanism of charging and supercharging molecules in electrospray ionization.* Journal of the American Chemical Society, 2003. **125**(8): p. 2319-2327.
168. Lomeli, S.H., et al., *Increasing Charge While Preserving Noncovalent Protein Complexes for ESI-MS.* Journal of the American Society for Mass Spectrometry, 2009. **20**(4): p. 593-596.

169. Sterling, H.J. and E.R. Williams, *Origin of supercharging in electrospray ionization of noncovalent complexes from aqueous solution.* Journal of the American Society for Mass Spectrometry, 2009. **20**(10): p. 1933-1943.
170. Rubin, E., K. Andrews, and Y. Kan, *Newborn screening by DNA analysis of dried blood spots.* Human Genetics, 1989. **82**(2): p. 134-136.
171. McDade, T.W., S. Williams, and J.J. Snodgrass, *What a drop can do: dried blood spots as a minimally invasive method for integrating biomarkers into population-based research.* Demography, 2007. **44**(4): p. 899-925.
172. Olsen, J.V., et al., *A dual pressure linear ion trap Orbitrap instrument with very high sequencing speed.* Molecular & cellular proteomics, 2009. **8**(12): p. 2759-2769.
173. Martin, N.J., J. Bunch, and H.J. Cooper, *Dried Blood Spot Proteomics: Surface Extraction of Endogenous Proteins Coupled with Automated Sample Preparation and Mass Spectrometry Analysis.* Journal of the American Society for Mass Spectrometry, 2013: p. 1-8.
174. Chace, D.H., et al., *Rapid diagnosis of phenylketonuria by quantitative analysis for phenylalanine and tyrosine in neonatal blood spots by tandem mass spectrometry.* Clinical chemistry, 1993. **39**(1): p. 66-71.

Appendices

Appendix 1. Results of one-way ANOVA. Does formic acid % in ESI solution effect the intenstity of obserbed β- globin chains.

SUMMARY

Groups	*Count*	*Sum*	*Average*	*Variance*
1%	9	362.3965	40.26628	372.8786
2%	9	390.3501	43.37223	201.5902
3%	9	376.717	41.85744	312.5474
5%	9	502.4478	55.82753	358.6493

ANOVA

Source of Variation	*SS*	*df*	*MS*	*F*	*P-value*	*F crit*
Between Groups	1365.578	3	455.1926	1.461685	0.243459	2.90112
Within Groups	9965.324	32	311.4164			
Total	11330.9	35				

Appendix 2. Results of one-way ANOVA. Does MeOH % in ESI solution effect the intenstity of obserbed β- globin chains.

SUMMARY

Groups	*Count*	*Sum*	*Average*	*Variance*
0.1	9	258.8943	28.76604	502.8608
0.3	9	242.9414	26.99349	152.0132
0.5	9	376.717	41.85744	312.5474
0.7	9	431.3282	47.92536	2283.784

ANOVA

Source of Variation	*SS*	*df*	*MS*	*F*	*P-value*	*F crit*
Between Groups	2784.389	3	928.1298	1.14189	0.347059	2.90112
Within Groups	26009.64	32	812.8014			
Total	28794.03	35				

Appendix 3. Results of one-way ANOVA. Does sampling time delay effect the intenstity of obserbed β- globin chains.

SUMMARY

Groups	*Count*	*Sum*	*Average*	*Variance*
0	9	18.59248	2.065831	3.473802
2.5	9	167.5195	18.61328	91.40132
5	9	327.7643	36.41825	12.90067
7.5	9	333.3878	37.04309	52.94357
10	9	268.9366	29.88184	22.97202

ANOVA

Source of Variation	*SS*	*df*	*MS*	*F*	*P-value*	*F crit*
Between Groups	7792.379	4	1948.095	53.0263	1.82E-15	2.605975
Within Groups	1469.531	40	36.73828			
Total	9261.91	44				

Appendix 4. Results of one-way ANOVA. Does sampling time delay effect the intenstity of obserbed β- globin chains.

SUMMARY

Groups	*Count*	*Sum*	*Average*	*Variance*
1 mm	3	99.49147	33.16382	46.85932
1.2 mm	3	124.6958	41.56525	63.54393
1.6 mm	3	106.4071	35.46904	8.924575
2 mm	3	87.86103	29.28701	55.29712
2.4 mm	3	105.1101	35.03671	38.27925
2.8 mm	3	103.2488	34.41626	33.28988

ANOVA

Source of Variation	*SS*	*df*	*MS*	*F*	*P-value*	*F crit*
Between Groups	238.4594	5	47.69188	1.1623	0.381919	3.105875
Within Groups	492.3882	12	41.03235			
Total	730.8475	17				

Appendix 5. CID (normalized collision energy 30 %) fragment ions of normal adult α-globin chain

Meas m/z	Calc m/z	Δ ppm	Fragment
338.1822	338.1823	-0.30	y_2
433.7592	433.7584	1.84	y_7^{2+}
466.2777	466.2772	1.07	y_3
484.2827	484.2822	1.03	y_8^{2+}
527.7986	527.7982	0.76	y_9^{2+}
553.3096	553.3093	0.54	y_4
583.3089	583.3086	0.51	b_6
612.8513	612.8510	0.49	b_{12}^{2+}
620.8487	620.8484	0.48	y_{11}^{2+}
648.3699	648.3695	0.62	b_{13}^{2+}
654.3574	654.3570	0.61	y_5
656.3681	656.3670	1.68	y_{12}^{2+}
672.3757	672.3772	-2.23	y_{18}^{3+}
677.7099	677.7093	0.89	b_{20}^{3+}
696.0566	696.0563	0.43	y_{19}^{3+}
701.3889	701.3884	0.71	b_{21}^{3+}
711.4044	711.4036	1.12	b_7
712.9094	712.9090	0.56	y_{13}^{2+}
720.3962	720.3955	0.97	b_{22}^{3+}
741.4101	741.4092	1.21	b_{14}^{2+}
759.6610	759.6605	0.66	y_{28}^{4+}
763.4101	763.4097	0.52	b_{23}^{3+}
767.4417	767.4410	0.91	y_6
774.7658	774.7654	0.52	y_{21}^{3+}
786.4438	786.4432	0.76	y_{14}^{2+}
787.9321	787.9315	0.76	y_{29}^{4+}
795.1673	795.1665	1.01	b_{31}^{4+}
798.4407	798.4444	-4.63	y_{22}^{3+}
817.7649	817.7642	0.86	b_{24}^{3+}
822.1969	822.1962	0.85	y_{30}^{4+}

827.9268	827.9266	0.24	b_{32}^{4+}
830.7961	830.7953	0.96	y_{23}^{3+}
833.9681	833.9674	0.84	b_{16}^{2+}
839.9567	839.9555	1.39	y_{31}^{4+}
842.2601	842.2605	-0.47	y_{39}^{5+}
850.4915	850.4907	0.94	y_{15}^{2+}
860.4508	860.4503	0.58	b_{26}^{3+}
864.4788	864.4779	1.04	y_{24}^{3+}
864.6945	864.6937	0.93	b_{33}^{4+}
866.5103	866.5094	1.04	y_{7}
867.0523	867.0514	1.04	b_{41}^{5+}
883.0631	883.0656	-2.83	y_{56}^{7+}
883.5036	883.5016	2.26	b_{17}^{2+}
892.9660	892.9647	1.46	b_{34}^{4+}
903.4656	903.4645	1.22	b_{27}^{3+}
904.9014	904.9006	0.88	y_{42}^{5+}
908.0052	908.0042	1.10	y_{16}^{2+}
911.2480	911.2477	0.33	y_{34}^{4+}
912.0126	912.0123	0.33	b_{18}^{2+}
913.2971	913.2964	0.77	b_{50}^{6+}
913.5017	913.5007	1.09	y_{25}^{3+}
914.7238	914.7227	1.20	b_{35}^{4+}
918.6145	918.6136	0.98	b_{60}^{7+}
922.8014	922.8000	1.52	b_{51}^{6+}
926.4951	926.4942	0.97	b_{9}
927.1444	927.1436	0.86	b_{28}^{3+}
936.0169	936.0148	2.24	y_{35}^{4+}
936.9110	936.9128	-1.92	b_{61}^{7+}
947.5319	947.5309	1.06	b_{19}^{2+}
950.6678	950.6674	0.42	y_{61}^{7+}
952.7433	952.7429	0.42	b_{72}^{8+}
956.5161	956.5149	1.25	y_{26}^{3+}
964.2871	964.2858	1.35	y_{36}^{4+}
964.5475	964.5462	1.35	y_{17}^{2+}
964.8387	964.8383	0.41	b_{29}^{3+}
965.1266	965.1264	0.21	b_{73}^{8+}
966.8235	966.8222	1.34	y_{62}^{7+}
967.5581	967.5571	1.03	y_{8}
975.7542	975.7530	1.23	b_{37}^{4+}
975.9030	975.9001	2.97	b_{45}^{5+}
977.6475	977.6461	1.43	b_{64}^{7+}
980.1950	980.1939	1.12	y_{27}^{3+}
992.5591	992.5568	2.32	y_{37}^{4+}
993.8811	993.8832	-2.11	b_{75}^{8+}

1001.0169	1001.0149	2.00	b_{38}^{4+}
1005.3194	1005.3138	5.57	b_{46}^{5+}
1007.8582	1007.8525	5.66	b_{30}^{3+}
1008.0637	1008.0622	1.49	y_{18}^{2+}
1012.5461	1012.5449	1.19	y_{28}^{3+}
1016.0617	1016.0603	1.38	b_{20}^{2+}
1017.8595	1017.8521	7.27	b_{57}^{6+}
1018.3102	1018.3091	1.08	y_{38}^{4+}
1021.9671	1021.9661	0.98	y_{47}^{5+}
1025.5636	1025.5626	0.98	b_{10}
1026.2774	1026.2768	0.58	b_{39}^{4+}
1028.3208	1028.3192	1.56	b_{47}^{5+}
1030.0769	1030.0754	1.46	y_{56}^{6+}
1043.5821	1043.5808	1.25	y_{19}^{2+}
1044.8239	1044.8245	-0.57	b_{69}^{7+}
1050.2406	1050.2396	0.95	y_{29}^{3+}
1051.5789	1051.5789	0.00	b_{21}^{2+}
1052.5714	1052.5739	-2.38	y_{39}^{4+}
1054.5905	1054.5891	1.33	y_{9}
1089.1168	1089.1153	1.38	$b_{112}1^{1+}$
1094.4401	1094.4387	1.28	y_{60}^{6+}
1099.3977	1099.3957	1.82	b_{113}^{11+}
1108.9458	1108.9441	1.53	y_{61}^{6+}
1112.1123	1112.1102	1.89	y_{20}^{2+}
1127.3811	1127.3844	-2.93	b_{105}^{10+}
1130.8770	1130.8739	2.74	y_{42}^{4+}
1132.5057	1132.5028	2.56	y_{105}^{10+}
1140.8393	1140.8304	7.80	y_{138}^{13+}
1147.5302	1147.5252	4.36	y_{139}^{13+}
1153.6593	1153.6575	1.56	y_{10}
1153.6593	1153.6575	1.56	b_{11}
1154.4457	1154.4426	2.69	b_{76}^{7+}
1161.6458	1161.6444	1.21	y_{21}^{2+}
1170.0069	1170.0128	-5.04	b_{109}^{10+}
1174.8155	1174.8135	1.70	y_{65}^{6+}
1177.1134	1177.1165	-2.63	b_{110}^{10+}
1190.2855	1190.2838	1.43	b_{34}^{3+}
1194.7492	1194.7473	1.59	b_{79}^{7+}
1206.4017	1206.4011	0.50	y_{91}^{8+}
1209.2393	1209.2345	3.97	b_{113}^{10+}
1210.7496	1210.7530	-2.81	y_{101}^{9+}
1214.6612	1214.6612	0.00	y_{34}^{3+}
1219.7977	1219.7940	3.03	b_{69}^{6+}
1234.9976	1234.9959	1.38	y_{68}^{6+}

1240.6909	1240.6896	1.05	y_{11}
1245.6907	1245.6894	1.04	y_{23}^{2+}
1247.1453	1247.1449	0.32	b_{71}^{6+}
1254.6584	1254.6533	4.06	b_{25}^{2+}
1268.3184	1268.3173	0.87	b_{36}^{3+}
1274.3440	1274.3505	-5.10	y_{70}^{6+}
1277.2068	1277.2058	0.78	y_{47}^{4+}
1296.2146	1296.2132	1.08	y_{24}^{2+}
1311.7280	1311.7267	0.99	y_{12}
1324.8417	1324.8418	-0.08	b_{75}^{6+}
1330.5340	1330.5314	1.95	y_{61}^{5+}
1346.6811	1346.6819	-0.59	b_{76}^{6+}
1354.6960	1354.6932	2.07	b_{27}^{2+}
1357.4090	1357.4098	-0.59	y_{38}^{3+}
1368.0320	1368.0333	-0.95	b_{39}^{3+}
1369.7490	1369.7474	1.17	y_{25}^{2+}
1393.6997	1393.7040	-3.09	b_{79}^{6+}
1403.0982	1403.0961	1.50	y_{39}^{3+}
1409.5746	1409.5748	-0.14	y_{65}^{5+}
1410.7316	1410.7317	-0.07	b_{40}^{3+}
1424.8119	1424.8108	0.77	y_{13}
1469.7883	1469.7873	0.68	y_{27}^{2+}
1518.3149	1518.3137	0.79	y_{28}^{2+}
1571.8806	1571.8792	0.89	y_{14}
1574.8571	1574.8557	0.89	y_{29}^{2+}

Appendix 6. CID (normalized collision energy 30 %) fragment ions of normal adult β-globin chain

Meas m/z	Calc m/z	Δ ppm	Fragment
350.2179	350.2187	-2.28	b_3
447.2348	447.2350	-0.45	y_3
451.2660	451.2663	-0.66	b_4
511.2690	511.2693	-0.59	b_9^{2+}
512.7693	512.7698	-0.98	y_9^{2+}
526.6342	526.6352	-1.90	y_{15}^{3+}
546.7873	546.7878	-0.91	b_{10}^{2+}
562.3029	562.3040	-1.96	y_{10}^{2+}
584.2933	584.2940	-1.20	y_4
590.8140	590.8147	-1.18	y_{11}^{2+}
596.3214	596.3220	-1.01	b_{11}^{2+}
608.8346	608.8354	-1.31	y_{23}^{4+}
623.6753	623.6758	-0.80	y_{17}^{3+}
626.3327	626.3333	-0.96	y_{12}^{2+}
646.8451	646.8459	-1.24	b_{12}^{2+}
647.3535	647.3549	-2.16	y_{18}^{3+}
649.6942	649.6948	-0.92	b_{18}^{3+}
655.3304	655.3311	-1.07	y_5
671.0330	671.0339	-1.34	y_{19}^{3+}
675.8668	675.8675	-1.04	y_{13}^{2+}
677.3611	677.3617	-0.89	b_6
682.3637	682.3644	-1.03	b_{13}^{2+}
687.7083	687.7091	-1.16	b_{19}^{3+}
694.5838	694.5828	1.44	b_{33}^{5+}
713.7194	713.7201	-0.98	y_{20}^{3+}
720.7312	720.7319	-0.97	b_{20}^{3+}
725.4011	725.4017	-0.83	y_{14}^{2+}
738.9058	738.9065	-0.95	b_{14}^{2+}
747.0090	747.0092	-0.27	b_{35}^{5+}
759.0736	759.0742	-0.79	b_{21}^{3+}
761.2002	761.2018	-2.10	y_{35}^{5+}
768.4145	768.4151	-0.78	y_6
779.0931	779.0938	-0.90	y_{22}^{3+}
781.0148	781.0155	-0.90	y_{36}^{5+}
786.6664	786.6676	-1.53	b_{30}^{4+}

789.4485	789.4492	-0.89	y_{15}^{2+}
802.0878	802.0884	-0.75	b_{22}^{3+}
803.6342	803.6356	-1.74	b_{37}^{5+}
806.4037	806.4043	-0.74	b_{7}
811.4441	811.4448	-0.86	y_{23}^{3+}
814.9379	814.9386	-0.86	b_{31}^{4+}
820.4351	820.4360	-1.10	y_{30}^{4+}
823.8485	823.8451	4.13	b_{38}^{5+}
831.9455	831.9461	-0.72	b_{15}^{2+}
835.1106	835.1112	-0.72	b_{23}^{3+}
839.4515	839.4522	-0.83	y_{7}
843.2090	843.2096	-0.71	b_{32}^{4+}
845.1268	845.1273	-0.59	y_{24}^{3+}
853.4779	853.4785	-0.70	y_{16}^{2+}
854.1175	854.1184	-1.05	b_{24}^{3+}
854.7001	854.7007	-0.70	y_{31}^{4+}
859.7956	859.7962	-0.70	y_{47}^{6+}
867.9761	867.9767	-0.69	b_{33}^{4+}
872.4601	872.4600	0.11	y_{32}^{4+}
880.6765	880.6770	-0.57	b_{40}^{5+}
888.6131	888.6139	-0.90	y_{56}^{7+}
892.7431	892.7438	-0.78	b_{34}^{4+}
894.1492	894.1501	-1.01	y_{25}^{3+}
900.7302	900.7310	-0.89	y_{33}^{4+}
916.1391	916.1397	-0.65	b_{26}^{3+}
918.3206	918.3220	-1.52	y_{50}^{6+}
919.4805	919.4817	-1.31	y_{58}^{7+}
924.5037	924.5043	-0.65	b_{17}^{2+}
925.4985	925.4981	0.43	y_{34}^{4+}
933.5090	933.5096	-0.64	b_{35}^{4+}
934.4994	934.4993	0.11	b_{8}
937.1637	937.1643	-0.64	y_{26}^{3+}
939.8182	939.8188	-0.64	b_{27}^{3+}
949.1375	949.1397	-2.32	y_{97}^{11+}
951.2499	951.2504	-0.53	y_{35}^{4+}
953.4945	953.4952	-0.73	y_{8}
958.5162	958.5185	-2.40	y_{52}^{6+}
968.5166	968.5097	7.12	y_{70}^{8+}
970.5281	970.5287	-0.62	y_{18}^{2+}
974.0381	974.0386	-0.51	b_{18}^{2+}
976.0172	976.0175	-0.31	y_{36}^{4+}
977.5119	977.5135	-1.64	b_{28}^{3+}
977.6892	977.6899	-0.72	y_{53}^{6+}
982.7166	982.7193	-2.75	b_{44}^{5+}

986.3351	986.3350	0.10	y_{45}^{5+}
994.8571	994.8578	-0.70	y_{54}^{6+}
996.5208	996.5206	0.20	b_{29}^{3+}
998.6509	998.6525	-1.60	y_{73}^{8+}
998.8693	998.8698	-0.50	y_{28}^{3+}
1003.8111	1003.8112	-0.10	y_{64}^{7+}
1004.2871	1004.2885	-1.39	y_{37}^{4+}
1006.0470	1006.0472	-0.20	y_{19}^{2+}
1011.6075	1011.6106	-3.06	y_{111}^{12+}
1017.7001	1017.7010	-0.88	y_{55}^{6+}
1024.5315	1024.5323	-0.78	y_{9}
1025.1945	1025.1992	-4.58	y_{112}^{12+}
1031.5523	1031.5540	-1.65	y_{47}^{5+}
1033.8461	1033.8482	-2.03	y_{96}^{10+}
1048.5539	1048.5543	-0.38	b_{30}^{3+}
1052.6534	1052.6561	-2.56	y_{98}^{10+}
1069.1601	1069.1595	0.56	b_{48}^{5+}
1070.0765	1070.0765	0.00	y_{20}^{2+}
1071.4683	1071.4589	8.77	b_{99}^{10+}
1072.5598	1072.5607	-0.84	y_{58}^{6+}
1075.4656	1075.4672	-1.49	y_{100}^{10+}
1080.5940	1080.5942	-0.19	b_{20}^{2+}
1081.1679	1081.1641	3.51	b_{100}^{10+}
1081.1679	1081.1694	-1.39	y_{101}^{10+}
1085.3623	1085.3569	4.98	y_{140}^{14+}
1086.2491	1086.2490	0.09	b_{31}^{3+}
1091.5880	1091.5832	4.40	y_{91}^{9+}
1093.5769	1093.5789	-1.83	y_{30}^{3+}
1100.5956	1100.5945	1.00	b_{40}^{4+}
1103.4821	1103.4837	-1.45	y_{111}^{11+}
1107.2619	1107.2728	-9.84	y_{132}^{13+}
1113.9167	1113.9188	-1.89	y_{123}^{12+}
1115.9714	1115.9715	-0.09	y_{133}^{13+}
1116.7974	1116.8017	-3.85	y_{144}^{14+}
1118.3025	1118.3076	-4.56	y_{112}^{11+}
1123.9434	1123.9437	-0.27	b_{32}^{3+}
1137.3597	1137.3616	-1.67	b_{41}^{4+}
1141.1725	1141.1732	-0.61	y_{73}^{7+}
1148.6069	1148.6083	-1.22	y_{96}^{9+}
1151.3864	1151.3808	4.86	b_{96}^{9+}
1156.9662	1156.9665	-0.26	b_{33}^{3+}
1159.8330	1159.8358	-2.41	y_{97}^{9+}
1166.6020	1166.6096	-6.51	b_{97}^{9+}
1168.1368	1168.1371	-0.26	y_{22}^{2+}

1169.5041	1169.5060	-1.62	y_{98}^{9+}
1174.1284	1174.1287	-0.26	b_{4}^{24+}
1177.4504	1177.4497	0.59	b_{65}^{6+}
1180.6227	1180.6222	0.42	y_{11}
1182.0697	1182.0709	-1.02	y_{99}^{9+}
1185.4191	1185.4181	0.84	y_{109}^{10+}
1185.4191	1185.4197	-0.51	b_{109}^{10+}
1189.9888	1189.9893	-0.42	b_{34}^{3+}
1190.3980	1190.3979	0.08	b_{99}^{9+}
1191.6402	1191.6368	2.85	b_{11}
1194.8529	1194.8517	1.00	y_{100}^{9+}
1201.1846	1201.1816	2.50	b_{100}^{9+}
1201.1846	1201.1874	-2.33	y_{101}^{9+}
1202.6283	1202.6290	-0.58	b_{22}^{2+}
1206.3890	1206.3893	-0.25	b_{43}^{4+}
1209.3424	1209.3427	-0.25	y_{78}^{7+}
1213.7287	1213.7313	-2.14	y_{111}^{10+}
1216.6628	1216.6635	-0.58	y_{23}^{2+}
1221.5420	1221.5470	-4.09	b_{123}^{11+}
1225.4916	1225.4975	-4.81	y_{79}^{7+}
1228.1459	1228.1473	-1.14	b_{44}^{4+}
1230.0349	1230.0376	-2.20	y_{112}^{10+}
1239.6480	1239.6502	-1.77	y_{80}^{7+}
1244.3430	1244.3437	-0.56	b_{35}^{3+}
1251.6594	1251.6593	0.08	y_{12}
1252.1637	1252.1632	0.40	b_{23}^{2+}
1257.9404	1257.9494	-7.15	y_{81}^{7+}
1264.9140	1264.9145	-0.40	b_{45}^{4+}
1267.1863	1267.1873	-0.79	y_{24}^{2+}
1268.1649	1268.1673	-1.89	y_{69}^{6+}
1279.1689	1279.1698	-0.70	b_{46}^{4+}
1289.1906	1289.1907	-0.08	y_{47}^{4+}
1291.0107	1291.0105	0.15	y_{70}^{6+}
1292.0563	1292.0584	-1.63	y_{96}^{8+}
1302.8489	1302.8500	-0.84	y_{71}^{6+}
1307.9255	1307.9266	-0.84	b_{47}^{4+}
1313.6912	1313.6886	1.98	b_{73}^{6+}
1315.5643	1315.5683	-3.04	y_{98}^{8+}
1336.1961	1336.1976	-1.12	b_{48}^{4+}
1340.7220	1340.7215	0.37	y_{25}^{2+}
1350.7271	1350.7277	-0.44	y_{13}
1357.9555	1357.9556	-0.07	b_{49}^{4+}
1373.7039	1373.7060	-1.53	b_{26}^{2+}
1383.2152	1383.2175	-1.66	b_{50}^{4+}

1405.2417	1405.2428	-0.78	y_{26}^{2+}
1409.2229	1409.2245	-1.14	b_{27}^{2+}
1410.7269	1410.7319	-3.54	y_{78}^{6+}
1412.7318	1412.7382	-4.53	b_{65}^{5+}
1449.7947	1449.7961	-0.97	y_{14}
1476.8045	1476.8057	-0.81	b_{14}
1497.7973	1497.8011	-2.54	y_{28}^{2+}
1498.3018	1498.2925	6.21	y_{83}^{6+}
1571.3352	1571.3353	-0.06	y_{29}^{2+}
1577.8898	1577.8911	-0.82	y_{15}
1662.8840	1662.8850	-0.60	b_{15}

Appendix 7. CID (normalized collision energy 30 %) fragment ions of normal neonatal α-globin chain

Meas *m/z*	Calc *m/z*	Δ ppm	Fragment
466.2792	466.2772	4.29	y_3
527.7999	527.7982	3.22	y_9^{2+}
553.3110	553.3093	3.07	y_4
577.3344	577.3324	3.46	b_{11}^{2+}
583.3104	583.3086	3.09	b_6
612.8532	612.8510	3.59	b_{12}^{2+}
620.8498	620.8484	2.25	y_{11}^{2+}
648.3713	648.3695	2.78	b_{13}^{2+}
654.3588	654.3570	2.75	y_5
677.7101	677.7093	1.18	b_{20}^{3+}
701.3899	701.3884	2.14	b_{21}^{3+}
712.9108	712.9090	2.52	y_{13}^{2+}
720.3958	720.3955	0.42	b_{22}^{3+}
741.4120	741.4092	3.78	b_{14}^{2+}
741.7438	741.7426	1.62	y_{20}^{3+}
759.6620	759.6605	1.97	y_{28}^{4+}
763.4113	763.4097	2.10	b_{23}^{3+}
767.4429	767.4410	2.48	y_6
774.7663	774.7654	1.16	y_{21}^{3+}
786.4451	786.4432	2.42	y_{14}^{2+}
787.9330	787.9315	1.90	y_{29}^{4+}
795.1677	795.1665	1.51	b_{31}^{4+}
817.7661	817.7642	2.32	b_{24}^{3+}
822.1977	822.1962	1.82	y_{30}^{4+}
827.9272	827.9266	0.72	b_{32}^{4+}
830.7971	830.7953	2.17	y_{23}^{3+}
833.9696	833.9674	2.64	b_{16}^{2+}
850.4928	850.4907	2.47	y_{15}^{2+}

860.4530	860.4503	3.14	b_{26}^{3+}
864.4796	864.4779	1.97	y_{24}^{3+}
866.5118	866.5094	2.77	y_{7}
883.5046	883.5016	3.40	b_{17}^{2+}
892.9669	892.9647	2.46	b_{34}^{4+}
903.4673	903.4645	3.10	b_{27}^{3+}
908.0065	908.0042	2.53	y_{16}^{2+}
911.2501	911.2477	2.63	y_{34}^{4+}
912.0140	912.0123	1.86	b_{18}^{2+}
913.5032	913.5007	2.74	y_{25}^{3+}
914.7230	914.7227	0.33	b_{35}^{4+}
926.4966	926.4942	2.59	b_{9}
927.1463	927.1436	2.91	b_{28}^{3+}
936.0170	936.0148	2.35	y_{35}^{4+}
947.5336	947.5309	2.85	b_{19}^{2+}
956.5174	956.5149	2.61	y_{26}^{3+}
964.5490	964.5462	2.90	y_{17}^{2+}
967.5599	967.5571	2.89	y_{8}
980.1966	980.1939	2.75	y_{27}^{3+}
992.5604	992.5568	3.63	y_{37}^{4+}
993.8851	993.8832	1.91	b_{75}^{8+}
1008.0652	1008.0622	2.98	y_{18}^{2+}
1012.5478	1012.5449	2.86	y_{28}^{3+}
1016.0634	1016.0603	3.05	b_{20}^{2+}
1018.3096	1018.3091	0.49	y_{38}^{4+}
1021.9686	1021.9661	2.45	y_{47}^{5+}
1025.5657	1025.5626	3.02	b_{10}
1028.3208	1028.3192	1.56	b_{47}^{5+}
1030.0766	1030.0754	1.16	y_{56}^{6+}
1043.5839	1043.5808	2.97	y_{19}^{2+}
1044.8273	1044.8245	2.68	b_{69}^{7+}
1050.2425	1050.2396	2.76	y_{29}^{3+}
1052.5716	1052.5739	-2.19	y_{39}^{4+}
1054.5923	1054.5891	3.03	y_{9}
1089.1205	1089.1153	4.77	b_{1121}^{1+}

1091.5765	1091.5722	3.94	y_{121}^{12+}
1094.4403	1094.4387	1.46	y_{60}^{6+}
1095.9289	1095.9259	2.74	y_{30}^{3+}
1099.3966	1099.3957	0.82	b_{113}^{11+}
1100.6752	1100.6754	-0.18	y_{111}^{11+}
1102.5806	1102.5880	-6.71	y_{102}^{10+}
1108.9465	1108.9441	2.16	y_{6}^{16+}
1112.1138	1112.1102	3.24	y_{20}^{2+}
1113.4631	1113.4618	1.17	b_{94}^{9+}
1119.6090	1119.6049	3.66	y_{31}^{3+}
1127.7885	1127.7914	-2.57	y_{62}^{6+}
1130.8758	1130.8739	1.68	y_{42}^{4+}
1132.4917	1132.5028	-9.80	y_{105}^{10+}
1135.7258	1135.7226	2.82	b_{75}^{7+}
1140.8752	1140.8760	-0.70	y_{115}^{11+}
1142.0975	1142.0974	0.09	b_{128}^{12+}
1147.5282	1147.5252	2.61	y_{139}^{13+}
1153.6607	1153.6575	2.77	b_{10}
1153.6607	1153.6575	2.77	y_{10}
1154.4429	1154.4426	0.26	b_{76}^{7+}
1161.6465	1161.6444	1.81	y_{21}^{2+}
1174.8153	1174.8135	1.53	y_{65}^{6+}
1177.1162	1177.1165	-0.25	b_{110}^{10+}
1184.2223	1184.2202	1.77	b_{111}^{10+}
1194.7493	1194.7473	1.67	b_{79}^{7+}
1209.2370	1209.2345	2.07	b_{113}^{10+}
1218.7960	1218.7940	1.64	b_{69}^{6+}
1219.2968	1219.2945	1.89	b_{35}^{3+}
1234.9987	1234.9959	2.27	y_{68}^{6+}
1240.6929	1240.6896	2.66	y_{11}
1245.6926	1245.6894	2.57	y_{23}^{2+}
1247.1451	1247.1449	0.16	b_{71}^{6+}
1268.3195	1268.3173	1.73	b_{36}^{3+}
1277.2075	1277.2085	-0.78	y_{47}^{4+}
1296.2165	1296.2132	2.55	y_{24}^{2+}

1307.8007	1307.7953	4.13	b_{110}^{9+}
1311.7302	1311.7267	2.67	y_{12}
1346.6827	1346.6819	0.59	b_{76}^{6+}
1369.7510	1369.7474	2.63	y_{25}^{2+}
1424.8144	1424.8108	2.53	y_{13}
1434.2723	1434.2687	2.51	y_{26}^{2+}
1518.3176	1518.3137	2.57	y_{28}^{2+}
1571.8832	1571.8793	2.48	y_{14}
1574.8603	1574.8557	2.92	y_{29}^{2+}
1699.9788	1699.9741	2.76	y_{15}

Appendix 8. CID (normalized collision energy 30 %) fragment ions of normal neonatal β-globin chain

Meas *m/z*	Calc *m/z*	Δ ppm	Fragment
350.2192	350.2187	1.43	b_3
451.2678	451.2663	3.32	b_4
512.7711	512.7698	2.54	y_9^{2+}
546.7895	546.7878	3.11	b_{10}^{2+}
584.2957	584.2940	2.91	y_4
590.8164	590.8147	2.88	y_{11}^{2+}
596.3237	596.3220	2.85	b_{11}^{2+}
608.8370	608.8354	2.63	y_{23}^{4+}
623.6776	623.6758	2.89	y_{17}^{3+}
626.3352	626.3333	3.03	y_{12}^{2+}
646.8478	646.8459	2.94	b_{12}^{2+}
649.6961	649.6948	2.00	b_{18}^{3+}
655.3331	655.3311	3.05	y_5
671.0362	671.0339	3.43	y_{19}^{3+}
675.8694	675.8675	2.81	y_{13}^{2+}
677.3637	677.3617	2.95	b_6
682.3665	682.3644	3.08	b_{13}^{2+}
687.7108	687.7091	2.47	b_{19}^{3+}
694.5849	694.5828	3.02	b_{33}^{5+}
713.7220	713.7201	2.66	y_{20}^{3+}
714.3916	714.3965	-6.86	b_{34}^{5+}
720.7341	720.7319	3.05	b_{20}^{3+}
725.4039	725.4017	3.03	y_{14}^{2+}
738.9088	738.9065	3.11	b_{14}^{2+}
747.0115	747.0092	3.08	b_{35}^{5+}
759.0768	759.0742	3.43	b_{21}^{3+}
761.2044	761.2018	3.42	y_{35}^{5+}
768.4176	768.4151	3.25	y_6
779.0963	779.0938	3.21	y_{22}^{3+}
781.0175	781.0155	2.56	y_{36}^{5+}
786.1738	786.1713	3.18	y_{29}^{4+}
786.6694	786.6676	2.29	b_{30}^{4+}
789.4516	789.4492	3.04	y_{15}^{2+}
802.0909	802.0884	3.12	b_{22}^{3+}

806.4070	806.4043	3.35	b_{7}
811.4473	811.4448	3.08	y_{23}^{3+}
814.9412	814.9386	3.19	b_{31}^{4+}
820.4386	820.4360	3.17	y_{30}^{4+}
831.9488	831.9461	3.25	b_{15}^{2+}
835.1139	835.1112	3.23	b_{23}^{3+}
839.4547	839.4522	2.98	y_{7}
843.2123	843.2096	3.20	b_{32}^{4+}
845.1302	845.1273	3.43	y_{24}^{3+}
853.4816	853.4785	3.63	y_{16}^{2+}
854.1214	854.1184	3.51	b_{24}^{3+}
854.7033	854.7007	3.04	y_{31}^{4+}
859.7991	859.7962	3.37	y_{47}^{6+}
867.9795	867.9767	3.23	b_{33}^{4+}
872.4633	872.4600	3.78	y_{32}^{4+}
873.1281	873.1255	2.98	b_{25}^{3+}
888.6148	888.6139	1.01	y_{56}^{7+}
891.1355	891.1341	1.57	b_{48}^{6+}
892.7467	892.7438	3.25	b_{34}^{4+}
894.1534	894.1501	3.69	y_{25}^{3+}
900.7335	900.7310	2.78	y_{33}^{4+}
905.6342	905.6395	-5.85	b_{49}^{6+}
916.1429	916.1397	3.49	b_{26}^{3+}
918.3231	918.3220	1.20	y_{50}^{6+}
919.4830	919.4817	1.41	y_{58}^{7+}
924.5074	924.5043	3.35	b_{17}^{2+}
933.5128	933.5096	3.43	b_{35}^{4+}
934.5029	934.4993	3.85	b_{8}
935.0133	935.0101	3.42	y_{17}^{2+}
937.1674	937.1693	-2.03	y_{51}^{6+}
939.8221	939.8188	3.51	b_{27}^{3+}
939.9557	939.9535	2.34	y_{96}^{11+}
949.1309	949.1397	-9.27	y_{97}^{11+}
951.2536	951.2504	3.36	y_{35}^{4+}
953.4984	953.4952	3.36	y_{8}
958.5201	958.5185	1.67	y_{52}^{6+}
968.5034	968.5097	-6.50	y_{70}^{8+}
970.5321	970.5287	3.50	y_{18}^{2+}
974.0419	974.0386	3.39	b_{18}^{2+}
976.0209	976.0175	3.48	y_{36}^{4+}
977.5158	977.5135	2.35	b_{28}^{3+}
977.6926	977.6896	3.07	y_{53}^{6+}
982.7199	982.7193	0.61	b_{44}^{5+}
986.3388	986.3350	3.85	y_{45}^{5+}

994.8593	994.8578	1.51	y_{54}^{6+}
996.5268	996.5206	6.22	b_{29}^{3+}
998.6554	998.6525	2.90	y_{73}^{8+}
998.8734	998.8698	3.60	y_{28}^{3+}
1003.8108	1003.8112	-0.40	y_{64}^{7+}
1004.2922	1004.2926	-0.40	b_{37}^{4+}
1006.0511	1006.0472	3.88	y_{19}^{2+}
1011.6053	1011.6106	-5.24	y_{111}^{12+}
1017.7053	1017.7010	4.23	y_{55}^{6+}
1024.5350	1024.5323	2.64	y_{9}
1025.1979	1025.1992	-1.27	y_{112}^{12+}
1031.5566	1031.5540	2.52	y_{47}^{5+}
1033.8506	1033.8482	2.32	y_{96}^{10+}
1043.9543	1043.9529	1.34	y_{97}^{10+}
1069.1641	1069.1595	4.30	b_{48}^{5+}
1070.0805	1070.0765	3.74	y_{20}^{2+}
1071.4658	1071.4589	6.44	b_{99}^{10+}
1072.5659	1072.5607	4.85	y_{58}^{6+}
1075.4730	1075.4672	5.39	y_{100}^{10+}
1080.5982	1080.5942	3.70	b_{20}^{2+}
1085.3582	1085.3569	1.20	y_{140}^{14+}
1086.2533	1086.2490	3.96	b_{31}^{3+}
1093.5805	1093.5789	1.46	y_{30}^{3+}
1103.4877	1103.4837	3.62	y_{111}^{11+}
1107.2639	1107.2728	-8.04	y_{132}^{13+}
1108.7224	1108.7243	-1.71	y_{143}^{14+}
1118.3069	1118.3076	-0.63	y_{112}^{11+}
1123.9475	1123.9437	3.38	b_{32}^{3+}
1137.3623	1137.3616	0.62	b_{41}^{4+}
1141.1753	1141.1732	1.84	y_{73}^{7+}
1148.6115	1148.6083	2.79	y_{96}^{9+}
1151.3910	1151.3808	8.86	b_{96}^{9+}
1156.9705	1156.9665	3.46	b_{33}^{3+}
1159.8386	1159.8358	2.41	y_{97}^{9+}
1166.6173	1166.6096	6.60	b_{97}^{9+}
1168.1411	1168.1371	3.42	y_{22}^{2+}
1169.5085	1169.5060	2.14	y_{98}^{9+}
1174.1331	1174.1287	3.75	b_{42}^{4+}
1177.4500	1177.4497	0.25	b_{65}^{6+}
1180.6265	1180.6222	3.64	y_{11}
1182.0738	1182.0709	2.45	y_{99}^{9+}
1185.4211	1185.4181	2.53	y_{109}^{10+}
1185.4211	1185.4197	1.18	b_{109}^{10+}
1189.9934	1189.9893	3.45	b_{34}^{3+}

1190.3950	1190.3979	-2.44	b_{99}^{9+}
1194.8565	1194.8517	4.02	y_{100}^{9+}
1200.6338	1200.6389	-4.25	y_{33}^{3+}
1201.1901	1201.1874	2.25	y_{101}^{9+}
1202.6327	1202.6290	3.08	b_{22}^{2+}
1206.3938	1206.3893	3.73	b_{43}^{4+}
1209.3351	1209.3427	-6.28	y_{78}^{7+}
1213.7349	1213.7313	2.97	y_{111}^{10+}
1216.6676	1216.6635	3.37	y_{23}^{2+}
1225.4956	1225.4975	-1.55	y_{79}^{7+}
1228.1510	1228.1473	3.01	b_{44}^{4+}
1230.0354	1230.0376	-1.79	y_{112}^{10+}
1239.6546	1239.6502	3.55	y_{80}^{7+}
1244.3478	1244.3437	3.29	b_{35}^{3+}
1251.6649	1251.6593	4.47	y_{12}
1252.1681	1252.1632	3.91	b_{23}^{2+}
1257.9451	1257.9494	-3.42	y_{81}^{7+}
1264.9187	1264.9145	3.32	b_{45}^{5+}
1267.1913	1267.1873	3.16	y_{24}^{2+}
1268.1718	1268.1673	3.55	y_{69}^{6+}
1276.6854	1276.6947	-7.28	b_{36}^{3+}
1289.1965	1289.1907	4.50	y_{47}^{4+}
1291.0206	1291.0105	7.82	y_{70}^{6+}
1292.0629	1292.0584	3.48	y_{96}^{8+}
1292.6890	1292.6845	3.48	b_{12}
1295.1798	1295.1775	1.78	b_{96}^{8+}
1307.9307	1307.9266	3.13	b_{47}^{4+}
1313.6970	1313.6886	6.39	b_{73}^{6+}
1321.6986	1321.6973	0.98	y_{72}^{6+}
1336.2015	1336.1976	2.92	b_{48}^{4+}
1340.7268	1340.7215	3.95	y_{25}^{2+}
1350.7327	1350.7277	3.70	y_{13}
1357.9603	1357.9556	3.46	b_{49}^{4+}
1363.7256	1363.7216	2.93	b_{13}
1373.7130	1373.7060	5.10	b_{26}^{2+}
1383.2215	1383.2175	2.89	b_{50}^{4+}
1405.2484	1405.2428	3.99	y_{26}^{2+}
1476.8103	1476.8057	3.11	b_{14}

Appendix 9. CID (normalized collision energy 30 %) fragment ions of normal neonatal γ_G-globin chain

Meas *m/z*	Calc *m/z*	Δ ppm	Fragment
558.7490	558.7515	-4.47	b_{10}^{2+}
562.2728	562.2732	-0.71	y_4
615.2935	615.2935	0.00	b_{11}^{2+}
649.3039	649.3052	-2.00	y_5
665.8170	665.8173	-0.45	b_{12}^{2+}
701.2885	701.2889	-0.57	b_6
705.6872	705.6884	-1.70	b_{19}^{3+}
709.3310	709.3333	-3.24	b_{13}^{2+}
738.7109	738.7112	-0.41	b_{20}^{3+}
739.8735	739.8747	-1.62	y_{14}^{2+}
762.3874	762.3893	-2.49	y_6
765.8739	765.8754	-1.96	b_{14}^{2+}
769.3939	769.3952	-1.69	y_{21}^{3+}
781.7250	781.7254	-0.51	b_{21}^{3+}
800.6454	800.6468	-1.75	b_{30}^{4+}
811.1575	811.1579	-0.49	y_{29}^{4+}
816.3138	816.3159	-2.57	b_7
820.0672	820.0677	-0.61	b_{22}^{3+}
828.9171	828.9178	-0.84	b_{31}^{4+}
833.4236	833.4264	-3.36	y_7
843.7447	843.7467	-2.37	b_{23}^{3+}
845.4236	845.4227	1.06	y_{30}^{4+}
857.1867	857.1889	-2.57	b_{32}^{4+}
858.9129	858.9150	-2.44	b_{15}^{2+}
862.7523	862.7539	-1.85	b_{24}^{3+}
867.9491	867.9514	-2.65	y_{16}^{2+}
873.6938	873.6957	-2.17	y_{31}^{4+}
881.7587	881.7610	-2.61	b_{25}^{3+}

881.9552	881.9560	-0.91	b_{33}^{4+}
887.4231	887.4258	-3.04	b_{16}^{2+}
891.4529	891.4530	-0.11	y_{32}^{4+}
897.9512	897.9537	-2.78	b_{48}^{6+}
906.7247	906.7231	1.76	b_{34}^{4+}
917.7362	917.7349	1.42	y_{66}^{8+}
919.7203	919.7240	-4.02	y_{33}^{4+}
920.4550	920.4585	-3.80	y_{8}
924.7724	924.7752	-3.03	b_{26}^{3+}
927.4639	927.4657	-1.94	y_{25}^{3+}
944.4115	944.4108	0.74	b_{8}
947.4857	947.4889	-3.38	b_{35}^{4+}
951.4700	951.4732	-3.36	b_{17}^{2+}
966.1857	966.1858	-0.10	y_{52}^{6+}
969.7510	969.7530	-2.06	y_{35}^{4+}
977.7602	977.7595	0.72	y_{70}^{8+}
980.0727	980.0738	-1.12	y_{80}^{9+}
991.4927	991.4956	-2.92	y_{9}
994.5189	994.5201	-1.21	y_{36}^{4+}
995.5324	995.5358	-3.42	y_{45}^{5+}
1001.0083	1001.0074	0.90	b_{18}^{2+}
1004.5066	1004.5071	-0.50	y_{18}^{2+}
1016.7852	1016.7866	-1.38	y_{73}^{8+}
1017.6171	1017.6180	-0.88	y_{111}^{12+}
1022.7897	1022.7911	-1.37	y_{37}^{4+}
1032.1854	1032.1853	0.10	y_{28}^{3+}
1032.1829	1032.1853	-2.33	y_{28}^{3+}
1040.7528	1040.7549	-2.02	y_{47}^{5+}
1048.6939	1048.6960	-2.00	y_{66}^{7+}
1077.3399	1077.3430	-2.88	b_{48}^{5+}
1079.6505	1079.6590	-7.87	b_{99}^{10+}
1081.2082	1081.2081	0.09	y_{29}^{3+}
1082.4399	1082.4365	3.14	b_{80}^{8+}
1090.3284	1090.3243	3.76	y_{40}^{4+}
1098.6499	1098.6565	-6.01	y_{131}^{13+}

1104.8870	1104.8880	-0.91	b_{31}^{3+}
1110.0375	1110.0372	0.27	y_{111}^{11+}
1122.4354	1122.4270	7.48	y_{123}^{12+}
1142.5784	1142.5827	-3.76	b_{32}^{3+}
1148.6843	1148.6859	-1.39	y_{126}^{12+}
1159.2191	1159.2215	-2.07	y_{52}^{5+}
1169.5127	1169.5122	0.43	y_{97}^{9+}
1175.6029	1175.6055	-2.21	b_{33}^{3+}
1178.8884	1178.8901	-1.44	y_{43}^{4+}
1179.1795	1179.1825	-2.54	y_{98}^{9+}
1183.1138	1183.1143	-0.42	y_{86}^{8+}
1188.1067	1188.1080	-1.09	b_{42}^{4+}
1199.5149	1199.5092	4.75	b_{99}^{9+}
1208.6262	1208.6283	-1.74	b_{34}^{3+}
1216.8670	1216.8647	1.89	b_{43}^{4+}
1220.9359	1220.9402	-3.52	y_{111}^{10+}
1225.9633	1225.9629	0.33	y_{33}^{3+}
1229.5991	1229.5979	0.98	b_{22}^{2+}
1236.9345	1236.9264	6.55	b_{80}^{7+}
1238.6199	1238.6227	-2.26	b_{44}^{4+}
1242.4827	1242.4820	0.56	y_{67}^{6+}
1262.9791	1262.9828	-2.93	b_{35}^{3+}
1266.6329	1266.6368	-3.08	y_{23}^{2+}
1275.3876	1275.3898	-1.72	b_{45}^{4+}
1289.6423	1289.6452	-2.25	b_{46}^{4+}
1292.6634	1292.6682	-3.71	y_{35}^{3+}
1300.6893	1300.6918	-1.92	y_{47}^{4+}
1303.3459	1303.3436	1.76	y_{70}^{6+}
1318.1513	1318.1559	-3.49	b_{47}^{4+}
1325.6887	1325.6910	-1.73	y_{36}^{3+}
1344.2948	1344.3008	-4.46	y_{60}^{5+}
1346.4239	1346.4269	-2.23	b_{48}^{4+}
1354.2132	1354.2156	-1.77	y_{49}^{4+}
1363.3841	1363.3857	-1.17	y_{37}^{3+}
1434.4193	1434.4228	-2.44	y_{39}^{3+}

1490.7649	1490.7769	-8.05	y_{67}^{5+}
1490.9491	1490.9563	-4.83	y_{81}^{6+}
1521.7981	1521.8090	-7.16	y_{83}^{6+}
1563.8093	1563.8109	-1.02	y_{70}^{5+}
1571.5106	1571.5177	-4.52	y_{43}^{3+}
1658.5542	1658.5548	-0.36	y_{45}^{3+}
1697.8949	1697.8835	6.71	y_{61}^{4+}

Appendix 10. CID (normalized collision energy 30 %) fragment ions of normal neonatal γ_A- globin chain

Meas *m/z*	Calc *m/z*	Δ ppm	Fragment
558.7532	558.7515	3.04	b_{10}^{2+}
562.2701	562.2732	-5.51	y_4
615.2919	615.2935	-2.60	b_{11}^{2+}
649.3059	649.3052	1.08	y_5
665.8153	665.8173	-3.00	b_{12}^{2+}
701.2872	701.2889	-2.42	b_6
705.6860	705.6884	-3.40	b_{19}^{3+}
709.3339	709.3333	0.85	b_{13}^{2+}
738.7124	738.7112	1.62	b_{20}^{3+}
762.3875	762.3893	-2.36	y_6
765.8741	765.8754	-1.70	b_{14}^{2+}
781.7243	781.7254	-1.41	b_{21}^{3+}
800.6448	800.6468	-2.50	b_{30}^{4+}
816.3134	816.3159	-3.06	b_7
820.0663	820.0677	-1.71	b_{22}^{3+}
828.9159	828.9178	-2.29	b_{31}^{4+}
833.4239	833.4264	-3.00	y_7
843.7445	843.7467	-2.61	b_{23}^{3+}
849.4314	849.4322	-0.94	y_{23}^{3+}
857.1874	857.1889	-1.75	b_{32}^{4+}
858.9129	858.9150	-2.44	b_{15}^{2+}
862.7533	862.7539	-0.70	b_{24}^{3+}
881.7592	881.7610	-2.04	b_{25}^{3+}
881.9538	881.9560	-2.49	b_{33}^{4+}
887.4235	887.4258	-2.59	b_{16}^{2+}
897.9531	897.9537	-0.67	b_{48}^{6+}
906.7204	906.7231	-2.98	b_{34}^{4+}
920.4577	920.4585	-0.87	y_8

923.2261	923.2279	-1.95	y_{33}^{4+}
924.7728	924.7752	-2.60	b_{26}^{3+}
932.1367	932.1376	-0.97	y_{25}^{3+}
944.4094	944.4108	-1.48	b_{8}
947.4859	947.4889	-3.17	b_{35}^{4+}
951.4766	951.4732	3.57	b_{17}^{2+}
973.2581	973.2569	1.23	y_{35}^{4+}
979.5079	979.5115	-3.68	y_{70}^{8+}
991.4928	991.4956	-2.82	y_{9}
998.0262	998.0240	2.20	y_{36}^{4+}
1001.0094	1001.0074	2.00	b_{18}^{2+}
1043.5554	1043.5580	-2.49	y_{47}^{5+}
1050.6944	1050.6983	-3.71	y_{66}^{7+}
1077.3398	1077.3430	-2.97	b_{48}^{5+}
1079.6513	1079.6590	-7.13	b_{99}^{10+}
1082.4373	1082.4365	0.74	b_{80}^{8+}
1099.7327	1099.7346	-1.73	y_{131}^{13+}
1104.8849	1104.8880	-2.81	b_{31}^{3+}
1111.3099	1111.3113	-1.26	y_{111}^{11+}
1114.0467	1114.0484	-1.53	y_{132}^{13+}
1123.5933	1123.5950	-1.51	y_{123}^{12+}
1142.5789	1142.5827	-3.33	b_{32}3+
1175.6013	1175.6055	-3.57	b_{33}^{3+}
1188.1066	1188.1080	-1.18	b_{42}^{4+}
1199.5143	1199.5092	4.25	b_{99}^{9+}
1208.6295	1208.6283	0.99	b_{34}^{3+}
1216.8627	1216.8647	-1.64	b_{43}^{4+}
1229.5991	1229.5979	0.98	b_{22}^{2+}
1236.9349	1236.9264	6.87	b_{80}^{7+}
1238.6195	1238.6227	-2.58	b_{44}^{4+}
1262.9789	1262.9828	-3.09	b_{35}^{3+}
1275.3879	1275.3898	-1.49	b_{45}^{4+}
1289.6403	1289.6452	-3.80	b_{46}^{4+}
1318.1533	1318.1559	-1.97	b_{47}^{4+}
1346.4239	1346.4269	-2.23	b_{48}^{4+}

Appendix 11**.** CID (normalized collision energy 30 %) fragment ions of the sickle globin chain in a neonatal sample.

Meas m/z	Calc m/z	Δ ppm	Fragment
451.2661	451.2663	-0.44	b_4
581.3341	581.3350	-1.55	b_{11}^{2+}
584.2932	584.2940	-1.37	y_4
608.8344	608.8354	-1.64	y_{23}^{4+}
631.8590	631.8588	0.32	b_{12}^{2+}
647.3854	647.3875	-3.24	b_6
655.3306	655.3311	-0.76	y_5
667.3767	667.3774	-1.05	b_{13}^{2+}
675.8667	675.8675	-1.18	y_{13}^{2+}
723.9188	723.9194	-0.83	b_{14}^{2+}
725.4009	725.4017	-1.10	y_{14}^{2+}
749.0819	749.0828	-1.20	b_{21}^{3+}
768.4146	768.4151	-0.65	y_6
776.4296	776.4301	-0.64	b_7
779.0940	779.0938	0.26	y_{22}^{3+}
779.1732	779.1740	-1.03	b_{30}^{4+}
781.0157	781.0155	0.26	y_{36}^{5+}
789.4487	789.4492	-0.63	y_{15}^{2+}
792.0964	792.0970	-0.76	b_{22}^{3+}
807.4430	807.4450	-2.48	b_{31}^{4+}
811.4441	811.4448	-0.86	y_{23}^{3+}
816.9584	816.9590	-0.73	b_{15}^{2+}
820.4356	820.4360	-0.49	y_{30}^{4+}
825.1187	825.1198	-1.33	b_{23}^{3+}
835.7155	835.7160	-0.60	b_{32}^{4+}
844.1260	844.1270	-1.18	b_{24}^{3+}
845.1273	845.1273	0.00	y_{24}^{3+}
845.4694	845.4698	-0.47	b_{16}^{2+}
853.4784	853.4785	-0.12	y_{16}^{2+}
854.7014	854.7007	0.82	y_{31}^{4+}

859.7960	859.7962	-0.23	y_{47}^{6+}
860.4825	860.4831	-0.70	b_{33}^{4+}
872.4592	872.4600	-0.92	y_{32}^{4+}
885.2497	885.2502	-0.56	b_{34}^{4+}
900.7307	900.7310	-0.33	y_{33}^{4+}
904.5243	904.5251	-0.88	b_{8}
906.1465	906.1483	-1.99	b_{26}^{3+}
909.5175	909.5173	0.22	b_{17}^{2+}
918.3249	918.3220	3.16	y_{50}^{6+}
925.4938	925.4981	-4.65	y_{34}^{4+}
926.0156	926.0161	-0.54	b_{35}^{4+}
929.8265	929.8274	-0.97	b_{27}^{3+}
934.1133	934.1127	0.64	y_{43}^{5+}
935.0094	935.0101	-0.75	y_{17}^{2+}
937.1652	937.1643	0.96	y_{26}^{3+}
939.9561	939.9535	2.77	y_{96}^{11+}
950.2736	950.2793	-6.00	b_{36}^{4+}
953.4946	953.4952	-0.63	y_{8}
959.0509	959.0515	-0.63	b_{18}^{2+}
967.5210	967.5221	-1.14	b_{28}^{3+}
970.5286	970.5287	-0.10	y_{18}^{2+}
976.0171	976.0175	-0.41	y_{36}^{4+}
979.8645	979.8626	1.94	y_{27}^{3+}
998.6500	998.6525	-2.50	y_{73}^{8+}
998.8708	998.8698	1.00	y_{28}^{3+}
1006.0480	1006.0472	0.80	y_{19}^{2+}
1024.5332	1024.5323	0.88	y_{9}
1031.5542	1031.5540	0.19	y_{47}^{5+}
1033.8462	1033.8482	-1.93	y_{96}^{10+}
1076.2585	1076.2576	0.84	b_{31}^{3+}
1093.5763	1093.5789	-2.38	y_{30}^{3+}
1103.4810	1103.4837	-2.45	y_{111}^{11+}
1113.9524	1113.9523	0.09	b_{32}^{3+}
1146.9748	1146.9751	-0.26	b_{33}^{3+}
1148.6074	1148.6083	-0.78	y_{96}^{9+}

1159.8341	1159.8358	-1.47	y_{97}^{9+}
1166.6343	1166.6351	-0.69	b_{42}^{4+}
1169.5027	1169.5060	-2.82	y_{98}^{9+}
1179.9977	1179.9979	-0.17	b_{34}^{3+}
1187.0606	1187.0675	-5.81	b_{99}^{9+}
1198.8956	1198.8958	-0.17	b_{43}^{4+}
1201.1939	1201.1874	5.41	y_{101}^{9+}
1213.7291	1213.7313	-1.81	y_{111}^{10+}
1216.6649	1216.6635	1.15	y_{23}^{2+}
1220.6550	1220.6538	0.98	b_{44}^{4+}
1234.3516	1234.3523	-0.57	b_{35}^{3+}
1257.4185	1257.4209	-1.91	b_{45}^{4+}
1268.0014	1267.9981	2.60	y_{35}^{3+}
1271.6818	1271.6763	4.33	b_{46}^{4+}
1300.4324	1300.4330	-0.46	b_{47}^{4+}
1318.1903	1318.1965	-4.70	b_{74}^{6+}
1328.7058	1328.7040	1.35	b_{48}^{4+}
1375.7227	1375.7240	-0.94	b_{50}^{4+}

Appendix 12**.** CID (normalized collision energy 30 %) fragment ions of the HbC globin chain in a neonatal sample.

Meas *m/z*	Calc *m/z*	Δ ppm	Fragment
451.2667	451.2663	0.89	b_4
584.2941	584.2940	0.17	y_4
608.8355	608.8354	0.16	y_{23}^{4+}
655.3311	655.3311	0.00	y_5
671.0337	671.0339	-0.30	y_{19}^{3+}
675.8678	675.8675	0.44	y_{13}^{2+}
681.8906	681.8906	0.00	b_{13}^{2+}
713.7207	713.7201	0.84	y_{20}^{3+}
720.4157	720.4160	-0.42	b_{20}^{3+}
725.4016	725.4017	-0.14	y_{14}^{2+}
738.4330	738.4327	0.41	b_{14}^{2+}
758.7587	758.7583	0.53	b_{21}^{3+}
768.4150	768.4151	-0.13	y_6
779.0939	779.0938	0.13	y_{22}^{3+}
786.1729	786.1713	2.04	y_{29}^{4+}
786.4308	786.4306	0.25	b_{30}^{4+}
789.4497	789.4492	0.63	y_{15}^{2+}
801.7727	801.7725	0.25	b_{22}^{3+}
811.4450	811.4448	0.25	y_{23}^{3+}
820.4374	820.4360	1.71	y_{30}^{4+}
834.7956	834.7953	0.36	b_{23}^{3+}
842.9729	842.9727	0.24	b_{32}^{4+}
845.1277	845.1273	0.47	y_{24}^{3+}
853.4782	853.4785	-0.35	y_{16}^{2+}
853.8031	853.8025	0.70	b_{24}^{3+}
854.7007	854.7007	0.00	y_{31}^{4+}
859.7964	859.7962	0.23	y_{47}^{6+}
867.7404	867.7398	0.69	b_{33}^{4+}
872.4612	872.4600	1.38	y_{32}^{4+}
892.5073	892.5069	0.45	b_{34}^{4+}
900.7321	900.7310	1.22	y_{33}^{4+}

933.2721	933.2727	-0.64	b_{35}^{4+}
935.0111	935.0101	1.07	y_{17}^{2+}
939.9543	939.9535	0.85	y_{96}^{11+}
953.4956	953.4952	0.42	y_{8}
970.5296	970.5287	0.93	y_{18}^{2+}
976.0187	976.0175	1.23	y_{36}^{4+}
998.6521	998.6525	-0.40	y_{73}^{8+}
998.8716	998.8698	1.80	y_{28}^{3+}
1006.0484	1006.0472	1.19	y_{19}^{2+}
1024.5322	1024.5323	-0.10	y_{9}
1031.5549	1031.5540	0.87	y_{47}^{5+}
1033.8483	1033.8482	0.10	y_{96}^{10+}
1103.4820	1103.4837	-1.54	y_{111}^{11+}
1148.6090	1148.6083	0.61	y_{96}^{9+}
1156.6505	1156.6506	-0.09	b_{33}^{3+}
1159.8394	1159.8358	3.10	y_{97}^{9+}
1169.5072	1169.5060	1.03	y_{98}^{9+}
1173.8883	1173.8918	-2.98	b_{42}^{4+}
1189.6753	1189.6734	1.60	b_{34}^{3+}
1202.1539	1202.1552	-1.08	b_{22}^{2+}
1206.1546	1206.1524	1.82	b_{43}^{4+}
1213.7287	1213.7313	-2.14	y_{111}^{10+}
1216.6638	1216.6635	0.25	y_{23}^{2+}
1227.9149	1227.9104	3.66	b_{44}^{4+}
1244.0288	1244.0279	0.72	b_{35}^{3+}
1251.6605	1251.6593	0.96	y_{12}
1264.9286	1264.9275	0.87	y_{46}^{4+}
1307.6917	1307.6896	1.61	b_{47}^{4+}
1382.9813	1382.9806	0.51	b_{50}^{4+}

Appendix 13**.** CID (normalized collision energy 30 %) fragment ions of HbD globin chain in a neonatal sample.

Meas *m/z*	Calc *m/z*	Δ ppm	Fragment
350.2181	350.2187	-1.71	b_3
451.2664	451.2663	0.22	b_4
512.7696	512.7698	-0.39	y_9^{2+}
546.7876	546.7878	-0.37	b_{10}^{2+}
584.2937	584.2940	-0.51	y_4
590.8144	590.8147	-0.51	y_{11}^{2+}
596.3217	596.3220	-0.50	b_{11}^{2+}
608.8350	608.8354	-0.66	y_{23}^{4+}
626.3331	626.3333	-0.32	y_{12}^{2+}
646.8456	646.8459	-0.46	b_{12}^{2+}
649.6942	649.6948	-0.92	b_{18}^{3+}
655.3309	655.3311	-0.31	y_5
671.0337	671.0339	-0.30	y_{19}^{3+}
675.8672	675.8675	-0.44	y_{13}^{2+}
677.3615	677.3617	-0.30	b_6
682.3641	682.3644	-0.44	b_{13}^{2+}
687.7088	687.7091	-0.44	b_{19}^{3+}
713.7199	713.7201	-0.28	y_{20}^{3+}
720.7318	720.7319	-0.14	b_{20}^{3+}
725.4015	725.4017	-0.28	y_{14}^{2+}
738.9063	738.9065	-0.27	b_{14}^{2+}
759.0741	759.0742	-0.13	b_{21}^{3+}
768.4150	768.4151	-0.13	y_6
779.0937	779.0938	-0.13	y_{22}^{3+}
780.8183	780.8187	-0.51	y_{36}^{5+}
786.6671	786.6676	-0.64	b_{30}^{4+}
789.4490	789.4492	-0.25	y_{15}^{2+}
802.0883	802.0884	-0.12	b_{22}^{3+}
806.4042	806.4043	-0.12	b_7
811.4446	811.4448	-0.25	y_{23}^{3+}
814.9384	814.9386	-0.25	b_{31}^{4+}

820.1899	820.1900	-0.12	y_{30}^{4+}
831.9461	831.9461	0.00	b_{15}^{2+}
835.1110	835.1112	-0.24	b_{23}^{3+}
839.4519	839.4522	-0.36	y_{7}
843.2096	843.2096	0.00	b_{32}^{4+}
845.1272	845.1273	-0.12	y_{24}^{3+}
853.4783	853.4785	-0.23	y_{16}^{2+}
854.1183	854.1184	-0.12	b_{24}^{3+}
854.4531	854.4547	-1.87	y_{31}^{4+}
859.6322	859.6322	0.00	y_{47}^{6+}
867.9766	867.9767	-0.12	b_{33}^{4+}
872.2138	872.2140	-0.23	y_{32}^{4+}
873.1259	873.1255	0.46	b_{25}^{3+}
892.7436	892.7438	-0.22	b_{34}^{4+}
894.1502	894.1501	0.11	y_{25}^{3+}
900.4850	900.4850	0.00	y_{33}^{4+}
916.1393	916.1397	-0.44	b_{26}^{3+}
924.5043	924.5043	0.00	b_{17}^{2+}
925.2515	925.2521	-0.65	y_{34}^{4+}
933.5097	933.5096	0.11	b_{35}^{4+}
936.8368	936.8363	0.53	y_{26}^{3+}
939.8188	939.8188	0.00	b_{27}^{3+}
939.8610	939.8641	-3.30	y_{96}^{11+}
949.0511	949.0502	0.95	y_{97}^{11+}
951.0045	951.0044	0.11	y_{35}^{4+}
953.4951	953.4952	-0.10	y_{8}
958.3555	958.3545	1.04	y_{52}^{6+}
968.3866	968.3867	-0.10	y_{70}^{8+}
970.5288	970.5287	0.10	y_{18}^{2+}
974.0386	974.0386	0.00	b_{18}^{2+}
975.7714	975.7715	-0.10	y_{36}^{4+}
977.5131	977.5135	-0.41	b_{28}^{3+}
977.5259	977.5256	0.31	y_{53}^{6+}
998.5288	998.5295	-0.70	y_{73}^{8+}
998.5420	998.5418	0.20	y_{28}^{3+}

1006.0478	1006.0472	0.60	y_{19}^{2+}
1017.5365	1017.5370	-0.49	y_{55}^{6+}
1021.9651	1021.9699	-4.70	y_{65}^{7+}
1024.5311	1024.5323	-1.17	y_{9}
1031.3582	1031.3572	0.97	y_{47}^{5+}
1033.7480	1033.7498	-1.74	y_{96}^{10+}
1069.1602	1069.1595	0.65	b_{48}^{5+}
1103.3934	1103.3942	-0.73	y_{111}^{11+}
1123.9438	1123.9437	0.09	b_{32}^{3+}
1137.3597	1137.3616	-1.67	b_{41}^{4+}
1148.4970	1148.4989	-1.65	y_{96}^{9+}
1156.9667	1156.9665	0.17	b_{33}^{3+}
1159.7241	1159.7264	-1.98	y_{97}^{9+}
1168.1372	1168.1371	0.09	y_{22}^{2+}
1169.3943	1169.3967	-2.05	y_{98}^{9+}
1174.1293	1174.1287	0.51	b_{42}^{4+}
1180.6228	1180.6222	0.51	y_{11}
1189.9895	1189.9893	0.17	b_{34}^{3+}
1190.3995	1190.3979	1.34	b_{99}^{9+}
1202.6289	1202.6290	-0.08	b_{22}^{2+}
1206.3895	1206.3893	0.17	b_{43}^{4+}
1216.6635	1216.6635	0.00	y_{23}^{2+}
1228.1469	1228.1473	-0.33	b_{44}^{4+}
1244.3437	1244.3437	0.00	b_{35}^{3+}
1251.6600	1251.6593	0.56	y_{12}
1252.1647	1252.1632	1.20	b_{23}^{2+}
1264.9141	1264.9145	-0.32	b_{45}^{4+}
1267.1870	1267.1873	-0.24	y_{24}^{2+}
1279.1704	1279.1698	0.47	b_{46}^{4+}
1288.9404	1288.9447	-3.34	y_{47}^{4+}
1291.9325	1291.9354	-2.24	y_{96}^{8+}
1307.9264	1307.9266	-0.15	b_{47}^{4+}
1336.1971	1336.1976	-0.37	b_{48}^{4+}
1340.7220	1340.7215	0.37	y_{25}^{2+}
1350.7279	1350.7277	0.15	y_{13}

1357.9552	1357.9556	-0.29	b_{49}^{4+}
1363.7217	1363.7216	0.07	b_{13}
1383.2169	1383.2175	-0.43	b_{50}^{4+}
1449.7961	1449.7961	0.00	y_{14}
1476.8056	1476.8057	-0.07	b_{14}
1662.8850	1662.8850	0.00	b_{15}

Appendix 14. CID (normalized collision energy 30 %) fragment ions of HbE globin chain in a neonatal sample.

Meas *m/z*	Calc *m/z*	Δ ppm	Fragment
350.2185	350.2187	-0.57	b_3
451.2669	451.2663	1.33	b_4
546.7882	546.7878	0.73	b_{10}^{2+}
584.2945	584.2940	0.86	y_4
596.3224	596.3220	0.67	b_{11}^{2+}
608.8359	608.8354	0.82	y_{23}^{4+}
626.3338	626.3333	0.80	y_{12}^{2+}
646.8466	646.8459	1.08	b_{12}^{2+}
655.3318	655.3311	1.07	y_5
675.8682	675.8675	1.04	y_{13}^{2+}
677.3625	677.3617	1.18	b_6
682.3651	682.3644	1.03	b_{13}^{2+}
713.7208	713.7201	0.98	y_{20}^{3+}
720.7325	720.7319	0.83	b_{20}^{3+}
725.4025	725.4017	1.10	y_{14}^{2+}
738.9072	738.9065	0.95	b_{14}^{2+}
759.0751	759.0742	1.19	b_{21}^{3+}
768.4160	768.4151	1.17	y_6
779.0946	779.0938	1.03	y_{22}^{3+}
781.0174	781.0155	2.43	y_{36}^{5+}
786.1718	786.1713	0.64	y_{29}^{4+}
789.4501	789.4492	1.14	y_{15}^{2+}
802.0894	802.0884	1.25	b_{22}^{3+}
806.4051	806.4043	0.99	b_7
811.4456	811.4448	0.99	y_{23}^{3+}
820.4366	820.4360	0.73	y_{30}^{4+}
831.9472	831.9461	1.32	b_{15}^{2+}
835.1123	835.1112	1.32	b_{23}^{3+}
839.4530	839.4522	0.95	y_7
842.9724	842.9727	-0.36	b_{32}^{4+}
845.1285	845.1273	1.42	y_{24}^{3+}
853.4796	853.4785	1.29	y_{16}^{2+}
854.1195	854.1184	1.29	b_{24}^{3+}
854.7018	854.7007	1.29	y_{31}^{4+}
859.7974	859.7962	1.40	y_{47}^{6+}
872.4616	872.4600	1.83	y_{32}^{4+}
892.5066	892.5069	-0.34	b_{34}^{4+}

900.7321	900.7310	1.22	y_{33}^{4+}
924.5055	924.5043	1.30	b_{17}^{2+}
933.2719	933.2727	-0.86	b_{35}^{4+}
935.0115	935.0101	1.50	y_{17}^{2+}
937.1652	937.1693	-4.37	y_{51}^{6+}
939.9464	939.9535	-7.55	y_{96}^{11+}
951.2515	951.2504	1.16	y_{35}^{4+}
953.4966	953.4952	1.47	y_{8}
958.5188	958.5185	0.31	y_{52}^{6+}
965.1238	965.1234	0.41	b_{43}^{5+}
968.5056	968.5097	-4.23	y_{70}^{8+}
970.5301	970.5297	0.41	y_{18}^{2+}
974.0398	974.0386	1.23	b_{18}^{2+}
976.0189	976.0175	1.43	y_{36}^{4+}
982.5315	982.5298	1.73	b_{44}^{5+}
986.3367	986.3350	1.72	y_{45}^{5+}
998.6529	998.6525	0.40	y_{73}^{8+}
998.8708	998.8698	1.00	y_{28}^{3+}
1003.8165	1003.8112	5.28	y_{64}^{7+}
1006.0490	1006.0472	1.79	y_{19}^{2+}
1011.6153	1011.6106	4.65	y_{111}^{12+}
1017.7028	1017.7010	1.77	y_{55}^{6+}
1023.3508	1023.3478	2.93	b_{46}^{5+}
1025.1977	1025.1992	-1.46	y_{112}^{12+}
1031.5546	1031.5540	0.58	y_{47}^{5+}
1033.8484	1033.8482	0.19	y_{96}^{10+}
1068.9674	1068.9700	-2.43	b_{48}^{5+}
1075.4676	1075.4672	0.37	y_{100}^{10+}
1092.8780	1092.8861	-7.41	y_{131}^{13+}
1103.4838	1103.4837	0.09	y_{111}^{11+}
1116.7441	1116.7340	9.04	y_{144}^{14+}
1148.6091	1148.6083	0.70	y_{96}^{9+}
1159.8331	1159.8358	-2.33	y_{97}^{9+}
1168.1382	1168.1371	0.94	y_{22}^{2+}
1169.5077	1169.5060	1.45	y_{98}^{9+}
1170.9423	1170.9451	-2.39	y_{64}^{6+}
1201.1908	1201.1874	2.83	y_{101}^{9+}
1202.6301	1202.6290	0.91	b_{22}^{2+}
1209.3361	1209.3427	-5.46	y_{78}^{7+}
1213.7303	1213.7313	-0.82	y_{111}^{10+}
1216.6651	1216.6635	1.32	y_{23}^{2+}
1227.9034	1227.9104	-5.70	b_{44}^{4+}
1230.0329	1230.0376	-3.82	y_{112}^{10+}
1244.0267	1244.0279	-0.96	b_{35}^{3+}

1252.1646	1252.1632	1.12	b_{23}^{2+}
1264.6703	1264.6775	-5.69	b_{45}^{4+}
1278.9291	1278.9329	-2.97	b_{46}^{4+}
1280.6755	1280.6739	1.25	b_{24}^{2+}
1292.0485	1292.0584	-7.66	y_{96}^{8+}
1307.6914	1307.6896	1.38	b_{47}^{4+}
1313.5358	1313.5307	3.88	b_{73}^{6+}
1350.7306	1350.7277	2.15	y_{13}
1363.7225	1363.7216	0.66	b_{13}
1382.9860	1382.9806	3.90	b_{50}^{4+}
1476.8071	1476.8057	0.95	b_{14}

Appendix 15**.** CID (normalized collision energy 30 %) fragment ions of HbC globin chain in a neonatal compound heterozygote FSC sample.

Meas *m/z*	Calc *m/z*	Δ ppm	Fragment
350.2222	350.2187	9.99	b_3
451.2705	451.2663	9.31	b_4
584.2897	584.2940	-7.36	y_4
590.8201	590.8147	9.14	y_{11}^{2+}
608.8415	608.8354	10.02	y_{23}^{4+}
623.6723	623.6758	-5.61	y_{17}^{3+}
626.3388	626.3333	8.78	y_{12}^{2+}
725.4084	725.4017	9.24	y_{14}^{2+}
738.4401	738.4327	10.02	b_{14}^{2+}
758.7652	758.7583	9.09	b_{21}^{3+}
768.4228	768.4151	10.02	y_6
779.1011	779.0938	9.37	y_{22}^{3+}
786.4376	786.4306	8.90	b_{30}^{4+}
801.7803	801.7725	9.73	b_{22}^{3+}
820.4278	820.4360	-9.99	y_{30}^{4+}
845.1240	845.1273	-3.90	y_{24}^{4+}
859.9746	859.9830	-9.77	b_{16}^{2+}
872.4682	872.4600	9.40	y_{32}^{4+}
892.5157	892.5069	9.86	b_{34}^{4+}
900.7400	900.7310	9.99	y_{33}^{4+}
918.3309	918.3220	9.69	y_{50}^{6+}
925.5069	925.4981	9.51	y_{34}^{4+}
935.0192	935.0101	9.73	y_{17}^{2+}
939.9591	939.9535	5.96	y_{96}^{11+}
951.2598	951.2504	9.88	y_{35}^{4+}
953.5051	953.4952	10.38	y_8
958.5091	958.5185	-9.81	y_{52}^{6+}
970.5191	970.5287	-9.89	y_{18}^{2+}
973.5744	973.5647	9.96	b_{18}^{2+}
976.0273	976.0175	10.04	y_{36}^{4+}
998.6525	998.6525	0.00	y_{73}^{8+}
1024.5428	1024.5329	9.66	y_9
1031.5449	1031.5540	-8.82	y_{47}^{5+}
1033.8512	1033.8482	2.90	y_{96}^{10+}
1103.4939	1103.4837	9.24	y_{111}^{11+}
1148.6195	1148.6083	9.75	y_{96}^{9+}
1156.6621	1156.6506	9.94	b_{33}^{3+}
1168.1484	1168.1371	9.67	y_{22}^{2+}
1189.6852	1189.6734	9.92	b_{34}^{3+}

1216.6755	1216.6635	9.86	y_{23}^{2+}
1244.0398	1244.0279	9.57	b_{35}^{3+}
1307.6914	1307.6896	1.38	b_{47}^{4+}

Appendix 16**.** CID (normalized collision energy 30 %) fragment ions of HbD globin chain in a neonatal compound heterozygote FSD sample.

Meas *m/z*	Calc *m/z*	Δ ppm	Fragment
738.9069	738.9065	0.54	b_{14}^{2+}
802.0876	802.0884	-1.00	b_{22}^{3+}
811.4454	811.4448	0.74	y_{23}^{3+}
831.9465	831.9461	0.48	b_{15}^{2+}
867.9769	867.9767	0.23	b_{33}^{4+}
872.2143	872.2140	0.34	y_{32}^{4+}
977.5241	977.5256	-1.53	y_{53}^{6+}
1024.5328	1024.5323	0.49	y_{9}
1031.3566	1031.3572	-0.58	y_{47}^{5+}
1033.7489	1033.7498	-0.87	y_{96}^{10+}
1103.3966	1103.3942	2.18	y_{111}^{11+}
1123.9450	1123.9437	1.16	b_{32}^{3+}
1146.5972	1146.5970	0.17	b_{63}^{6+}
1148.4982	1148.4989	-0.61	y_{96}^{9+}
1156.9669	1156.9665	0.35	b_{33}^{3+}
1168.1412	1168.1371	3.51	y_{22}^{2+}
1169.3942	1169.3967	-2.14	y_{98}^{9+}
1174.1325	1174.1287	3.24	b_{42}^{4+}
1189.9908	1189.9893	1.26	b_{34}^{3+}
1202.6303	1202.6290	1.08	b_{22}^{2+}
1213.6274	1213.6329	-4.53	y_{111}^{10+}
1216.6656	1216.6635	1.73	y_{23}^{2+}
1220.6552	1220.6432	9.83	b_{91}^{8+}
1228.1469	1228.1473	-0.33	b_{44}^{4+}
1244.3448	1244.3437	0.88	b_{35}^{3+}
1307.9273	1307.9266	0.54	b_{47}^{4+}

Appendix 17**.** CID (normalized collision energy 30 %) fragment ions of HbD -Iran globin chain in a previously undiagnosed (FAV1) neonatal sample.

Meas *m/z*	Calc *m/z*	Δ ppm	Fragment
350.2179	350.2187	-2.28	b_3
451.2663	451.2663	0.00	b_4
512.7696	512.7698	-0.39	y_9^{2+}
546.7874	546.7878	-0.73	b_{10}^{2+}
584.2934	584.2940	-1.03	y_4
590.8139	590.8147	-1.35	y_{11}^{2+}
596.3215	596.3220	-0.84	b_{11}^{2+}
608.8349	608.8354	-0.82	y_{23}^{4+}
626.3323	626.3333	-1.60	y_{12}^{2+}
646.8451	646.8459	-1.24	b_{12}^{2+}
655.3305	655.3311	-0.92	y_5
675.8670	675.8675	-0.74	y_{13}^{2+}
677.3611	677.3617	-0.89	b_6
682.3638	682.3644	-0.88	b_{13}^{2+}
687.7080	687.7091	-1.60	b_{19}^{3+}
713.7199	713.7201	-0.28	y_{20}^{3+}
720.7312	720.7319	-0.97	b_{20}^{3+}
725.4010	725.4017	-0.96	y_{14}^{2+}
738.9058	738.9065	-0.95	b_{14}^{2+}
759.0737	759.0742	-0.66	b_{21}^{3+}
768.4145	768.4151	-0.78	y_6
779.0931	779.0938	-0.90	y_{22}^{3+}
781.0142	781.0155	-1.66	y_{36}^{5+}
786.1702	786.1713	-1.40	y_{29}^{4+}
789.4485	789.4492	-0.89	y_{15}^{2+}
801.7598	801.7604	-0.75	b_{22}^{3+}
806.4037	806.4043	-0.74	b_7
811.4441	811.4448	-0.86	y_{23}^{3+}
820.4352	820.4360	-0.98	y_{30}^{4+}
831.9455	831.9461	-0.72	b_{15}^{2+}
834.7824	834.7832	-0.96	b_{23}^{3+}
839.4515	839.4522	-0.83	y_7
842.9634	842.9636	-0.24	b_{32}^{4+}
845.1267	845.1273	-0.71	y_{24}^{3+}
853.4780	853.4785	-0.59	y_{16}^{2+}
853.7901	853.7904	-0.35	b_{24}^{3+}
854.7001	854.7007	-0.70	y_{31}^{4+}
859.7955	859.7962	-0.81	y_{47}^{6+}
867.7299	867.7307	-0.92	b_{33}^{4+}
872.4602	872.4600	0.23	y_{32}^{4+}
880.4768	880.4802	-3.86	b_{40}^{5+}
892.4969	892.4978	-1.01	b_{34}^{4+}

894.1495	894.1501	-0.67	y_{25}^{3+}
900.7305	900.7310	-0.56	y_{33}^{4+}
919.4805	919.4817	-1.31	y_{58}^{7+}
924.5035	924.5043	-0.87	b_{17}^{2+}
925.5067	925.4981	9.29	y_{34}^{4+}
933.2629	933.2636	-0.75	b_{35}^{4+}
934.4988	934.4993	-0.54	b_{8}
937.1633	937.1693	-6.40	y_{51}^{6+}
939.9490	939.9535	-4.79	y_{96}^{11+}
951.2497	951.2504	-0.74	y_{35}^{4+}
953.4945	953.4952	-0.73	y_{8}
958.5189	958.5185	0.42	y_{52}^{6+}
968.5116	968.5097	1.96	y_{70}^{8+}
970.5281	970.5287	-0.62	y_{18}^{2+}
974.0379	974.0386	-0.72	b_{18}^{2+}
976.0173	976.0175	-0.20	y_{36}^{4+}
977.6872	977.6896	-2.45	y_{53}^{6+}
986.3337	986.3350	-1.32	y_{45}^{5+}
998.6506	998.6525	-1.90	y_{73}^{8+}
998.8696	998.8698	-0.20	y_{28}^{3+}
1003.8139	1003.8112	2.69	y_{64}^{7+}
1006.0469	1006.0472	-0.30	y_{19}^{2+}
1011.6013	1011.6106	-9.19	y_{111}^{12+}
1017.6995	1017.7010	-1.47	y_{55}^{6+}
1024.5310	1024.5323	-1.27	y_{9}
1031.5519	1031.5540	-2.04	y_{47}^{5+}
1033.8463	1033.8482	-1.84	y_{96}^{10+}
1036.2487	1036.2450	3.57	b_{96}^{10+}
1075.4673	1075.4672	0.09	y_{100}^{10+}
1081.0700	1081.0657	3.98	b_{100}^{10+}
1103.4818	1103.4837	-1.72	y_{111}^{11+}
1104.5769	1104.5794	-2.26	y_{103}^{10+}
1113.9170	1113.9188	-1.62	y_{123}^{12+}
1116.8958	1116.8954	0.36	b_{133}^{13+}
1118.3032	1118.3076	-3.93	y_{112}^{11+}
1123.6147	1123.6157	-0.89	b_{32}^{3+}
1137.1131	1137.1156	-2.20	b_{41}^{4+}
1148.6068	1148.6083	-1.31	y_{96}^{9+}
1149.9892	1149.9832	5.22	y_{85}^{8+}
1156.6379	1156.6385	-0.52	b_{33}^{3+}
1159.8328	1159.8358	-2.59	y_{97}^{9+}
1169.5036	1169.5060	-2.05	y_{98}^{9+}
1180.6214	1180.6222	-0.68	y_{11}
1185.3194	1185.3213	-1.60	b_{109}^{10+}
1189.6604	1189.6613	-0.76	b_{34}^{3+}
1190.2843	1190.2886	-3.61	b_{99}^{9+}
1201.1868	1201.1874	-0.50	y_{101}^{9+}
1202.1367	1202.1370	-0.25	b_{22}^{2+}

1206.1431	1206.1433	-0.17	b_{43}^{4+}
1209.2321	1209.2238	6.86	b_{55}^{5+}
1209.9141	1209.9088	4.38	y_{122}^{11+}
1213.7274	1213.7313	-3.21	y_{111}^{10+}
1215.0933	1215.0925	0.66	y_{123}^{11+}
1216.6626	1216.6635	-0.74	y_{23}^{2+}
1221.4617	1221.4576	3.36	b_{123}^{11+}
1227.9013	1227.9013	0.00	b_{44}^{4+}
1230.2870	1230.2805	5.28	b_{124}^{11+}
1244.0149	1244.0157	-0.64	b_{35}^{3+}
1249.3141	1249.3200	-4.72	y_{68}^{6+}
1251.6594	1251.6593	0.08	y_{12}
1264.6687	1264.6684	0.24	b_{45}^{4+}
1267.1867	1267.1873	-0.47	y_{24}^{2+}
1307.6794	1307.6806	-0.92	b_{47}^{4+}
1317.0231	1317.0193	2.89	y_{109}^{9+}
1335.9526	1335.9516	0.75	b_{48}^{4+}
1338.7100	1338.7156	-4.18	y_{37}^{3+}
1340.7204	1340.7215	-0.82	y_{25}^{2+}
1350.7260	1350.7277	-1.26	y_{13}
1363.7212	1363.7216	-0.29	b_{13}
1477.8077	1477.8057	1.35	b_{14}

Appendix 18**.** CID (normalized collision energy 30 %) fragment ions of HbD -Iran globin chain in a previously undiagnosed (FAV2) neonatal sample.

Meas *m/z*	Calc *m/z*	Δ ppm	Fragment
451.2688	451.2663	5.54	b_4
512.7716	512.7698	3.51	y_9^{2+}
562.3058	562.3040	3.20	y_{10}^{2+}
584.2959	584.2940	3.25	y_4
590.8167	590.8147	3.39	y_{11}^{2+}
596.3241	596.3220	3.52	b_{11}^{2+}
608.8373	608.8354	3.12	y_{23}^{4+}
623.6776	623.6758	2.89	y_{17}^{3+}
626.3355	626.3333	3.51	y_{12}^{2+}
646.8481	646.8459	3.40	b_{12}^{2+}
655.3332	655.3311	3.20	y_5
675.8698	675.8675	3.40	y_{13}^{2+}
677.3641	677.3617	3.54	b_6
682.3666	682.3644	3.22	b_{13}^{2+}
687.7108	687.7091	2.47	b_{19}^{3+}
713.7222	713.7201	2.94	y_{20}^{3+}
720.7344	720.7319	3.47	b_{20}^{3+}
738.9086	738.9065	2.84	b_{14}^{2+}
759.0764	759.0742	2.90	b_{21}^{3+}
768.4177	768.4151	3.38	y_6
779.0963	779.0938	3.21	y_{22}^{3+}
781.0176	781.0155	2.69	y_{36}^{5+}
789.4513	789.4492	2.66	y_{15}^{2+}
801.7624	801.7604	2.49	b_{22}^{3+}
806.4068	806.4043	3.10	b_7
820.4375	820.4360	1.83	y_{30}^{4+}
831.9485	831.9461	2.88	b_{15}^{2+}
834.7852	834.7832	2.40	b_{23}^{3+}
839.4548	839.4522	3.10	y_7
842.9663	842.9636	3.20	b_{32}^{4+}
845.1296	845.1273	2.72	y_{24}^{3+}
853.4810	853.4785	2.93	y_{16}^{2+}
853.7928	853.7904	2.81	b_{24}^{3+}
854.7028	854.7007	2.46	y_{31}^{4+}
859.7981	859.7962	2.21	y_{47}^{6+}
860.4562	860.4569	-0.81	b_{16}^{2+}
867.7331	867.7307	2.77	b_{33}^{4+}
872.4639	872.4600	4.47	y_{32}^{4+}
892.5001	892.4978	2.58	b_{34}^{4+}
894.1528	894.1501	3.02	y_{25}^{3+}
900.7343	900.7310	3.66	y_{33}^{4+}
924.5070	924.5043	2.92	b_{17}^{2+}

935.0130	935.0101	3.10	y_{17}^{2+}
939.9563	939.9535	2.98	y_{96}^{11+}
951.2533	951.2504	3.05	y_{35}^{4+}
953.4983	953.4952	3.25	y_{8}
958.5215	958.5185	3.13	y_{52}^{6+}
970.5320	970.5287	3.40	y_{18}^{2+}
974.0415	974.0386	2.98	b_{18}^{2+}
976.0205	976.0175	3.07	y_{36}^{4+}
977.6928	977.6896	3.27	y_{53}^{6+}
979.8654	979.8626	2.86	y_{27}^{3+}
982.5214	982.5256	-4.27	y_{91}^{10+}
986.3379	986.3350	2.94	y_{45}^{5+}
998.6549	998.6525	2.40	y_{73}^{8+}
998.8728	998.8698	3.00	y_{28}^{3+}
1006.0507	1006.0472	3.48	y_{19}^{2+}
1011.6044	1011.6106	-6.13	y_{111}^{12+}
1017.7028	1017.7010	1.77	y_{55}^{6+}
1024.5352	1024.5323	2.83	y_{9}
1031.5559	1031.5540	1.84	y_{47}^{5+}
1033.8493	1033.8482	1.06	y_{96}^{10+}
1036.2529	1036.2450	7.62	b_{96}^{10+}
1048.2304	1048.2263	3.91	b_{30}^{3+}
1052.6589	1052.6561	2.66	y_{98}^{10+}
1054.5602	1054.5594	0.76	y_{48}^{5+}
1070.0806	1070.0765	3.83	y_{20}^{2+}
1072.5649	1072.5607	3.92	y_{58}^{6+}
1073.8994	1073.8897	9.03	b_{59}^{6+}
1093.9657	1093.9700	-3.93	b_{101}^{10+}
1103.4857	1103.4837	1.81	y_{111}^{11+}
1106.1418	1106.1432	-1.27	y_{92}^{9+}
1106.3092	1106.3075	1.54	b_{112}^{11+}
1108.2493	1108.2494	-0.09	y_{60}^{6+}
1113.9107	1113.9188	-7.27	y_{123}^{12+}
1116.9023	1116.8954	6.18	b_{133}^{13+}
1118.3066	1118.3076	-0.89	y_{112}^{11+}
1137.8238	1137.8246	-0.70	y_{95}^{9+}
1141.1001	1141.1036	-3.07	y_{84}^{8+}
1144.6057	1144.6003	4.72	y_{62}^{6+}
1146.6050	1146.6004	4.01	y_{115}^{11+}
1148.6104	1148.6083	1.83	y_{96}^{9+}
1151.2798	1151.2715	7.21	b_{96}^{9+}
1156.6419	1156.6385	2.94	b_{33}^{3+}
1159.8388	1159.8358	2.59	y_{97}^{9+}
1166.5084	1166.5002	7.03	b_{97}^{9+}
1168.1408	1168.1371	3.17	y_{22}^{2+}
1169.5091	1169.5060	2.65	y_{98}^{9+}
1177.2902	1177.2857	3.82	b_{65}^{6+}
1180.6263	1180.6222	3.47	y_{11}

1185.3173	1185.3113	5.06	b_{109}^{10+}
1189.6653	1189.6613	3.36	b_{34}^{3+}
1190.2938	1190.2886	4.37	b_{99}^{9+}
1201.1928	1201.1874	4.50	y_{101}^{9+}
1202.1415	1202.1370	3.74	b_{22}^{2+}
1206.1477	1206.1433	3.65	b_{43}^{4+}
1213.7336	1213.7313	1.89	y_{111}^{10+}
1216.6673	1216.6635	3.12	y_{23}^{2+}
1224.0689	1224.0615	6.05	b_{135}^{12+}
1224.1025	1224.0988	3.02	y_{124}^{11+}
1227.9056	1227.9013	3.50	b_{44}^{4+}
1230.0354	1230.0376	-1.79	y_{112}^{10+}
1244.0191	1244.0157	2.73	b_{35}^{3+}
1246.1943	1246.1974	-2.49	y_{126}^{11+}
1251.6632	1251.6712	-6.39	b_{23}^{2+}
1264.6714	1264.6684	2.37	b_{45}^{4+}
1264.9213	1264.9275	-4.90	y_{46}^{4+}
1267.1903	1267.1873	2.37	y_{24}^{2+}
1278.9309	1278.9238	5.55	b_{46}^{4+}
1289.1953	1289.1907	3.57	y_{47}^{4+}
1292.0571	1292.0584	-1.01	y_{96}^{8+}
1307.6839	1307.6806	2.52	b_{47}^{4+}
1313.5352	1313.5246	8.07	b_{73}^{6+}
1317.0250	1317.0193	4.33	y_{109}^{9+}
1335.9541	1335.9516	1.87	b_{48}^{4+}
1338.7058	1338.7156	-7.32	y_{37}^{3+}
1340.7276	1340.7215	4.55	y_{25}^{2+}
1350.7318	1350.7277	3.04	y_{13}
1357.7068	1357.7096	-2.06	b_{49}^{4+}
1363.7258	1363.7216	3.08	b_{13}
1382.9755	1382.9715	2.89	b_{50}^{4+}
1405.2453	1405.2428	1.78	y_{26}^{2+}
1449.8004	1449.7961	2.97	y_{14}
1476.8096	1476.8057	2.64	b_{14}

Appendix 19**.** CID (normalized collision energy 30 %) fragment ions of Hb Headington globin chain in a previously undiagnosed (FAV3) neonatal sample.

Meas *m/z*	Calc *m/z*	Δ ppm	Fragment
350.2177	350.2187	-2.86	b_3
451.2658	451.2663	-1.11	b_4
584.2931	584.2940	-1.54	y_4
596.3208	596.3220	-2.01	b_{11}^{2+}
608.8343	608.8354	-1.81	y_{23}^{4+}
626.3323	626.3333	-1.60	y_{12}^{2+}
646.8442	646.8459	-2.63	b_{12}^{2+}
655.3299	655.3311	-1.83	y_5
675.8662	675.8675	-1.92	y_{13}^{2+}
677.3607	677.3617	-1.48	b_6
682.3631	682.3644	-1.91	b_{13}^{2+}
713.7182	713.7201	-2.66	y_{20}^{3+}
720.7304	720.7319	-2.08	b_{20}^{3+}
725.4006	725.4017	-1.52	y_{14}^{2+}
738.9051	738.9065	-1.89	b_{14}^{2+}
759.0729	759.0742	-1.71	b_{21}^{3+}
768.4137	768.4151	-1.82	y_6
779.0924	779.0938	-1.80	y_{22}^{3+}
781.0146	781.0155	-1.15	y_{36}^{5+}
786.1701	786.1713	-1.53	y_{29}^{4+}
789.4476	789.4492	-2.03	y_{15}^{2+}
802.0868	802.0884	-1.99	b_{22}^{3+}
806.4031	806.4043	-1.49	b_7
811.4434	811.4448	-1.73	y_{23}^{3+}
814.9379	814.9386	-0.86	b_{31}^{4+}
820.4345	820.4360	-1.83	y_{30}^{4+}
831.9447	831.9461	-1.68	b_{15}^{2+}
835.1099	835.1112	-1.56	b_{23}^{3+}
839.4507	839.4522	-1.79	y_7
843.2080	843.2096	-1.90	b_{32}^{4+}
845.1258	845.1273	-1.77	y_{24}^{3+}
853.4771	853.4785	-1.64	y_{16}^{2+}
854.1169	854.1184	-1.76	b_{24}^{3+}
854.6989	854.7007	-2.11	y_{31}^{4+}
859.7944	859.7962	-2.09	y_{47}^{6+}
867.9751	867.9767	-1.84	b_{33}^{4+}
872.4588	872.4600	-1.38	y_{32}^{4+}
888.6144	888.6139	0.56	y_{56}^{7+}
892.7423	892.7438	-1.68	b_{34}^{4+}
894.1483	894.1501	-2.01	y_{25}^{3+}
900.7293	900.7310	-1.89	y_{33}^{4+}
916.1373	916.1397	-2.62	b_{26}^{3+}
924.5028	924.5043	-1.62	b_{17}^{2+}
925.5049	925.4981	7.35	y_{34}^{4+}
933.5083	933.5096	-1.39	b_{35}^{4+}
934.4988	934.4993	-0.54	b_8

935.0087	935.0101	-1.50	y_{17}^{2+}
937.1624	937.1643	-2.03	y_{26}^{3+}
939.8171	939.8188	-1.81	b_{27}^{3+}
939.9051	939.9044	0.74	y_{86}^{10+}
946.2234	946.2325	-9.62	y_{96}^{11+}
951.2486	951.2504	-1.89	y_{35}^{4+}
953.4937	953.4952	-1.57	y_{8}
958.5174	958.5185	-1.15	y_{56} 6^{+}
970.5278	970.5287	-0.93	y_{18}^{2+}
974.0371	974.0386	-1.54	b_{18}^{2+}
976.0161	976.0175	-1.43	y_{36}^{4+}
977.6881	977.6896	-1.53	y_{53}^{6+}
998.8684	998.8698	-1.40	y_{28}^{3+}
1003.8107	1003.8112	-0.50	y_{64}^{7+}
1006.0459	1006.0472	-1.29	y_{19}^{2+}
1017.3679	1017.3664	1.47	y_{111}^{12+}
1031.5516	1031.5540	-2.33	y_{47}^{5+}
1040.7531	1040.7551	-1.92	y_{96}^{10+}
1069.1589	1069.1595	-0.56	b_{48}^{5+}
1086.2483	1086.2490	-0.64	b_{31}^{3+}
1123.9418	1123.9437	-1.69	b_{32}^{3+}
1137.3570	1137.3616	-4.04	b_{41}^{4+}
1146.4904	1146.4902	0.17	b_{95}^{9+}
1156.2811	1156.2826	-1.30	y_{96}^{9+}
1164.1489	1164.1551	-5.33	y_{139}^{13+}
1167.5091	1167.5101	-0.86	y_{97}^{9+}
1174.1267	1174.1287	-1.70	b_{42}^{4+}
1189.9874	1189.9893	-1.60	b_{34}^{3+}
1198.0752	1198.0723	2.42	b_{99}^{9+}
1202.6268	1202.6290	-1.83	b_{22}^{2+}
1206.3877	1206.3893	-1.33	b_{43}^{4+}
1213.5347	1213.5419	-5.93	b_{111}^{10+}
1216.6616	1216.6635	-1.56	y_{23}^{2+}
1220.6404	1220.6382	1.80	y_{111}^{10+}
1227.8349	1227.8260	7.25	b_{123}^{11+}
1228.1446	1228.1473	-2.20	b_{44}^{4+}
1244.3418	1244.3437	-1.53	b_{35}^{3+}
1251.6581	1251.6593	-0.96	y_{12}
1252.1617	1252.1632	-1.20	b_{23}^{2+}
1261.0784	1261.0841	-4.52	y_{139}^{12+}
1264.9121	1264.9145	-1.90	b_{45}^{4+}
1279.1679	1279.1698	-1.49	b_{46}^{4+}
1292.6849	1292.6845	0.31	b_{12}
1307.9242	1307.9266	-1.83	b_{47}^{4+}
1334.6968	1334.7037	-5.17	b_{74}^{6+}
1336.1952	1336.1976	-1.80	b_{48}^{4+}
1357.9525	1357.9556	-2.28	b_{49}^{4+}
1363.7189	1363.7216	-1.98	b_{13}
1375.6293	1375.6365	-5.23	y_{139}^{11+}
1383.2151	1383.2175	-1.74	b_{50}^{4+}

Appendix 20. ETD (activation energy 20 ms) fragment ions of Hb Headington globin chain in a previously undiagnosed (FAV3) neonatal sample.

Meas *m/z*	Calc *m/z*	Δ ppm	Fragment
367.2435	367.2452	-4.63	c_3
565.3440	565.3457	-3.01	c_5
781.4366	781.4398	-4.10	z_{15}^{2+}
789.4470	789.4492	-2.79	y_{15}^{2+}
823.4286	823.4308	-2.67	c_7
839.7847	839.7877	-3.57	z_{24}^{3+}
840.7888	840.7867	2.50	c_{23}^{3+}
896.9743	896.9783	-4.46	z'_{33}^{4+}
926.9979	927.0008	-3.13	z_{17}^{2+}
931.8220	931.8247	-2.90	z_{26}^{3+}
933.0149	933.0176	-2.89	c_{17}^{2+}
951.5229	951.5258	-3.05	c_8
962.5165	962.5193	-2.91	z_{18}^{2+}
970.5257	970.5287	-3.09	y_{18}^{2+}
974.5202	974.5231	-2.98	z_{27}^{3+}
982.5491	982.5518	-2.75	c_{18}^{2+}
983.1293	983.1312	-1.93	z_{45}^{5+}
993.5267	993.5302	-3.52	z_{28}^{3+}
998.0350	998.0379	-2.91	z_{19}^{2+}
998.8670	998.8698	-2.80	y_{28}^{3+}
1042.5498	1042.5530	-3.07	z_{29}^{3+}
1047.8896	1047.8936	-3.82	y_{29}^{3+}
1051.5538	1051.5572	-3.23	z'_{48}^{5+}
1053.5583	1053.5617	-3.23	z_{39}^{4+}
1068.8431	1068.8452	-1.96	z'_{68}^{7+}
1071.1648	1071.1694	-4.29	z_{49}^{5+}
1088.2362	1088.2393	-2.85	z_{30}^{3+}
1089.1037	1089.1075	-3.49	c_{20}^{2+}
1093.5754	1093.5789	-3.20	y_{30}^{3+}
1098.7773	1098.7827	-4.91	z'_{50}^{5+}
1104.8477	1104.8511	-3.08	c_{40}^{4+}

1117.5833	1117.5871	-3.40	z'_{61}^{6+}
1124.6078	1124.6110	-2.85	z'_{42}^{4+}
1128.3739	1128.3638	8.95	y_{42}^{4+}
1133.9262	1133.9256	0.53	z_{31}^{3+}
1141.9420	1141.9305	10.07	z_{62}^{6+}
1146.6172	1146.6210	-3.31	c_{21}^{2+}
1146.8156	1146.8169	-1.13	z_{52}^{5+}
1149.5966	1149.6019	-4.61	$c+H_{63}^{6+}$
1159.1043	1159.1055	-1.04	$c+H_{64}^{6+}$
1163.3791	1163.3844	-4.56	z_{43}^{4+}
1170.0209	1170.0239	-2.56	z'_{53}^{5+}
1195.6315	1195.6353	-3.18	z'_{33}^{3+}
1200.1409	1200.1515	-8.83	z_{44}^{4+}
1208.7861	1208.7754	8.85	z_{77}^{7+}
1210.6379	1210.6460	-6.69	c_{43}^{4+}
1227.6399	1227.6470	-5.78	z'_{67}^{6+}
1228.9100	1228.9142	-3.42	z'_{45}^{4+}
1259.1742	1259.1780	-3.02	z_{24}^{2+}
1265.4978	1265.4975	0.24	z_{69}^{6+}
1288.5052	1288.5086	-2.64	z'_{70}^{6+}
1292.1225	1292.1172	4.10	z'_{83}^{7+}
1309.0297	1309.0339	-3.21	$c+H_{72}^{6+}$
1309.7093	1309.7110	-1.30	c_{12}
1312.0797	1312.0827	-2.29	$c+H_{60}^{5+}$
1312.9538	1312.9428	8.38	z_{48}^{4+}
1337.4957	1337.5010	-3.96	c_{61}^{5+}
1338.9569	1338.9618	-3.66	z'_{49}^{4+}
1340.4636	1340.4542	7.01	c_{48}^{4+}
1347.6965	1347.7023	-4.30	z_{74}^{6+}
1351.6994	1351.7084	-6.66	c_{62}^{5+}
1370.3158	1370.3167	-0.66	z'_{62}^{5+}
1379.1164	1379.1202	-2.76	c_{63}^{5+}
1390.3177	1390.3247	-5.03	z_{63}^{5+}
1410.0831	1410.0700	9.29	z_{77}^{6+}
1472.7654	1472.7734	-5.43	z_{67}^{5+}
1507.1296	1507.1342	-3.05	z_{83}^{6+}
1529.7792	1529.7840	-3.14	$c\cdot_{56}^{4+}$
1530.1337	1530.1454	-7.65	z'_{84}^{6+}

1617.2371	1617.2428	-3.52	z'_{74}^{5+}
1632.3530	1632.3593	-3.86	z'_{30}^{2+}
1671.6155	1671.6244	-5.32	c_{61}^{4+}
1675.8771	1675.8770	0.06	z'_{61}^{4+}
1691.8865	1691.8826	2.31	z_{77}^{5+}
1712.6354	1712.6441	-5.08	z'_{62}^{4+}
1716.3929	1716.3968	-2.27	y_{62}^{4+}
1723.6444	1723.6484	-2.32	c_{63}^{4+}
1751.9170	1751.9239	-3.94	z'_{48}^{3+}
1808.5590	1808.5612	-1.22	z'_{83}^{5+}
1840.9592	1840.9668	-4.13	z'_{67}^{4+}

Appendix 21**.** CID (normalised collision energy 30%) fragment ions of Hb J -Baltimore globin chain in a previously undiagnosed (FAV4) neonatal sample.

Meas *m/z*	Calc *m/z*	Δ ppm	Fragment
451.2680	451.2663	3.77	b_4
584.2954	584.2940	2.40	y_4
596.3232	596.3220	2.01	b_{11}^{2+}
608.8366	608.8354	1.97	y_{23}^{4+}
655.3327	655.3311	2.44	y_5
677.3632	677.3617	2.21	b_6
682.3655	682.3644	1.61	b_{13}^{2+}
725.4032	725.4017	2.07	y_{14}^{2+}
738.9074	738.9065	1.22	b_{14}^{2+}
768.4162	768.4151	1.43	y_6
789.4506	789.4492	1.77	y_{15}^{2+}
801.1671	801.1689	-2.25	b_{30}^{4+}
806.4051	806.4043	0.99	b_7
811.4455	811.4448	0.86	y_{23}^{3+}
820.4365	820.4360	0.61	y_{30}^{4+}
821.4222	821.4236	-1.70	b_{22}^{3+}
831.9470	831.9461	1.08	b_{15}^{2+}
845.1290	845.1273	2.01	y_{24}^{3+}
854.4459	854.4464	-0.59	b_{23}^{3+}
857.7121	857.7110	1.28	b_{32}^{4+}
859.7967	859.7962	0.58	y_{47}^{6+}
872.4610	872.4600	1.15	y_{32}^{4+}
882.4785	882.4781	0.45	b_{33}^{4+}
907.2457	907.2452	0.55	b_{34}^{4+}
934.5014	934.4993	2.25	b_8
935.0118	935.0101	1.82	y_{17}^{2+}
948.0132	948.0110	2.32	b_{35}^{4+}
951.2525	951.2504	2.21	y_{35}^{4+}
958.5190	958.5185	0.52	y_{52}^{6+}
970.5309	970.5287	2.27	y_{18}^{2+}
976.0194	976.0175	1.95	y_{36}^{4+}
977.6915	977.6896	1.94	y_{53}^{6+}
1017.7052	1017.7010	4.13	y_{55}^{6+}
1025.1970	1025.1992	-2.15	y_{112}^{12+}
1031.5550	1031.5540	0.97	y_{47}^{5+}
1033.8500	1033.8482	1.74	y_{96}^{10+}
1044.0531	1044.0559	-2.68	b_{38}^{4+}
1062.3773	1062.3721	4.89	b_{58}^{6+}
1080.2855	1080.2829	2.41	y_{139}^{14+}
1103.4746	1103.4837	-8.25	y_{111}^{11+}
1148.6092	1148.6083	0.78	y_{96}^{9+}
1149.9727	1149.9832	-9.13	y_{85}^{8+}
1159.8375	1159.8358	1.47	y_{97}^{9+}
1169.5059	1169.5060	-0.09	y_{98}^{9+}

1176.3046	1176.3017	2.47	b_{33}^{3+}
1201.1870	1201.1874	-0.33	y_{101}^{9+}
1209.3270	1209.3245	2.07	b_{34}^{3+}
1213.7315	1213.7313	0.16	y_{111}^{10+}
1216.6661	1216.6635	2.14	y_{23}^{2+}
1220.8900	1220.8907	-0.57	b_{43}^{4+}
1322.4299	1322.4279	1.51	b_{47}^{4+}
1374.6416	1374.6307	7.93	y_{139}^{11+}

Appendix 22**.** CID (normalised collision energy 30%) fragment ions of the normal α - globin chain in a previously undiagnosed (FAV5) neonatal sample.

Meas *m/z*	Calc *m/z*	Δ ppm	Fragment
466.2792	466.2772	4.29	y_3
527.7999	527.7982	3.22	y_9^{2+}
553.3110	553.3093	3.07	y_4
577.3344	577.3324	3.46	b_{11}^{2+}
583.3104	583.3086	3.09	b_6
612.8532	612.8510	3.59	b_{12}^{2+}
620.8498	620.8484	2.25	y_{11}^{2+}
648.3713	648.3695	2.78	b_{13}^{2+}
654.3588	654.3570	2.75	y_5
677.7101	677.7093	1.18	b_{20}^{3+}
701.3899	701.3884	2.14	b_{21}^{3+}
712.9108	712.9090	2.52	y_{13}^{2+}
720.3958	720.3955	0.42	b_{22}^{3+}
741.4120	741.4092	3.78	b_{14}^{2+}
741.7438	741.7426	1.62	y_{20}^{3+}
759.6620	759.6605	1.97	y_{28}^{4+}
763.4113	763.4097	2.10	b_{23}^{3+}
767.4429	767.4410	2.48	y_6
774.7663	774.7654	1.16	y_{21}^{3+}
786.4451	786.4432	2.42	y_{14}^{2+}
787.9330	787.9315	1.90	y_{29}^{4+}
795.1677	795.1665	1.51	b_{31}^{4+}
817.7661	817.7642	2.32	b_{24}^{3+}
822.1977	822.1962	1.82	y_{30}^{4+}
827.9272	827.9266	0.72	b_{32}^{4+}
830.7971	830.7953	2.17	y_{23}^{3+}
833.9696	833.9674	2.64	b_{16}^{2+}
850.4928	850.4907	2.47	y_{15}^{2+}
860.4530	860.4503	3.14	b_{26}^{3+}
864.4796	864.4779	1.97	y_{24}^{3+}
866.5118	866.5094	2.77	y_7
883.5046	883.5016	3.40	b_{17}^{2+}

892.9669	892.9647	2.46	b_{34}^{4+}
903.4673	903.4645	3.10	b_{27}^{3+}
908.0065	908.0042	2.53	y_{16}^{2+}
911.2501	911.2477	2.63	y_{34}^{4+}
912.0140	912.0123	1.86	b_{18}^{2+}
913.5032	913.5007	2.74	y_{25}^{3+}
914.7230	914.7227	0.33	b_{35}^{4+}
926.4966	926.4942	2.59	b_{9}
927.1463	927.1436	2.91	b_{28}^{3+}
936.0170	936.0148	2.35	y_{35}^{4+}
947.5336	947.5309	2.85	b_{19}^{2+}
956.5174	956.5149	2.61	y_{26}^{3+}
964.5490	964.5462	2.90	y_{17}^{2+}
967.5599	967.5571	2.89	y_{8}
980.1966	980.1939	2.75	y_{27}^{3+}
992.5604	992.5568	3.63	y_{37}^{4+}
993.8851	993.8832	1.91	b_{75}^{8+}
1008.0652	1008.0622	2.98	y_{18}^{2+}
1012.5478	1012.5449	2.86	y_{28}^{3+}
1016.0634	1016.0603	3.05	b_{20}^{2+}
1018.3096	1018.3091	0.49	y_{38}^{4+}
1021.9686	1021.9661	2.45	y_{47}^{5+}
1025.5657	1025.5626	3.02	b_{10}
1028.3208	1028.3192	1.56	b_{47}^{5+}
1030.0766	1030.0754	1.16	y_{56}^{6+}
1043.5839	1043.5808	2.97	y_{19}^{2+}
1044.8273	1044.8245	2.68	b_{69}^{7+}
1050.2425	1050.2396	2.76	y_{29}^{3+}
1052.5716	1052.5739	-2.19	y_{39}^{4+}
1054.5923	1054.5891	3.03	y_{9}
1089.1205	1089.1153	4.77	b_{1121}^{1+}
1091.5765	1091.5722	3.94	y_{121}^{12+}
1094.4403	1094.4387	1.46	y_{60}^{6+}
1095.9289	1095.9259	2.74	y_{30}^{3+}
1099.3966	1099.3957	0.82	b_{113}^{11+}

1100.6752	1100.6754	-0.18	y_{111}^{11+}
1102.5806	1102.5880	-6.71	y_{102}^{10+}
1108.9465	1108.9441	2.16	y_{6}^{16+}
1112.1138	1112.1102	3.24	y_{20}^{2+}
1113.4631	1113.4618	1.17	b_{94}^{9+}
1119.6090	1119.6049	3.66	y_{31}^{3+}
1127.7885	1127.7914	-2.57	y_{62}^{6+}
1130.8758	1130.8739	1.68	y_{42}^{4+}
1132.4917	1132.5028	-9.80	y_{105}^{10+}
1135.7258	1135.7226	2.82	b_{75}^{7+}
1140.8752	1140.8760	-0.70	y_{115}^{11+}
1142.0975	1142.0974	0.09	b_{128}^{12+}
1147.5282	1147.5252	2.61	y_{139}^{13+}
1153.6607	1153.6575	2.77	b_{10}
1153.6607	1153.6575	2.77	y_{10}
1154.4429	1154.4426	0.26	b_{76}^{7+}
1161.6465	1161.6444	1.81	y_{21}^{2+}
1174.8153	1174.8135	1.53	y_{65}^{6+}
1177.1162	1177.1165	-0.25	b_{110}^{10+}
1184.2223	1184.2202	1.77	b_{111}^{10+}
1194.7493	1194.7473	1.67	b_{79}^{7+}
1209.2370	1209.2345	2.07	b_{113}^{10+}
1218.7960	1218.7940	1.64	b_{69}^{6+}
1219.2968	1219.2945	1.89	b_{35}^{3+}
1234.9987	1234.9959	2.27	y_{68}^{6+}
1240.6929	1240.6896	2.66	y_{11}
1245.6926	1245.6894	2.57	y_{23}^{2+}
1247.1451	1247.1449	0.16	b_{71}^{6+}
1268.3195	1268.3173	1.73	b_{36}^{3+}
1277.2075	1277.2085	-0.78	y_{47}^{4+}
1296.2165	1296.2132	2.55	y_{24}^{2+}
1307.8007	1307.7953	4.13	b_{110}^{9+}
1311.7302	1311.7267	2.67	y_{12}
1346.6827	1346.6819	0.59	b_{76}^{6+}
1369.7510	1369.7474	2.63	y_{25}^{2+}

1424.8144	1424.8108	2.53	y_{13}
1434.2723	1434.2687	2.51	y_{26}^{2+}
1518.3176	1518.3137	2.57	y_{28}^{2+}
1571.8832	1571.8793	2.48	y_{14}
1574.8603	1574.8557	2.92	y_{29}^{2+}
1699.9788	1699.9741	2.76	y_{15}

Appendix 23**.** CID (normalised collision energy 30%) fragment ions of the Hb Phnom Penh variant chain in a previously undiagnosed (FAV5) neonatal sample.

Meas *m/z*	Calc *m/z*	Δ ppm	Fragment
338.1832	338.1823	2.66	y_2
466.2796	466.2772	5.15	y_3
484.2848	484.2822	5.37	y_8^{2+}
527.8005	527.7982	4.36	y_9^{2+}
553.3115	553.3093	3.98	y_4
577.3349	577.3324	4.33	b_{11}^{2+}
583.3110	583.3086	4.11	b_6
612.8533	612.8510	3.75	b_{12}^{2+}
623.3499	623.3483	2.57	y_{23}^{4+}
648.3719	648.3695	3.70	b_{13}^{2+}
654.3594	654.3570	3.67	y_5
677.7114	677.7093	3.10	b_{20}^{3+}
701.3908	701.3884	3.42	b_{21}^{3+}
711.4071	711.4036	4.92	b_7
712.9121	712.9090	4.35	y_{13}^{2+}
720.3981	720.3955	3.61	b_{22}^{3+}
741.7448	741.7426	2.97	y_{20}^{3+}
763.4118	763.4097	2.75	b_{23}^{3+}
767.4436	767.4410	3.39	y_6
774.7670	774.7654	2.07	y_{21}^{3+}
786.4459	786.4432	3.43	y_{14}^{2+}
787.9338	787.9315	2.92	y_{29}^{4+}
795.1687	795.1665	2.77	b_{31}^{4+}
817.7665	817.7642	2.81	b_{24}^{3+}
827.9294	827.9266	3.38	b_{32}^{4+}
830.7979	830.7953	3.13	y_{23}^{3+}
833.9703	833.9674	3.48	b_{16}^{2+}
836.7739	836.7713	3.11	b_{25}^{3+}
850.4937	850.4907	3.53	y_{15}^{2+}
860.4529	860.4503	3.02	b_{26}^{3+}
864.4810	864.4779	3.59	y_{24}^{3+}
866.5127	866.5094	3.81	y_7

868.2277	868.2265	1.38	y_{32}^{4+}
883.5061	883.5016	5.09	b_{17}^{2+}
892.9675	892.9647	3.14	b_{34}^{4+}
902.1746	902.1726	2.22	y_{25}^{3+}
903.4676	903.4645	3.43	b_{27}^{3+}
908.0074	908.0042	3.52	y_{16}^{2+}
912.0147	912.0123	2.63	b_{18}^{2+}
926.4962	926.4942	2.16	b_{9}
927.1472	927.1436	3.88	b_{28}^{3+}
947.5345	947.5309	3.80	b_{19}^{2+}
951.1994	951.1954	4.21	y_{26}^{3+}
964.2895	964.2858	3.84	y_{36}^{4+}
967.5609	967.5571	3.93	y_{8}
975.9027	975.9001	2.66	b_{45}^{5+}
977.6489	977.6461	2.86	b_{64}^{7+}
992.5609	992.5568	4.13	y_{37}^{4+}
993.7614	993.7651	-3.72	y_{83}^{9+}
1002.2199	1002.2164	3.49	b_{94}^{10+}
1008.0662	1008.0622	3.97	y_{18}^{2+}
1025.5664	1025.5626	3.71	b_{10}
1028.3221	1028.3192	2.82	b_{47}^{5+}
1030.0776	1030.0754	2.14	y_{56}^{6+}
1031.1016	1031.0969	4.56	y_{105}^{11+}
1043.5849	1043.5808	3.93	y_{19}^{2+}
1050.2435	1050.2396	3.71	y_{29}^{3+}
1054.5933	1054.5891	3.98	y_{9}
1099.3990	1099.3957	3.00	b_{113}^{11+}
1102.8551	1102.8577	-2.36	b_{73}^{7+}
1112.1146	1112.1102	3.96	y_{20}^{2+}
1118.8098	1118.8169	-6.35	b_{85}^{8+}
1152.5879	1152.5891	-1.04	b_{33}^{3+}
1153.6619	1153.6575	3.81	b_{11}
1219.2964	1219.2945	1.56	b_{35}^{3+}
1240.6938	1240.6896	3.39	y_{11}
1245.6937	1245.6894	3.45	y_{23}^{2+}

1247.1460	1247.1449	0.88	b_{71}^{6+}
1268.3203	1268.3173	2.37	b_{36}^{3+}
1296.2178	1296.2132	3.55	y_{24}^{2+}
1298.9215	1298.9176	3.00	y_{59}^{5+}
1305.4803	1305.4768	2.68	y_{48}^{4+}
1311.7313	1311.7267	3.51	y_{12}
1349.5184	1349.5284	-7.41	$y_{138}1^{1+}$
1352.7613	1352.7553	4.44	y_{25}^{2+}
1410.7327	1410.7317	0.71	b_{40}^{3+}
1424.8158	1424.8108	3.51	y_{13}
1426.2903	1426.2895	0.56	y_{26}^{2+}

Appendix 24**.** CID and ETD fragment ions of the β -globin chain in a previously undiagnosed (FAV6) neonatal sample.

Meas *m/z*	Calc *m/z*	Δ ppm	Fragment
350.2193	350.2187	1.71	b_3
451.2688	451.2663	5.54	b_4
546.7895	546.7878	3.11	b_{10}^{2+}
565.3450	565.3457	-1.24	c_5
584.2959	584.2940	3.25	y_4
590.8167	590.8147	3.39	y_{11}^{2+}
608.8371	608.8354	2.79	y_{23}^{4+}
626.3355	626.3333	3.51	y_{12}^{2+}
646.8480	646.8459	3.25	b_{12}^{2+}
655.3333	655.3311	3.36	y_5
671.0357	671.0339	2.68	y_{19}^{3+}
675.8699	675.8675	3.55	y_{13}^{2+}
677.3640	677.3617	3.40	b_6
682.3667	682.3644	3.37	b_{13}^{2+}
687.7089	687.7091	-0.29	b_{19}^{2+}
713.7219	713.7201	2.52	y_{20}^{3+}
720.7342	720.7319	3.19	b_{20}^{3+}
725.4039	725.4017	3.03	y_{14}
738.9088	738.9065	3.11	b_{14}^{2+}
759.0769	759.0742	3.56	b_{21}^{3+}
768.4177	768.4151	3.38	y_6
779.0959	779.0938	2.70	y_{22}^{3+}
781.0182	781.0155	3.46	y_{36}^{5+}
781.4392	781.4398	-0.77	z_{15}^{2+}
786.1730	786.1713	2.16	y_{29}^{4+}
789.4482	789.4492	-1.27	y_{15}^{2+}
789.4517	789.4492	3.17	y_{15}^{2+}
802.0907	802.0884	2.87	b_{22}^{3+}
806.4069	806.4043	3.22	b_7
811.4467	811.4448	2.34	y_{23}^{3+}
820.4378	820.4360	2.19	y_{30}^{4+}
831.9486	831.9461	3.01	b_{15}^{2+}

835.1136	835.1112	2.87	b_{23}^{3+}
843.2113	843.2096	2.02	b_{32}^{4+}
845.1293	845.1273	2.37	y_{24}^{3+}
859.7982	859.7963	2.21	y_{47}^{6+}
867.9795	867.9767	3.23	b_{33}^{4+}
872.4641	872.4600	4.70	y_{32}^{4+}
892.7463	892.7438	2.80	b_{34}^{4+}
900.7338	900.7310	3.11	y_{33}^{4+}
916.1408	916.1397	1.20	b_{26}^{3+}
924.5068	924.5043	2.70	b_{17}^{2+}
925.5003	925.4981	2.38	y_{34}^{4+}
931.8239	931.8247	-0.86	z_{26}^{3+}
933.0165	933.0176	-1.18	c_{17}^{2+}
933.5120	933.5096	2.57	b_{35}^{4+}
935.0130	935.0101	3.10	y_{17}^{2+}
937.1672	937.1643	3.09	y_{26}^{3+}
939.8212	939.8188	2.55	b_{27}^{3+}
951.2535	951.2504	3.26	y_{35}^{4+}
951.5247	951.5258	-1.16	c_{8}
953.4981	953.4952	3.04	y_{8}
958.5194	958.5185	0.94	y_{52}^{6+}
962.5185	962.5193	-0.83	z_{18}^{2+}
970.5274	970.5287	-1.34	y_{18}^{2+}
970.5317	970.5287	3.09	y_{18}^{2+}
974.0418	974.0386	3.29	b_{18}^{2+}
974.5219	974.5231	-1.23	z_{27}^{3+}
976.0200	976.0175	2.56	y_{36}^{4+}
977.5158	977.5135	2.35	b_{28}^{3+}
982.5508	982.5518	-1.02	c_{18}^{2+}
993.5294	993.5302	-0.81	z_{28}^{3+}
998.0369	998.0379	-1.00	z_{19}^{2+}
998.6567	998.6525	4.21	y_{73}^{8+}
998.8694	998.8698	-0.40	y_{28}^{3+}
1003.8171	1003.8112	5.88	y_{64}^{7+}
1006.0506	1006.0472	3.38	y_{19}^{2+}

1017.7029	1017.7010	1.87	y_{55}^{6+}
1024.5355	1024.5323	3.12	y_{9}
1031.5562	1031.5540	2.13	y_{47}^{5+}
1033.8495	1033.8482	1.26	y_{96}^{10+}
1038.5573	1038.5580	-0.48	c_{9}
1042.5527	1042.5530	-0.29	z_{29}^{3+}
1047.8922	1047.8930	-0.38	y_{29}^{3+}
1062.0669	1062.0670	-0.28	z_{20}^{2+}
1069.1642	1069.1595	4.40	b_{48}^{5+}
1075.4652	1075.4672	-1.86	y_{100}^{10+}
1088.2380	1088.2390	-1.19	z_{30}^{3+}
1089.1049	1089.1080	-2.39	c_{20}^{2+}
1093.5786	1093.5790	-0.27	y_{30}^{3+}
1103.4852	1103.4837	1.36	y_{111}^{11+}
1107.2625	1107.2728	-9.30	y_{132}^{13+}
1108.7294	1108.7243	4.60	y_{143}^{14+}
1111.5999	1111.6010	-1.35	z_{21}^{2+}
1116.8035	1116.8017	1.61	y_{144}^{14+}
1118.3070	1118.3076	-0.54	y_{112}^{11+}
1123.9473	1123.9437	3.20	b_{32}^{3+}
1134.2597	1134.2620	-1.68	z'_{31}^{3+}
1148.6109	1148.6083	2.26	y_{96}^{9+}
1156.9700	1156.9665	3.03	b_{33}^{3+}
1159.8389	1159.8358	2.67	y_{97}^{9+}
1168.1404	1168.1371	2.83	y_{22}^{2+}
1169.5073	1169.5060	1.11	y_{98}^{9+}
1174.1320	1174.1287	2.81	b_{42}^{4+}
1180.6259	1180.6222	3.13	y_{11}
1185.4210	1185.4197	1.10	b_{109}^{10+}
1189.9929	1189.9893	3.03	b_{34}^{3+}
1190.3878	1190.3979	-8.48	b_{99}^{9+}
1194.8419	1194.8517	-8.20	y_{100}^{9+}
1195.2989	1195.2990	-0.42	z_{33}^{3+}
1195.6620	1195.6650	-2.34	c_{34}^{3+}
1201.1810	1201.1874	-5.33	y_{101}^{9+}

1202.6324	1202.6290	2.83	b_{22}^{2+}
1206.3935	1206.3893	3.48	b_{43}^{4+}
1208.6629	1208.6630	-0.41	c_{11}
1211.1406	1211.1420	-1.40	c_{22}^{2+}
1213.7300	1213.7313	-1.07	y_{111}^{10+}
1216.6670	1216.6635	2.88	y_{23}^{2+}
1221.5398	1221.5470	-5.89	b_{123}^{11+}
1224.1496	1224.1435	4.98	b_{135}^{12+}
1228.1501	1228.1473	2.28	b_{44}^{4+}
1230.0284	1230.0376	-7.48	y_{112}^{10+}
1244.3470	1244.3437	2.65	b_{35}^{3+}
1251.6635	1251.6593	3.36	y_{12}
1252.1667	1252.1632	2.80	b_{23}^{2+}
1259.1778	1259.1780	-0.16	z_{24}^{2+}
1264.9178	1264.9275	-7.67	y_{46}^{4+}
1267.1902	1267.1873	2.29	y_{24}^{2+}
1279.1728	1279.1698	2.35	b_{46}^{4+}
1289.1933	1289.1907	2.02	y_{47}^{4+}
1292.0563	1292.0584	-1.63	y_{96}^{8+}
1307.9299	1307.9266	2.52	b_{47}^{4+}
1309.7096	1309.7110	-1.07	c_{12}
1313.6757	1313.6886	-9.82	b_{73}^{6+}
1314.1929	1314.1950	-1.37	z'_{48}^{4+}
1336.2015	1336.1976	2.92	b_{48}^{4+}
1338.7051	1338.7100	-3.59	z_{49}^{4+}
1340.7291	1340.7215	5.67	y_{25}^{2+}
1357.9581	1357.9556	1.84	b_{49}^{4+}
1363.7257	1363.7216	3.01	b_{13}
1383.2212	1383.2175	2.67	b_{50}^{4+}
1397.2328	1397.2340	-0.50	z_{26}^{2+}
1449.7998	1449.7961	2.55	y_{14}
1476.8095	1476.8057	2.57	b_{14}

Appendix 25**.** CID and ETD fragment ions of the α -globin chain in a previously undiagnosed (FAV6) neonatal sample.

Meas *m/z*	Calc *m/z*	Δ ppm	Fragment
466.2797	466.2772	5.36	y_3
485.3082	485.3082	0.00	c_5
521.7981	521.7982	-0.19	c_{10}^{2+}
527.7999	527.7982	3.22	y_9^{2+}
553.3112	553.3093	3.43	y_4
583.3106	583.3086	3.43	b_6
585.8455	585.8457	-0.34	c_{11}^{2+}
600.3350	600.3352	-0.33	c_6
612.8530	612.8510	3.26	b_{12}^{2+}
621.3640	621.3642	-0.32	c_{12}^{2+}
648.3718	648.3695	3.55	b_{13}^{2+}
654.3590	654.3570	3.06	y_5
656.8826	656.8828	-0.30	c_{13}^{2+}
677.7115	677.7114	0.15	b_{20}^{3+}
701.3911	701.3884	3.85	b_{21}^{3+}
707.0635	707.0639	-0.57	c_{21}^{3+}
712.9114	712.9090	3.37	y_{13}^{2+}
720.3969	720.3955	1.94	b_{22}^{3+}
728.4299	728.4301	-0.27	c_7
741.7453	741.7426	3.64	y_{20}^{3+}
749.9225	749.9225	0.00	c_{14}^{2+}
759.6631	759.6605	3.42	y_{28}^{4+}
763.4119	763.4097	2.88	b_{23}^{3+}
767.4432	767.4410	2.87	y_6
769.0851	769.0852	-0.13	c_{23}^{3+}
774.7675	774.7654	2.71	y_{21}^{3+}
778.4332	778.4332	0.00	c_{15}^{2+}
778.4332	778.4339	-0.90	z_{14}^{2+}
786.4431	786.4432	-0.13	y_{14}^{2+}
786.4462	786.4432	3.81	y_{14}^{2+}
787.9339	787.9315	3.05	y_{29}^{4+}
795.1689	795.1665	3.02	b_{31}^{4+}

799.6741	799.6739	0.25	$c+H_{31}^{4+}$
817.7667	817.7642	3.06	b_{24}^{3+}
822.1983	822.1982	0.12	y_{30}^{4+}
823.4392	823.4397	-0.61	c_{24}^{3+}
827.9295	827.9266	3.50	b_{32}^{4+}
829.4776	829.4778	-0.24	c_{8}
830.7980	830.7953	3.25	y_{23}^{3+}
833.9703	833.9774	-8.51	b_{16}^{2+}
842.4805	842.4807	-0.24	c_{16}^{2+}
850.4911	850.4907	0.47	z_{7}
850.4934	850.4907	3.17	y_{15}^{2+}
859.1374	859.1383	-1.05	z_{24}^{3+}
860.4536	860.4503	3.84	b_{26}^{3+}
864.4798	864.4779	2.20	y_{24}^{3+}
866.1258	866.1259	-0.12	c_{26}^{3+}
866.5122	866.5094	3.23	y_{7}
883.5052	883.5016	4.07	b_{17}^{2+}
892.0148	892.0149	-0.11	c_{17}^{2+}
892.9668	892.9647	2.35	b_{34}^{4+}
897.2215	897.2213	0.22	c_{34}^{4+}
903.2710	903.2701	1.00	$c+H_{42}^{5+}$
903.4670	903.4645	2.77	b_{27}^{3+}
908.0069	908.0042	2.97	y_{16}^{2+}
908.1609	908.1611	-0.22	z_{25}^{3+}
909.1392	909.1401	-0.99	c_{27}^{3+}
911.2512	911.2477	3.84	y_{34}^{4+}
913.5033	913.5007	2.85	y_{25}^{3+}
914.7247	914.7227	2.19	b_{35}^{4+}
918.6184	918.6136	5.23	b_{60}^{7+}
918.9792	918.9793	-0.11	c_{35}^{4+}
936.0181	936.0148	3.53	y_{35}^{4+}
943.5208	943.5207	0.11	c_{9}
947.5341	947.5309	3.38	b_{19}^{2+}
956.0441	956.0442	-0.10	c_{19}^{2+}
956.5175	956.5149	2.72	y_{26}^{3+}

964.5502	964.5462	4.15	y_{17}^{2+}
966.8305	966.8222	8.58	y_{62}^{7+}
967.5602	967.5571	3.20	y_{8}
979.3057	979.3054	0.31	c_{45}^{5+}
980.1967	980.1939	2.86	y_{27}^{3+}
992.5588	992.5568	2.01	y_{37}^{4+}
1000.0528	1000.0529	-0.10	z_{18}^{2+}
1005.2718	1005.2715	0.30	c_{38}^{4+}
1008.0614	1008.0622	-0.79	y_{18}^{2+}
1008.0655	1008.0622	3.27	y_{18}^{2+}
1008.7190	1008.7191	-0.10	c_{46}^{5+}
1011.1864	1011.1862	0.20	c_{56}^{6+}
1012.5477	1012.5449	2.77	y_{28}^{3+}
1016.0639	1016.0603	3.54	b_{20}^{2+}
1018.3123	1018.3091	3.14	y_{38}^{4+}
1020.6903	1020.6898	0.49	c_{57}^{6+}
1021.9691	1021.9661	2.94	y_{47}^{5+}
1024.5736	1024.5736	0.00	c_{20}^{2+}
1025.5658	1025.5626	3.12	b_{10}
1028.3235	1028.3192	4.18	b_{47}^{5+}
1030.0774	1030.0754	1.94	y_{56}^{6+}
1030.5339	1030.5335	0.39	c_{39}^{4+}
1035.5715	1035.5714	0.10	z_{19}^{2+}
1042.5892	1042.5891	0.10	c_{10}
1043.5343	1043.5330	1.25	c_{58}^{6+}
1043.5843	1043.5808	3.35	y_{19}^{2+}
1045.2344	1045.2359	-1.44	z'_{29}^{3+}
1045.5286	1045.5298	-1.15	b_{79}^{8+}
1048.5688	1048.5692	-0.38	z_{39}^{4+}
1050.2426	1050.2424	0.19	y_{29}^{3+}
1052.5727	1052.5739	-1.14	y_{39}^{4+}
1053.2021	1053.2038	-1.61	$c+H_{59}^{6+}$
1054.3407	1054.3413	-0.57	c_{48}^{5+}
1054.5925	1054.5891	3.22	y_{9}
1060.0921	1060.0922	-0.09	c_{21}^{2+}

1062.5563	1062.5572	-0.85	c_{40}^{4+}
1065.5616	1065.5617	-0.09	c_{31}^{3+}
1070.3276	1070.3272	0.37	z_{40}^{4+}
1074.5513	1074.5529	-1.49	$c+H_{60}^{6+}$
1087.8197	1087.8191	0.55	c_{41}^{4+}
1088.6029	1088.6029	0.00	c_{22}^{2+}
1089.1164	1089.1153	1.01	b_{112}^{11+}
1094.4423	1094.4387	3.29	y_{60}^{6+}
1095.9295	1095.9259	3.28	y_{30}^{3+}
1099.1591	1099.1595	-0.36	c_{50}^{5+}
1099.3986	1099.3957	2.64	b_{113}^{11+}
1100.6758	1100.6754	0.36	y_{111}^{11+}
1102.5823	1102.5880	-5.17	y_{102}^{10+}
1108.9485	1108.9441	3.97	y_{61}^{6+}
1109.2417	1109.2419	-0.18	c_{32}^{3+}
1110.7648	1110.7645	0.27	$c+H_{51}^{5+}$
1112.1144	1112.1102	3.78	y_{20}^{2+}
1113.4663	1113.4618	4.04	b_{94}^{9+}
1126.8695	1126.8692	0.27	z_{42}^{4+}
1128.5850	1128.5850	0.00	c_{42}^{4+}
1130.8728	1130.8739	-0.97	y_{42}^{4+}
1132.5100	1132.5028	6.36	y_{105}^{10+}
1135.7265	1135.7226	3.43	b_{75}^{7+}
1137.9442	1137.9444	-0.18	z_{32}^{3+}
1140.8367	1140.8304	5.52	y_{138}^{13+}
1143.4238	1143.4242	-0.35	$c+H_{64}^{6+}$
1147.5306	1147.5252	4.71	y_{139}^{13+}
1153.1241	1153.1242	-0.09	c_{23}^{2+}
1154.4465	1154.4426	3.38	b_{76}^{7+}
1158.2641	1158.2647	-0.52	c_{33}^{3+}
1158.8927	1158.8930	-0.26	z_{43}^{4+}
1162.8967	1162.8976	-0.77	y_{43}^{4+}
1170.6840	1170.6841	-0.09	c_{11}
1175.3709	1175.3681	2.38	y_{131}^{12+}
1175.6386	1175.6390	-0.34	z_{33}^{3+}

1177.1170	1177.1165	0.42	b_{110}^{10+}
1182.8570	1182.8582	-1.01	z'_{54}^{5+}
1184.2274	1184.2202	6.08	b_{111}^{10+}
1189.8667	1189.8661	0.50	$c+H_{44}^{4+}$
1194.7502	1194.7473	2.43	b_{79}^{7+}
1195.6588	1195.6601	-1.09	z_{44}^{4+}
1195.9593	1195.9593	0.00	c_{34}^{3+}
1209.2327	1209.2345	-1.49	b_{113}^{10+}
1209.3221	1209.3216	0.41	z_{34}^{3+}
1210.6456	1210.6422	2.81	y_{111}^{10+}
1213.2216	1213.2220	-0.33	c_{56}^{5+}
1218.7900	1218.7940	-3.28	b_{69}^{6+}
1224.9698	1224.9700	-0.16	c_{35}^{3+}
1234.6549	1234.6559	-0.81	c_{24}^{2+}
1240.6929	1240.6896	2.66	y_{11}
1241.7210	1241.7212	-0.16	c_{12}
1245.6927	1245.6894	2.65	y_{23}^{2+}
1252.0363	1252.0381	-1.44	c_{58}^{5+}
1267.2525	1267.2568	-3.39	z'_{83}^{7+}
1268.3202	1268.3173	2.29	b_{36}^{3+}
1274.3544	1274.3505	3.06	y_{70}^{6+}
1277.2086	1277.2058	2.19	y_{47}^{4+}
1296.2164	1296.2132	2.47	y_{24}^{2+}
1301.9573	1301.9578	-0.38	z_{48}^{4+}
1307.7946	1307.7953	-0.54	b_{110}^{9+}
1311.7301	1311.7267	2.59	y_{12}
1311.9267	1311.9265	0.15	$c+H_{98}^{8+}$
1315.6942	1315.6883	4.48	b_{111}^{9+}
1317.6745	1317.6748	-0.23	c_{48}^{4+}
1325.0666	1325.0603	4.75	b_{137}^{11+}
1330.5349	1330.5314	2.63	y_{61}^{5+}
1340.0257	1340.0263	-0.45	c_{38}^{3+}
1346.6837	1346.6819	1.34	b_{76}^{6+}
1354.6977	1354.6932	3.32	b_{27}^{2+}
1357.4116	1357.4098	1.33	y_{38}^{3+}

1361.7377	1361.7381	-0.29	z_{25}^{2+}
1363.2063	1363.2065	-0.15	c_{27}^{2+}
1368.0360	1368.0333	1.97	b_{39}^{3+}
1369.7509	1369.7474	2.56	y_{25}^{2+}
1387.9615	1387.9529	6.20	c_{51}^{4+}
1393.7063	1393.7040	1.65	b_{79}^{6+}
1397.7564	1397.7565	-0.07	z_{39}^{3+}
1403.0944	1403.0961	-1.21	y_{39}^{3+}
1416.4070	1416.4072	-0.14	c_{40}^{3+}
1424.8141	1424.8108	2.32	y_{13}
1427.1010	1427.1031	-1.47	z'_{40}^{3+}
1431.7590	1431.7579	0.77	z_{106}^{8+}
1434.2722	1434.2687	2.44	y_{36}^{2+}
1478.3180	1478.3209	-1.96	z'_{54}^{4+}
1544.8538	1544.8549	-0.71	z_{43}^{3+}
1550.1930	1550.1944	-0.90	y_{43}^{3+}
1564.8079	1564.7958	7.73	c_{58}^{4+}
1566.8460	1566.8463	-0.19	z_{29}^{2+}
1588.7244	1588.7209	2.20	z_{133}^{9+}
1636.1598	1636.1508	5.50	z_{106}^{7+}
1735.9409	1735.9440	-1.79	z'_{48}^{3+}
1836.9481	1836.9514	-1.80	c_{35}^{2+}

Appendix 26**.** CID and ETD fragment ions of the Gγ -globin chain in a previously undiagnosed (FAV6) neonatal sample.

Meas *m/z*	Calc *m/z*	Δ ppm	Fragment
459.2211	459.2225	-3.05	z_3
558.7497	558.7515	-3.22	b_{10}^{2+}
562.2715	562.2732	-3.02	y_4
615.2915	615.2935	-3.25	b_{11}^{2+}
649.3032	649.3052	-3.08	y_5
665.8152	665.8173	-3.15	b_{12}^{2+}
701.2866	701.2889	-3.28	b_6
705.6861	705.6884	-3.26	b_{19}^{3+}
709.3310	709.3333	-3.24	b_{13}^{2+}
738.7089	738.7112	-3.11	b_{20}^{3+}
739.8730	739.8747	-2.30	y_{14}^{2+}
762.3870	762.3893	-3.02	y_6
765.8730	765.8754	-3.13	b_{14}^{2+}
769.3928	769.3952	-3.12	y_{21}^{3+}
781.7229	781.7254	-3.20	b_{21}^{3+}
800.6442	800.6468	-3.25	b_{30}^{4+}
811.1557	811.1579	-2.71	y_{29}^{4+}
816.3133	816.3159	-3.19	b_7
820.0652	820.0677	-3.05	b_{22}^{3+}
828.9155	828.9178	-2.77	b_{31}^{4+}
833.4237	833.4264	-3.24	y_7
843.7441	843.7467	-3.08	b_{23}^{3+}
845.4267	845.4227	4.73	y_{30}^{4+}
857.1863	857.1889	-3.03	b_{32}^{4+}
858.9124	858.9150	-3.03	b_{15}^{2+}
862.7511	862.7539	-3.25	b_{24}^{3+}
867.4245	867.4283	-4.38	c_{15}^{2+}
867.9483	867.9514	-3.57	y_{16}^{2+}
873.6918	873.6957	-4.46	y_{31}^{4+}
881.7581	881.7610	-3.29	b_{25}^{3+}
881.9532	881.9560	-3.17	b_{33}^{4+}
887.4231	887.4258	-3.04	b_{16}^{2+}

891.4502	891.4530	-3.14	y_{32}^{4+}
897.9506	897.9537	-3.45	b_{48}^{6+}
906.7201	906.7231	-3.31	b_{34}^{4+}
917.7312	917.7349	-4.03	y_{66}^{8+}
919.7210	919.7240	-3.26	y_{33}^{4+}
920.4557	920.4585	-3.04	y_{8}
922.1215	922.1261	-4.99	z_{25}^{3+}
924.7720	924.7752	-3.46	b_{26}^{3+}
927.4633	927.4657	-2.59	y_{25}^{3+}
944.4082	944.4108	-2.75	b_{8}
947.4857	947.4889	-3.38	b_{35}^{4+}
951.4706	951.4732	-2.73	b_{17}^{2+}
965.1366	965.1403	-3.83	z_{26}^{3+}
966.1831	966.1858	-2.79	y_{52}^{6+}
969.7499	969.7530	-3.20	y_{35}^{4+}
977.7561	977.7595	-3.48	y_{70}^{8+}
980.0719	980.0738	-1.94	y_{80}^{9+}
991.4924	991.4956	-3.23	y_{9}
992.3272	992.3320	-4.84	z_{45}^{5+}
994.5171	994.5201	-3.02	y_{36}^{4+}
995.5321	995.5358	-3.72	y_{45}^{5+}
1001.0045	1001.0074	-2.90	b_{18}^{2+}
1004.5036	1004.5071	-3.48	y_{18}^{2+}
1009.5163	1009.5207	-4.36	c_{18}^{2+}
1016.7802	1016.7866	-6.29	y_{73}^{8+}
1017.6123	1017.6180	-5.60	y_{111}^{12+}
1022.7882	1022.7911	-2.84	y_{37}^{4+}
1026.8408	1026.8458	-4.87	z_{28}^{3+}
1032.0126	1032.0163	-3.59	z_{19}^{2+}
1032.1814	1032.1853	-3.78	y_{28}^{3+}
1032.1826	1032.1853	-2.62	y_{28}^{3+}
1032.4703	1032.4745	-4.07	c_{9}
1040.7524	1040.7549	-2.40	y_{47}^{5+}
1048.6934	1048.6960	-2.48	y_{66}^{7+}
1072.0609	1072.0643	-3.17	z_{39}^{4+}

1075.8641	1075.8686	-4.18	z_{29}^{3+}
1077.3396	1077.3430	-3.16	b_{48}^{5+}
1079.6505	1079.6590	-7.87	b_{99}^{10+}
1081.2042	1081.2081	-3.61	y_{29}^{3+}
1082.4390	1082.4365	2.31	b_{80}^{8+}
1086.3124	1086.3196	-6.63	z_{40}^{4+}
1090.3207	1090.3243	-3.30	y_{40}^{4+}
1098.6466	1098.6565	-9.01	y_{131}^{13+}
1104.8847	1104.8880	-2.99	b_{31}^{3+}
1110.0357	1110.0372	-1.35	y_{111}^{11+}
1114.5860	1114.5906	-4.13	z_{41}^{4+}
1121.5507	1121.5549	-3.74	z_{30}^{3+}
1122.4368	1122.4270	8.73	y_{123}^{12+}
1129.5839	1129.5883	-3.90	z_{61}^{6+}
1139.6053	1139.6062	-0.79	z_{83}^{8+}
1142.5782	1142.5827	-3.94	b_{32}^{3+}
1147.4142	1147.4198	-4.88	$c+H_{63}^{6+}$
1148.6804	1148.6859	-4.79	y_{126}^{12+}
1154.1005	1154.0997	0.69	z_{62}^{6+}
1156.2134	1156.2193	-5.10	z_{52}^{5+}
1156.9200	1156.9233	-2.85	$c\cdot_{64}^{6+}$
1159.2186	1159.2215	-2.50	y_{52}^{5+}
1159.2448	1159.2496	-4.14	z_{31}^{3+}
1169.5120	1169.5122	-0.17	y_{97}^{9+}
1170.9460	1170.9410	4.27	z_{63}^{6+}
1174.8799	1174.8854	-4.68	z_{43}^{4+}
1175.6011	1175.6055	-3.74	b_{33}^{3+}
1178.8860	1178.8901	-3.48	y_{43}^{4+}
1179.1788	1179.1825	-3.14	y_{98}^{9+}
1180.5929	1180.5977	-4.07	c_{21}^{2+}
1183.1108	1183.1143	-2.96	y_{86}^{8+}
1188.1064	1188.1080	-1.35	b_{42}^{4+}
1199.5144	1199.5092	4.34	b_{99}^{9+}
1208.6241	1208.6283	-3.48	b_{34}^{3+}
1211.6476	1211.6576	-8.25	z_{44}^{4+}

1216.8607	1216.8647	-3.29	b_{43}^{4+}
1220.9337	1220.9402	-5.32	y_{111}^{10+}
1221.1165	1221.1213	-3.93	c_{43}^{4+}
1225.9683	1225.9629	4.40	y_{33}^{3+}
1229.5933	1229.5979	-3.74	b_{22}^{2+}
1236.9346	1236.9264	6.63	b_{80}^{7+}
1238.1054	1238.1112	-4.68	c_{22}^{2+}
1238.6193	1238.6227	-2.74	b_{44}^{4+}
1240.1588	1240.1632	-3.55	z_{45}^{4+}
1242.4822	1242.4820	0.16	y_{67}^{6+}
1262.9788	1262.9828	-3.17	b_{35}^{3+}
1266.6327	1266.6368	-3.24	y_{23}^{2+}
1272.4184	1272.4239	-4.32	z_{46}^{4+}
1273.6221	1273.6297	-5.97	c_{23}^{2+}
1275.3875	1275.3898	-1.80	b_{45}^{4+}
1289.6403	1289.6452	-3.80	b_{46}^{4+}
1292.6629	1292.6682	-4.10	y_{35}^{3+}
1300.6893	1300.6918	-1.92	y_{47}^{4+}
1302.2606	1302.2632	-2.00	z_{83}^{7+}
1303.3439	1303.3436	0.23	y_{70}^{6+}
1309.4570	1309.4640	-5.35	$c+H_{60}^{5+}$
1317.4054	1317.4040	1.06	c_{85}^{7+}
1318.1503	1318.1559	-4.25	b_{47}^{4+}
1325.4372	1325.4438	-4.98	z_{48}^{4+}
1325.6866	1325.6910	-3.32	y_{36}^{3+}
1335.0771	1335.0830	-4.42	$c+H_{61}^{5+}$
1341.2935	1341.2986	-3.80	z'_{60}^{5+}
1344.2918	1344.3008	-6.69	y_{60}^{5+}
1346.4234	1346.4269	-2.60	b_{48}^{4+}
1347.6480	1347.6539	-4.38	c_{12}
1349.0844	1349.0898	-4.00	c_{62}^{5+}
1350.4564	1350.4629	-4.81	z'_{49}^{4+}
1354.2113	1354.2156	-3.18	y_{49}^{4+}
1355.4970	1355.5060	-6.64	z'_{61}^{5+}
1363.3811	1363.3857	-3.37	y_{37}^{3+}

1376.4955	1376.5016	-4.43	c_{63}^{5+}
1404.9173	1404.9277	-7.40	z_{63}^{5+}
1426.7360	1426.7468	-7.57	$c+H_{79}^{6+}$
1429.0774	1429.0833	-4.13	z_{39}^{3+}
1434.4190	1434.4228	-2.65	y_{39}^{3+}
1487.5829	1487.5732	6.52	z_{67}^{5+}
1490.7643	1490.7769	-8.45	y_{67}^{5+}
1490.9488	1490.9563	-5.03	y_{81}^{6+}
1521.7979	1521.8090	-7.29	y_{83}^{6+}
1523.4718	1523.4798	-5.25	z_{42}^{3+}
1527.0099	1527.0135	-2.36	$c+H_{56}^{4+}$
1536.8038	1536.8035	0.20	c_{85}^{6+}
1553.8196	1553.8219	-1.48	z_{85}^{6+}
1563.8011	1563.8109	-6.27	y_{70}^{5+}
1566.1697	1566.1781	-5.36	z_{43}^{3+}
1571.5126	1571.5177	-3.25	y_{43}^{3+}
1576.8145	1576.8134	0.70	$C+H_{101}^{7+}$
1627.8185	1627.8160	1.54	c_{43}^{3+}
1653.5431	1653.5412	1.15	z'_{45}^{3+}
1658.5509	1658.5548	-2.35	y_{45}^{3+}
1668.5962	1668.6020	-3.48	$c+H_{61}^{4+}$
1686.3580	1686.3613	-1.96	$c+H_{62}^{4+}$
1697.8943	1697.8835	6.36	y_{61}^{4+}
1720.6194	1720.6294	-5.81	$C+H_{63}^{4+}$
1756.1549	1756.1598	-2.79	z'_{63}^{4+}
1822.9666	1822.9672	-0.33	z'_{83}^{5+}

Appendix 27. CID and ETD fragment ions of the **A**γ -globin chain in a previously undiagnosed (FAV6) neonatal sample.

Meas *m/z*	Calc *m/z*	Δ ppm	Fragment
459.2211	459.2225	-3.05	z_3
558.7497	558.7515	-3.22	b_{10}^{2+}
562.2715	562.2732	-3.02	y_4
615.2915	615.2935	-3.25	b_{11}^{2+}
649.3032	649.3052	-3.08	y_5
665.8152	665.8173	-3.15	b_{12}^{2+}
701.2866	701.2889	-3.28	b_6
705.6861	705.6884	-3.26	b_{19}^{3+}
709.3310	709.3333	-3.24	b_{13}^{2+}
738.7089	738.7112	-3.11	b_{20}^{3+}
762.3870	762.3893	-3.02	y_6
765.8730	765.8754	-3.13	b_{14}^{2+}
781.7229	781.7254	-3.20	b_{21}^{3+}
800.6442	800.6468	-3.25	b_{30}^{4+}
816.3133	816.3159	-3.19	b_7
820.0652	820.0677	-3.05	b_{22}^{3+}
828.9155	828.9178	-2.77	b_{31}^{4+}
833.4237	833.4264	-3.24	y_7
843.7441	843.7467	-3.08	b_{23}^{3+}
849.4302	849.4322	-2.35	y_{23}^{3+}
857.1863	857.1889	-3.03	b_{32}^{4+}
858.9124	858.9150	-3.03	b_{15}^{2+}
862.7511	862.7539	-3.25	b_{24}^{3+}
867.4245	867.4283	-4.38	c_{15}^{2+}
881.7581	881.7610	-3.29	b_{25}^{3+}
881.9532	881.9560	-3.17	b_{33}^{4+}
887.4231	887.4258	-3.04	b_{16}^{2+}
897.9506	897.9537	-3.45	b_{48}^{6+}
906.7201	906.7231	-3.31	b_{34}^{4+}

919.2262	919.2232	3.26	z_{33}^{4+}
920.4557	920.4585	-3.04	y_{8}
923.2260	923.2279	-2.06	y_{33}^{4+}
924.7720	924.7752	-3.46	b_{26}^{3+}
932.1366	932.1376	-1.07	y_{25}^{3+}
944.4082	944.4108	-2.75	b_{8}
947.4857	947.4889	-3.38	b_{35}^{4+}
951.4706	951.4732	-2.73	b_{17}^{2+}
973.2545	973.2569	-2.47	y_{35}^{4+}
979.5071	979.5115	-4.49	y_{70}^{8+}
991.4924	991.4956	-3.23	y_{9}
995.3303	995.3367	-6.43	z'_{45}^{5+}
998.0214	998.0240	-2.61	y_{36}^{4+}
1001.0045	1001.0074	-2.90	b_{18}^{2+}
1009.5163	1009.5207	-4.36	c_{18}^{2+}
1032.4703	1032.4745	-4.07	c_{9}
1043.5557	1043.5580	-2.20	y_{47}^{5+}
1050.6944	1050.6983	-3.71	y_{66}^{7+}
1077.3396	1077.3430	-3.16	b_{48}^{5+}
1079.6505	1079.6590	-7.87	b_{99}^{10+}
1080.5361	1080.5405	-4.07	z_{29}^{3+}
1082.4390	1082.4365	2.31	b_{80}^{8+}
1099.7307	1099.7346	-3.55	y_{131}^{13+}
1104.8847	1104.8880	-2.99	b_{31}^{3+}
1111.3095	1111.3113	-1.62	y_{111}^{11+}
1114.0465	1114.0484	-1.71	y_{132}^{13+}
1123.5937	1123.5950	-1.16	y_{123}^{12+}
1142.5782	1142.5827	-3.94	$b_{32}3+$
1147.4142	1147.4198	-4.88	$c+H_{63}^{6+}$
1156.9200	1156.9233	-2.85	$c+H_{64}^{6+}$
1175.6011	1175.6055	-3.74	b_{33}^{3+}
1178.3837	1178.3893	-4.75	z_{43}^{4+}
1180.5929	1180.5977	-4.07	c_{21}^{2+}
1188.1064	1188.1080	-1.35	b_{42}^{4+}
1199.5144	1199.5092	4.34	b_{99}^{9+}

1208.6241	1208.6283	-3.48	b_{34}^{3+}
1216.8607	1216.8647	-3.29	b_{43}^{4+}
1221.1165	1221.1213	-3.93	c_{43}^{4+}
1225.2998	1225.2952	3.75	z_{33}^{3+}
1229.5933	1229.5979	-3.74	b_{22}^{2+}
1236.9346	1236.9264	6.63	b_{80}^{7+}
1238.1054	1238.1112	-4.68	c_{22}^{2+}
1238.6193	1238.6227	-2.74	b_{44}^{4+}
1262.9788	1262.9828	-3.17	b_{35}^{3+}
1273.6221	1273.6297	-5.97	c_{23}^{2+}
1275.3875	1275.3898	-1.80	b_{45}^{4+}
1289.6403	1289.6452	-3.80	b_{46}^{4+}
1309.4570	1309.4640	-5.35	$c+H_{60}^{5+}$
1317.4054	1317.4040	1.06	c_{85}^{7+}
1318.1503	1318.1559	-4.25	b_{47}^{4+}
1335.0771	1335.0830	-4.42	$c+H_{61}^{5+}$
1346.4234	1346.4269	-2.60	b_{48}^{4+}
1347.6480	1347.6539	-4.38	c_{12}
1349.0844	1349.0898	-4.00	c_{62}^{5+}
1354.7148	1354.7148	0.00	z_{49}^{4+}
1376.4955	1376.5016	-4.43	c_{63}^{5+}
1426.7360	1426.7468	-7.57	$c+H_{79}^{6}+$
1527.0099	1527.0135	-2.36	$c+H_{56}^{4+}$
1536.8038	1536.8035	0.20	c_{85}^{6+}
1576.8145	1576.8134	0.70	$c+H_{101}^{7+}$
1627.8185	1627.8160	1.54	c_{43}^{3+}
1668.5962	1668.6020	-3.48	$c+H_{61}^{4+}$
1686.3580	1686.3613	-1.96	$c+H_{62}^{4+}$
1720.6194	1720.6294	-5.81	$c+H_{63}^{4+}$